

DOE/SF/10535-1/1

**ALTERNATE CENTRAL RECEIVER POWER SYSTEM PROGRAM
PHASE II**

Midterm Technical Report, Volume 1—Commercial Plant Design Refinement

By

**J. C. Amos
A. V. Curinga
J. A. Elsner
E. E. Gerrels**

**C. C. Hussey
D. J. Muller
H. P. Offer
G. Oganowski**

**E. Olich
B. D. Pomeroy
P. J. Ring
S. I. Schwartz**

July 1980

Work Performed Under Contract No. AC03-79SF10535

**General Electric Company
Energy Systems Programs Department
Schenectady, New York**



U.S. Department of Energy



Solar Energy

Cat. No: 22-0041
VOL 1

DISCLAIMER

"This book was prepared as an account of work sponsored by an agency of the United States Government. Neither the United States Government nor any agency thereof, nor any of their employees, makes any warranty, express or implied, or assumes any legal liability or responsibility for the accuracy, completeness, or usefulness of any information, apparatus, product, or process disclosed, or represents that its use would not infringe privately owned rights. Reference herein to any specific commercial product, process, or service by trade name, trademark, manufacturer, or otherwise, does not necessarily constitute or imply its endorsement, recommendation, or favoring by the United States Government or any agency thereof. The views and opinions of authors expressed herein do not necessarily state or reflect those of the United States Government or any agency thereof."

This report has been reproduced directly from the best available copy.

Available from the National Technical Information Service, U. S. Department of Commerce, Springfield, Virginia 22161.

Price: Printed Copy A11
Microfiche A01

MIDTERM TECHNICAL REPORT
VOLUME I - COMMERCIAL PLANT DESIGN REFINEMENT

**ALTERNATE
CENTRAL RECEIVER POWER
SYSTEM PROGRAM
PHASE II**

July 1980

PREPARED FOR
UNITED STATES DEPARTMENT OF ENERGY
(CONTRACT NO. DE-AC03-79SF10535)

GENERAL ELECTRIC COMPANY
ENERGY SYSTEMS PROGRAMS DEPARTMENT
SCHENECTADY, NEW YORK

GENERAL  ELECTRIC

ABSTRACT

This Midterm Technical Report documents progress during the first year of the Alternate Central Receiver Power System Program Phase II (DoE Contract No. DE-AC03-79SF10535). The Phase II program is an extension of the "Conceptual Design of Advanced Central Receiver Power System-Phase I (DoE Contract No. DE-AC03-78ET20500)" completed in February 1979.

The objective of the Phase II program is "the near term application of sodium central receiver power plants for low cost electric power generation." This Midterm Technical Report documents technical accomplishments on the three principal program activities:

- Refinement of the Phase I conceptual design of a 100 MWe sodium cooled central receiver power plant to incorporate improvements in performance and cost. The results are described in Volume I of this report.
- Design, fabrication, installation, and testing of a 2.5 MW thermal Sodium Receiver Test Assembly (SRTA). Volume II describes progress during the first year of the program.
- Materials experiments including development of a brazing fabrication procedure for joining the thin-walled tubes of sodium central receivers. Materials efforts are documented in Volume III.

ACKNOWLEDGEMENTS

This report was prepared by the General Electric Company Energy Systems Programs Department for the U.S. Department of Energy under Contract No. DE-AC03-79SF10535. In May 1980 the program was shifted to Sandia Livermore Laboratories Contract No. 83-7550. The principal authors are:

J.C. Amos
A.V. Curinga
J.A. Elsner
E.E. Gerrels
C.C. Hussey
D.J. Muller
H.P. Offer
G. Oganowski
E. Olich
B.D. Pomeroy
P.J. Ring
S.I. Schwartz

J.A. Elsner is the Program Manager and C.C. Hussey is the Technical Manager for this program.

The General Electric Company Advanced Reactor Systems Department is a major contributor to the program and the GE Corporate Research and Development (CRD) Center provided significant technical consultation. Particular appreciation is expressed to Dr. B.D. Pomeroy of CRD whose personal technical leadership allowed a successful transition of the program from Phase I to Phase II.

This report is based upon work performed by the above listed authors and by the following additional technical contributors:

D.B. Drendel
K.L. Lee
C.E. Messervl
T.V. Narayanan
A. Robertson
D. Reed
P. Roy
P.W. Swartz

VOLUME I

TABLE OF CONTENTS

<u>Section</u>		<u>Page</u>
	LIST OF FIGURES	iv
	LIST OF TABLES	vii
	PHASE II PROGRAM OVERVIEW	1
1	INTRODUCTION	1-1
	1.1 Receiver Subsystem	1-1
	1.2 Storage Subsystem	1-2
	1.3 Plant Analysis	1-2
	1.4 Plant Integration	1-3
2	PANEL CONFIGURATION ANALYSIS	2-1
	2.1 Introduction	2-1
	2.2 Thermal Loss Comparison	2-2
	2.3 Flow Distribution and Control Comparison	2-5
	2.4 Mechanical Design Comparison	2-8
	2.5 Thermal Stress Comparison	2-9
	2.5.1 Definition of Cases	2-10
	2.5.2 Definition of Operating Thermal Cycles	2-11
	2.5.3 Thermal Stress Analysis	2-15
	2.6 Design Criteria	2-16
	2.6.1 Estimate of Panel Life	2-23
	2.6.2 Generalized Fatigue Evaluation Chart	2-26
	2.7 Conclusions	2-29
3	RECEIVER FLOW CONTROL SYSTEM COST REDUCTION	3-1
	3.1 Introduction	3-1
	3.2 Approach	3-1
	3.3 Panel Grouping Analysis	3-3
	3.3.1 Panel Outlet ΔT Limit	3-3
	3.3.2 Receiver Efficiency Degradation	3-4
	3.3.3 Grouping Thermal Analysis	3-4
	3.3.4 Grouping Cost Impact	3-7
	3.4 EM Pump Vs. Throttle Valves	3-7
	3.5 Conclusions	3-8
4	STORAGE SUBSYSTEM DESIGN IMPROVEMENTS	4-1
	4.1 Introduction	4-1
	4.2 Sodium-Iron Storage	4-1
	4.2.1 Conceptual Design	4-1
	4.2.2 Cost Estimate	4-2
	4.2.3 Development Issues	4-9
	4.2.4 Summary and Conclusions	4-12
	4.3 Storage System Redesign	4-12
	4.3.1 Storage Vessel Design	4-12
	4.3.2 Potential Improvements	4-16

VOLUME I

TABLE OF CONTENTS (Continued)

<u>Section</u>		<u>Page</u>
5	OPERATING MODE ANALYSIS	5-1
5.1	Introduction	5-1
5.2	Background	5-1
5.3	Operating Mode Description	5-12
5.3.1	Standby Modes	5-13
5.3.1.1	Short Term (Hot) Standby	5-13
5.3.1.2	Intermediate Term (Warm) Standby	5-21
5.3.1.3	Long Term (Cold) Standby	5-25
5.3.2	Startup Modes	5-27
5.3.2.1	Cold Start	5-27
5.3.2.2	Warm Start	5-30
5.3.2.3	Hot Start	5-31
5.3.3	Normal Operation Modes	5-31
5.3.4	Shutdown Modes	5-32
5.3.4.1	Normal Shutdown	5-32
5.3.4.2	Emergency Shutdown	5-32
5.3.5	Other Topics	5-34
5.3.5.1	Cloud Cover Standby	5-34
5.3.5.2	Drainage Approach	5-34
5.3.5.3	Initial Fill and Refill of Sodium	5-35
5.4	Recommended Revisions to the Phase I Plant Design	5-39
5.5	Areas for Future Study and Resolution	5-39
6	SYSTEM ANNUAL PERFORMANCE ANALYSIS	6-1
6.1	Introduction	6-1
6.2	Computer Model Description	6-1
6.2.1	Program Structure	6-1
6.2.2	Operating Plan Logic	6-3
6.2.3	Model Description	6-6
6.3	Plant Performance	6-17
6.3.1	Design Point	6-17
6.3.2	Hourly Variation During Typical Days	6-17
6.3.3	Monthly and Annual Variation	6-22
7	REFINED CONCEPTUAL DESIGN	7-1
7.1	Introduction	7-1
7.2	Field Optimization Analysis	7-1
7.2.1	Optimum Field Layout	7-4
7.2.2	Receiver Design	7-6
7.3	Overall Plant Performance	7-14
8	REFINED PLANT COST ESTIMATE	8-1
8.1	Receiver Equipment	8-1
8.1.1	Absorber Unit	8-1
8.1.2	Receiver Circulation Equipment	8-3
8.2	Thermal Storage Equipment	8-3

VOLUME I

TABLE OF CONTENTS (Continued)

<u>Section</u>		<u>Page</u>
	8.3 Collector Equipment	8-8
	8.4 Revised First Solar Power Plant Capital Cost Summary	8-8
	8.5 Revised Mature Solar Power Plant Capital Cost Summary ...	8-8
9	REFERENCES	9-1
<u>Appendices</u>		
A	RECEIVER LOSS ANALYSIS CODE - PANELGR2	A-1
B	PANELGR2 OUTPUT FOR SELECTED GROUPING SCHEME	B-1
C	COMPONENT COOLDOWN ANALYSIS (INITIAL UNIFORM TEMPERATURE)	C-1
D	COMPONENT COOLDOWN ANALYSIS (INITIAL NONUNIFORM TEMPERATURE) .	D-1
E	TEMPERATURE CYCLING CONSIDERATIONS IN THE DOWNCOMER PIPE	E-1
F	TRICKLE FLOW SCHEME FOR SHORT TERM STANDBY	F-1
G	COMPUTER PROGRAM LISTING FOR SYSTEM ANNUAL PERFORMANCE ANALYSIS	G-1

VOLUME I

LIST OF FIGURES

<u>Figure</u>		<u>Page</u>
2-1	Comparison of Two- and Three-Header Panels	2-2
2-2	Receiver Efficiency	2-3
2-3	Tube Temperatures - 100% Power	2-4
2-4	Tube Temperatures - 30% Power	2-5
2-5	Flux Plots	2-6
2-6	Effect of Gross Aiming Errors on Sodium Outlet Temperatures for Three-Header Panel	2-7
2-7	Comparison of Pressure Distributions	2-8
2-8	Effect of Orifice on Sodium Flow Imbalance in the Three-Header Panel	2-9
2-9	Three-Header Temperatures and Fluxes - 100% Power	2-10
2-10	Two-Header Temperatures and Fluxes - 100% Power	2-11
2-11	North Panel Fluxes - Alternate Aiming Strategies	2-12
2-12	North Panel Temperatures and Fluxes - Two-Point Aiming	2-13
2-13	Absorber Panel Thermal Cycle Histogram	2-14
2-14	Finite Element Model for Thermal and Stress Analysis	2-15
2-15	Thermal and Mechanical Properties of Incoloy 800	2-17
2-16	Temperature Profile - Case 4	2-18
2-17	Definition of Frequency	2-19
2-18	Curve Fit of Data at 593°C (1100°F) to Determine Constants β and β' for Case of Zero Hold Time (Constant Frequency)	2-20
2-19	Curve Fit of Data at 593°C (1100°F) to Determine Frequency Exponents (K and K')	2-21
2-20	Correlation of Data for 593°C (1100°F)	2-22
2-21	Preliminary Design Curves for 538°C (1000°F)	2-23
2-22	Preliminary Design Curves for 593°C (1100°F)	2-24
2-23	Preliminary Design Curves for 649°C (1200°F)	2-25
2-24	Fatigue Evaluation Chart	2-27
2-25	Fatigue Evaluation of Three Previously Analyzed Cases	2-28
3-1	Panel Grouping Concept	3-2
3-2	Grouped Panel Header Configurations	3-3
3-3	Panel Numbering Sequence	3-6
3-4	Final Grouping Configuration	3-6

VOLUME I

LIST OF FIGURES (Continued)

<u>Figure</u>		<u>Page</u>
3-5	Throttle Valve Manifold	3-8
4-1	Sodium-Iron Storage Concept	4-3
4-2	Sodium-Iron Storage Layout	4-6
4-3	Sodium-Iron Tank Concept	4-7
4-4	Thermal Energy Storage Vessel	4-13
5-1	ACR Control Schematic	5-3/4
5-2	Cooldown of Riser/Downcomer	5-7
5-3	Cooldown of Receiver Panels	5-8
5-4	Cooldown of Cold Sodium Storage Tank	5-9
5-5	Cooldown of Hot Sodium Storage Tank	5-10
5-6	Cooldown of Superheater (Reheater)	5-11
5-7	Receiver/Tower Loop Short Term Hold Mode (Phase I Natural Cir- culation Scheme)	5-15
5-8	Reverse Recirculation Scheme for Short Term Hold	5-16
5-9	Temperature Levels in Tower Loop (Reverse Recirculation Scheme During Short Term Standby)	5-18
5-10	Evaporator Circulation Loop and Temperature History During Inter- mediate Term Standby	5-24
5-11	Steam Generator Circulation Loop and Temperature History During Long Term Standby	5-26
5-12	Flow and Temperature History of Steam Generator During Cold Start	5-29
5-13	Sodium in Components/Piping Drained into Hot Storage Tanks	5-36
5-14	Sodium in Components/Piping Drained into Cold Storage Tank	5-37
5-15	Revision to Plant Design	5-41/42
6-1	System Annual Performance Model Program Structure	6-2
6-2	System Operation Logic Flow Chart	6-4
6-3	Daily Total Insulation Data for Barstow, California in 1976	6-7
6-4	Heliostat Field Efficiency Variation	6-8
6-5	Receiver Efficiency Variation	6-10
6-6	EPGS Efficiency Variation with Condensing Condition	6-13
6-7	Steam Turbine/Generator Performance Variation with Load	6-14

VOLUME I
LIST OF FIGURES (Continued)

<u>Figure</u>		<u>Page</u>
6-8	Variation of Condensing Condition with Ambient Wet Bulb Temperature	6-15
6-9	Condenser Part Load Performance	6-16
6-10	Daily Output Variation, June 21	6-19
6-11	Daily Output Variation, December 23	6-20
6-12	Monthly Plant Output Variation	6-24
6-13	Annual Plant Energy Flow	6-25
7-1	Modified Subsystems in Phase I Commercial Plant Configuration ..	7-2
7-2	Optimized Field Layout	7-5
7-3	Design Point Circumferential Flux Variation of Receiver Midline	7-7
7-4	Design Point Axial Flux Variations	7-4
7-5	Design Point Incident Flux (1st Plant)	7-9
7-6	Design Point Incident Flux (Nth Plant)	7-10
7-7	Variations in Field Efficiency	7-11
7-8	ACR Phase II Receiver Concept	7-13
7-9	Revised Receiver Plan View	7-15
7-10	Refined Energy Cascade at Design Point (Noon, Summer Solstice) .	7-16
8-1	Phase I - Commercial Plant Configuration with Changes Highlighted	8-2
8-2	Comparison of Two- and Three-Header Panels	8-4
8-3	Hourglass Insert	8-5
8-4	Panel Grouping Concept	8-10
8-5	Thermal Energy Storage Vessel	8-16

VOLUME I
LIST OF TABLES

<u>Table</u>		<u>Page</u>
2-1	Absorber Panel Data	2-3
2-2	Effect of Flux Distribution on Efficiency	2-6
2-3	Results of Thermal Stress Analysis	2-19
2-4	Constants for Frequency Modified Fatigue Equations	2-21
2-5	Fatigue Damage Results	2-25
2-6	Comparison of Panel Types	2-29
3-1	Panel Grouping Analysis Results	3-5
3-2	Throttle Valve Versus EM Pump Direct Costs	3-7
4-1	Storage Subsystem Cost Summary - 1100°F System	4-3
4-2	Comparison of Storage Concepts	4-4
4-3	Analysis of Iron Tank Pressure Drop and Thermocline Losses	4-5
4-4	Cost Summary and Comparison	4-8
4-5	Cost Details	4-10
4-6	Storage Tank Costs	4-11
4-7	Storage System Cost Comparison	4-14
4-8	Details, Cost Account 4600	4-15
5-1	Summary of Operating Modes	5-2
5-2	ACR Solar Plant Component Operation Restrictions	5-6
5-3	Candidate Schemes for Standby Modes	5-13
5-4	Revisions to Overall Plant Schematic	5-40
5-5	Areas of Concern for Future Study and Resolution	5-43
6-1	Insulation Loss Summary	6-11
6-2	Summary of Auxiliary Loads	6-11
6-3	Design Point Energy Balance	6-18
6-4	Monthly Performance Variation (Unit: MWhr per Month)	6-23
6-5	Energy Loss Due to Heliostat Defocusing	6-26
7-1	Impact of Changes to Phase I Conceptual Design	7-3
7-2	DELSOL - Capabilities	7-3
7-3	Revised Heliostat Specifications	7-4
7-4	Annual Performance Summary	7-12
7-5	Plant Energy Balance	7-17

VOLUME I

LIST OF TABLES (Continued)

<u>Table</u>		<u>Page</u>
8-1	Commercial Revised Receiver Panel Manufacturing Operations	8-6
8-2	Absorber Panel Cost Detail	8-7
8-3	Absorber Panel Materials and Factory Labor (One Panel)	8-8
8-4	Commercial Plant Storage Cost	8-11
8-5	1st Commercial Heliostat Cost	8-12
8-6	Mature Heliostat Cost	8-13
8-7	First Solar Power Plant	8-14
8-8	Mature Solar Power Plant	8-15

PHASE II PROGRAM OVERVIEW

This Midterm Technical Report documents progress during the first year of the Alternate Central Receiver Power System Program Phase II (DoE Contract No. DE-AC03-79SF10535). The report consists of the following three volumes:

- Volume I - Commercial Plant Design Refinement
- Volume II - Sodium Test Receiver Experiment
- Volume III - Materials Experiments

BACKGROUND

The Phase II program is a follow-on program to the completed Conceptual Design of Advanced Central Receiver Power Systems - Phase I (DoE Contract No. DE-AC03-78ET20500) led by General Electric Corporate Research and Development.

During Phase I, parametric analyses were performed to select the preferred commercial scale (100 MWe) sodium cooled central receiver power plant. The reference concept selected utilizes an external cylindrical receiver with a surrounding field of heliostats. The plant loop schematic is shown in Figure 1 and an artist's concept of the plant in Figure 2. There are approximately three hours of storage, ground level steam generators, and a high efficiency reheat steam power conversion cycle.

A conceptual design was prepared for the reference plant concept and detailed cost estimates were calculated. A number of potential improvements to be examined during Phase II were identified, as were a number of Subsystem Research Experiments (SRE's). The SRE's were selected as those technical steps necessary for advancement of the sodium central receiver technology towards commercialization and addressed critical technical uncertainties.

The Phase II program is a logical extension of the Phase I effort and has as its objective "the near term application of sodium solar central receiver power plants for low cost electric power generation." The specific Phase II activities, shown graphically on Figure 3, include the following efforts:

- Performance of a receiver panel test at the Central Receiver Test Facility (CRTF)

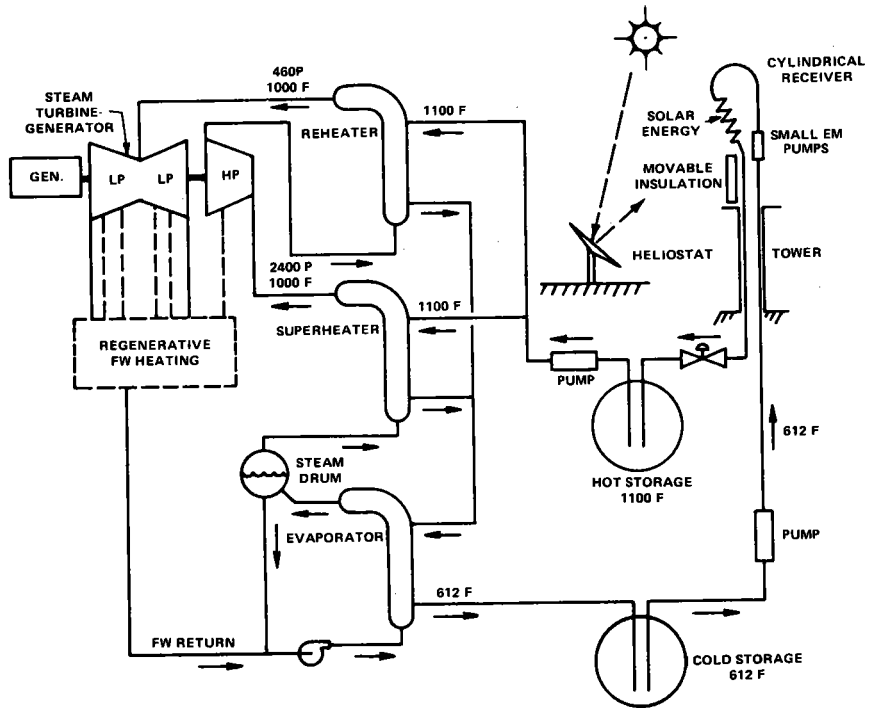


Figure 1. Plant Schematic

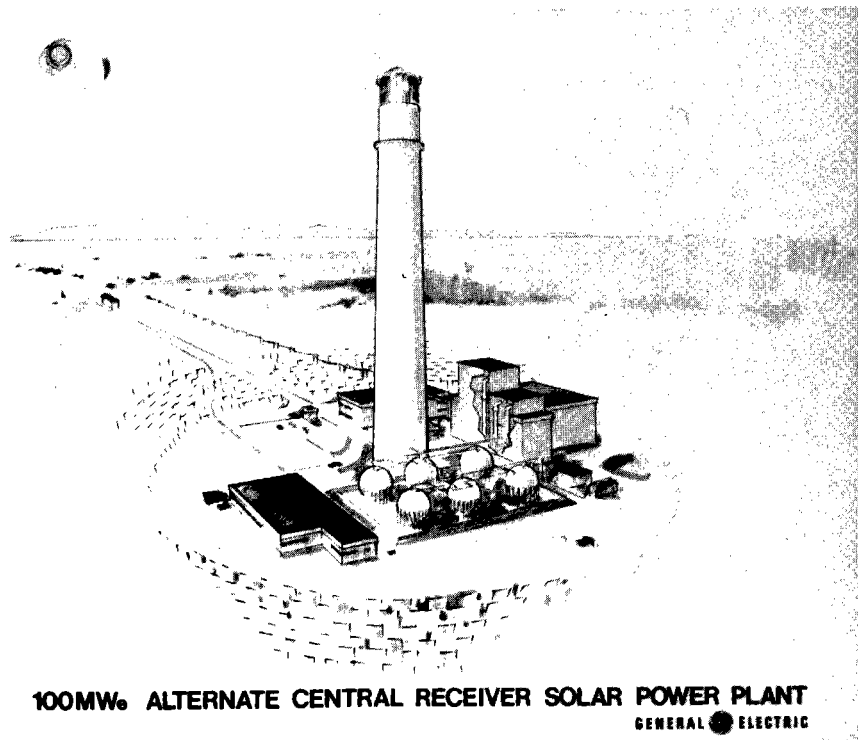
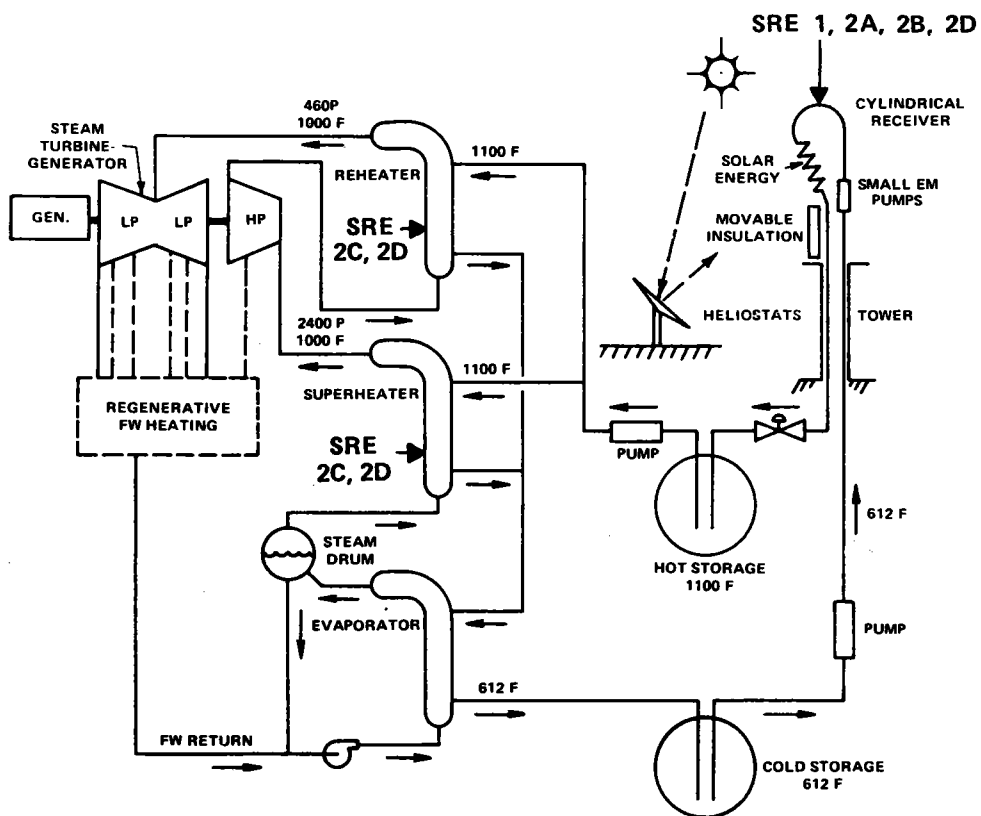


Figure 2. Plant Arrangement

**SYSTEM ENGINEERING
AND ANALYSIS**

**SUBSYSTEM RESEARCH
EXPERIMENTS (SRE'S)**



● SRE 1	ABSORBER PANEL TEST
● SRE 2	MATERIALS SRE'S
SRE 2A	PANEL FABRICATION DEVELOPMENT
SRE 2B	PANEL INSPECTION AND EVALUATION
SRE 2C	STRESS CORROSION AND FATIGUE
SRE 2D	FATIGUE CRACK GROWTH AND FRACTURE TOUGHNESS

Figure 3. Major Phase II Activities

- Performance of materials experiments and panel fabrication development
- Commercial plant design updates
- Development planning.

PROGRAM WORK PLAN

The Phase II program consists of the five tasks described below that extend over two years.

- Task 1 - Subsystem Research Experiments (SRE's)
Perform the necessary hardware development efforts to move sodium central receiver technology from conceptual design status to commercial demonstration status. Key efforts are design, fabrication, and testing of a Sodium Receiver Test Assembly (SRTA) shown in Figure 4 and the conduct of critical materials experiments.
- Task 2 - Commercial Plant Design
Perform a revivification of the conceptual design, based on improvements identified during Phase I. Near the end of the program, update the design to reflect knowledge gained during Phase II.
- Task 3 - Critical Module Design
Define the next step in plant commercial plant development by conceptualizing a large scale critical module configuration. Update the critical module concept near the end of the program to reflect knowledge gained during Phase II.
- Task 4 - Development Planning
Prepare an update of the Phase I development plan for solar sodium receiver technology near the end of Phase II to reflect the knowledge gained during Phase II.
- Task 5 - Program Management
Perform appropriate program management.

The work flow for accomplishing these tasks is shown on Figure 5 and the related schedule shown on Figure 6.

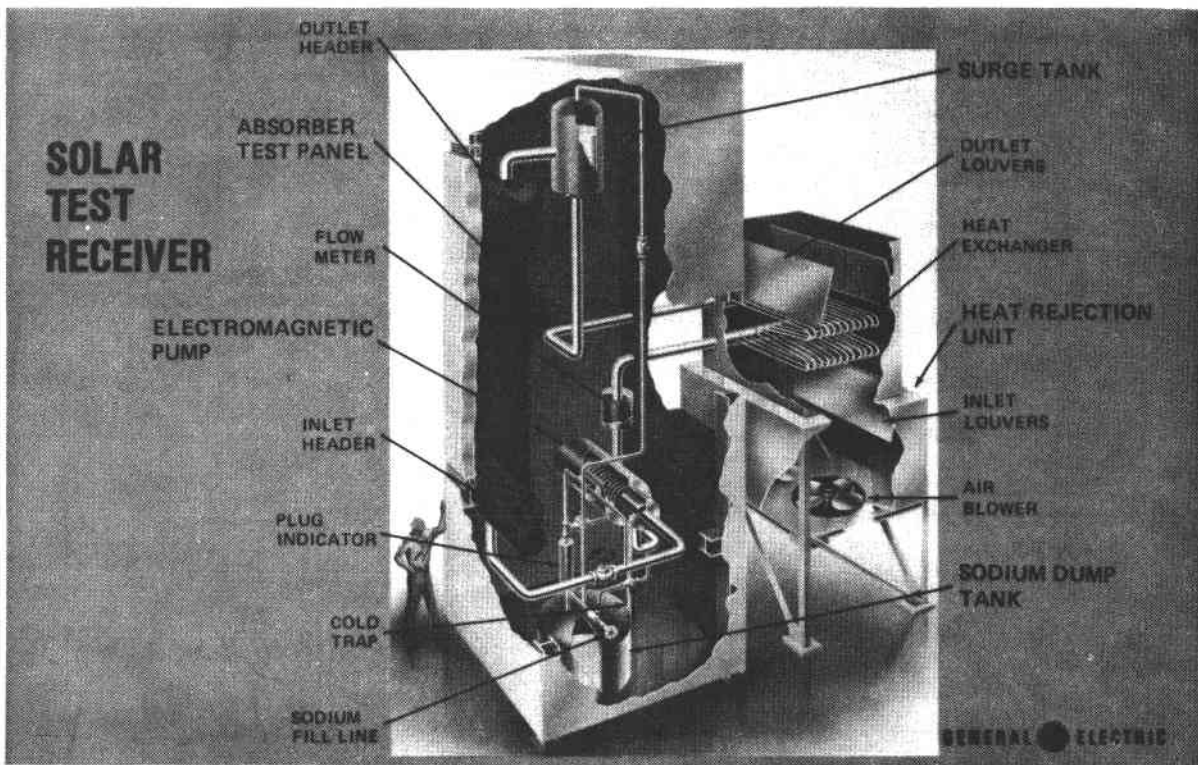
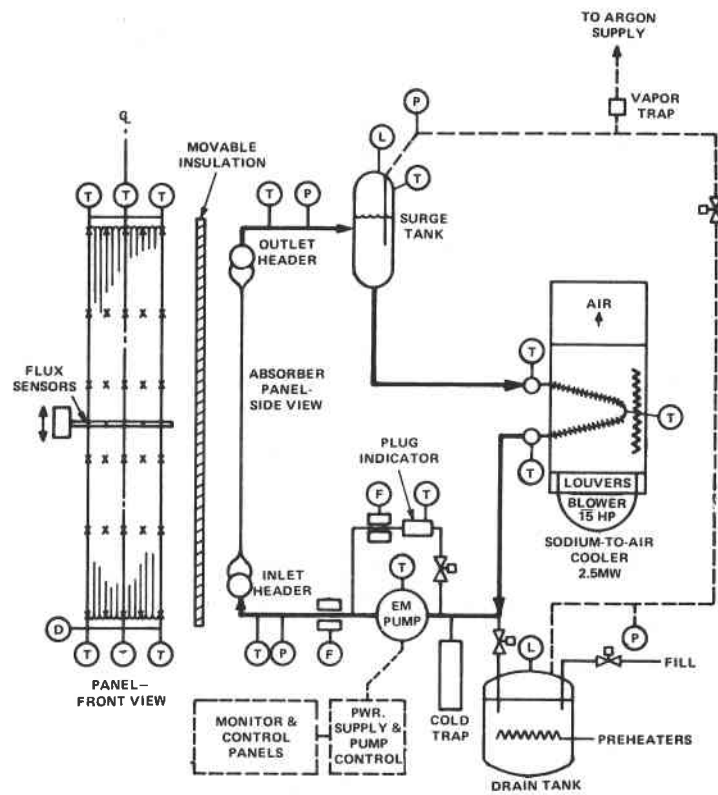


Figure 4. SRTA Schematic and Artist's Concept

ORGANIZATION

The Phase II program is being led by the General Electric Energy Systems Programs Department (ESPD). The transition of leadership from Corporate Research and Development (CRD) to ESPD is a normal activity for General Electric and represents the logical transition of a primarily R&D program into a primarily hardware and commercial application program. CRD played a major role in the plant design refinement task and ensured that a sound technical transition occurred. Kaiser Engineers, Incorporated of Oakland, CA was the Architect Engineer during Phase I and performed the storage tank design refinement described in Volume I of this report. The current organization is shown in Table 1.

TABLE 1

PROGRAM ORGANIZATION

- GENERAL ELECTRIC COMPANY
 - ENERGY SYSTEMS PROGRAMS DEPARTMENT (ESPD)
 - Program Management
 - Systems Engineering
 - Plant Integration
 - ADVANCED REACTOR SYSTEMS DEPARTMENT (ARSD)
 - Liquid Metal Engineering
 - Sodium Components
 - Brazing Development
- FOSTER WHEELER DEVELOPMENT CORPORATION (FWDC)
 - Absorber Test Panel Fabrication
- PYROMET INDUSTRIES, INC.
 - Test Panel Brazing
 - Temporary Brazing Furnace

PROGRAM STATUS

As of April 1980, the Phase II program is focused on fabrication of the 2.5 MWth Sodium Receiver Test Assembly (SRTA). The design refinement of the 100MWe commercial plant was completed in October 1979 and the analysis and results are detailed in Volume I of this report.

The SRTA design has been completed and fabrication of the components are underway. The panel fabrication scheme (horizontal furnace braze) has been selected and fabrication of a large temporary brazing furnace is well underway.

The design and fabrication status of the SRTA is reported in Volume II.

Significant progress has been made in the development of the panel fabrication techniques and several materials test efforts are underway. The materials experiments are discussed in Volume III.

Section 1

INTRODUCTION

The commercial plant configuration developed during Phase I was selected from a large number of candidate concepts through a detailed parametric analysis and comparison of alternatives (see Ref. 1-1). This comparison identified an approach which promised to meet the plant operating requirements in a cost effective manner. However, in performing the conceptual design analysis, it was not possible to fully optimize the plant concept because a number of identified potential improvements in performance and cost could not be incorporated due to schedule and resource constraints.

As part of Task 2.1 of this Alternate Central Receiver - Phase II Program certain of the above improvements were singled out for further evaluation. Those selected design improvements are outlined below along with the remaining Task 2.1 studies including an operating mode analysis, the system annual performance and the refined plant configuration and cost estimates. Details of the specific analyses are contained in the following sections of this report.

1.1 RECEIVER SUBSYSTEM

The three-header absorber panel design used in Phase I was originally conceived to accommodate high peak solar fluxes on the order of 4 MW/m^2 , which were anticipated prior to the final selection of the 360° surround heliostat field configuration. Since the peak flux in the present design is significantly lower than 4 MW/m^2 , a less expensive two-header panel design has been evaluated and compared to the three-header configuration. As discussed in Section 2 the two-header panel is the preferred approach. It will meet all design criteria and offers advantages in terms of efficiency, performance and cost over the three-header panel.

In Phase I, electromagnetic (EM) pumps were selected to control the sodium flow in each absorber panel because they offer smooth, wide-range with high reliability. The alternative use of control valves was rejected for this service due to anticipated reliability problems. However, the high cost of EM pumps has prompted a review of the control options. Furthermore, the panel cooling requirements for a 360° field configuration are less severe than for a north field configuration.

Therefore, reducing the number of panel trim pumps has also been considered as a means of reducing the total receiver cost. Section 3 contains an evaluation of the above control options. It was concluded that a reduced number of EM pumps is the preferred approach since the potential savings with throttle valves is now very small and does not offset the proven high reliability of EM pumps.

1.2 STORAGE SUBSYSTEM

Sodium-iron storage was evaluated during Phase I and found to be more expensive than sodium storage primarily due to the high cost of iron (\$0.45/lb.). However, recently obtained price quotes indicate that scrap steel plate can be purchased for less than half the previous value (\$0.20/lb.). Section 4 presents a re-evaluation of sodium-iron storage incorporating the new iron costs plus a more realistic estimate of iron void space.

A six-tank storage system (three hot and three cold) was chosen in Phase I as the lowest cost configuration. The selected design utilized single wall construction, where, in general, the tank material requirement decreases as the number of tanks increase. However, by switching to double wall construction, typical of cryogenic storage vessels, the sodium storage system has been redesigned to a four-tank system (two hot and two cold). The new system, which is discussed in Section 4, offers improvement in structural integrity and cost while still maintaining the same storage capacity.

1.3 PLANT ANALYSIS

An operating mode analysis, described in Section 5, has been performed for the 100 MWe commercial plant. All modes were developed to meet a set of criteria representative of the various plant operating characteristics. The overall plant control schematic is also discussed which provides for smooth transition between operation and shutdown.

Section 6 describes a computer program that has been written to calculate system annual performance on an hour-by-hour basis utilizing characteristic insolation and weather data. The computer model considers three operating modes (normal operation, warmup and standby) following the plant operating logic developed in Section 5.

1.4 PLANT INTEGRATION

Four areas having improved costs and/or performance have been evaluated as part of an integrated total plant system. These four areas consist of (1) a redesigned two-header absorber panel, (2) reduction in the number of EM pumps, (3) a redesigned storage subsystem using only four tanks (two hot and two cold), and (4) a heliostat application specifying glass heliostats for the 1st plant and GE enclosed heliostats for the Nth plant.

These improvements were incorporated and modeled with the DELSOL computer code and a collector field optimization was performed. The resulting refined commercial plant configuration is described in Section 7. The associated refined capital cost estimates are described in Section 8.

Section 2

PANEL CONFIGURATION ANALYSIS

2.1 INTRODUCTION

Flowing sodium can absorb heat fluxes in excess of 4 MW/m^2 without boiling, even at modest pressures such as 15 kPa (2 psi). In Phase 1, we proposed to exploit this superior heat transfer capability to design a small, lightweight, and inexpensive sodium-cooled receiver. Although the high heat fluxes did not exceed sodium's convective cooling capacity, we recognized that the tube wall thermal stresses might be a limiting factor. Therefore, a three-header panel concept (see Figure 2-1) was adopted in which cool sodium enters the panel at its midpoint, thus minimizing temperatures in the region of highest heat flux and thermal stress.

Both flat and cylindrical receivers were designed in Phase 1 using the three-header panel, and the operating flux levels were estimated for a power plant with a 100 MW rating and a solar multiple of 1.5.* Peak fluxes ranged from about 4 MW/m^2 for the flat receiver when a single point heliostat aiming strategy was employed to about 2 MW/m^2 for a cylindrical receiver with an aim-at-the-belt heliostat strategy. The cylindrical receiver was eventually selected as the lower-cost option and has been carried into the Phase 2 program as the preferred configuration.

Since the cylindrical receiver experiences peak fluxes well below the initial target of 4 MW/m^2 , we considered replacement of the three-header panel with a simpler two-header configuration (also shown in Figure 2-1). Our recent work on alternate aiming strategies has indicated that peak fluxes can be reduced to as low as 1.2 MW/m^2 by distributing the aim points of the heliostats closest to the receiver, thus adding further impetus to reevaluate the three-header panel concept.

The two- and three-header configurations are compared below with respect to:

- Thermal losses and receiver efficiency
- Sodium flow distribution and control
- Mechanical design of the panel supports
- Thermal stresses and creep/fatigue failure.

*Ref. 1.1, Section 3.2

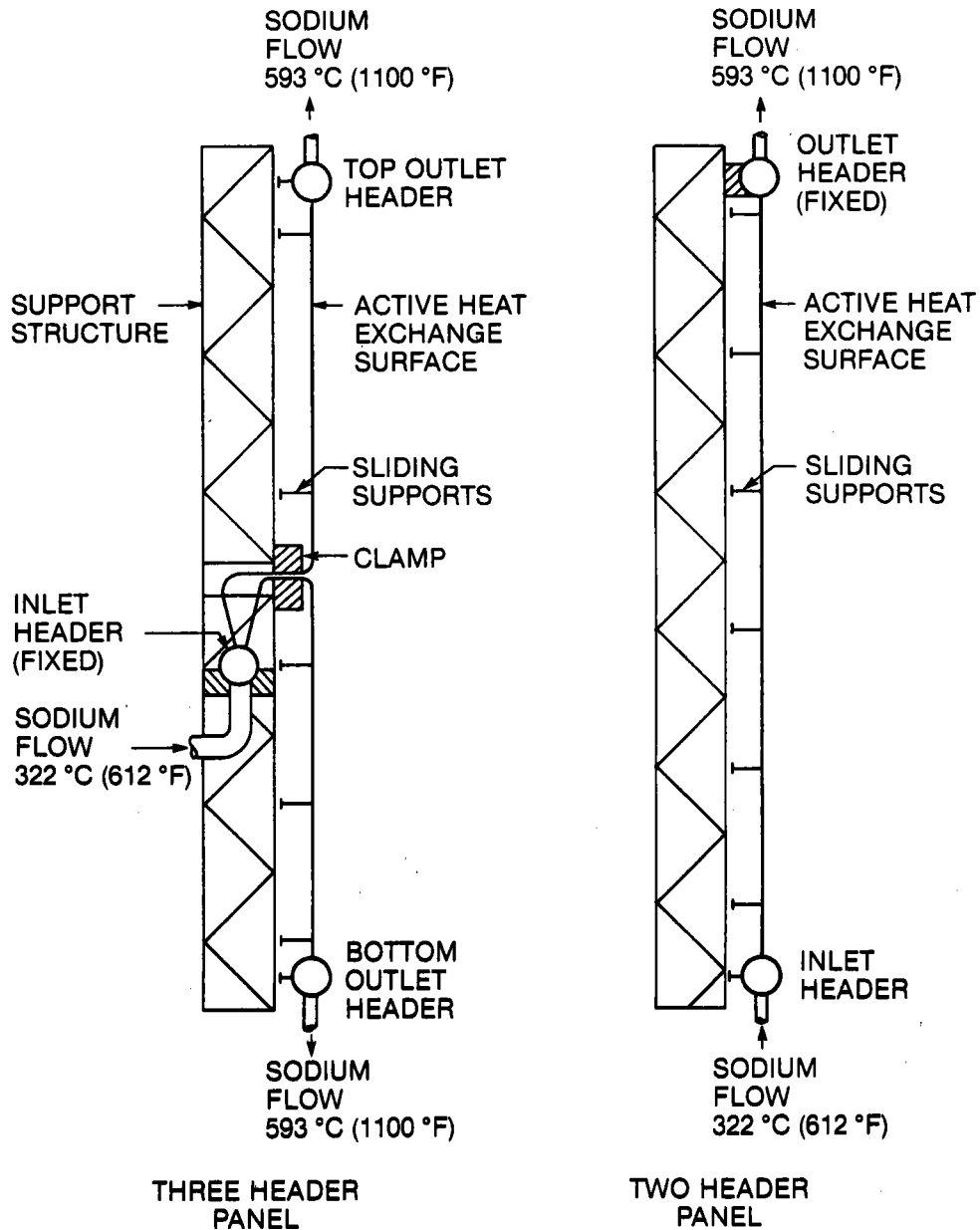


Figure 2-1. Comparison of Two- and Three-Header Panels

On the basis of this work, we conclude that the two-header panel offers efficiency, performance, and mechanical design advantages over the three-header concept, and that the two-header panel meets the design criteria for 30-year life with respect to thermal cycling for fluxes corresponding to a multipoint heliostat aiming strategy (1.2 MW/m^2). However, for higher flux environments, the three-header panel would still be preferred.

2.2 THERMAL LOSS COMPARISON

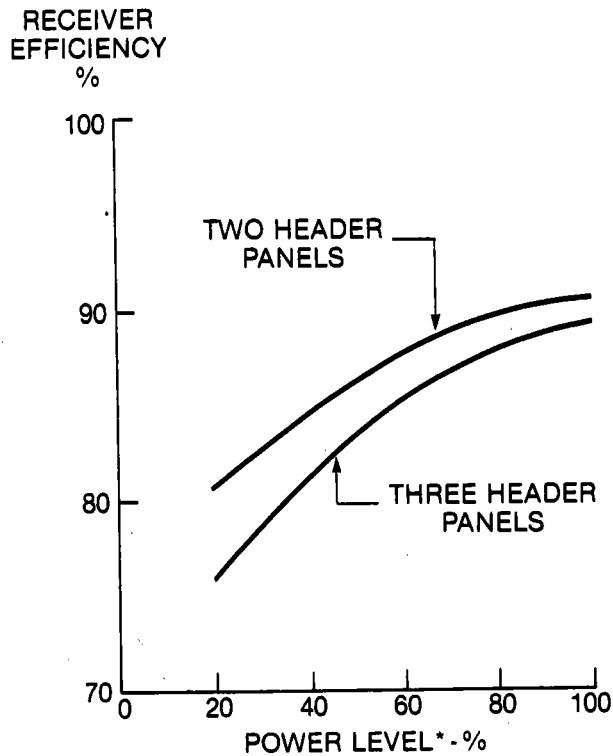
Thermal losses were estimated in Phase 1 for a cylindrical receiver with three-header panels.* The panel dimensions and thermal properties used in this

*Ref. 1.1, Section 5.3.2

calculation are summarized in Table 2-1, and the receiver efficiency results are plotted in Figure 2-2.

Table 2-1
 ABSORBER PANEL DATA

Tube Material	Incoloy 800
Tube OD (in.)	0.75
Tube ID (in.)	0.65
Solar Absortivity (%)	95
Infrared Emissivity (%)	90
Panel Width (m)	2.0944
Panel Length (m)	16.0
Tubes Per Panel	108
Absorber Diameter (m)	16
Absorber Height (m)	16



*INCIDENT SOLAR POWER AS A PERCENT OF MAXIMUM (414MW)

Figure 2-2. Receiver Efficiency

This receiver with a two-header panel using the same dimensions, thermal properties, and flux plots has been evaluated, and these results are also shown in Figure 2-2. The two header configuration was found to have higher efficiency over a wide range of receiver power levels. The reason for this difference can be seen in the absorber temperature profiles (Figure 2-3). Very low temperatures near the sodium inlet header result in lower overall radiation losses for the two-header panels. Convection and reflection losses are about the same for both panel concepts.

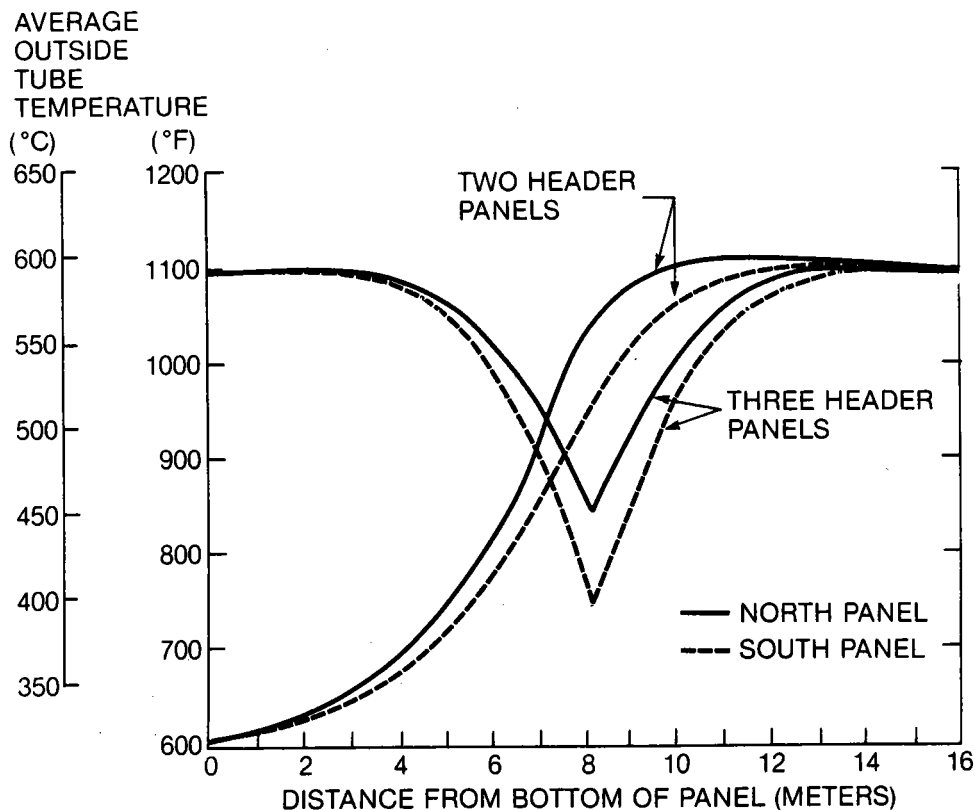


Figure 2-3. Tube Temperatures - 100% Power

Figure 2-4 shows the temperature distributions at the probable low power limit of receiver operation (30% power). Note that the tube temperatures rise well above the sodium outlet temperature in the region two to four meters upstream from the panel outlet headers. This temperature rise occurs because the hot ends of the panels have such low incident fluxes (less than 0.1 MW/m^2) that they are losing more power by radiation and convection than they are gaining from the incident beam. The resulting temperature "bulge" has serious implications with respect to controlling the sodium flows at low power. Note in Figure 2-4 that the two-header configuration has a smaller bulge than the three-header concept.

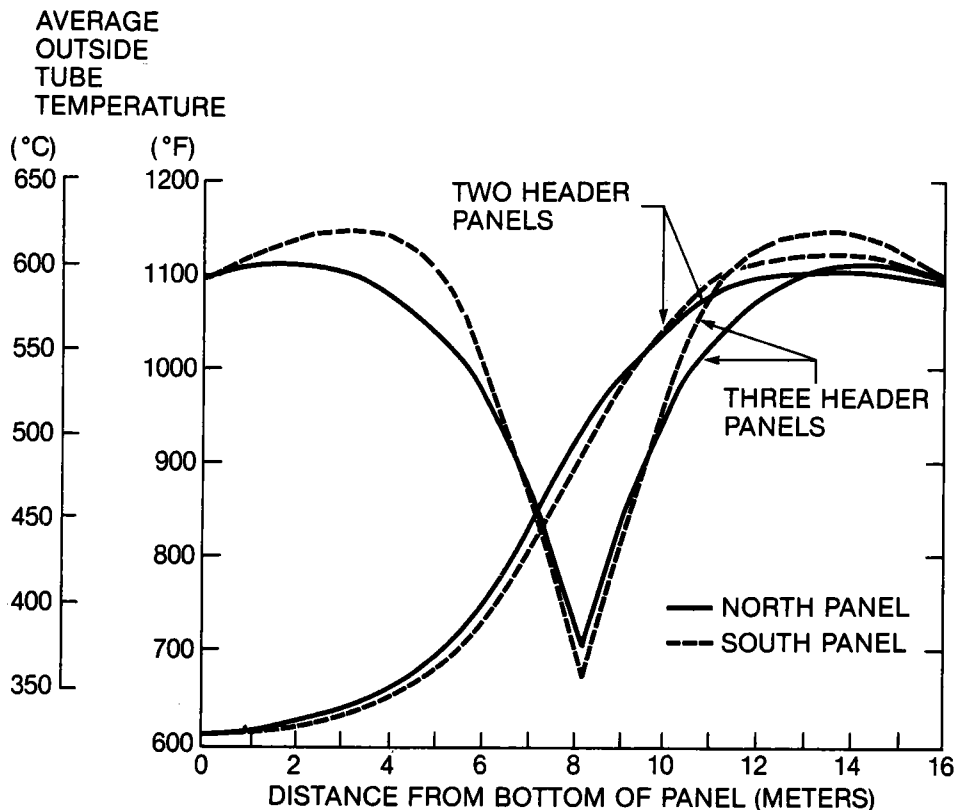


Figure 2-4. Tube Temperatures - 30% Power

Receiver performance was also evaluated with respect to the uniform flux distribution shown in Figure 2-5. The distributed flux shown in this figure is the flux plot used in the calculations discussed above. Table 2-2 shows the comparisons of performance for these two flux plots. Note that the efficiencies for the uniform fluxes are greater than for the distributed fluxes. Thus it appears desirable to adjust the heliostat aiming strategy to achieve the closest practical approximation to the uniform flux model. The difference in efficiency between the two panel concepts diminishes in the uniform flux case, but the two-header concept is still marginally superior.

2.3 FLOW DISTRIBUTION AND CONTROL COMPARISON

Three flow distribution and control problems which occur in the three-header panel were identified in Phase 1.* Although these problems are not insoluble, they do represent a disadvantage with respect to the two-header configuration.

The first problem is the "bulge" in the axial temperature distribution which occurs at low power levels (below 30%). This is a consequence of using a control

*Ref. 1.1, Section 5.3.1

DISTANCE
FROM BOTTOM
OF PANEL - METERS

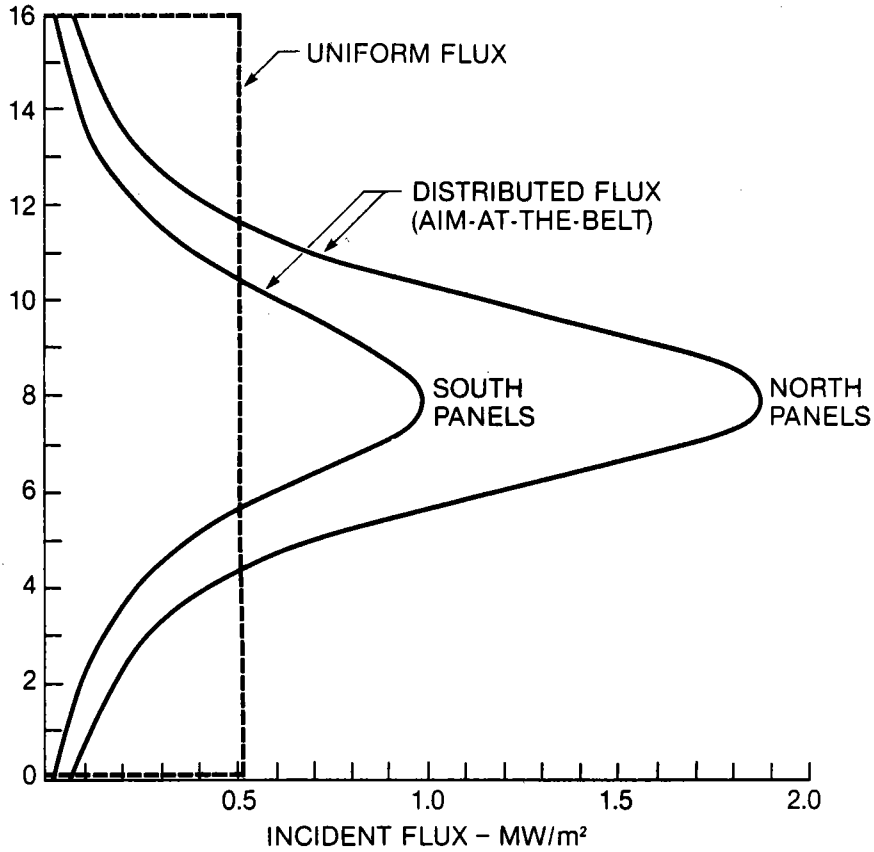


Figure 2-5. Flux Plots

Table 2-2

EFFECT OF FLUX DISTRIBUTION ON EFFICIENCY

	Three-Header Panels		Two-Header Panels	
	Distributed Flux	Uniform Flux	Distributed Flux	Uniform Flux
Incident Power (MW)	414.14	414.19	414.14	414.19
Losses:				
Radiation (MW)	19.60	14.35	15.13	14.26
Convection (MW)	4.83	4.21	4.19	4.19
Reflection (MW)	20.71	20.71	20.71	20.71
Receiver Efficiency (%)	89.1	90.5	90.3	90.6

strategy which adjusts the sodium flow in each panel to maintain a constant 593°C (1100°F) outlet sodium temperature. On cloudless days this phenomenon would not be a problem because the solar input from the heliostats varies between

100% at noon to about 35% at the field tracking cutoff point (10° sun elevation.) However, partial cloudiness could expose some panels to low level sunlight and induce failure by overheating in the region of the bulge. Under these conditions, the two-header panel would be superior because it has a smaller bulge.

The second problem involves control of the incident flux pattern to maintain equal temperatures in the top and bottom outlet headers. As illustrated in Figure 2-6, if the solar beam were shifted only one meter upward, the sodium outlet temperatures could diverge by as much as 200°C (360°F). This situation could cause failure of the receiver through overheating of the upper panel half and thermal shock in the downcomer manifold. The two-header panel, having only one flow path, is insensitive to changes in the axial flux distribution.

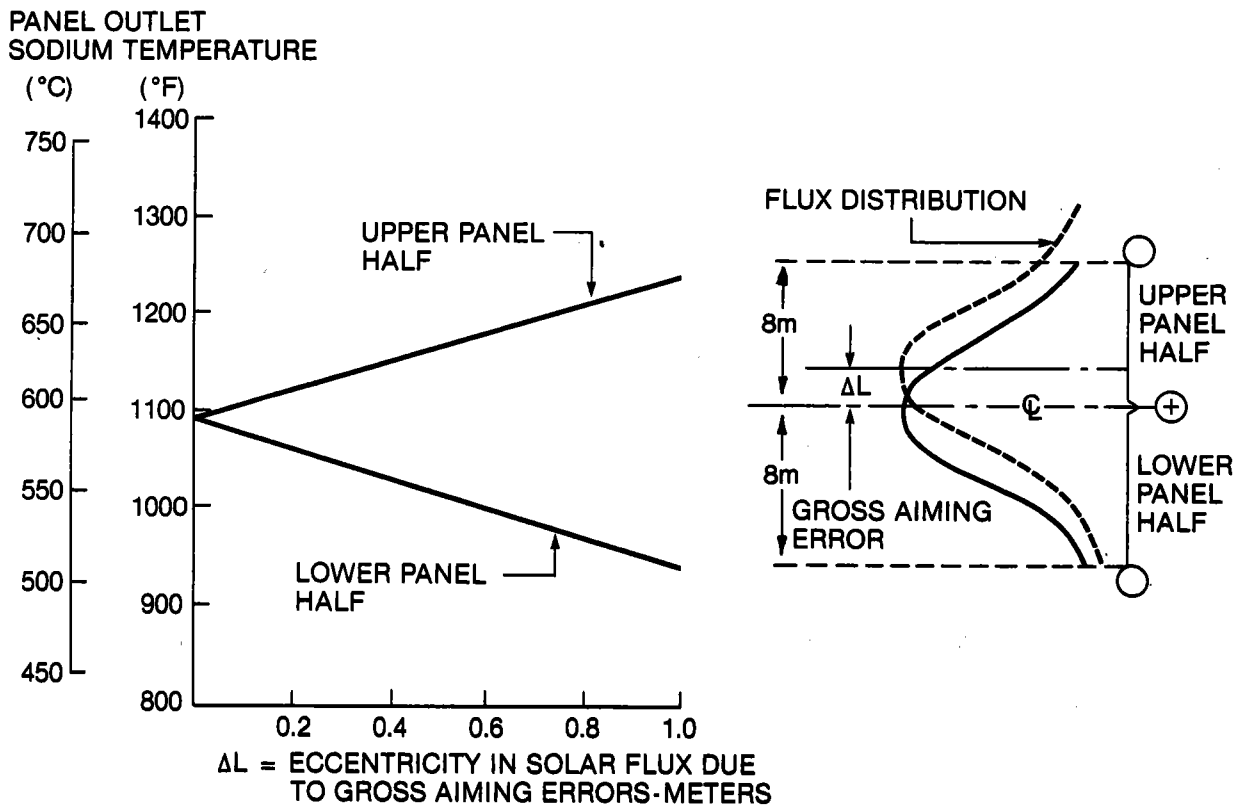


Figure 2-6. Effect of Gross Aiming Errors on Sodium Outlet Temperatures for the Three-Header Panel (Ref. 2.1)

The third flow control problem is induced by the changes in the density of sodium as it is heated in the panel. Figure 2-7 shows typical pressure distributions for the two- and three-header panels at full flow. Note that the pressure at the bottom outlet header on the three-header panel (0.24 MPa) is higher than the pressure at the same elevation on the downcomer (0.23 MPa). An orifice can be inserted as shown to prevent flow in the lower panel half

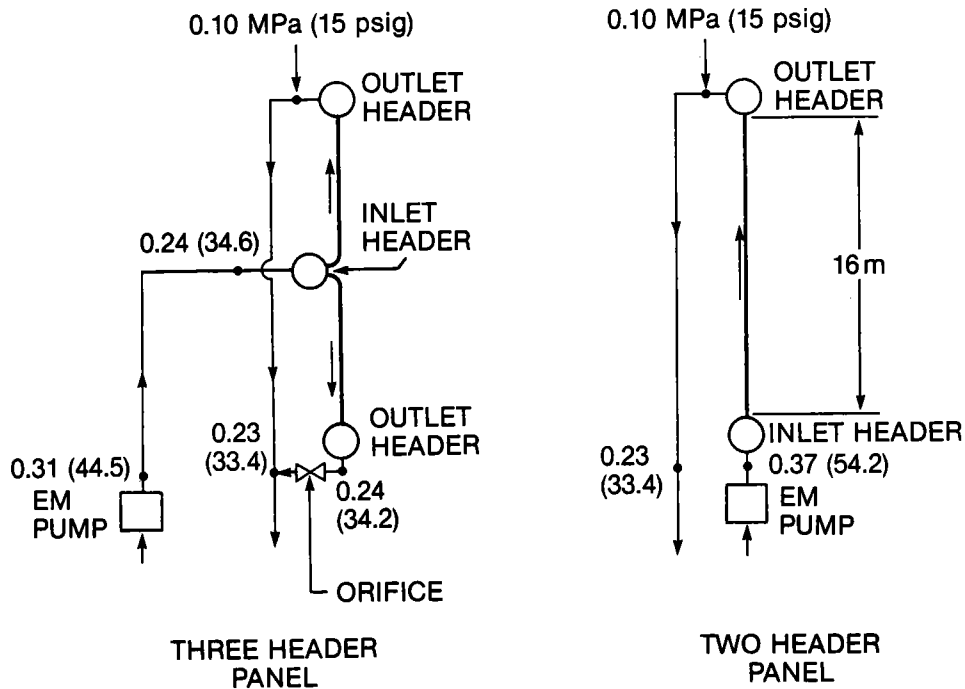


Figure 2-7. Comparison of Pressure Distributions

from being larger than that in the upper panel half. However, an orifice selected so as to balance the flows at full power would cause a significant imbalance at low power levels (Figure 2-8). The consequence of this imbalance is that the top and bottom outlet temperatures diverge. Instead of attempting to balance the flows, it might be possible to continually adjust the heliostat aiming strategy to shift more flux onto the flow-rich panel half. However, the two-header panel, because of its simple flow pattern, does not require an orifice or real-time interaction with the field controls.

2.4 MECHANICAL DESIGN COMPARISON

Both types of panels have 108 tubes across the panel width (Table 2-1). In the three-header case, these tubes are joined to all three headers by 432 welds. The two-header panel, on the other hand, has only 216 welds. Since tube-header welds have been found to be the most frequent area of failure in sodium-heated steam generators (Ref. 1.1), the smaller number of welds in the two-header configuration is a definite advantage with respect to reliability. Fewer welds will also have a favorable impact on the cost of fabricating the two-header panel, since each weld must be fully X-ray inspected.

As shown in Figure 2-1, the tubes in the center of the three-header panel bend sharply where fluxes are highest, while the tubes are straight on the two-

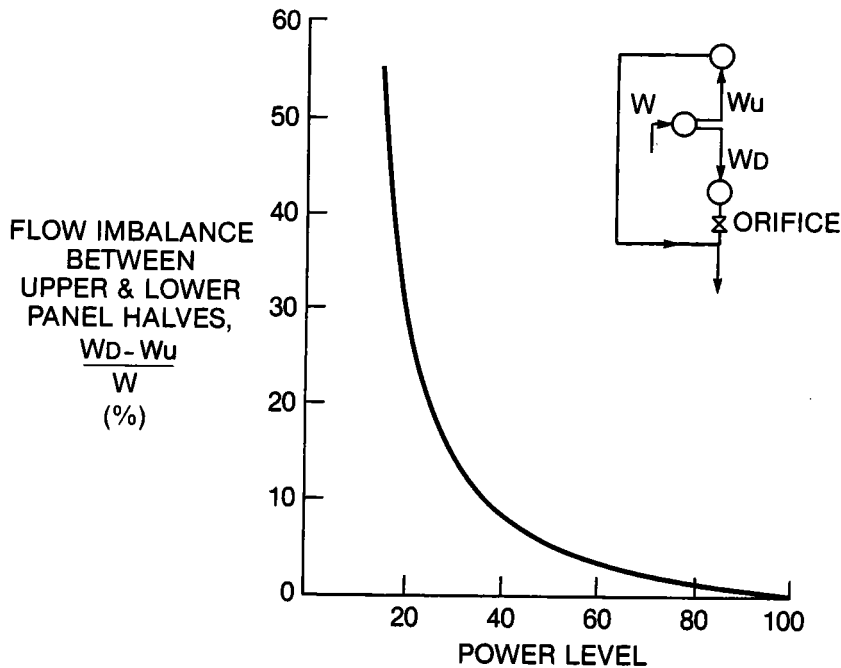


Figure 2-8. Effect of Orifice on Sodium Flow Imbalance in the Three-Header Panel (Ref. 1.1)

header panel. This is an advantage for the two-header concept because the straight tubes are more easily analyzed for stresses and would probably provide a more reliable design.

Thermal expansion in the tubes is accommodated in the three-header panel by clamping the two panel halves together in the center (Figure 2-1) and allowing vertical movement of the outlet headers. The two-header panel is hung from its upper header and expands downward only. The clamps which anchor the center of the three-header panel are a potential source of wear and stress concentration, and are therefore viewed as a disadvantage of the three-header concept.

2.5 THERMAL STRESS COMPARISON

Figure 2-3 shows that in the region of highest flux (north panels, eight meters from bottom) the average outside tube temperatures for the two- and three-header panels are 570°C (1050°F) and 450°C (850°F) respectively. This is potentially a serious disadvantage for the two-header concept because the combination of high flux and high temperature could significantly shorten panel life. To assess the importance of this difference, several panel segments have been analyzed for thermal stresses to estimate the panel life with respect to the cyclic fatigue failure mode. The analyzed segments are referred to as Cases 1 through 4 in the following discussion.

2.5.1 DEFINITION OF CASES

Figure 2-9 shows the temperature and flux profiles for a three-header panel. The sodium and average outside tube temperature curves are identical to those plotted for the north panel in Figure 2-3. The peak outside tube temperature is a rough estimate of the tube crown temperature, based on a one-dimensional heat flow model. As shown in Figure 2-9, the critical area for thermal fatigue failure lies between the point of highest flux (eight meters) and the point of highest peak tube temperature (six and ten meters). The eight-meter point was selected for analysis and has been designated as Case 1.

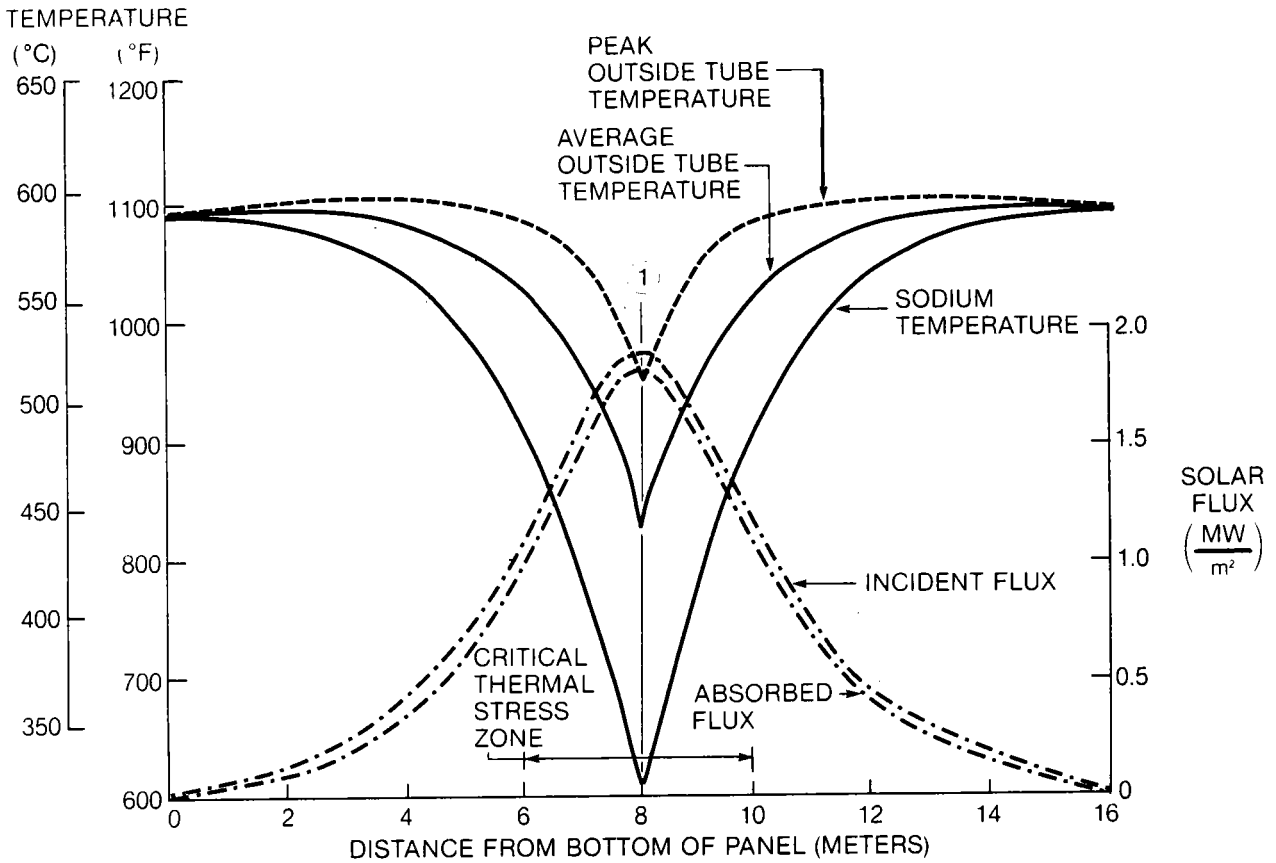


Figure 2-9. Three-Header Temperatures and Fluxes - 100% Power

Similarly, on the two-header panel (Figure 2-10), the critical stress zone lies between the points of highest flux and highest temperature, designated as Cases 2 and 3 respectively.

Figures 2-9 and 2-10 are based upon a sharply peaked flux distribution corresponding to an aim-at-the-belt (single line) heliostat control strategy. If a double line aiming strategy were adopted, the peak flux could be substantially

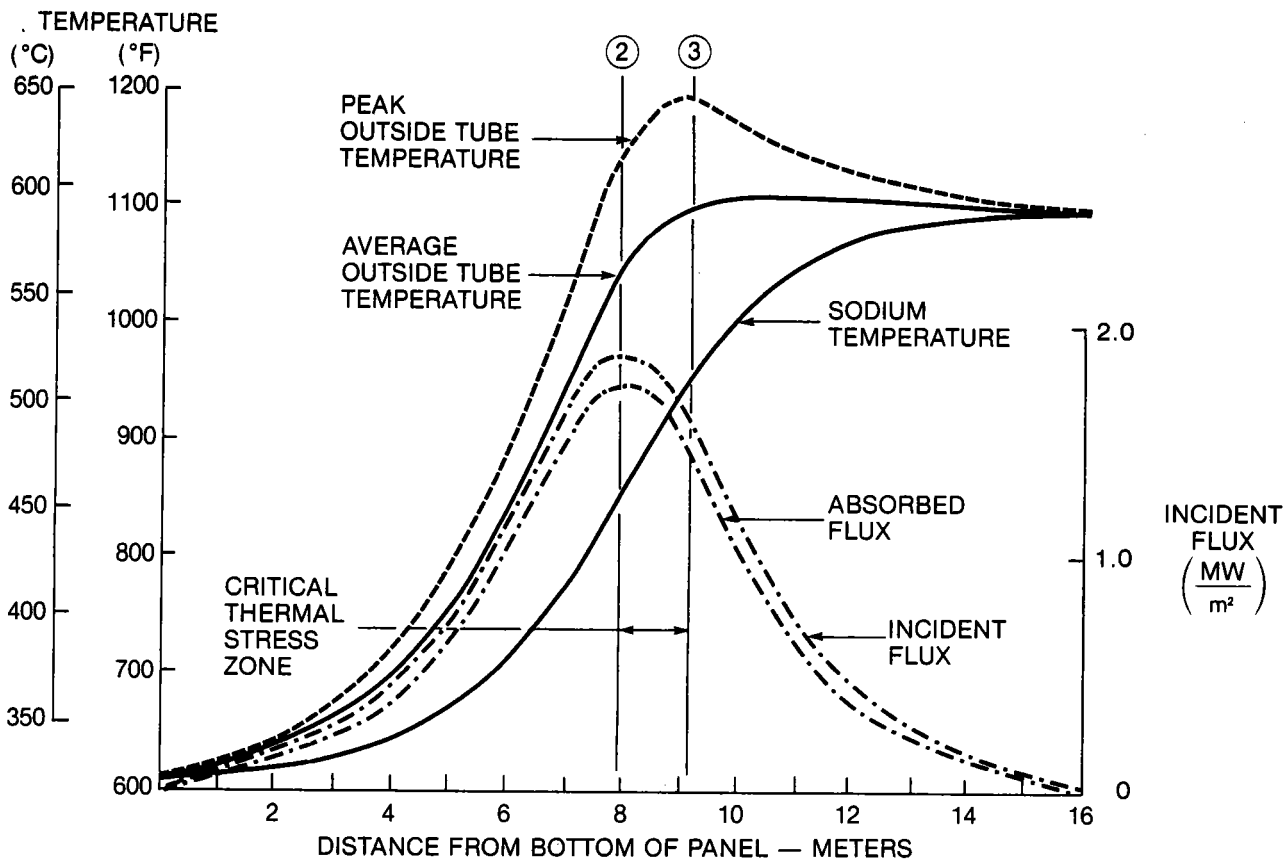


Figure 2-10. Two-Header Temperatures and Fluxes - 100% Power

reduced without significantly increasing receiver spillage losses (Figure 2-11). Similar reductions in peak flux can be achieved with even less spillage by using multipoint aiming only for the heliostats nearest the tower. In either case, peak fluxes of less than 1.2 MW/m^2 seem like a realistic design goal. Figure 2-12 shows a temperature profile for a two-header panel with this type of flux distribution. The point selected for stress analysis is shown as Case 4 in this figure.

2.5.2 DEFINITION OF OPERATING THERMAL CYCLES

Receiver panels will be subjected to at least six different kinds of thermal transients as shown in Figure 2-13. The first of these is the ramp to full temperature (Transient 1) which is the initial step in the startup procedure. The panel starts with a uniform temperature of 316°C (600°F). The sodium flow rate is brought up to 35% of full rated flow, and then the solar flux is ramped from zero to 35% power in 30 minutes while holding the flow constant, thus raising the sodium outlet temperature from 316°C (600°F) to 593°C (1100°F). This process avoids the potentially dangerous temperature excursion (bulge) noted in Figure 2-4.

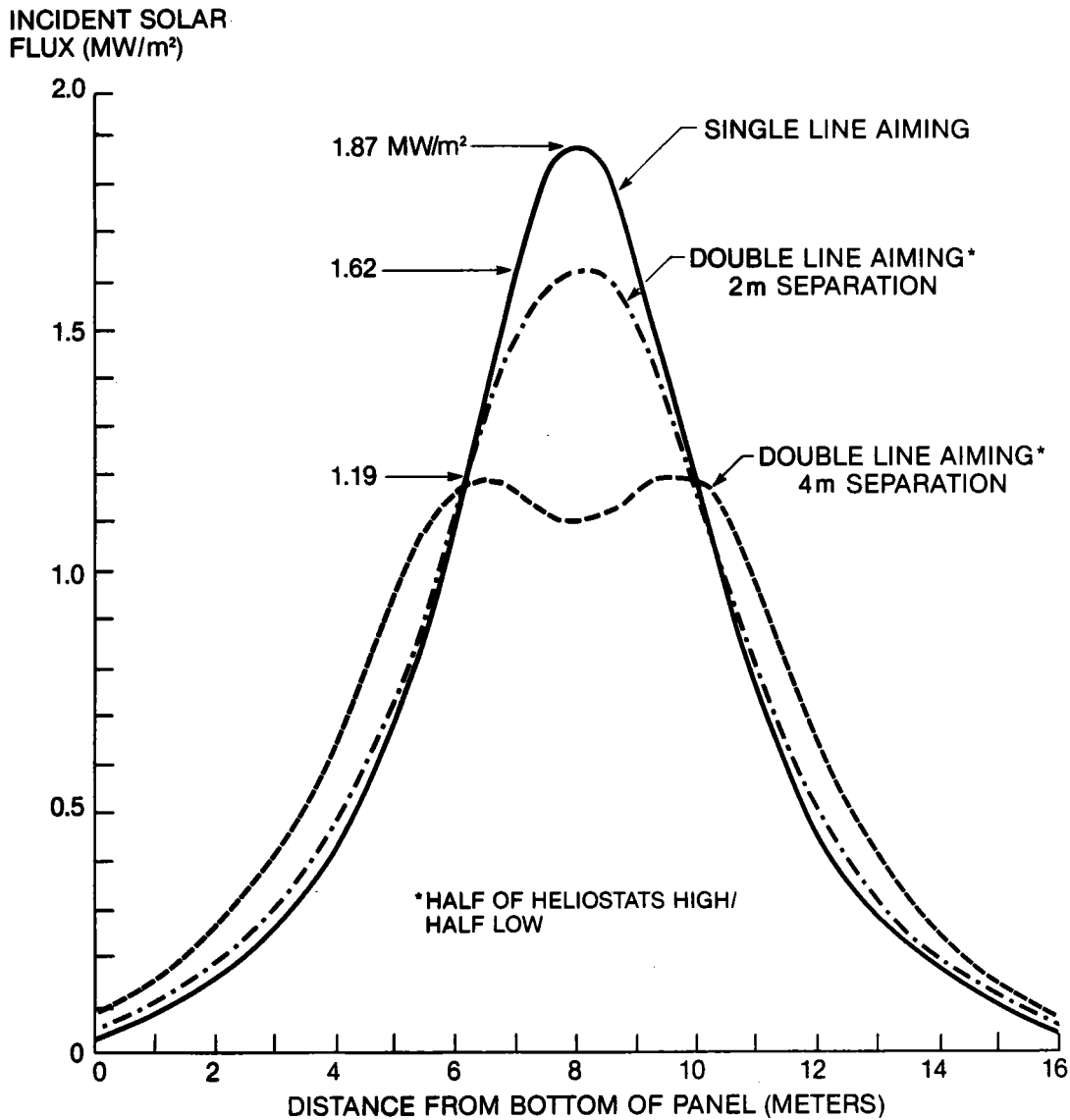


Figure 2-11. North Panel Fluxes - Alternate Aiming Strategies

When the panel's axial temperature distribution has been established, it is possible to complete the startup procedure by ramping the flux to full intensity while controlling flow to maintain the sodium outlet temperature at 593°C (1100°F) (Transient 2).

Cyclic fatigue experiments have indicated that the number of cycles to failure depends not only on the strain range and metal temperature, but also on the hold time at maximum strain. Thus the full power operating period for the receiver has been divided into classes of hold times corresponding to different types of cloud cover (Transient 3). Analysis of Barstow, California, insolation data (Ref. 2.1) has identified three types of cycles in which the

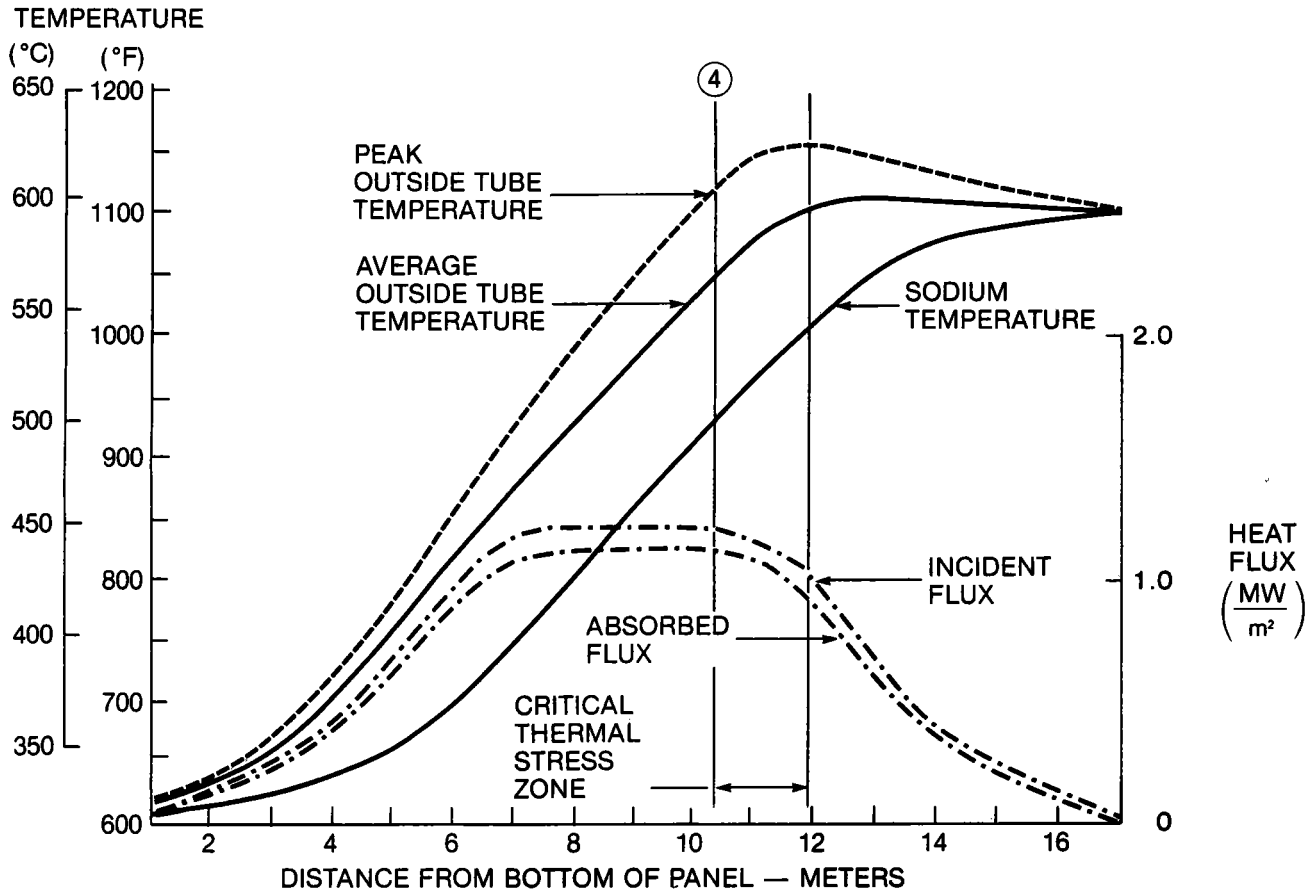
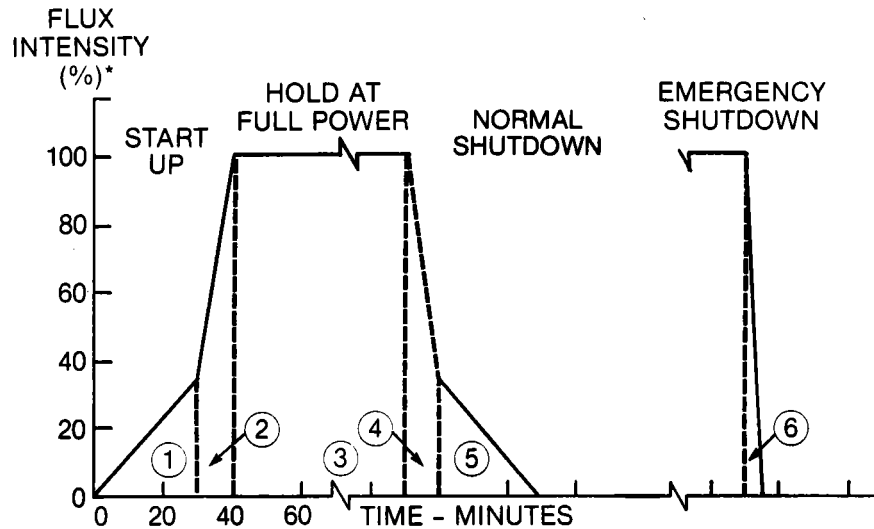


Figure 2-12. North Panel Temperatures and Fluxes - Two Point Aiming

solar intensity varies from zero to full flux and back to zero. The first class is clear days (about 225 per year) in which sunlight is available from eight to twelve hours per day; a nominal ten hour hold time has been selected as representative of these days. Half cloudy days (79 per year) either start clear and change to total or partial cloud cover around noon, or start cloudy and clear up around noon; a hold time of five hours has been assigned to the clear part of these days. There are also partly cloudy days when the sun is available for periods of roughly one hour, and the analysis of Barstow data indicates that there are roughly 279 of these periods per year. There are also numerous shorter duration flux variations, but these are either too short to operate the plant, or do not involve large variations in flux and so will probably not have a significant effect on panel life.

The plant shutdown procedure on clear and half cloudy days will be the reverse of the startup. First, the flux intensity will be reduced until the minimum sodium flow (35%) is reached (Transient 4); then, with flow held constant, the flux will be reduced to zero to bring the panel back to uniform temperature (Transient 5).



TYPE OF CYCLE	NUMBER OF CYCLES**	DURATION (MINUTES)
① RAMP TO FULL TEMPERATURE	18,000	30
② RAMP TO FULL FLUX	18,000	10
③ HOLD AT FULL FLUX		
CLEAR DAYS	7,000	600
HALF CLOUDY DAYS	2,500	300
PARTLY CLOUDY DAYS	8,500	60
④ RAMP TO MINIMUM FLOW	9,500	10
⑤ RAMP TO UNIFORM TEMPERATURE	9,500	30
⑥ EMERGENCY SHUTDOWN	8,500	5 SECONDS

*PERCENT OF FULL POWER FLUX INTENSITY
 **FOR 30 YEAR LIFE

Figure 2-13. Absorber Panel Thermal Cycle Histogram

On partly cloudy days, the shutdown transient is expected to be much more severe (Transient 6) because of the speed and random nature of the cloud shadows. Thus the flux may drop from full intensity to zero in five seconds, and, because the pumps are unable to reduce flow to zero immediately, there will be a rapid cooldown of the panel to a uniform temperature of 316°C (600°F). This transient also corresponds to the case of an emergency shutdown in which the heliostats are slewed away from the receiver.

In all of these transients, there are really only two types of thermal strains. The first type is associated with the axial temperature distribution.

These strains are primarily concentrated around the tube-header welds and points where the tubes are attached to the panel support structure. The stresses in these areas should be small, however, because the structure will be designed to accommodate axial and horizontal thermal expansion. Therefore Transients 1, 5, and 6 are not expected to limit the life of the panel.

The second type of strain is caused by the heat flux flowing through the tube walls. This heat flow sets up radial and circumferential temperature gradients in the wall which can induce high stresses and local yielding in the high flux regions of the panel. Transients 2, 3, and 4 are a constant temperature thermal stress cycle which will be repeated frequently and is a potential life-limiting process. This is the type of cycle evaluated in the analysis described below.

2.5.3 THERMAL STRESS ANALYSIS

This analysis was performed using two General Electric in-house programs: THERMAL, a generalized finite element conduction heat transfer program, and FINITE, a two-dimensional finite element algorithm for plane stress, plane strain, and axisymmetric structures. Figure 2-14 shows the division of a panel tube cross section into 384 elements for analysis. Since a line passing through the tube center and parallel to the solar rays forms an axis of symmetry, it was only necessary to analyze one side of the tube.

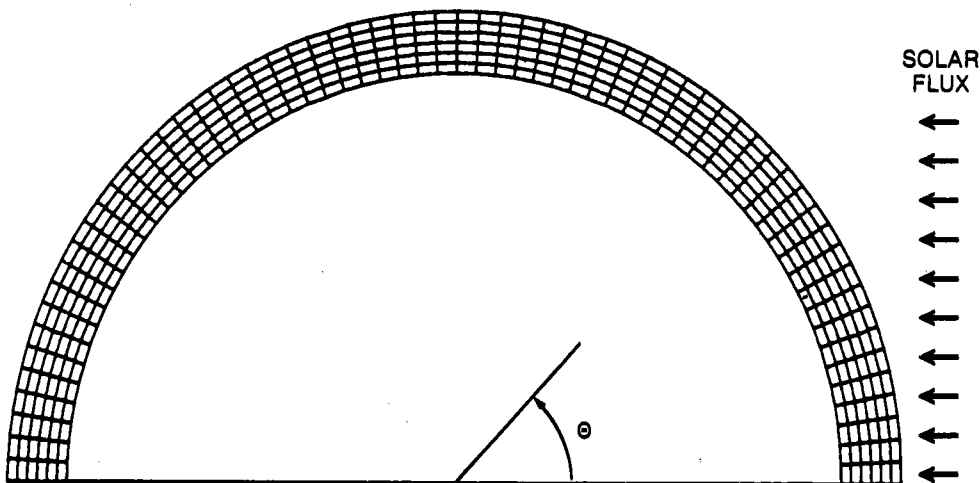


Figure 2-14. Finite Element Model for Thermal and Stress Analysis

Heat flux on the front surface of the tube was assumed to vary according to equation (1):

$$q'' = \begin{cases} q''_0 \cos \theta & (0 \leq \theta \leq 90^\circ) \\ 0 & (90^\circ < \theta \leq 180^\circ) \end{cases} \quad (1a)$$

$$(1b)$$

where:

q'' = local absorbed heat flux on curved tube surface

q''_0 = planar absorbed heat flux from Figures 2-9, 2-10, and 2-12

θ = angle from axis of symmetry (Figure 2-14).

Equation (1b) represents the insulation on the back side of the tube.

The thermal conductivity of the tube material (Incoloy 800) varies from 17 to 22 W/m-°K (10 to 13 Btu/hr-ft-°F) in the range of temperatures encountered (Figure 15), and this variation has been accounted for in the calculations.

Figure 2-16 shows a temperature plot from the two-dimensional thermal analysis of Case 4. The sharpest temperature gradients occur in the region of the tube crown (right-hand side of diagram) where the outside and inside metal temperatures are 624°C (1155°F) and 528°C (982°F) respectively. These temperatures are listed in Table 2-3 for all four cases considered here. The input data shown in Table 2-3 were derived from Figures 2-10, 2-11, and 2-13.

These temperature distributions were used as inputs to the two-dimensional analysis of thermal strains. Since the tube is a long cylinder assumed to expand freely in the axial direction, a generalized plane strain model was assumed. The mechanical properties of Incoloy 800 were allowed to vary with temperature, as shown in Figure 2-15. The peak total strain was found to occur at the crown of the tube; the strains at this location are listed in Table 2-3 for all four cases considered.

2.6 DESIGN CRITERIA

Thus in 30 years of service, calculations indicate that the north absorber panels will experience the strains listed in Table 2-3 in the cyclic pattern of hold times described by Transients 2, 3, and 4 of Figure 2-13. Incoloy 800 has been selected for the panel tubing. To assess whether this material will survive in this service, it is necessary to define a design failure criterion based upon the fatigue data available for Incoloy 800.

This effort has two steps:

1. Correlate the fatigue data using curve fitting with semi-theoretical relations.
2. Apply a factor of safety to the correlating equations to define a design failure criterion.

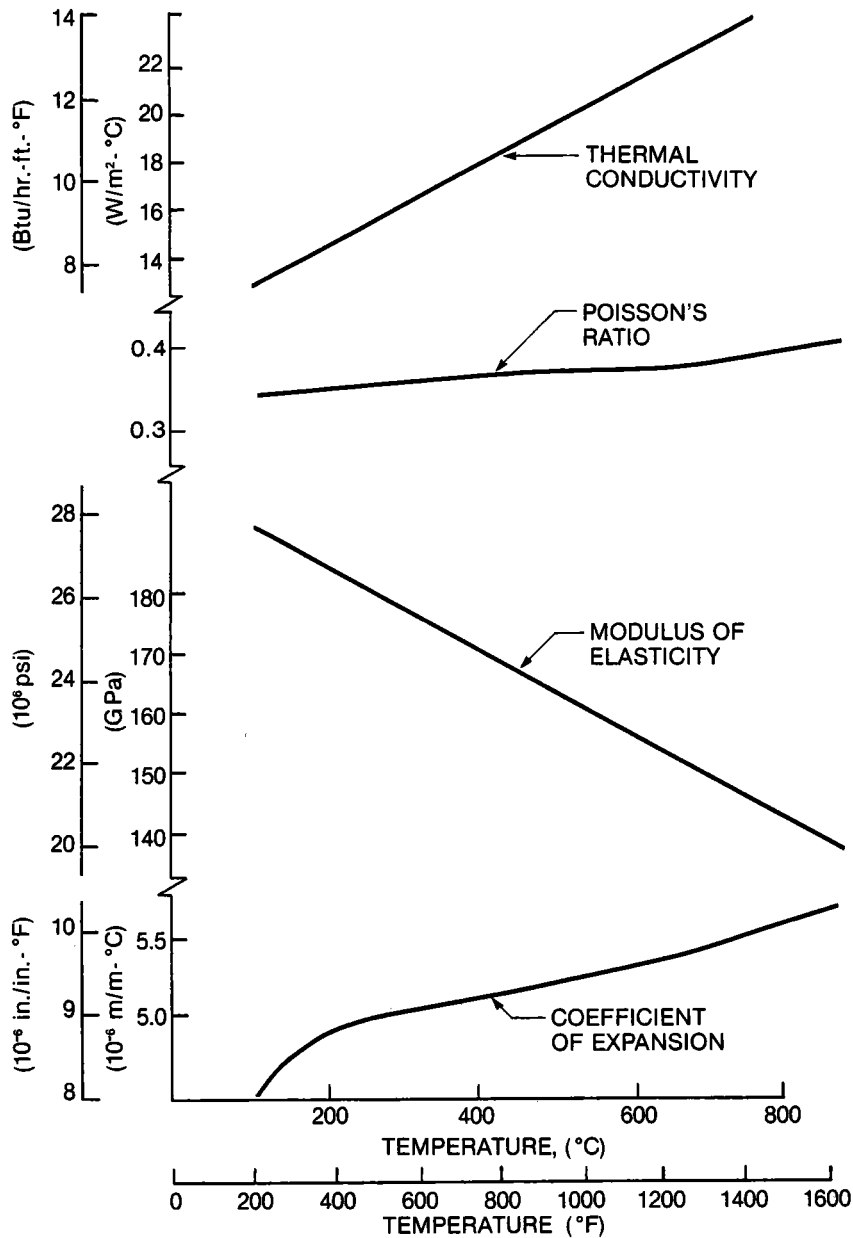
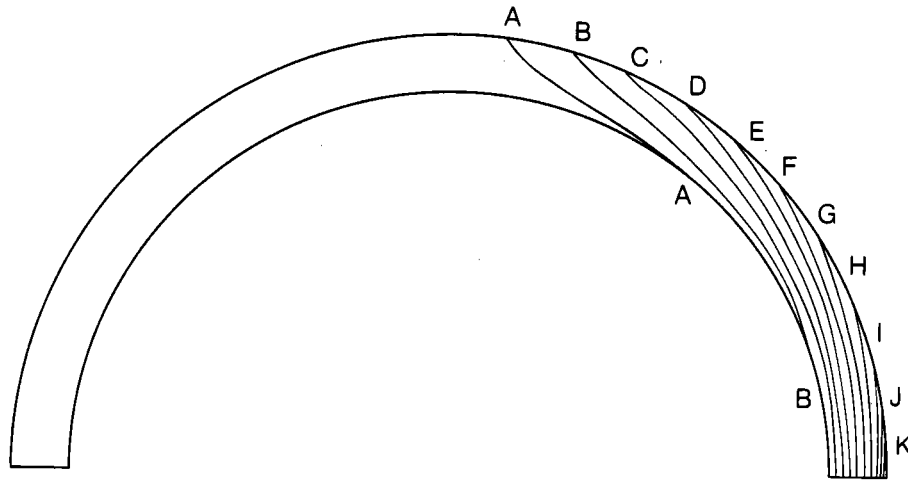


Figure 2-15. Thermal and Mechanical Properties of Incoloy 800

Cyclic strain fatigue resistance has been shown to decrease with increasing temperature and decreasing strain rate. Since Figure 2-13 shows panel cycles with hold times as long as ten hours, it is necessary to use correlating equations which predict the cycles to failure as a function of strain range, temperature, and hold time. The predictive methodology selected was to use the frequency modified Coffin-Manson equation (2) and the frequency modified Basquin equation (3) (Ref. 2.2).

$$\Delta \epsilon_p = C_2 (N_f \nu^{k-1})^{-\beta} \quad (2)$$



TEMPERATURE	
	(°F) (°C)
A =	960 516
B =	980 527
C =	1000 538
D =	1020 549
E =	1040 560
F =	1060 571
G =	1080 582
H =	1100 593
I =	1120 604
J =	1140 616
K =	1150 621

Figure 2-16. Temperature Profile - Case 4

$$\Delta\epsilon_e = A' N_f^{-\beta'} \nu^{K'_1} \quad (3)$$

where:

$\Delta\epsilon_p$ = plastic strain range

$\Delta\epsilon_e$ = elastic strain range

N_f = cycles to failure

ν = frequency (see definition Figure 2-17)

The empirical coefficients C_2 , A' , K , K'_1 , β , and β' were determined by curve fitting the Incoloy 800 fatigue data compiled by Majumdar (Ref. 2.3).

Equations (2) and (3) indicate that the data for a single frequency should fall on straight lines when plotted on log-log paper, and that the slope of the lines are the exponents of N_f . Figure 2-18 gives an example of this for zero hold time data and a temperature of 593°C (1100°F), showing the derived values for β and β' .

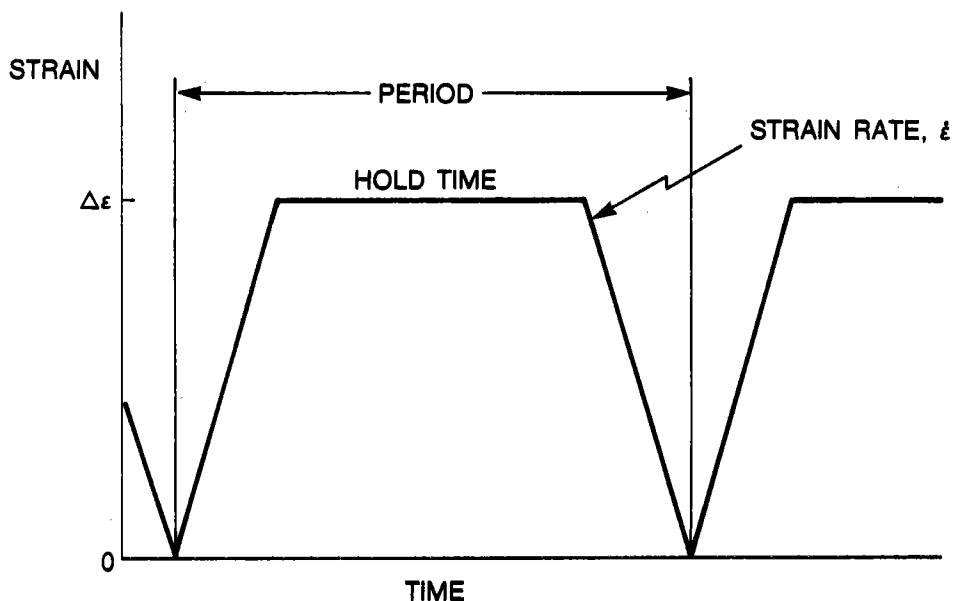
The exponent of ν can be determined by rewriting equations (2) and (3) as

Table 2-3
RESULTS OF THERMAL STRESS ANALYSIS

	Case Number			
	1	2	3	4
Input Data:				
Absorbed Heat Flux* - MW/m ²	1.75	1.75	1.50	1.10
Sodium Temperature - °C (°F)	323 (613)	460 (860)	510 (950)	504 (940)
Sodium Heat Transfer Coefficient - kW/m ² - °K (Btu/hr-ft ² - °F)	44.3 (7800)	50.5 (8900)	49.4 (8700)	49.4 (8700)
Output:				
Outside Tube Temperature [†] - °C (°F)	518 (965)	650 (1203)	673 (1244)	624 (1155)
Inside Tube Temperature [†] - °C (°F)	364 (688)	496 (925)	542 (1007)	528 (982)
Total Strain Range - m/m	2.54×10^{-3}	2.56×10^{-3}	2.21×10^{-3}	1.60×10^{-3}

* q_0'' in Equation (1a)

[†] Measured along a radius passing through the crown of the tube



$$\text{PERIOD} = \text{HOLD TIME} + 2\Delta\epsilon/\dot{\epsilon}$$

$$\text{FREQUENCY} = \nu = 1/\text{PERIOD}$$

Figure 2-17. Definition of Frequency

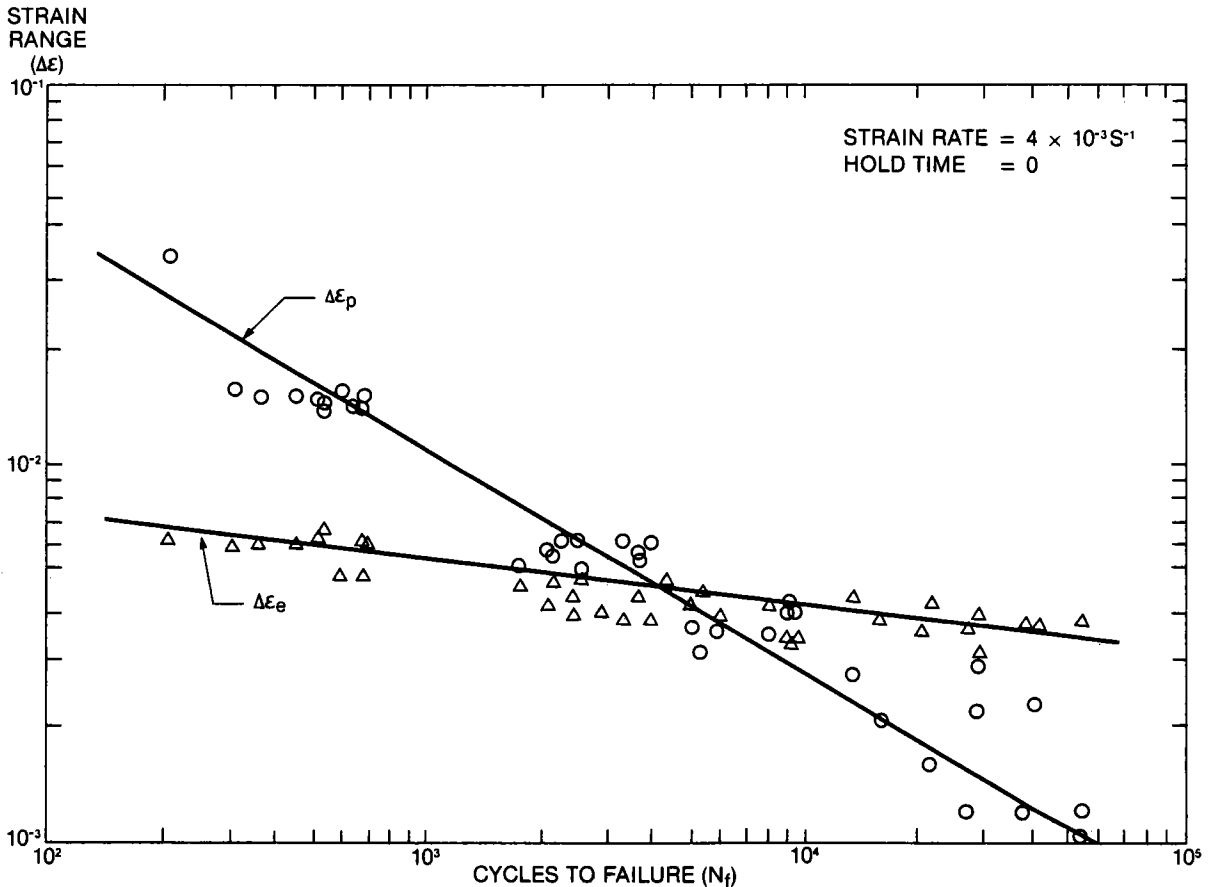


Figure 2-18. Curve Fit of Data at 593°C (1100°F) to Determine Constants β and β' for Case of Zero Hold Time (Constant Frequency) (Data from Ref. 2.3)

$$(\Delta\epsilon_p) N_f^\beta = C_2 (\nu^{k-1})^\beta \quad (4)$$

$$(\Delta\epsilon_e) N_f^{\beta'} = A' \nu^{K_1'} \quad (5)$$

and noting that these form functions of ν which are also straight lines on a log-log plot. The fatigue data (Ref. 2.3) were plotted in this form, and the exponents K and K_1' were determined as shown in Figure 2-19 for 593°C (1100°F). This procedure was carried out at several temperatures covering the range seen in Cases 1 through 4, and the results are summarized in Table 2-4.

Finally, the constants C_2 and A' were evaluated by selecting particular data points that the equations must intercept. The overall result of this curve fitting is compared with the 593°C (1100°F) data in Figure 2-20.

The frequency modified fatigue equations with empirically determined constants provide a means of extrapolating fatigue behavior of Incoloy 800 to longer hold times than those covered by the data. Because of the scatter in these data, however, correlating equations are not suitable for direct use in

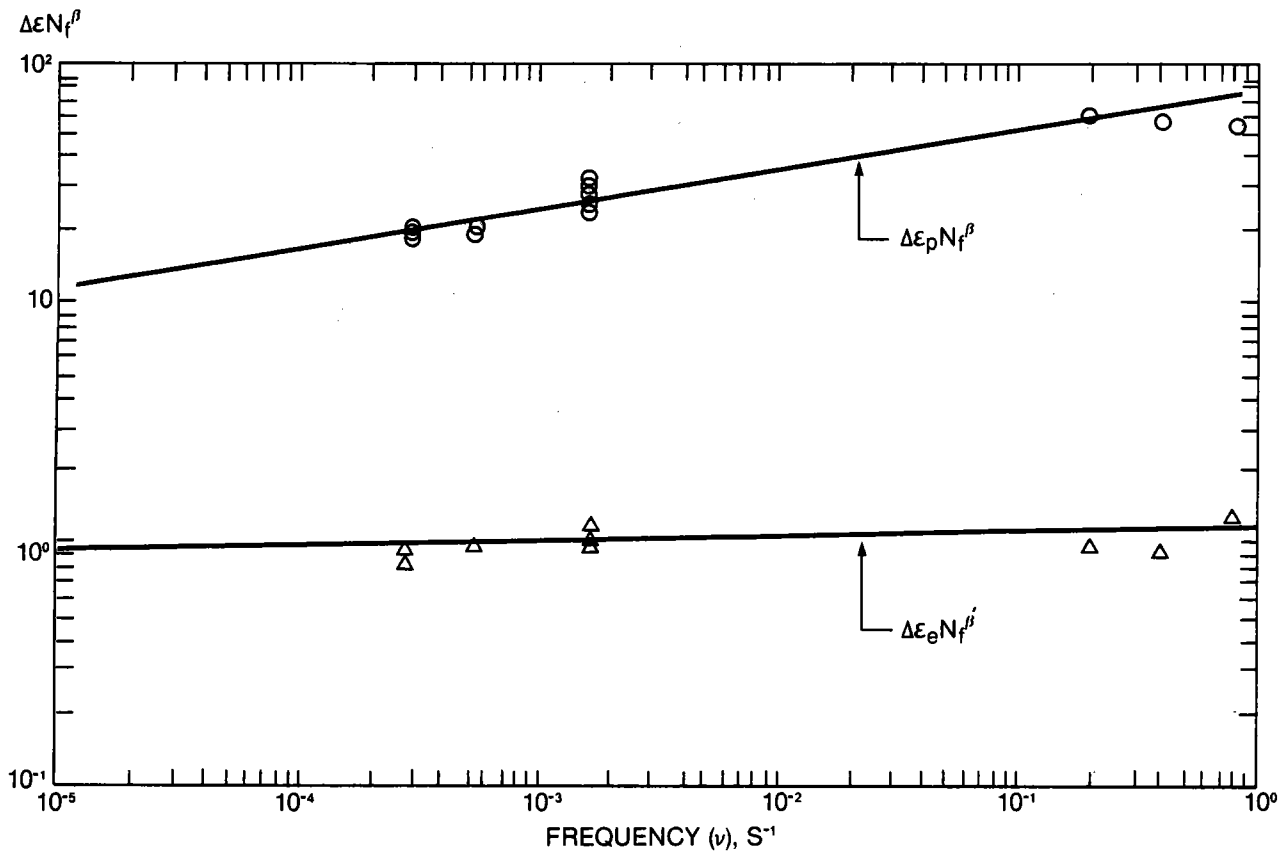


Figure 2-19. Curve Fit of Data at 593°C (1100°F) to Determine Frequency Exponents (K and K'_1) (Data from Ref. 2.3)

Table 2-4

CONSTANTS FOR FREQUENCY MODIFIED FATIGUE EQUATIONS

Temperature		β	β'	K	K'_1
°F	°C				
1000	538	0.567	0.0875	0.727	0.0200
1100	593	0.584	0.111	0.729	0.0214
1200	649	0.625	0.115	0.803	0.0686

design. Rather, a "reasonable" factor of safety must be applied which is conservative enough to provide assurance that the design will not fail, and, on the other hand, is not so conservative as to add heavy cost penalties. A number of approaches could be used including, for example, applying statistically determined "three sigma" (standard deviation) limits. The approach used here was to divide the cycles to failure determined by the correlating equations by a factor of twenty to determine the allowable cycles for design N_d . It should

2-22

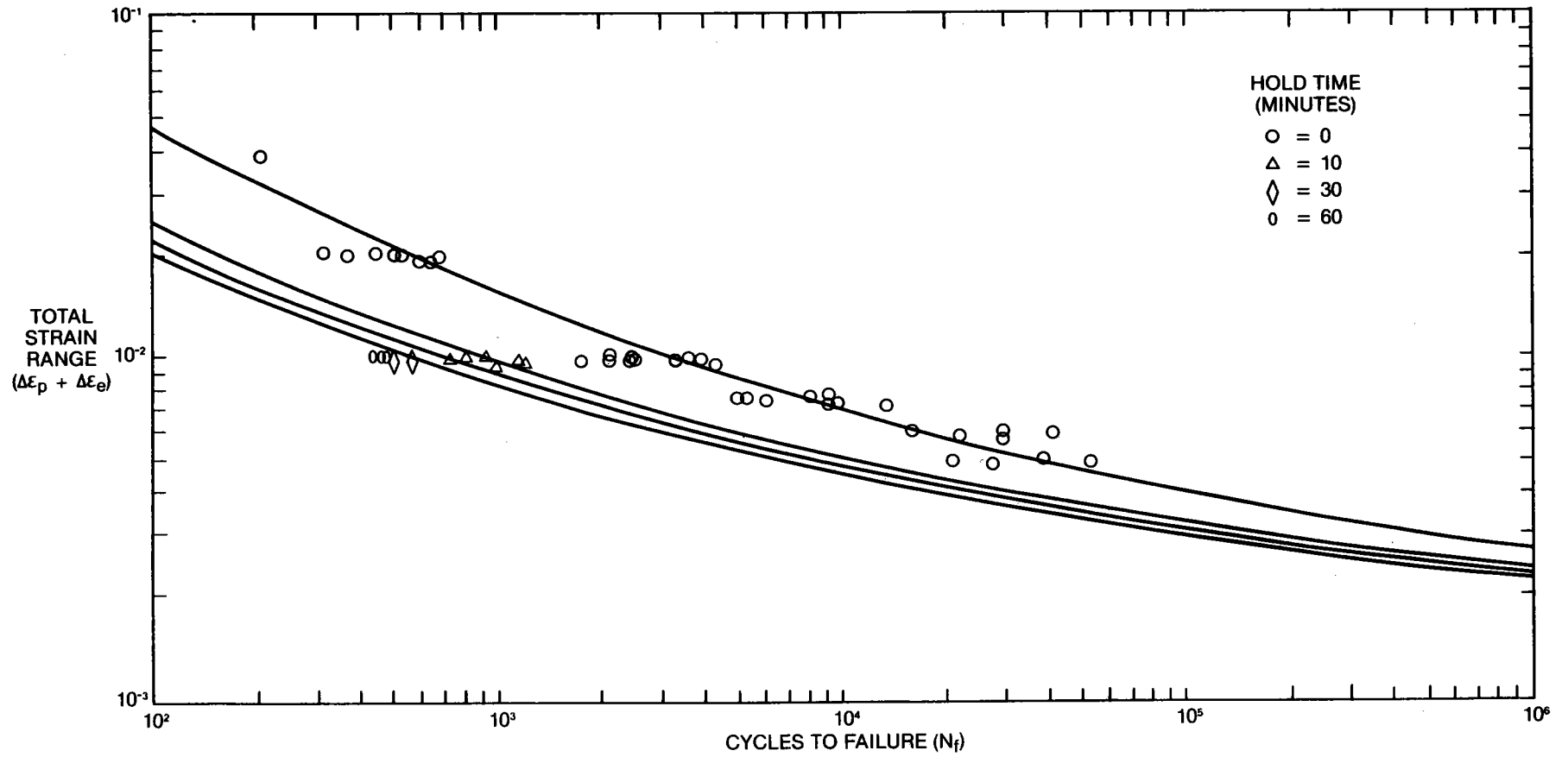


Figure 2-20. Correlation of Data for 593°C (1100°F) (Data from Ref. 2.3)

be noted that, although this is a good preliminary approach, it should not be construed as a recommended design standard for solar energy applications. Establishment of a standard would require more data and more effort in data analysis than was possible in this brief study. Such a standard is critically needed and is the subject of a current DOE-funded effort (Ref. 2.4) involving several metallurgical experts.

The preliminary design curves developed for the present comparison are shown in Figures 2-21 to 2-23 for a range of temperatures from 538°C (1000°F) to 649°C (1200°F) and hold times to ten hours.

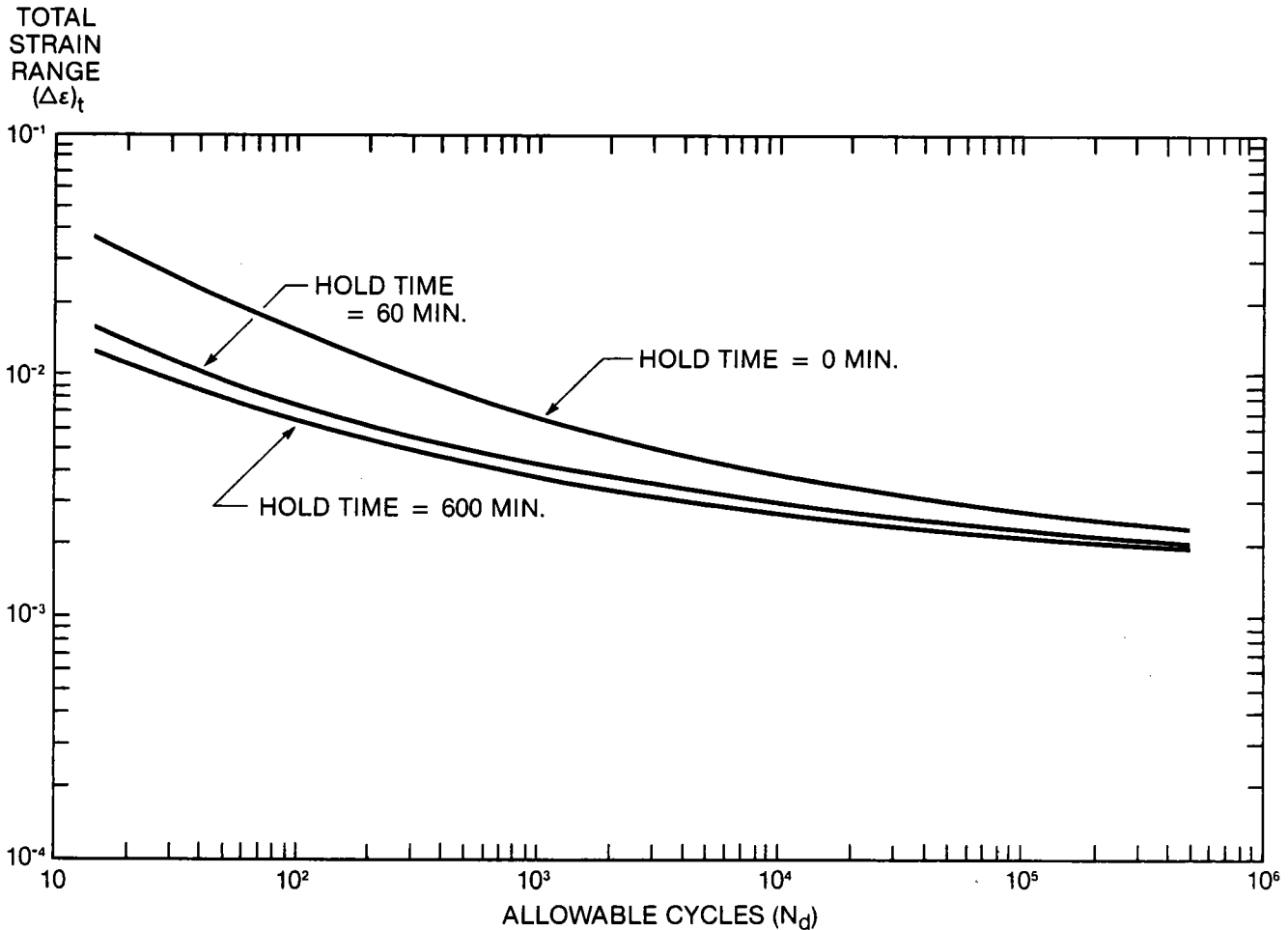


Figure 2-21. Preliminary Design Curves for 538°C (1000°F)

2.6.1 ESTIMATE OF PANEL LIFE

Table 2-5 shows the application of these curves to Cases 1 through 4. In this table "allowable cycles" represents the predicted panel life, based upon the calculated strain ranges, temperatures, hold times, and a safety factor of 20 on life. The number of "imposed cycles" is the life required by the thermal

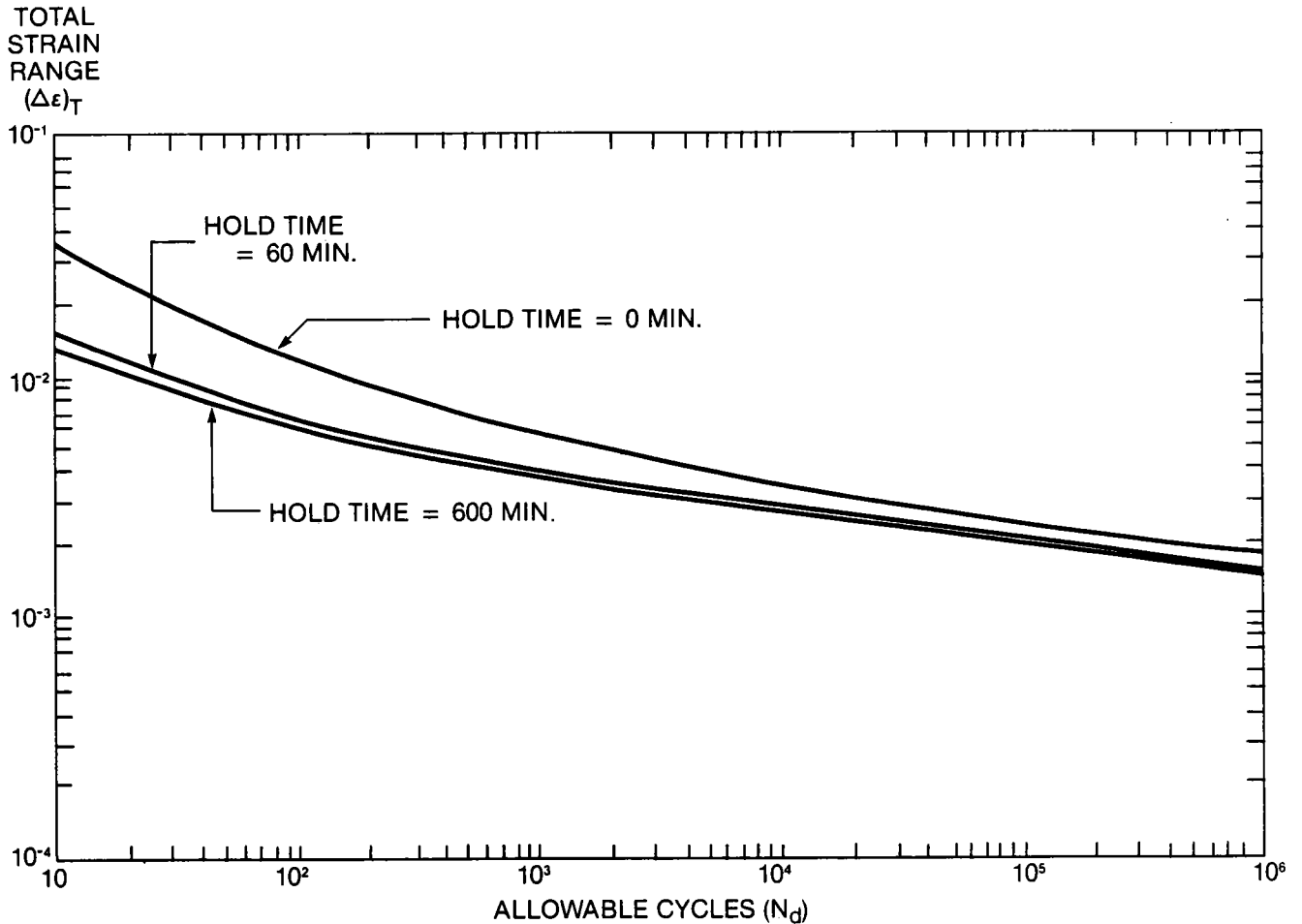


Figure 2-22. Preliminary Design Curves for 593°C (1100°F)

cycling histogram (Figure 2-13), and the "damage factor" is simply the ratio of imposed cycles to allowable cycles. The individual damage fractions for the various hold times are summed at the bottom of the table for each case. Consistent with prevailing practice, the fatigue design criterion applied to these results is that the sum of the damage fractions must be less than unity to assure a reliable panel.

Thus, the three-header panel (Case 1) is seen to have adequate design life for this application (damage factor = 0.625), while the two-header panel with aim-at-the-belt heliostat control (Cases 2 and 3) does not meet the design criteria for thirty-year life, and will need replacement several times during the power plant lifetime.

However, if multipoint heliostat aiming with lower peak fluxes is employed, then the two-header panel (Case 4) will have more than adequate life.

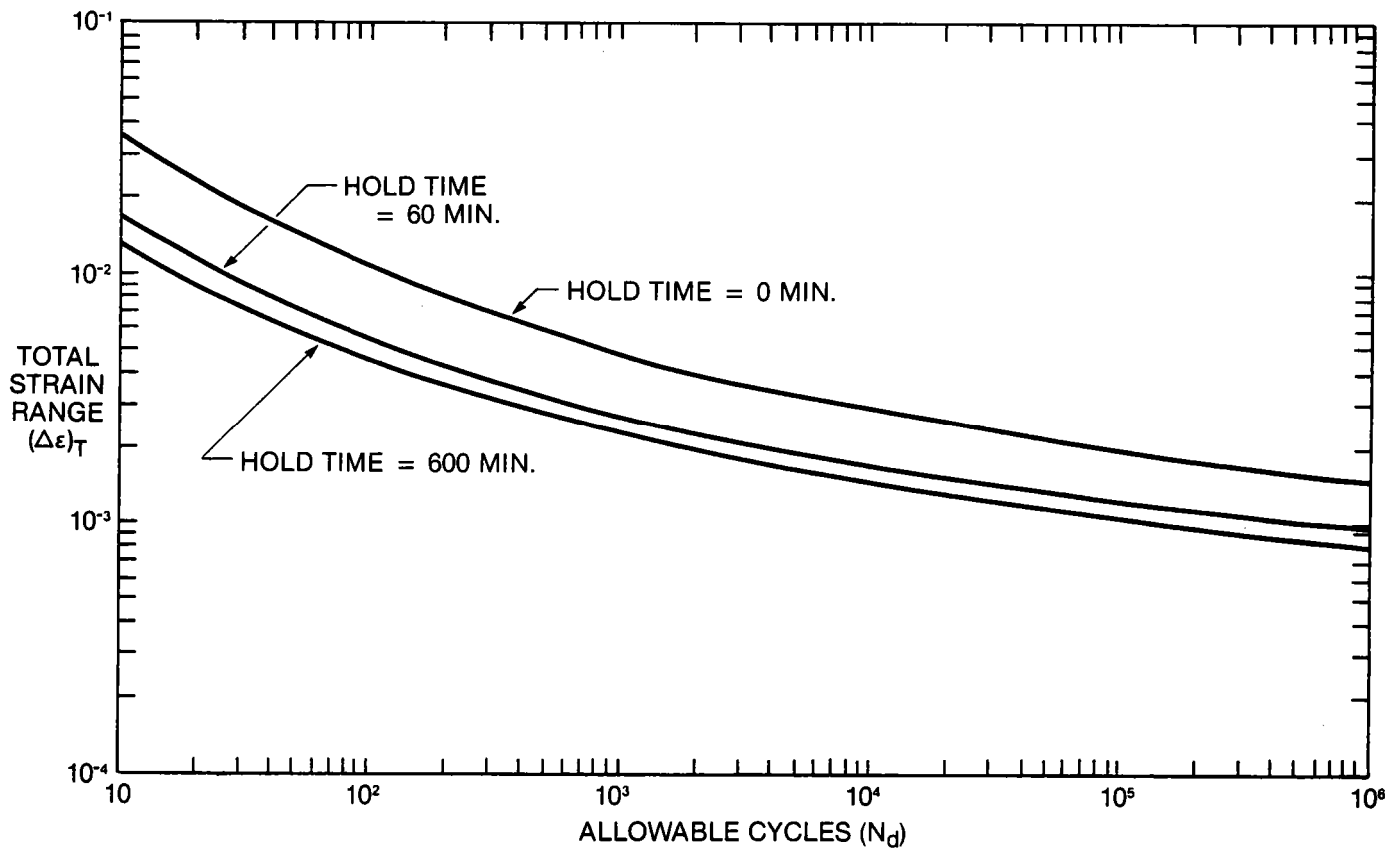


Figure 2-23. Preliminary Design Curves for 649°C (1200°F)

Table 2-5
FATIGUE DAMAGE RESULTS

	Case 1		Case 2		Case 3		Case 4	
<u>10 Hour Hold Time</u>								
Imposed Cycles	7,000	-	7,000	-	7,000	-	7,000	-
Available Cycles	30,000	-	610	-	760	-	42,000	-
Damage Factor	-	.233	-	11.5	-	9.21	-	.167
<u>5 Hour Hold Time</u>								
Imposed Cycles	2,500	-	2,500	-	2,500	-	2,500	-
Available Cycles	23,000	-	760	-	960	-	85,000	-
Damage Factor	-	.109	-	3.29	-	2.60	-	.0294
<u>1 Hour Hold Time</u>								
Imposed Cycles	8,500	-	8,500	-	8,500	-	8,500	-
Available Cycles	30,000	-	1,200	-	1,600	-	150,000	-
Damage Factor	-	.283	-	7.08	-	5.31	-	.0567
Cumulative Damage Factor	-	.625	-	21.9	-	17.1	-	.253

2.6.2 GENERALIZED FATIGUE EVALUATION CHART

Fatigue evaluations of the absorber panel tubes performed thus far have been at particular points judged to be worst case conditions such as peak flux points or peak temperature points (see Section 2.5.1). This approach begs the question concerning intermediate flux and temperature conditions.

In order to satisfy all conditions, a generalized fatigue evaluation chart has been prepared and is shown in Figure 2-24. Coordinates of the chart are absorbed heat flux on the ordinate and sodium temperature on the abscissa. The dashed lines running diagonally are lines of constant tube crown temperature. These lines, determined from the tube thermal analyses, illustrate the fact that the flux must be reduced with increasing sodium temperature to maintain a constant crown temperature. When the flux is zero, the tube temperature is equal to the sodium temperature.

The heavy line on top is the locus of all combinations of flux and sodium temperature for which $\Sigma(\text{damage fractions}) = 1.0$. All points in the plane below this line meet the design criterion for the hypothesized 30 year cycles. Points above the line do not meet the criterion. Consequently, in order to perform a fatigue evaluation of a proposed design, all that is needed is to plot flux/sodium temperature on the chart for each point along the tube. If all points fall below the fatigue damage line, the design is acceptable.

The fatigue evaluation chart has been applied to three cases previously analyzed. These results are shown in Figure 2-25. Line 1 on the chart corresponds to the three header design in which the flux and temperature profiles are symmetrical about the midpoint of the receiver (Case 1, Figure 2-9). The sodium enters at low temperature where the flux is high (this is the upper end of Line 1). Moving along the tube in the direction of sodium flow, the flux falls off rapidly as the sodium temperature increases as shown by Line 1. All points on this line fall below the damage line.

Line 2 corresponds to a two-header design with a high peak flux at the center of the receiver (Case 2, Figure 2-10). In this case, the Line 2 crosses the damage line near the center of the tube. This is consistent with previous results which showed that this design did not meet the criterion. It appears from the chart that Line 2 is only "slightly" above the damage line whereas previous calculations showed that the $\Sigma(\text{damage fractions}) = 21.9$ (Table 2-5) at the peak flux point. A partial explanation is that the peak

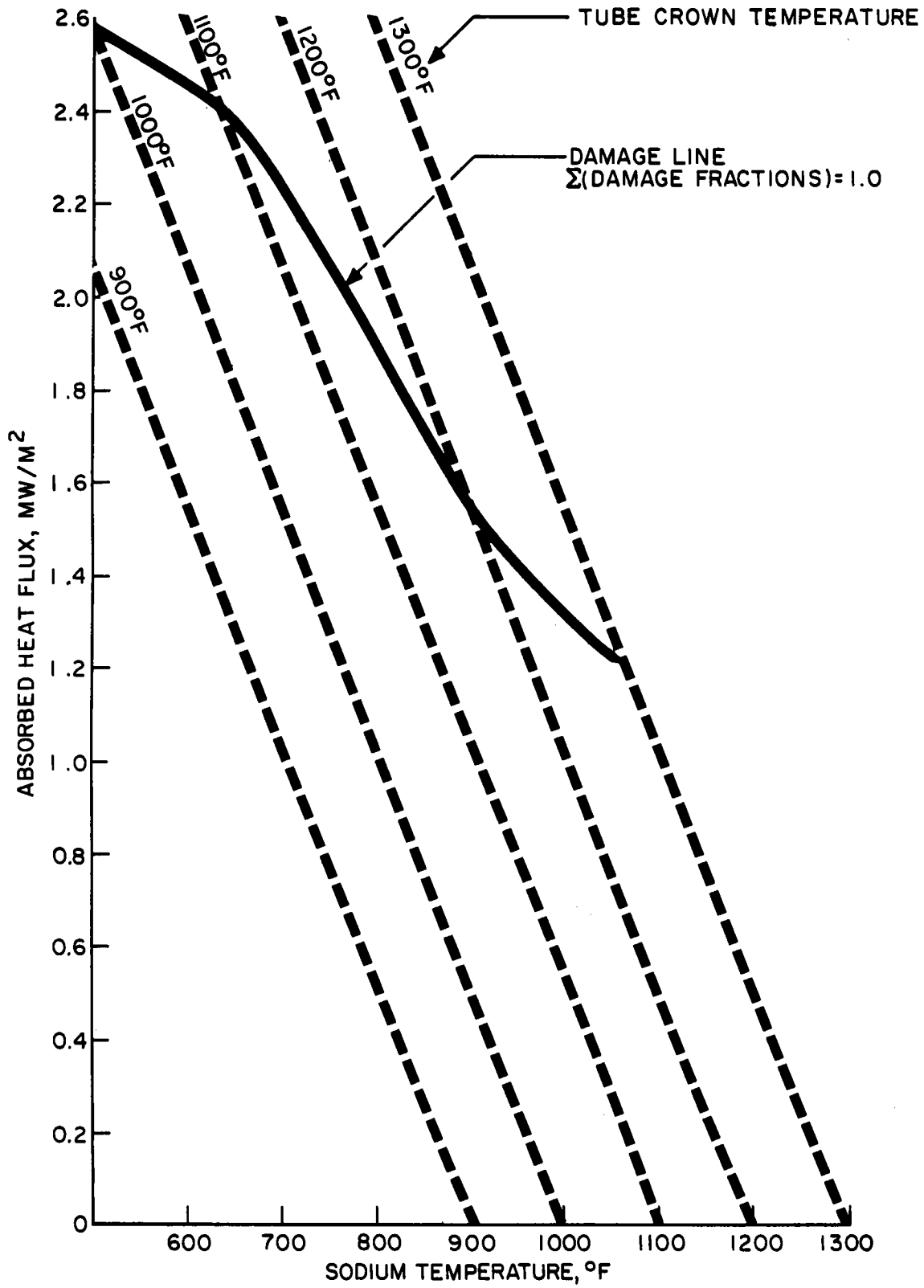


Figure 2-24. Fatigue Evaluation Chart

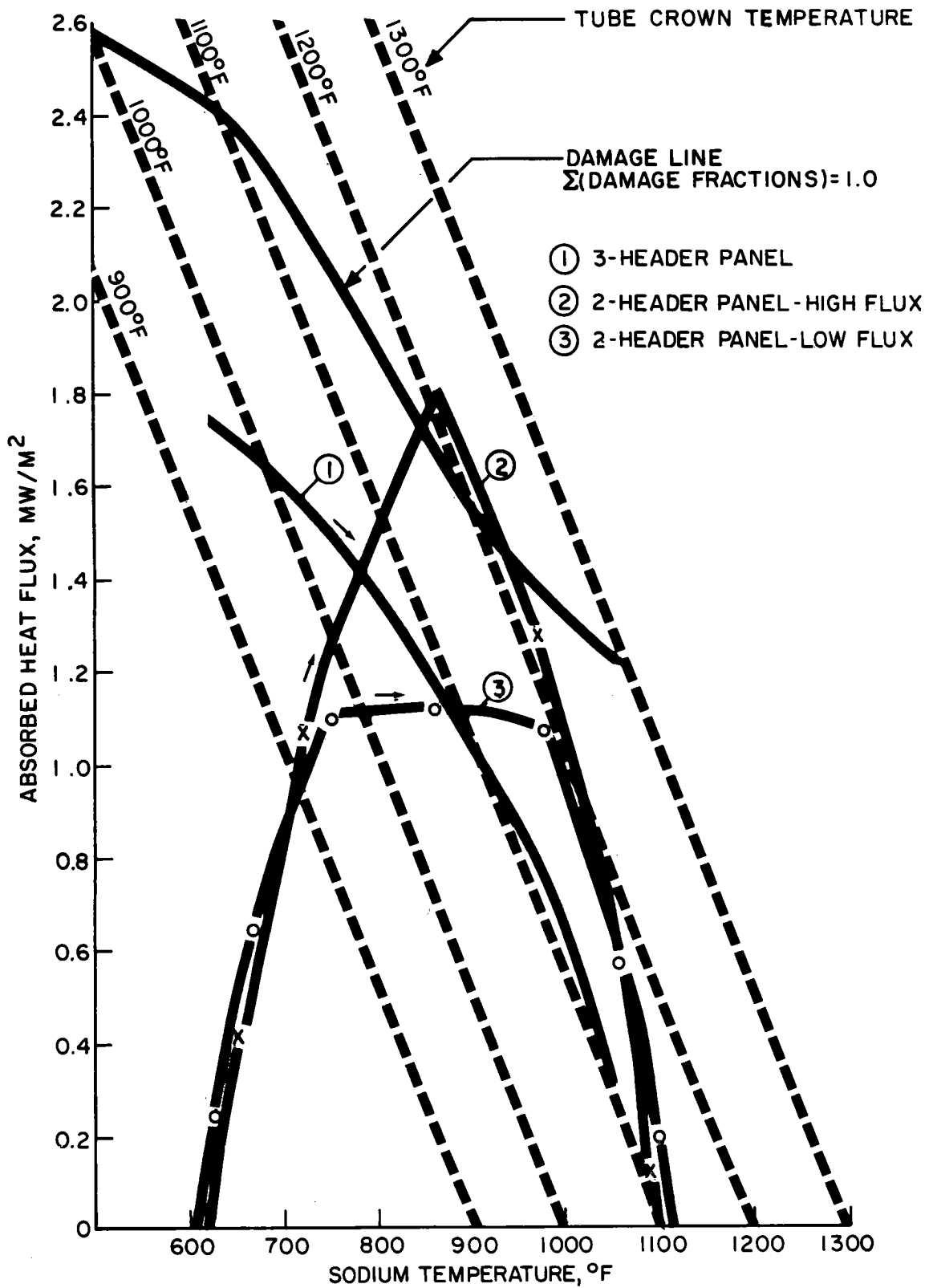


Figure 2-25. Fatigue Evaluation of Three Previously Analyzed Cases

metal temperatures used in the damage analyses were higher than those previously calculated and shown in the chart. However, more importantly, is the fact that local damage fraction sums are in no way proportional to the "distance" of a point from the damage line. This is due to the highly nonlinear dependence of allowable cycles on the flux level (strain range) and temperature.

Line 3 on the chart corresponds to a two-header design with a low, flat peak flux (Case 4, Figure 2-12). All points are below the damage line, consistent with previous results.

Finally, readers are cautioned not to interpret the phrase "generalized fatigue evaluation chart" too literally. The chart is general in terms of flux and temperature. It does not, however, apply to different tube sizes, tube materials, or to different flux cycle histograms than were used in the analysis.

2.7 CONCLUSIONS

Table 2-6 summarizes the major points of comparison between the three-header and two-header panel concepts.

Table 2-6
COMPARISON OF PANEL TYPES

Three Headers	Two Headers
<ul style="list-style-type: none"> ● Good Receiver Efficiency ● Requires an Axially Symmetrical Flux Distribution ● Possible Flow Distribution Problem Between Upper and Lower Halves ● 432 Tube-Header Welds ● Tubes Bend in High Flux Region ● Panel Halves are Clamped Together in High Flux Region ● 965 °F in High Stress Region; Meets Design Criteria for 30-Year Life at High Fluxes 	<ul style="list-style-type: none"> ● Slightly Better Receiver Efficiency ● Insensitive to Axial Flux Distribution ● Simple Flow Pattern ● 216 Welds ● Tubes are Straight ● Panel Hung from Top ● 1155 °F in High Stress Region; Not Suitable for High Flux Operation but Meets Design Criteria for 30-Year Life at Moderate Fluxes

The two-header panel was found to have superior thermal efficiency for the two flux distributions evaluated, and the two-header concept is more stable with respect to axial flux variations and sodium flow transients.

The two-header panel is a less complex structure than the three-header panel and, as a result, is likely to be less costly to manufacture and less prone to failures induced by axial expansion and contraction.

The single disadvantage of the two-header concept is that it cannot tolerate high fluxes (1.8 MW/m^2 incident). However, heliostat aiming strategies which redistribute the smaller close-in heliostat images so as to improve receiver efficiency by creating a more uniform flux pattern, result in peak fluxes of about 1.2 MW/m^2 for a 100 MW plant, and the two-header panel can easily survive this level of flux for 30 years of service.

Thus, this comparison supports the conclusion that the two-header panel concept is superior to the three-header panel for this application.

SECTION 3

RECEIVER FLOW CONTROL SYSTEM COST REDUCTION

3.1 INTRODUCTION

The 100 MW_e commercial plant conceptual design developed during Phase I had a single electromagnetic (EM) pump for sodium flow control on each of the 24 receiver panels. Each pump represents approximately \$191,000 (excluding distributables) of the plant cost. The total flow control equipment cost of \$4.6 million presents a significant opportunity for reducing plant costs.

Several technical approaches for reducing the flow control system were considered. The impact on overall plant costs and a discussion of the possible elimination of EM pumps in favor of throttle valves for flow control are discussed.

3.2 APPROACH

The approach taken was cost reduction by reducing the number of EM pumps in the receiver subsystem. Several concepts were considered as indicated below:

- Increasing the Panel Size

Increasing the panel size would reduce the number of panels and thus the number of pumps. To achieve a meaningful reduction in the number of pumps a panel size increase by a factor of two or more would be required. This would result in higher transverse panel temperature gradients due to the transverse flux distribution. These gradients would tend to warp the panels due to differential axial tube expansion. The larger panel concept would also increase problems in the receiver panel edge area due to the increase in the edge tube surface exposure. This concept was dropped for these reasons.

- Variable Panel Size

A variation on the initial concept involves reducing the number of panels by placing larger panels in the lower flux areas (south side panels) where the flux intensity is lower. This concept was discarded primarily because manufacturing different panel sizes would increase initial costs and also require additional spare panels to make each size available for replacement, offsetting any cost savings.

- Panel Grouping

This concept involves grouping of two or more panels on a single EM pump and is illustrated in Figure 3-1.

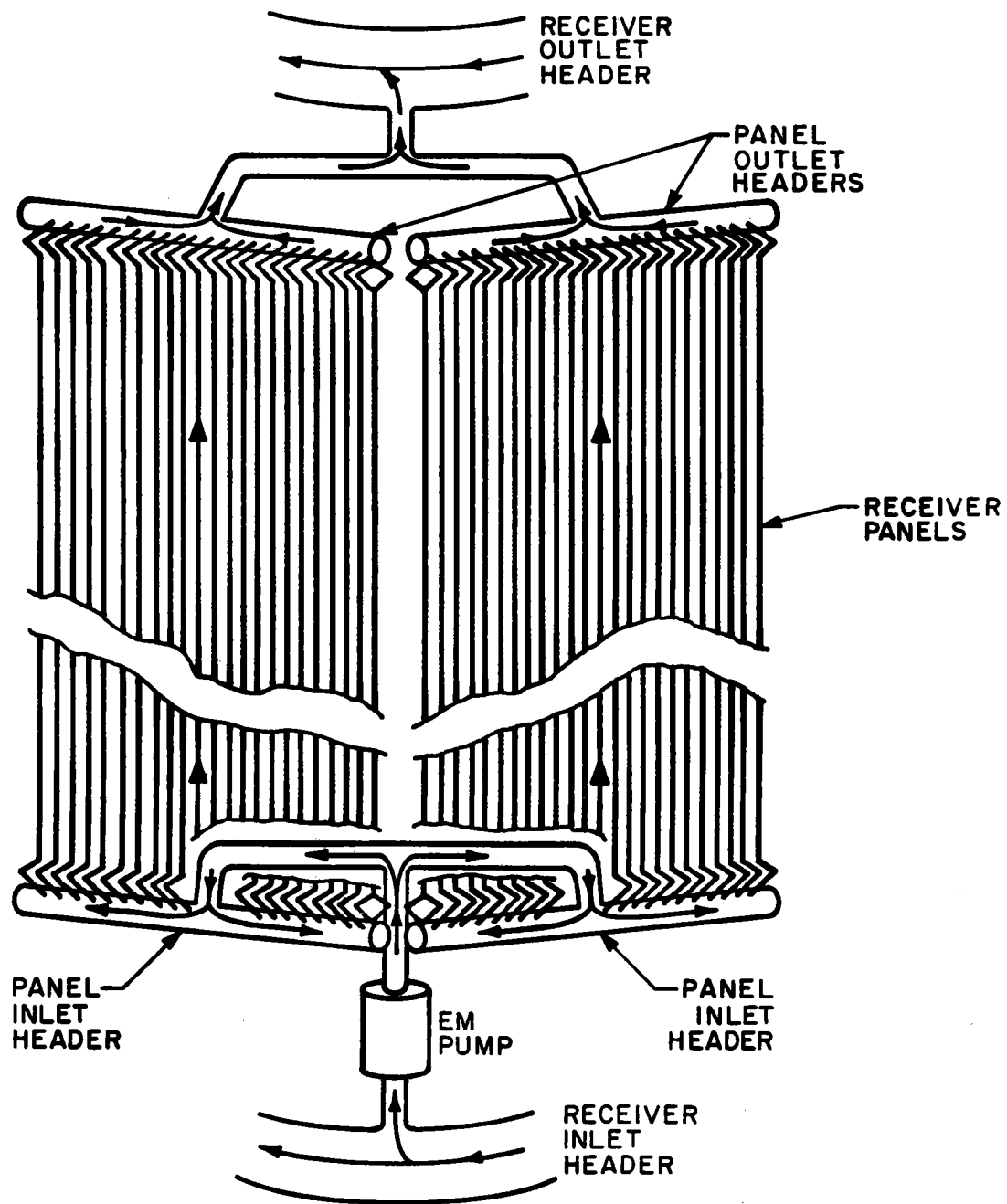


Figure 3-1. Panel Grouping Concept

This approach was selected as the most practical means of reducing the number of EM pumps. The only major concern related to this approach is that the outlet temperature of each panel cannot easily be controlled to exactly 1100°F, as was the case for one pump per panel. However, the average outlet temperature of the grouped panels can be controlled to 1100°F.

The different panel outlet temperatures result in a ΔT concern at the joint where the two panel flows merge. This concern will limit the extent of grouping as will be discussed in later sections.

3.3 PANEL GROUPING ANALYSIS

Following selection of the panel grouping approach, an analysis was undertaken to determine the minimum number of pumps required. Two criteria relating to outlet panel temperature differences and receiver efficiency were established to evaluate the acceptability of various configurations. Each criteria is discussed below:

3.3.1 PANEL OUTLET ΔT LIMIT

In order to control the pump flow to produce the required average 1100°F outlet temperature, the outlets from each panel must be combined to a common header where the mixed temperature can be determined. Possible configurations for two and three panel groupings are shown in Figure 3-2. Because the panel hydraulics are the same,

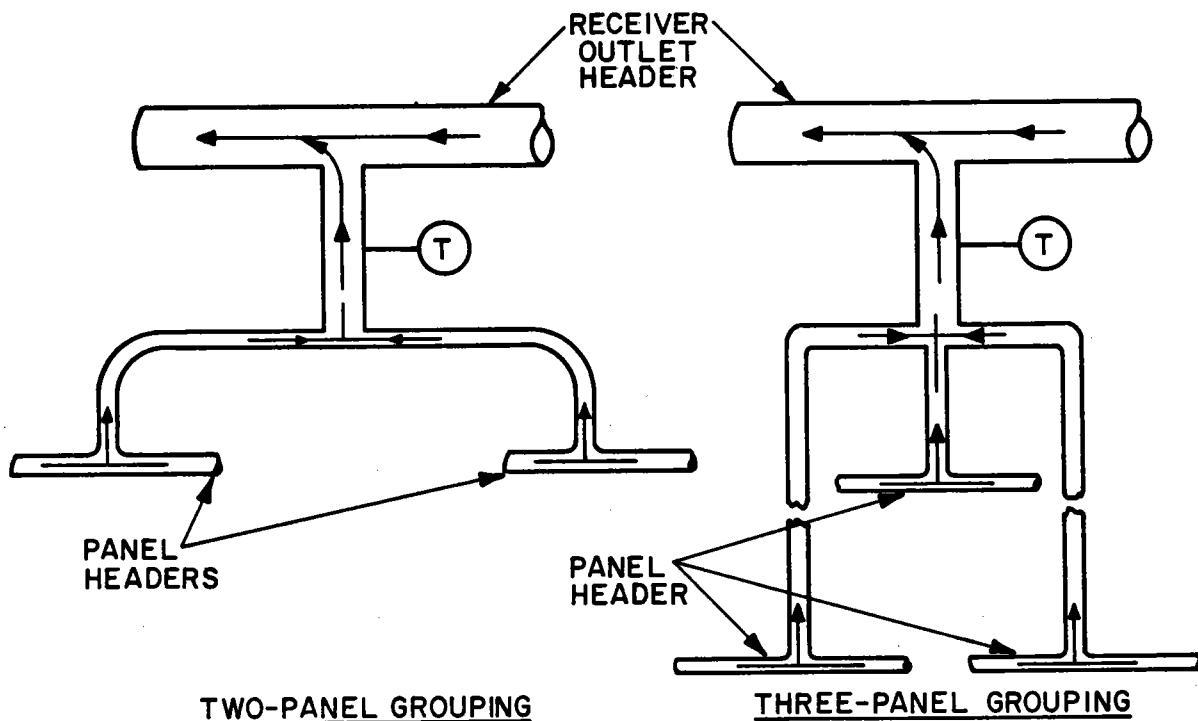


Figure 3-2. Grouped Panel Header Configurations

the same flow is produced through each panel of a group. Since the panel fluxes are different, the panel outlet temperatures will be different. The combining of the panel outlet flows at the common header results in stresses at the joint due to the temperature difference (ΔT). This ΔT must be limited to avoid overstress or fatigue failure of the joint.

Since detailed analysis of the joints were beyond the scope of this study, two conservative criteria were selected to determine the allowable panel outlet temperature difference:

- The ΔT should produce strains in the range satisfactory for one million cycles ($< 1.5 \times 10^{-4}$ in/in)
- The ΔT should produce stresses no greater than yield ($< 30,000$ psi).

The resultant allowable ΔT was calculated to be ~ 58 C (105 F). (It should be noted that detailed stress analysis and/or design features could significantly increase the allowable ΔT).

3.3.2 RECEIVER EFFICIENCY DEGRADATION

The overall efficiency of the receiver is significantly affected by the receiver temperature distribution. Since the loss relationships are not linear with temperature, raising and lowering adjacent panel temperatures such that the average temperature is the same will not necessarily result in the same overall efficiency as maintaining uniform panel outlet temperatures. Since each percentage point reduction in receiver efficiency results in added solar plant costs of $\sim \$550,000$, little receiver efficiency loss can be tolerated. Any loss must be traded off against the savings associated with EM pump reductions.

3.3.3 GROUPING THERMAL ANALYSIS

To analyze various configurations, the receiver loss computer program developed in the Phase I program was modified to allow grouping of the panels. A listing of the modified program, PANELGR2, is shown in Appendix A.

The design point, noon summer solstice, heat flux was utilized in the analysis. Consideration of off-design point fluxes resulted in the conclusion that the flux gradients are no more severe than those produced at the design point. Four baseline cases were run. The first case used no grouping. The second grouped the panels in pairs, the third in groups of three and the fourth in groups of four. Table 3-1 summarizes the critical results. Only twelve panels are shown since symmetry yields identical results for the other half of the receiver. Figure 3-3 shows the panel numbering sequence.

Table 3-1
PANEL GROUPING ANALYSIS RESULTS

CASE	ITEM	PANEL NUMBER											
		1	2	3	4	5	6	7	8	9	10	11	12
I (NO GROUPING)	EFFICIENCY - 90.33%												
II (2 PANEL GROUPING)	GROUP NUMBER	I	I	II	II	III	III	IV	IV	V	V	VI	VI
	MAX. GROUP ΔT ($^{\circ}F$)	22		23		26		29		34		38	
	EFFICIENCY - 90.33%												
III (3 PANEL GROUPING)	GROUP NUMBER	I	I	I	II	II	II	III	III	III	IV	IV	IV
	MAX. GROUP ΔT ($^{\circ}F$)		43			51			60			74	
	EFFICIENCY - 90.33%												
IV (4 PANEL GROUPING)	GROUP NUMBER	I	I	I	I	II	II	II	II	III	III	III	III
	MAX. GROUP ΔT ($^{\circ}F$)			68				88				115	
	EFFICIENCY - 90.33%												

The results in Table 3-1 indicate that the two, three and four panel groupings have no affect on receiver efficiency and thus are acceptable from that standpoint. However, the header ΔT criteria does require consideration.

All the panel header to panel header ΔT 's for the two-panel grouping are less than the criteria set forth. The three panel grouping also yielded acceptable results. The four panel grouping can be seen to exceed the ΔT limit for the third group of four. Therefore, three panel groupings were selected as the reference approach. Appendix B shows the detailed output from PANELGR2 for the selected three panel grouping.

This final configuration, shown in Figure 3-4, will require a total of 8 EM pumps as opposed to the 24 originally specified for the commercial plant.

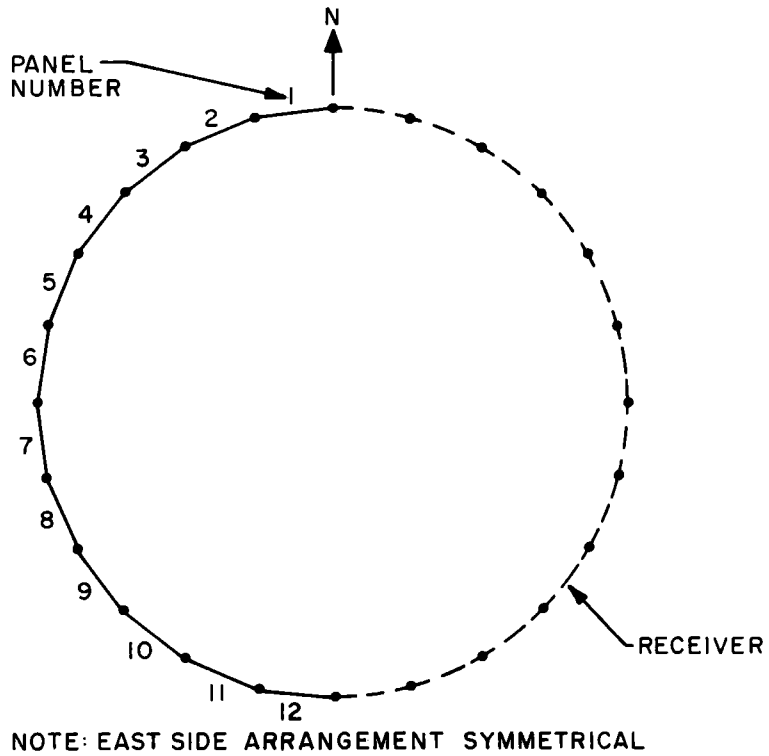


Figure 3-3. Panel Numbering Sequence

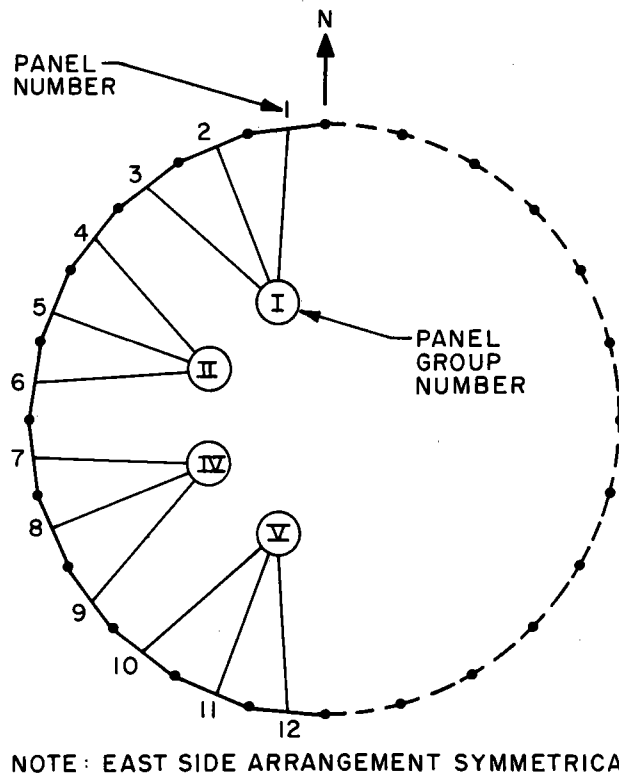


Figure 3-4. Final Grouping Configuration

3.3.4 GROUPING COST IMPACT

The EM pumps were estimated to cost \$191,000 each (excluding distributables) during the ACR Phase I program. The reduction in pumps from 24 to 8 will reduce direct costs from \$4.6 million to \$1.5 million for a net savings of \$3.1 million. Although the pump flow rating will increase for the new eight pump configuration, the cost per pump does not significantly change over this range. For estimating purposes the \$191,000 per pump is considered adequate.

The total distributables attributable to the 24 pump design was \$2 million. Reducing to an 8 pump design will save \$1.4 million of this total for a resulting distributable cost of \$.6 million.

Thus, the total receiver flow control cost, including distributables, will be \$2.1 million as opposed to the previous design which cost \$6.6 million. The \$4.5 million savings represents a 2.1% overall plant cost savings.

3.4 EM PUMPS VS. THROTTLE VALVES

Another avenue of approach for reducing receiver flow control equipment costs is the use of throttle valves rather than EM pumps. That concept was dropped from further consideration since the potential savings now available are very small, and there is a proven high level of EM pump reliability.

Table 3-2 shows a cost comparison of throttle valves versus EM pumps for the eight group flow control scheme discussed earlier. Only direct costs are compared.

Table 3-2
THROTTLE VALVE VERSUS EM PUMP
DIRECT COSTS

Group Number (see Fig. 4)	Number of Panels	Total Number of Valves		Valve Size	Valve Cost	EM Pump Cost
		Throttle	Stop			
I	3	4	6	10"	\$310,000	
II	3	4	6	8"	170,000	
III	3	4	6	8"	170,000	
IV	3	4	6	6"	\$.79 million	\$1.5 million

The analysis assumed that a throttle valve manifold will be utilized. The manifold would consist of two throttle valves in parallel, an upstream stop valve for each throttle valve and a single downstream stop valve. Figure 3-5 illustrates the configuration. A two throttle valve manifold is considered the minimum necessary to allow continued operation should a throttle valve fail. In reality, a parallel small throttle valve would most likely be required to control during low flow conditions.

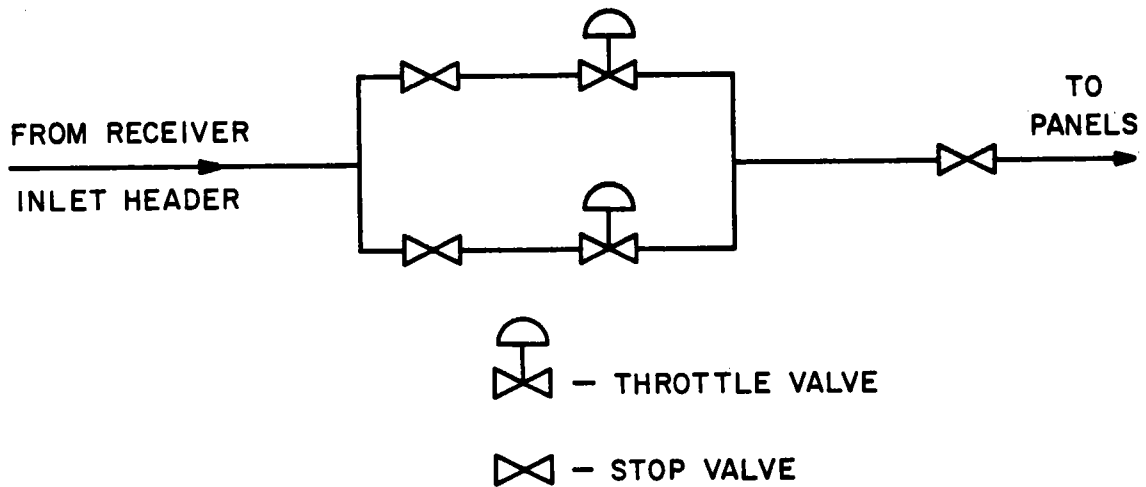


Figure 3-5. Throttle Valve Manifold

Therefore the two valve arrangement is optimistic (minimum throttle valve cost). In addition there is concern about sodium throttle valve reliability which could result in a third parallel full sized valve which would increase costs further.

The valve sizes shown in Table 3-2 are based on limiting flow to 20 ft/sec in adjacent piping. The valves are the same nominal size as the piping. The valve costs are based on Phase I data.

The data shows that approximately \$.7 million could potentially be saved if throttle valves were utilized. However, to determine the actual lifetime costs of the throttle valves versus EM pumps would require a complex reliability analysis which, in all likelihood, would considerably reduce or eliminate the potential savings.

Because the potential savings are so small (< .4% of plant cost) and uncertain, no further consideration of throttle valves for receiver flow control will be considered in this program.

3.5 CONCLUSIONS

A significant reduction in the cost of the receiver flow control system has been identified through the grouping of receiver panels onto a single pump rather than use of the one pump/one panel approach from Phase I. The concept will reduce the total number of EM pumps from 24 to 8 for a total savings of \$4.5 million.

SECTION 4

STORAGE SUBSYSTEM DESIGN IMPROVEMENTS

4.1 INTRODUCTION

During Phase I, sodium-iron storage was evaluated. Despite the fact that the iron storage had a lower sodium inventory and a smaller tank volume, it was found to be more expensive than the sodium storage. The principal reason for this was the high cost of iron (\$0.45/lb based on vendor quotes for low carbon steel plate stock). Recently obtained quotes from ARMCO, Inc. show that scrap steel plate can be purchased for \$0.20/lb. The impact of this new iron cost information is assessed in Section 4.2.

The Phase I analysis also assumed that the iron could be loaded into the tanks with only 25% void space. A further survey of the literature has uncovered evidence (see Ref. 4.3) that the actual void fraction would most likely be greater than 38%. The impact of higher void fractions is also assessed in Section 4.2.

As conceptually designed in Phase I, the storage system consisted of six spherical tanks, three of which were used for storage of cold sodium (612°F) and three were used for storage of hot sodium (1100°F). Section 4.3 presents a redesigned storage system that includes the following improvements:

- Better safety, by virtue of double-wall containment instead of single-wall.
- Four cylindrical/spherical tanks rather than six spherical tanks, with no increase of tank diameter.
- 37% cost reduction.

4.2 SODIUM-IRON STORAGE

An iron storage system has been designed that meets the same specifications as the conceptual design of sodium storage presented in Section 5.4 of the Phase I final report (Ref. 1.1). A revised cost estimate has been prepared and summarized in the standard format.

4.2.1 CONCEPTUAL DESIGN

Quotes recently obtained from ARMCO, Inc. show that scrap steel plate can be purchased at \$0.20/lb. These "roughly sheared bars" (about 2" square x 1/2" thick)

are the scrap resulting from plate trimming operations. ARMCO also manufactures grinding balls in sizes from 3/8" dia. up to 6" dia. at about \$0.55/lb. A mixture of 30% balls (by volume) with 70% bars would have an aggregate cost of \$0.30/lb. with about seven balls per plate to promote flow of sodium around the plates. With steel purchased at \$0.30/lb iron storage could be less expensive than sodium storage.

A schematic of the sodium-iron storage concept is shown in Figure 4-1. It consists of small sodium tanks with 0.25 hours capacity, and iron tanks with 2.75 hours capacity. A larger proportion of capacity has been located in the iron tanks in this example than was done in the parametric analysis case to maximize the savings in tank volume available from the iron storage concept. As shown in Table 4-1 the iron storage concept uses fifteen tanks, four for sodium and eleven for iron. These tanks are all cylindrical in shape and factory assembled. The sodium tank volumes have been selected to allow for about 5% cover gas volume and 5% sodium ullage; the iron tanks have no gas space but are large enough to provide 5% volume for a sodium flow distributor at the base of the tank. Thermocline losses have been estimated at 5% of the capacity (see Table 4-2) and these losses have been accounted for by designing the entire storage system to be 5% oversize.

Figure 4-2 shows a plan and elevation arrangement of these tanks. The overall height of this array is about 33.5 meters (110 ft). Note that each iron tank has a separate valve. These valves permit the iron tanks to be discharged singly as required by the small capacity of the sodium tanks. An electromagnetic pump is required rather than a centrifugal pump because the sodium flow reverses in going from charge to discharge mode. In either mode the pump operates on the cold side of the circuit.

The individual tank designs used in this example are basically those developed by Foster Wheeler as part of the Phase 1 parametric analysis (Ref. 1.1, pp. 3-89, 3-90). However, the iron tanks have been modified slightly by the addition of a tapered inner liner (Figure 4-3) whose function is to support the side loads (hoop stresses) imposed by the iron in the tank. This liner can support hoop loads equivalent to a pressure of 400 psi.

4.2.2 COST ESTIMATE

A comparison of the iron storage and sodium storage costs is presented in Table 4-3. The uncertainty in the iron storage estimate (probably $\pm 2M\$$) is larger than the difference in cost (1.08M\$) between these two systems.

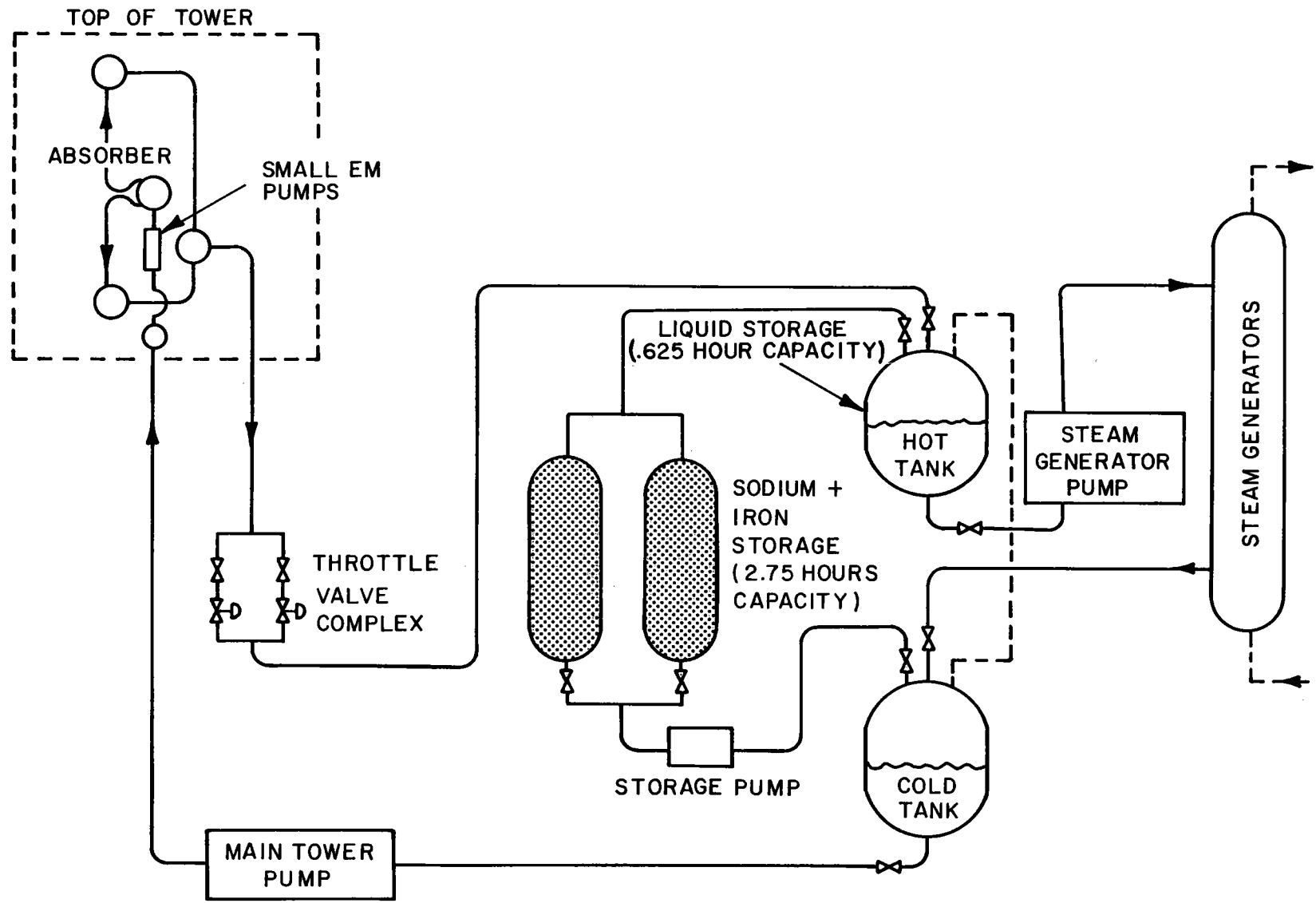


Figure 4-1. Sodium-Iron Storage Concept

Table 4-1

COMPARISON OF STORAGE CONCEPTS

	<u>Sodium-Iron Storage</u>	<u>Sodium Storage[†]</u>
Peak Temperature	1099.2°F, 866°K	1099.2°F
Low Temperature	611.9°F, 585°K	611.9°F
Sodium Tanks		
Number of Tanks	2 hot; 2 cold	3 hot; 3 cold
Volume per Tank	9905 cu. ft.	124,000 cu. ft.
Sodium in Tanks	1.623×10^6 lb	18.55×10^6 lb
Storage Capacity	0.25 hours (192 MW _h)*	3.00 hours (766 MW _h)**
Sodium-Iron Tanks		
Number of Tanks	11	
Volume per Tank	9900 cu. ft.	
Sodium in Tanks	2.64×10^6 lb.	
Iron in Tanks	28.38×10^6 lb.	
Storage Capacity	2.75 hours (574 MW _h)*	
Iron Description		
Balls (steel)	30% by volume, 1/2" dia.	
Plates (steel)	70% by volume, 2" sq. x 3/8" thk.	
Aggregate Cost	\$0.30/lb.	
Sodium Cost	\$0.33/lb	\$0.33/lb

*Net rating, includes allowance for 5% thermocline loss.

**See Ref. 1.1, pp. 5-97 for computation of this number

†Ref. 1.1, Section 5.4

Table 4-2.

ANALYSIS OF IRON TANK PRESSURE DROP
AND THERMOCLINE LOSSES

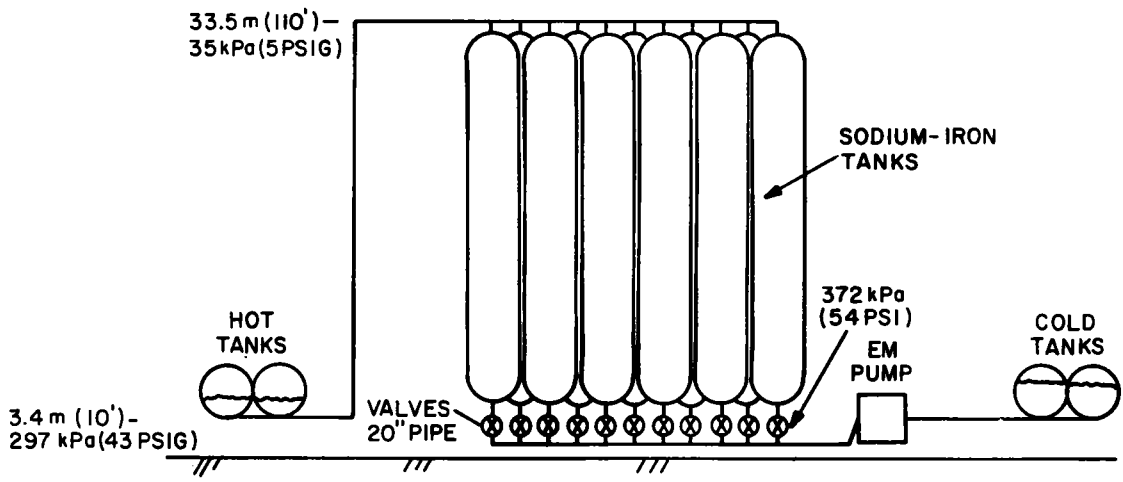
Volume Fraction of Solid (Iron) ^d	55%
Volume of Tank	9900 cu. ft
Surface Area of Iron	550,696 ft ²
Heat Transfer Coefficient	2000 Btu/Hr-ft ² -°F
Sodium Flow Speed in Bed	1947 Ft/ Hr.
Bed Discharge Time (t*) ^a	0.25 hours
Thermocline Spread (2Δτ/τ) ^a	0.322
Thermocline Loss (a/A) ^b	2.4% convection and conduction <u>2.6%</u> flow distribution 5.0% Total
Pressure Drop Across bed ^c	8.1 psi

a. Based on method in Ref. 1.1, Appendix F

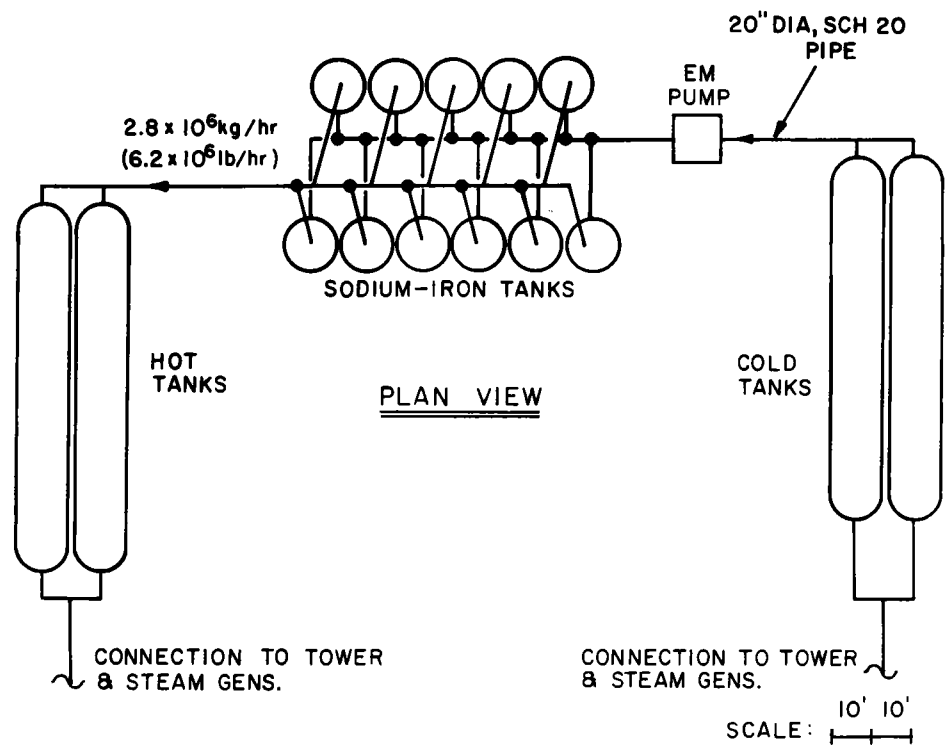
b. Based on method in Ref. 1.1, pp. 3-118

c. Based on Burke-Plummer Method, p. 198, Ref. 4.4

d. Maximum practical packing factor for spheres is about 62% (Ref. 4.1, p. 71) for mixed plates and spheres it will probably be somewhat lower.



ELEVATION VIEW



PLAN VIEW

Figure 4-2. Sodium-Iron Storage Layout

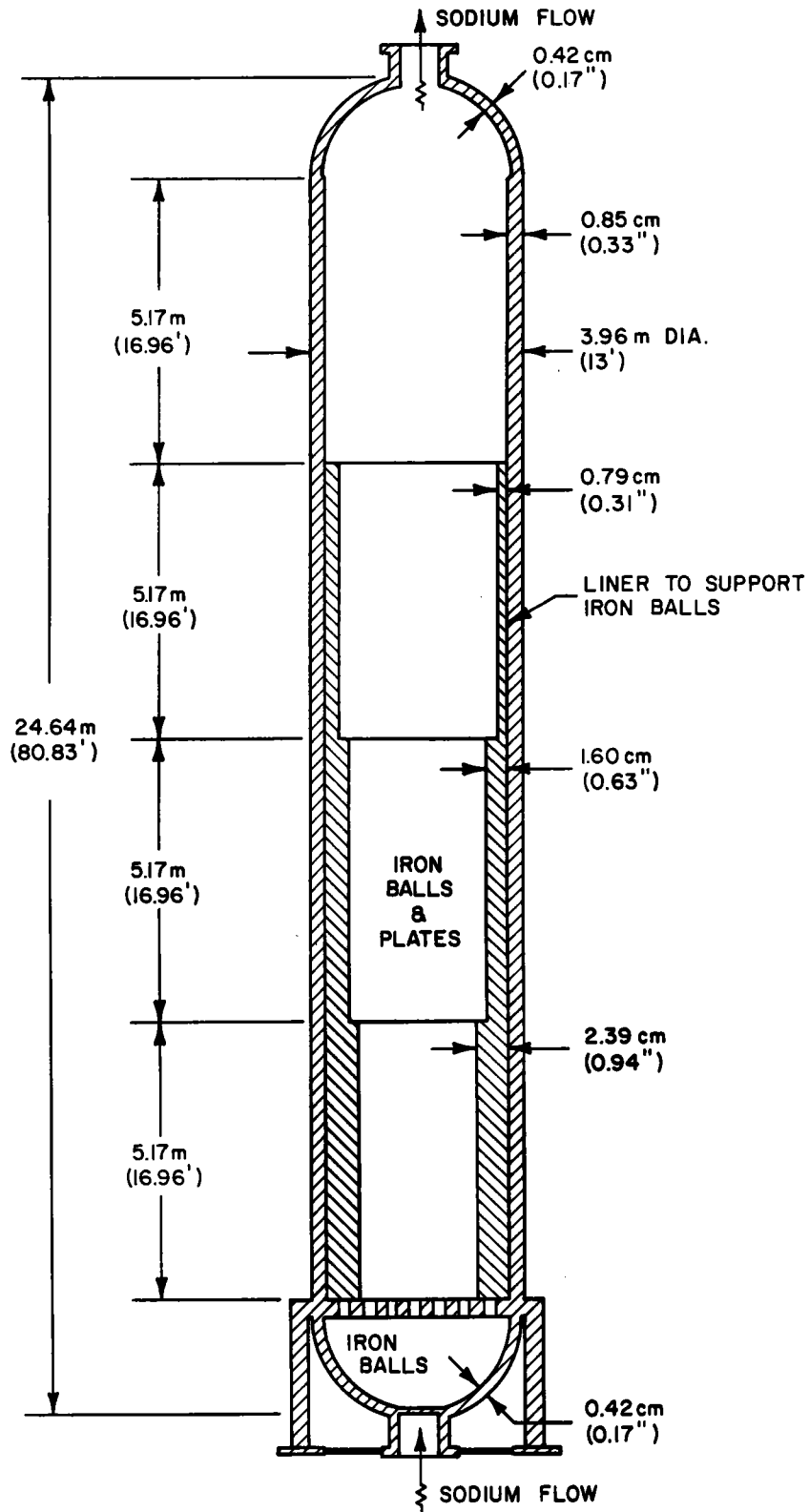


Figure 4-3. Sodium-Iron Tank Concept

Table 4-3

COST SUMMARY AND COMPARISON

<u>Cost Category</u>	<u>Sodium-Iron Storage</u>	<u>Sodium Storage*</u>
<u>4600 Thermal Storage Equipment</u>		
4610 Media Containment Equipment		
4611 Hot Sodium Tanks	0.60	10.07
4612 Cold Sodium Tanks	0.51	2.80
4613 Sodium-Iron Tanks	5.01	-
4614 Piping and Valves	1.18	-
4620 Media Circulation Equipment	3.05	-
4660 Foundations	-	0.19
4680 Media		
Sodium	1.41	6.12
Iron	8.50	-
4600 Subtotal	20.26	19.18

* Ref. 1.1, pp. 6-45

The details of the iron storage cost estimate are given in Table 4-4. The costs of the tanks were obtained by scaling the Foster Wheeler parametric analysis results as shown in Table 4-5. Tank installation costs were based on the estimates prepared by Kaiser Engineers for the parametric analysis. Piping costs were scaled from the conceptual design results presented in Appendix T of the Phase I Report (Ref. 1.1).

4.2.3 DEVELOPMENT ISSUES

If iron storage were to be pursued further because of its low sodium inventory, then there are two development issues which should be addressed. They are:

- Thermocline Losses

Available models for thermocline behavior during charging and discharging treat convection and axial conduction as separate processes within the packed bed of iron spheres. A more complete model is needed which not only treats the combined effects of convection and conduction but also accounts for conductive resistance within the iron spheres.

There is currently no method for predicting the sodium flow distribution within the bed or accounting for wall effects.

- Thermal Stresses

Charging and discharging subjects the tanks and iron to a 275°C (500°F) temperature change with relatively sharp temperature gradients. This may cause failure of the tanks due to creep-fatigue.

The iron balls may shift (ratcheting) due to temperature induced size changes and cause the bed diameter to grow, thereby placing additional stress on the tank walls.

These issues could be resolved by performing four subsystem research experiments as follows:

- SRE#1 - Thermocline Mathematical Modeling

Develop a model for the charge-discharge processes which includes the effects of combined convection, axial conduction and internal resistance of the iron balls.

- SRE#2 - Thermocline Experiment

Build a small model of a sodium-iron storage tank (.5 ft dia. x 3 ft. long) and instrument it to measure temperature at multiple locations. Run charge and discharge cycles to establish correspondence between measured performance and predicted performance.

Table 4-4
COST DETAILS
(M \$)

Description	Quantity	Installation	Material	Total
<u>4610 Media Containment Equipment</u>				
<u>4611 Hot Sodium Tanks</u>				
	2 ea.			
Metal, fabrication and freight (FOB Jobsite)		-	0.17	0.17
Field Installation Incl.-Steel Supports, Concrete Fdn's., Unloading Trace Htg, Insulation and Instrumentation		0.43	-	0.43
<u>4612 Cold Sodium Tanks</u>				
	2 ea.			
Metal, Fabrication and Freight		-	0.08	0.08
Field Installation Incl.-as 4611		0.43	-	0.43
<u>4613 Sodium-Iron Tanks</u>				
	11 ea.			
Metal, Fabrication and Freight		-	2.38	2.38
Field Installation Incl.-as 4611 Plus Filling with Iron Balls and Plates		2.63	-	2.63
<u>4614 Sodium Piping and Valves</u>				
Pipe (20" dia., Sch. 20)	200 lf	0.02	0.01	0.03
Elbows	30	0.001	0.03	0.03
Tees	20	0.004	0.02	0.02
Valves (20" pipe, 630°F service)	11	0.001	1.10	1.10
<u>4620 Media Circulation Equipment</u>				
Electromagnetic Pump 16,000 gpm, 75 ft. heat (Including Power Supply, Capacitor and Stator Cooling Equipment)	1 ea.	0.05	3.00	3.05
<u>4660 Foundations</u>				
	Included in Accts. 4611, 4612, 4613 Installation Costs			
<u>4680 Media</u>				
Sodium 0.33\$/lb	4.26x10 ⁶ lb	Incl. in 4611,4612	1.41	1.41
Iron (low carbon steel, 30% balls, 70% rates)				
Aggregate Cost 0.30\$/lb	28.32x10 ⁶ lb	Incl. in 4613	8.50	8.50

4-10

Table 4-5
STORAGE TANK COSTS

Storage Medium	Sodium	Sodium	Iron
Tank Orientation	Horizontal	Horizontal	Vertical
Design Temperature (°C)	593	322	593
Design Pressure (mPa)	0.34	0.34	0.34
Tank Material	316SS	Carbon Stl.	316SS
Tank Volume (m ³)	280.7	280.7	280.6
Tank Weight Empty (kg)	22,374	20,656	21,755 ^b
Liner Weight (kg)	-	-	24,579
Cost (1978 dollars)			
Tank Material	69,367	20,519 ^a	72,472 ^b
Liner Material	-	-	81,880 ^c
Factory Labor	17,450	19,504	60,956 ^c
Freight to Jobsite	494	456	1,022 ^c
Total (FOB Jobsite)	87,311	40,479	216,330
Field Installation	213,500	213,500	239,000
Cost Scaled from Ref. 1.1, pp. 3-91 Cases:	5b	4c	2b

NOTES:

- a. Scaled by (0.45/1.10) to change from 2 1/4 Cr-1Mo to Carbon Steel
- b. Scaled by (50/150) to change from 150 psi to 50 psi Design Pressure
- c. Scaled by weight from Case 2b.

- SRE#3 - Thermal Stress Analysis

Analyze the tank wall thermal stresses caused by temperature gradients in the thermocline and estimate the number of cycles to failure.

- SRE#4 - Large Scale Test

Construct a full scale tank (13 ft. dia. x 73 ft. long), fill with iron balls and test in a sodium loop with required pump and heat exchangers for thermal cycling. This test will verify not only the thermal design procedures but also the structural integrity under thermal cycling.

4.2.4 SUMMARY AND CONCLUSIONS

Iron storage can reduce the total volume of tankage required for sodium storage from 744,000 cu. ft. to 148,520 cu. ft. and reduce the sodium inventory from 18.6×10^6 lb to 4.3×10^6 lb. However, this reduction in system size does not result in a reduction in overall plant cost because of the increase in storage media cost and the added costs for auxiliary equipment, particularly the storage pump and sodium valves. In addition, considering that there are two development issues that need to be resolved, it was concluded that a storage subsystem using sensible heat stored in sodium should be retained.

4.3 STORAGE SYSTEM REDESIGN

In Phase I, a six-tank storage system (three hot and three cold) was chosen as the lowest cost configuration. Potential plant cost savings were believed possible if an eight-tank system (four hot and four cold) was used. This was based on the use of single-wall construction, where, in general, the tank material requirement decreases as the number of tanks increases.

According to Kaiser Engineers (Ref. 4.5), the diameter of a 3300 ton single-wall spherical tank would vary from thermal expansion and contraction by as much as 6 inches during operation. This made it very difficult to adequately support the tank and be capable of resisting seismic forces. Such a design problem is not unsolvable, but would require extensive analysis.

4.3.1 STORAGE VESSEL DESIGN

A more prudent solution appeared to be the application of a design approach often used for large cryogenic storage vessels. That is, use a double-wall structure wherein the inner tank is supported by suspension members between the tank and the supporting structure. In this manner, structural stresses due to thermal displacements are avoided. The resulting redesigned double-wall storage tank utilizing a hemispherical/cylindrical configuration is shown in Figure 4-4.

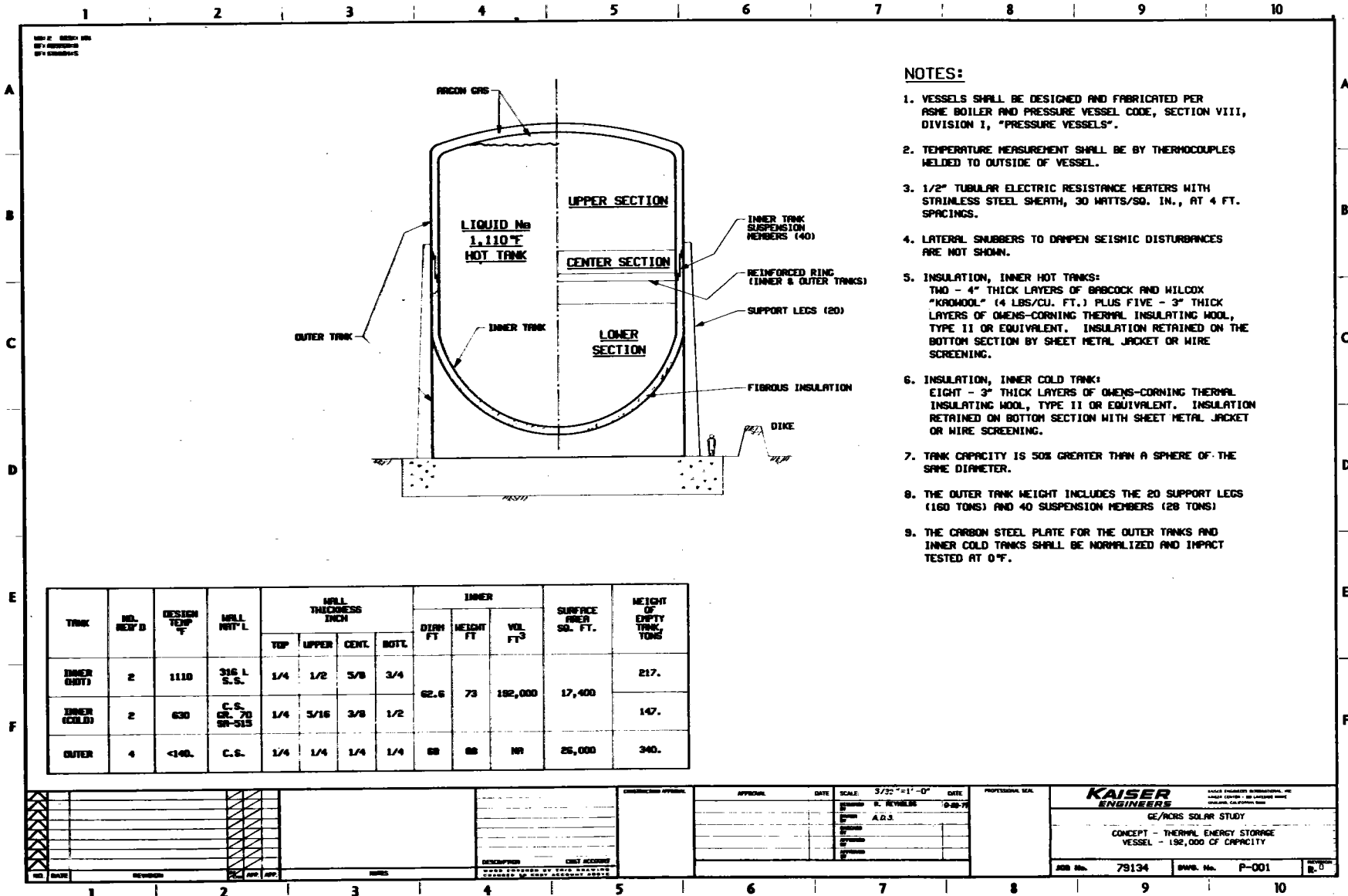


Figure 4-4. Thermal Energy Storage Vessel

Table 4-6
STORAGE SYSTEM COST COMPARISON

	Component	Component Cost	System Cost
Phase I System*	Hot Tank (3)	\$ 10,065,000	
	Cold Tank (3)	2,802,000	\$13,057,200
	Foundation	190,200	
Redesigned System	Hot Tank (2)	4,604,000	
	Cold Tank (2)	1,420,000	
	Outer Tank (4)	2,052,400	8,203,200
	Foundation	126,800	

NET SAVINGS = \$4,854,000

*Cost of Phase I system from Ref. 1.1, Table 6.2-11.

The double-wall vessel shown in Figure 4-4 has a volume of 192,000 cu. ft. Therefore, the redesigned storage system, having the same total volume as before, consists of four tanks (two hot and two cold). Table 4-6 presents a cost comparison between the Phase I system and the redesigned system. The costs for the Phase I system were taken from Ref. 1.1 and the costs for the redesigned system (details shown in Table 4-7) come from Table 4-7.

Notes 5 and 6 of Figure 4-4 specify blanket types of fibrous insulation. However, subsequent analysis has indicated that a bulk type fiber, such as Johns-Manville "Cerawool," would be more preferable from both cost (\$600,000 less per system) and performance (1600°F limiting temperature) standpoints. The bulk fiber would be blown into place, and could resist localized hot-spots (due to sheath heaters) better than fiberglass. The appropriate costs of "Cerawool" are reflected in the details shown in Table 4-7.

As shown in Table 4-6, the redesigned storage system provides for a net savings of \$4,854,000, while still maintaining the same storage capacity.

Table 4-7
 DETAILS, COST ACCOUNT 4600

<u>Cost Category</u>	<u>Quantity</u>	<u>Labor</u>	<u>Material</u>	<u>Total</u>
<u>4611 Hot Inner Storage Tank</u>	2 each			
Metal, Fabrication, Shipping and Installation		1,270,000	2,814,000	4,084,000
Insulation		85,000	315,000	400,000
Trace Heating		<u>50,000</u>	<u>70,000</u>	<u>120,000</u>
4611 Subtotal		1,405,000	3,199,000	4,604,000
<u>4612 Cold Inner Storage Tank</u>	2 each			
Metal, Fabrication, Shipping and Installation		360,000	540,000	900,000
Insulation		85,000	315,000	400,000
Trace Heating		<u>50,000</u>	<u>70,000</u>	<u>120,000</u>
4612 Subtotal		495,000	925,000	1,420,000
<u>4613 Outer Storage Tank</u>	4 each			
Metal, Fabrication, Shipping and Installation		657,600	1,394,800	2,052,400
<u>4660 Storage Foundations</u>				
4660 Subtotal		69,000	57,800	126,800
<u>4680 Media</u>				
Sodium	18.55x10 ⁶ lb			6,121,500

4.3.2 POTENTIAL IMPROVEMENTS

To further improve the design and reduce the cost of the storage system, it is recommended that the following refinements be considered in the future.

- Rather than supporting the Inner tank with 20 legs, support it with the lower cylindrical section of the Outer tank (i.e., the "skirt" principle). That section could be increased in thickness from 1/4" to 1" (if that much were necessary), with no increase in overall steel requirements and a substantial reduction of fabrication costs.
- Rather than placing insulation directly against the bottom or hemispherical surface of the Inner tank, locate it next to the inside surface of the Outer tank. Installation would be simpler and less expensive, and the bottom of the Inner tank would be readily visible for direct inspection.
- If analysis indicates that cooling of the foundation slab would be necessary, consider the use of cooling coils, embedded in the slab.

SECTION 5

OPERATING MODE ANALYSIS

5.1 INTRODUCTION

This section summarizes a study conducted to define the conditions associated with various major operating modes of the plant and to identify modifications to the plant design as a result of the analysis.

All of the operating modes have been developed based on the criteria listed below.

- The steady-state and transient operating temperature limits for all systems and components are not to be exceeded
- Use of auxiliary power sources (e.g., trace heating) to be avoided unless absolutely necessary
- Draining of sodium components to be considered only when maintenance on that component is necessary
- Consumption of energy during standby, startup and shutdown modes should be minimized
- Transition times between operating and hold modes should be minimized.

The modes developed meet the above criteria. They will result in controlled operation and smooth transition between operation and shutdown. A brief summary of the various operating modes is presented in Table 5-1. The overall plant control schematic is illustrated in Figure 5-1.

The report is organized as follows. The background information is given in Section 5.2. It is followed by the operating mode description in Section 5.3. Recommended revisions to the Phase I commercial plant design are then described in Section 5.4. Finally, areas of concern which require future study and resolution are identified in Section 5.5.

5.2 BACKGROUND

This study used the ACR Phase I design as a baseline. The background information was obtained by a review of the Phase I data and by consultation with cognizant personnel within the General Electric Company.

Table 5-1

SUMMARY OF OPERATING MODES

Operating Mode	Control Functions
Standby	<ul style="list-style-type: none"> ● Heliostats in stow position ● Tower loop and SG loop are bottled up. Circulate sodium from cold storage tanks periodically as necessary. ● Electrical power for auxiliary loads provided by grid with diesel-generator backup.
Startup	<ul style="list-style-type: none"> ● SG/EPGS warmup begins before sunrise in anticipation of startup if hot sodium is available. ● Receiver insulation curtain raised. ● Heliostats focused on receiver. ● Tower pump starts; sodium temperature and flow ramped up. ● Sodium from receiver admitted to cold or hot storage tanks depending on sodium temperature. ● All components warmed up while observing temperature increase rate limitations.
Normal Operation	<ul style="list-style-type: none"> ● Hot sodium generated at receiver admitted to storage. ● Partial defocus of heliostats if hot tanks fully charged. ● SG/EPGS side operation independent of tower/receiver side. ● Variable steam turbine pressure operation during part load.
Normal Shutdown	<ul style="list-style-type: none"> ● Occurs when insolation level decreases and master control indicates end of day. ● Heliostats to stow position. ● Receiver insulation curtain dropped, tower pump secured, sodium inside bottled up. ● SG/EPGS continue operation until hot sodium depleted; SG/EPGS will then be bottled up. ● Sequence of shutdown in reverse of startup, with plant ending in Standby mode.
Emergency Shutdown	<ul style="list-style-type: none"> ● Actuates for major malfunction indication. ● Initiates emergency shutdown sequence similar to normal shutdown. ● The side of plant not affected by emergency conditions continues to operate if status of hot storage tanks permits. ● Plant control must be reset prior to recommending plant startup.

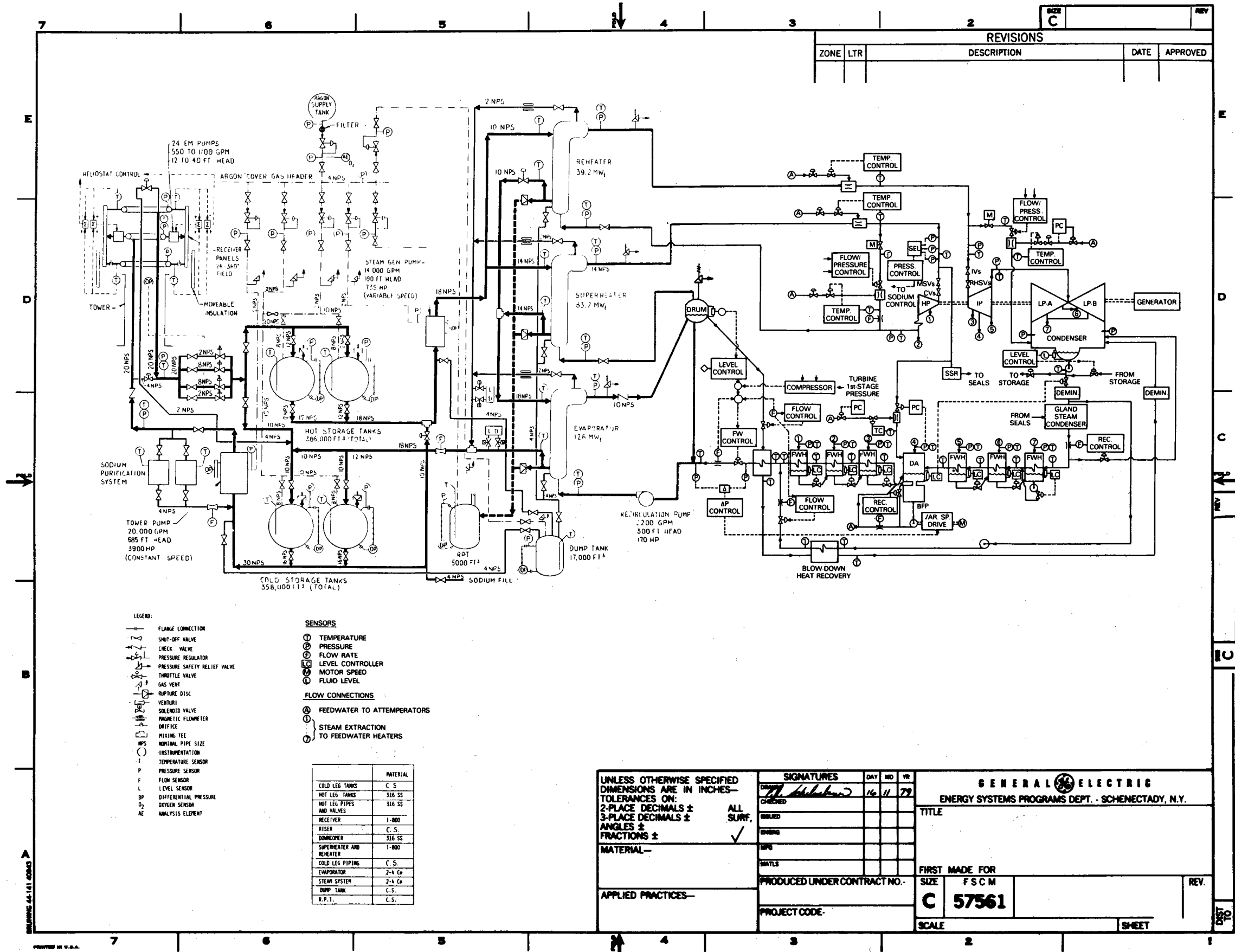


Figure 5-1. ACR Control Schematic

In analyzing the operating modes for the solar central receiver power plant, a key characteristic of the plant must be noted. Since all liquid sodium passes through the storage tanks to reach the steam generators, the receiver/tower side of the plant is effectively decoupled from the steam generator (SG)/electric power generation subsystem (EPGS) side. This allows the operation of one side of the plant to be independent of the other side. It is particularly important during a transient situation. For example, a transient in hot sodium generation at the receiver caused by passing clouds would not affect the operation of the SG/EPGS side of the plant.

Of major importance for the operating mode analysis are the component operation restrictions. A list of such constraints together with their impacts are given in Table 5-2. The restrictions on steam generator temperatures have the most significant impact on operating mode selection, since they affect the allowable shut-down/startup rates of the plant. The steam generator restrictions shown were developed in the Phase I study and can best be described as conservative estimates. Note that the 75°F/hr maximum ramp rate shown is for warmups from ambient temperature. The values for warmup rate from elevated temperatures were not given, but are expected to be higher. Values for these restrictions should be determined through detailed analyses performed on the steam generators for this particular solar application (e.g., steam generator geometry, materials and operating conditions). Values from such analyses can be used with increased confidence. In the absence of such analyses, it was decided to adopt in the present study, the temperature change rate limit of 150°F/hr published for the Clinch River Breeder Reactor Steam Generators (Ref. 5.3, 5.4) for warmups from elevated temperatures.

Information on the rate of temperature decrease of the various components of the plant during a standby period is important for determining the operating mode approach. The methods used to estimate the transient variations in component temperatures are presented in Appendixes C and D. The method in Appendix C is for a component initially at a uniform temperature (e.g., riser, downcomer, and storage tank), and the method in Appendix D is for a component which is initially hot at one end and cold at the other end with a linear temperature profile in between (e.g., receiver panel, superheater, and reheater). These methods are approximate in nature and are aimed at obtaining qualitative trends, rather than accurate quantitative values, to aid in the operating mode analysis. The results are shown in Figures 5-2 through 5-6. Several points should be noted:

Table 5-2

ACR SOLAR PLANT COMPONENT OPERATION RESTRICTIONS

Component	Restriction	Impact
Receiver Tower Loop	<ul style="list-style-type: none"> ● Riser piping material and insulation not rated for hot sodium temperature (1100°F) 	<ul style="list-style-type: none"> ● Use of riser/downcomer cross connect would require a redesign
Steam Turbine	<ul style="list-style-type: none"> ● Metal temperature ramp rate limit (life expenditure consideration). ● Max. ramp change (from Ambient) of 75°F/hr. 	<ul style="list-style-type: none"> ● Time required for Startup/Shutdown and load change. ● Operating Procedure must comply.
Steam Generators*	<ul style="list-style-type: none"> ● Max. transient temperature change ramped up or down in 60 min. or less (includes step change) - 180°F (upset), 250°F (emergency). ● Max. ΔT between Na and H₂O at any part (fill or operation) - 300°F. 	<ul style="list-style-type: none"> ● Violation of emergency condition requires requalification of steam generator.
Sodium Drain Tank	<ul style="list-style-type: none"> ● Made of carbon steel and not rated for hot sodium temperature (1100°F). 	<ul style="list-style-type: none"> ● 1100°F sodium must be cooled down to allowable temperature before being drained into the drain tank or must be drained to hot storage tanks.
Sodium Storage Tanks	<ul style="list-style-type: none"> ● Allowable rate of change of wall metal temperature: TBD**. ● Inner and outer wall metal differential temperature: TBD. ● Differential temperature limits from the top to the bottom: TBD. 	<ul style="list-style-type: none"> ● Allowable rates of warmup of storage tanks during cold start are limited.
All Other Sodium Piping and Components	<ul style="list-style-type: none"> ● Large thermal shocks undesirable. 	<ul style="list-style-type: none"> ● Large temperature shocks should be avoided by proper operating procedures.

*Estimates developed in the Phase I study.

**To Be Determined.

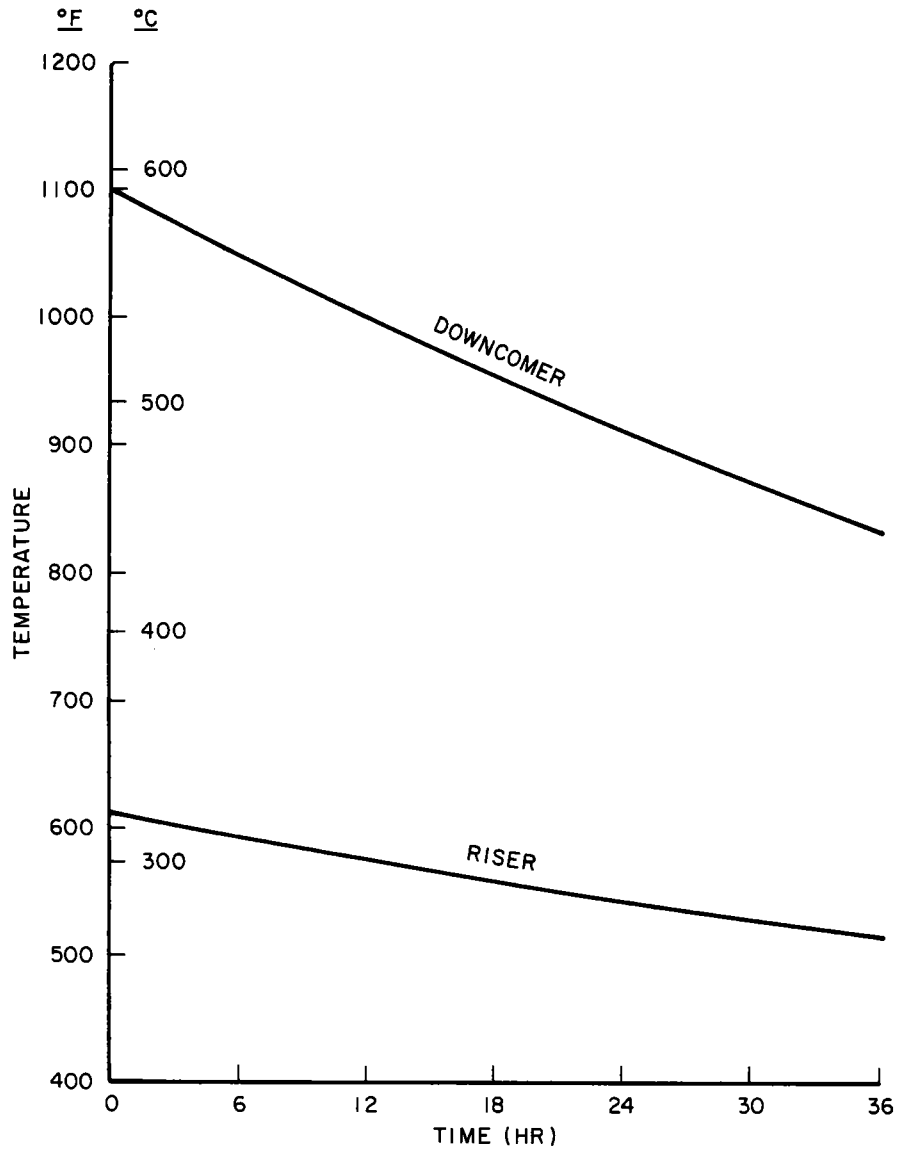


Figure 5-2. Cooldown of Riser/Downcomer

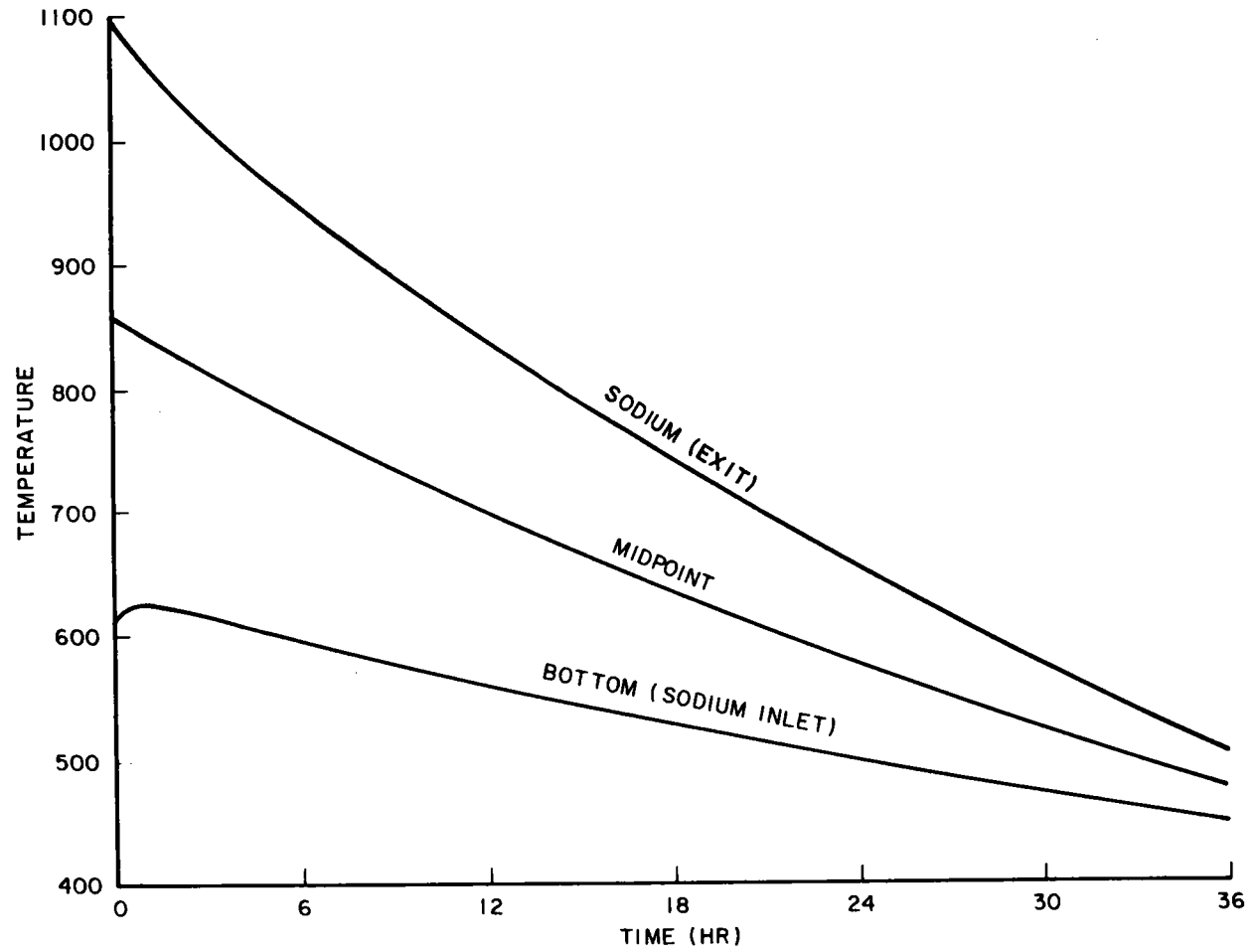


Figure 5-3. Cooldown of Receiver Panels.

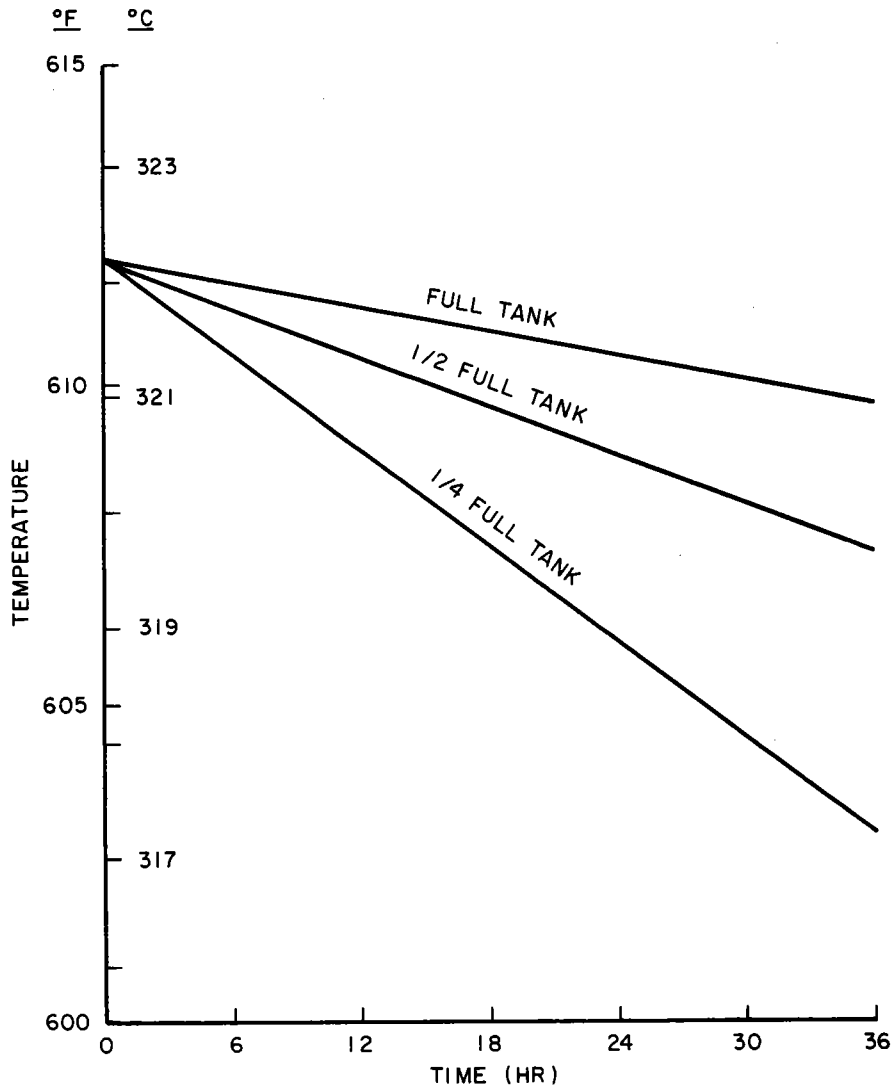


Figure 5-4. Cooldown of Cold Sodium Storage Tank

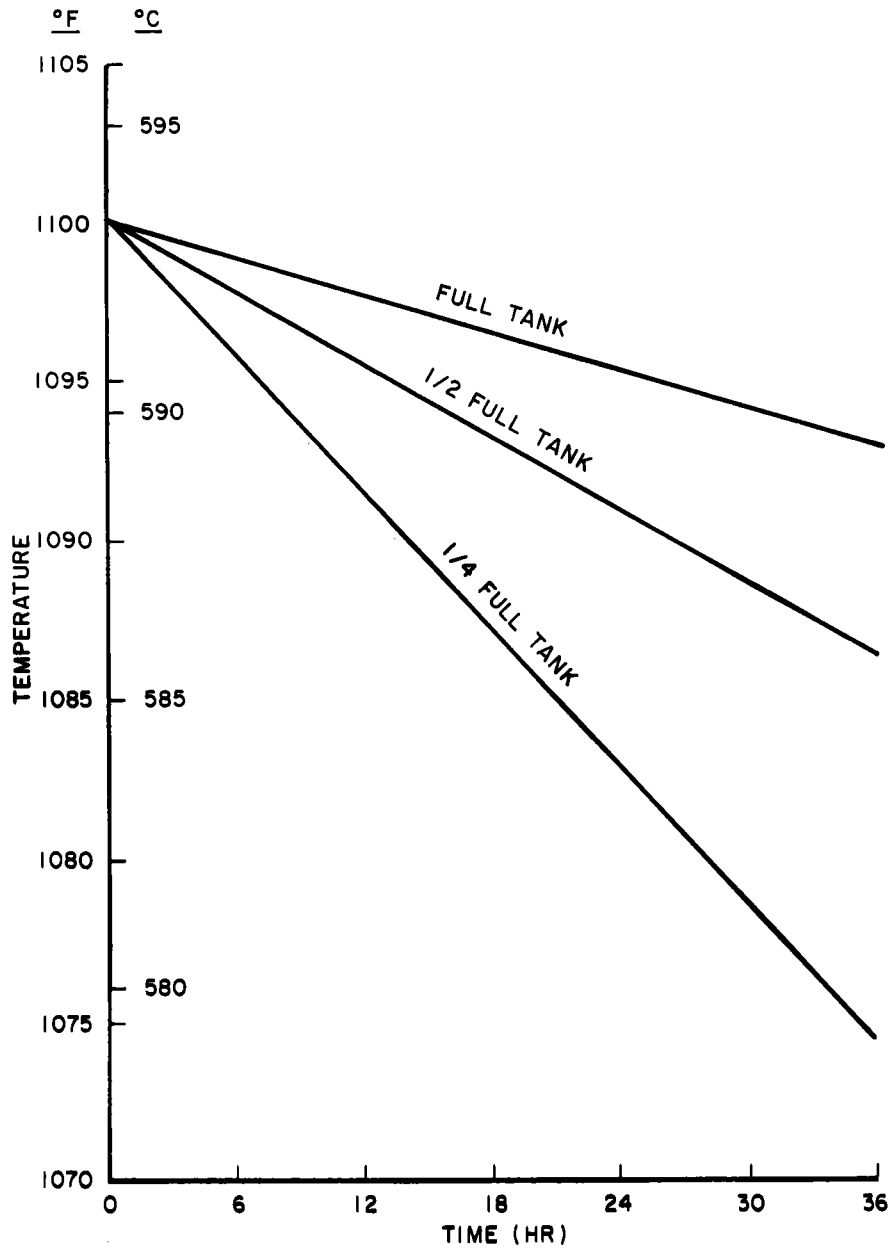


Figure 5-5. Cooldown of Hot Sodium Storage Tank

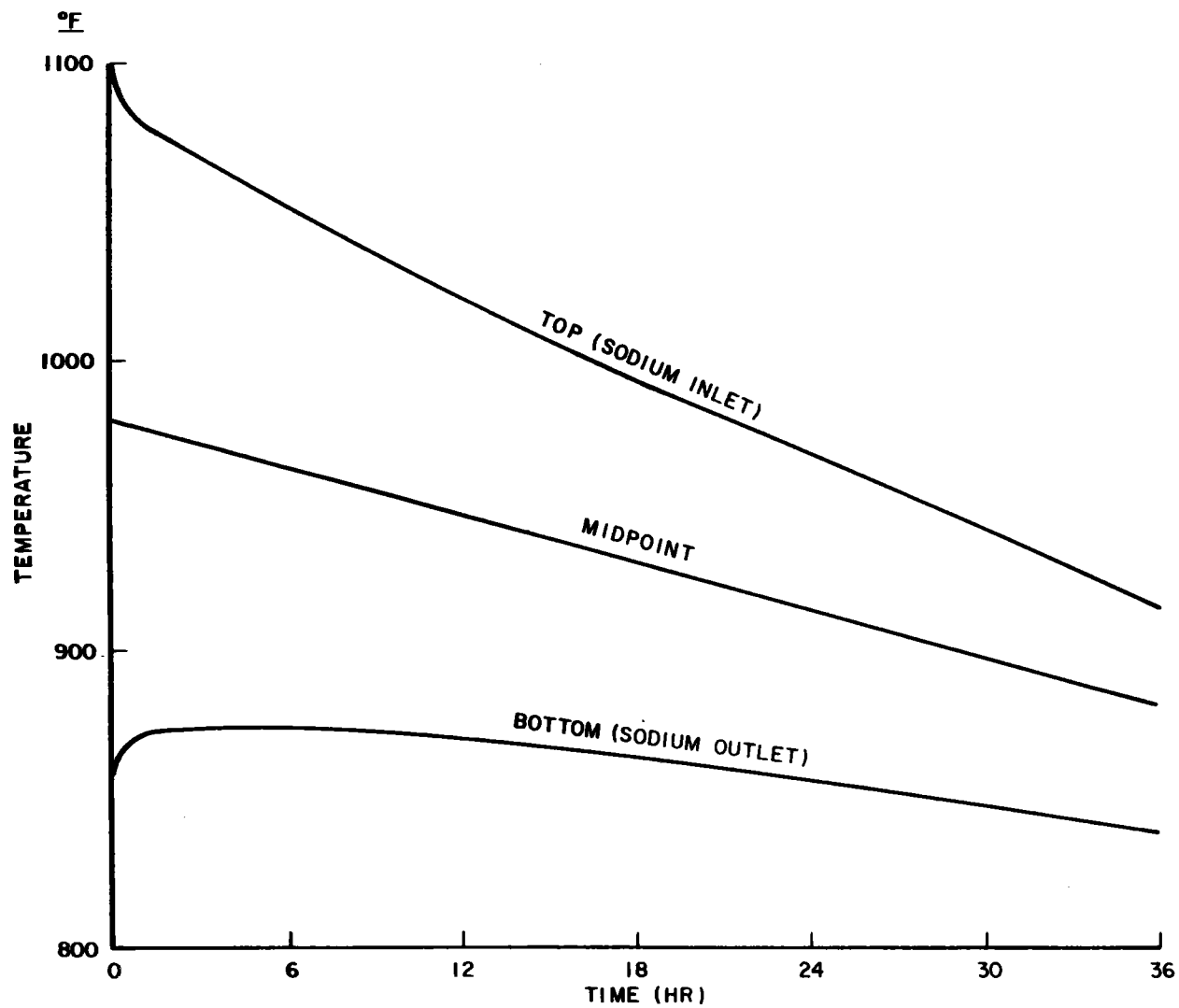


Figure 5-6. Cooldown of Superheater (Reheater)

- In Figures 5-3 and 5-6 for the receiver and the superheater (or reheater), which have linear temperature profiles initially, the variations of temperatures with time at the top, bottom and mid-point of the components are shown.
- The temperature variations of storage tanks, Figure 5-4 and 5-5, depend on the sodium inventories in the tank, with faster temperature drop for a tank with less sodium inventory.
- Figure 5-6 is applicable to both the superheater and the reheater, since their sodium temperatures are identical.
- No attempts were made to estimate the cooldown of the evaporator, since it would involve complicated water phase change and steam bleed-off processes.

5.3 OPERATING MODE DESCRIPTION

The plant operating modes investigated include the following:

- Standby Modes
- Startup Modes
- Normal Operation Modes
- Shutdown Modes

To avoid confusion, a few words about the distinctions among the terms used are warranted. Standby and Normal Operation Modes refer to the state the plant is in, while Startup and Shutdown refer to the process of going from one state to the other. For example, the plant goes through the shutdown mode from the Normal Operation mode to the Standby mode. Therefore, the plant would be in a transient in the Shutdown or the Startup mode, but would be more or less in a steady state (with the exception of some short term transients, e.g., periodic replenish of sodium in the tower loop during a standby) during the Standby or the Normal Operation modes.

Depending on the duration of the holding period, the Standby modes are divided into

- Short Term (Hot) Standby (<1 day)
- Intermediate Term (Warm) Standby (between 2 and 7 days)
- Long Term (Cold) Standby (>1 week)

The Startup modes are divided into Hot Start, Warm Start, and Cold Start, corresponding respectively to the three Standby modes from which the plant is started. The three time scales mentioned above which separate the three Standby modes were chosen to match the downtimes corresponding to the hot, warm, and cold starts of the steam turbine (Ref. 5.1).

A description of these major operating modes is presented in the following sections.

5.3.1 STANDBY MODES

In the Standby modes, the plant is shutdown, the heliostats are positioned in the stow position, and electric power for various auxiliary loads is supplied by the grid.

The candidate approaches for the three types of hold modes are summarized in Table 5-3. The selection of the candidates was made based on consideration of energy consumption, hardware requirements, and operational flexibility. Since the operation of the receiver/tower side is decoupled from the SG/EPGS side, the various alternative approaches considered for the two sides of the plant will be presented separately. For each operating mode, the referenced (selected) approach is described first.

Table 5-3
CANDIDATE SCHEMES FOR THE STANDBY MODES

Standby Mode	Short Term (< 1 day)	Intermediate Term (2 to 7 days)	Long Term (> 7 days)
Tower/Receiver Side	<ul style="list-style-type: none"> ● Bottling-up. ● Natural circulation. ● Reverse recirculation 	<ul style="list-style-type: none"> ● Bottling-up with periodic sodium replenishment. ● Bottling-up with trace heating. 	<ul style="list-style-type: none"> ● Bottling-up with periodic sodium replenishment, followed by trace heating. ● Draining.
Steam Generator Side	<ul style="list-style-type: none"> ● Bottling-up. ● Part load operation. ● Trickle flow. ● Shutdown by hot Na temperature control. 	<ul style="list-style-type: none"> ● Bottling-up with periodic sodium replenishment. ● Bottling-up with trace heating. ● Bottling-up with heating by auxiliary boiler. 	<ul style="list-style-type: none"> ● Bottling-up with periodic sodium replenishment. ● Draining.

5.3.1.1 Short Term (Hot) Standby

Receiver/Tower Side

Referenced Approach

In this approach, the tower loop will be allowed to stay idle with the tower pump secured after a shutdown. The throttle valves at the tower base will be shut off, and the tower loop is said to be "bottled-up."

The loop will gradually cool down by losing heat to the ambient. Figures 5-2 through 5-5 show that for an overnight standby, say 12 hours, the temperature losses (in °F) of the various components on the receiver/tower side are

Riser	37°
Downcomer	100°
Receiver Panel (Midpoint)	156°
Hot Tank (if the tank is 1/4 full)	9°
Cold Tank (if the tank is 1/4 full)	3°

The tower loop temperatures are seen to remain sufficiently high to allow a rapid start. This approach has been selected for the short term standby of the receiver/tower side.

Alternate Approaches

Natural Recirculation

The Phase I conceptual design provided a riser/downcomer cross-connect with a shunt valve which would be opened during short term standby to allow natural circulation of the sodium in the riser, downcomer and receiver. The circulation path (in reverse direction to the flow during normal operation mode) is illustrated in Figure 5-7. A closer examination of this scheme revealed the following drawbacks which eliminated the configuration from further consideration.

- Hot leg sodium (1100°F/593°C) would enter the cold leg (610°F/321°C) resulting in high, cyclic thermal stresses.
- The increased cold leg temperatures would necessitate a material change to stainless steel in the riser.
- The circulation flow would only be temporary and would eventually stop as the sodium stratified.

Reverse Recirculation

In the Reverse Recirculation Mode a very small amount of sodium would be pumped from the hot tanks backward through the system using the tower pump and a revised valving arrangement (Figure 5-8). Hot sodium would flow up the downcomer, through the receiver panels, down the riser and return to the cold storage tank. The flow-rate is set such that thermal losses to the ambient would cool the sodium to ~600°F by the time it arrived at the cold tanks. In this way the energy stored in the hot tank would make up that energy lost during a standby period and maintain fluid and component near their respective normal operating temperatures. The approach has the following drawbacks and was therefore dropped from further consideration.

- The tower pump design requirement is to operate in 600°F sodium. Using it to recirculate 1100°F sodium may require design or material modifications. The additional valves also add to the costs. An alternative is to add a pump solely for the reverse recirculation purpose.

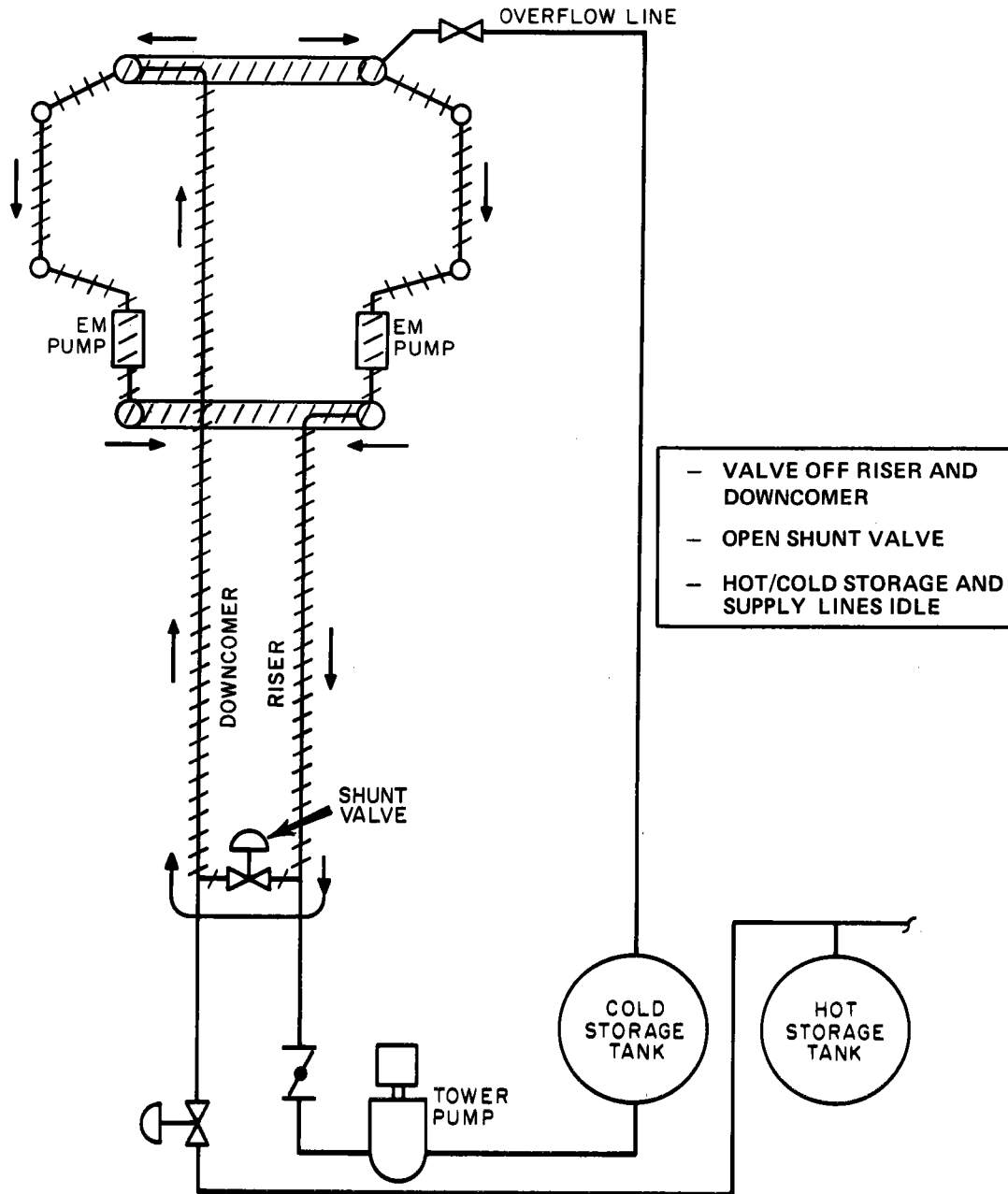


Figure 5-7. Receiver/Tower Loop Short Term Hold Mode
(Phase 1 Natural Circulation Scheme)

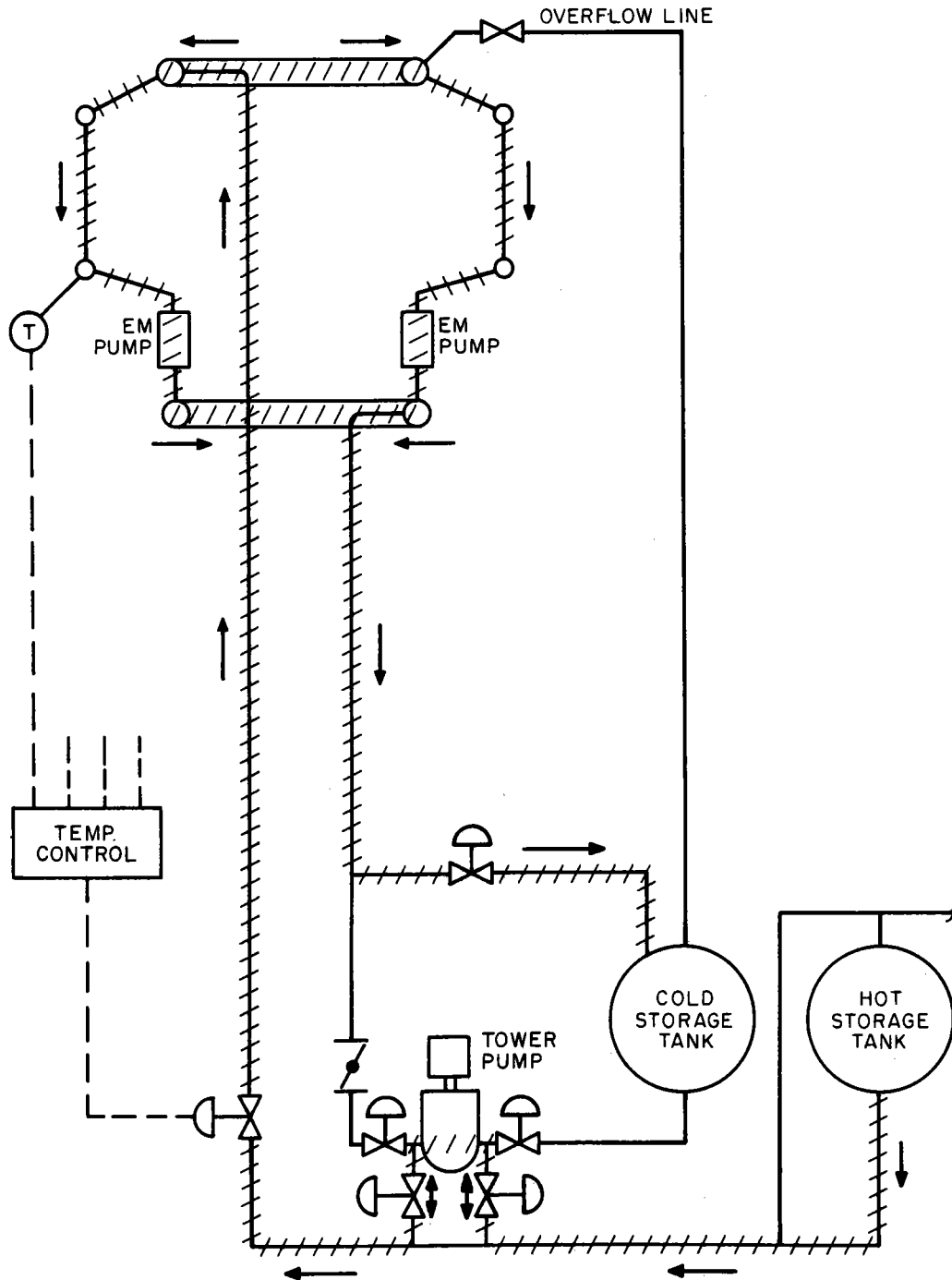


Figure 5-8. Reverse Recirculation Scheme for Short Term Hold

- To maintain the tower loop temperature near the normal operating levels, the major portion of the sodium heat loss must take place in the receiver panels. The situation is delineated in Figure 5-9. It is apparent that the poorer the receiver panels are insulated, the bigger the temperature gradient is and the closer the temperatures are to their normal levels. This approach is then dependent upon designing into the system a high level thermal energy loss to achieve the goal of normal operating temperature level maintenance.

SG/EPGS Side

Referenced Approach

The favored approach involves the "bottling-up" of the steam generator and steam turbine components. In this configuration, neither water/steam nor sodium flows through these components. The system is brought to this state by the normal shutdown mode described in Section 5.3.4.

At the start of this mode steam generator metal temperatures are spread over a wide range due to the fluid (H_2O and Na) temperature gradients from the inlet to the outlet of each component. A list of the range of fluid temperatures for each component is given below:

Steam Generator Temperature Levels (°F)

<u>Location</u>	<u>EVAP</u>	<u>SH</u>	<u>RH</u>
Na Inlet, Design Point	859	1100	1100
Na Outlet, Design Point	612	859	859
H_2O Inlet, Design Point	529	674	572
H_2O Outlet, Design Point	674	1000	1000
Bulk Temp, During Standby Mode if Bottled up and Perfectly Insulated	688	962	966

As flow through the components is stopped, heat will flow from hot to cold areas and, over a period of time, tend to stabilize at an average bulk temperature. The bulk temperatures for the steam generators are also shown in the table above. These values were derived without considering the heat losses to the ambient. From this table, it is seen that some metal components will experience a large temperature change when switching from their normal operating temperature to the component bulk temperature. If this happens too quickly, the component may possibly exceed the guidelines shown in Table 5-2. Knowledge of the rate of temperature change is therefore desirable.

CURVE ① - NORMAL OPERATION

CURVE ② - REVERSE RECIRCULATION WITH HIGH RECEIVER LOSS
(AND THEREFORE HIGH RECIRCULATION FLOW)

CURVE ③ - REVERSE RECIRCULATION WITH LOW RECEIVER LOSS
(AND THEREFORE LOW RECIRCULATION FLOW)

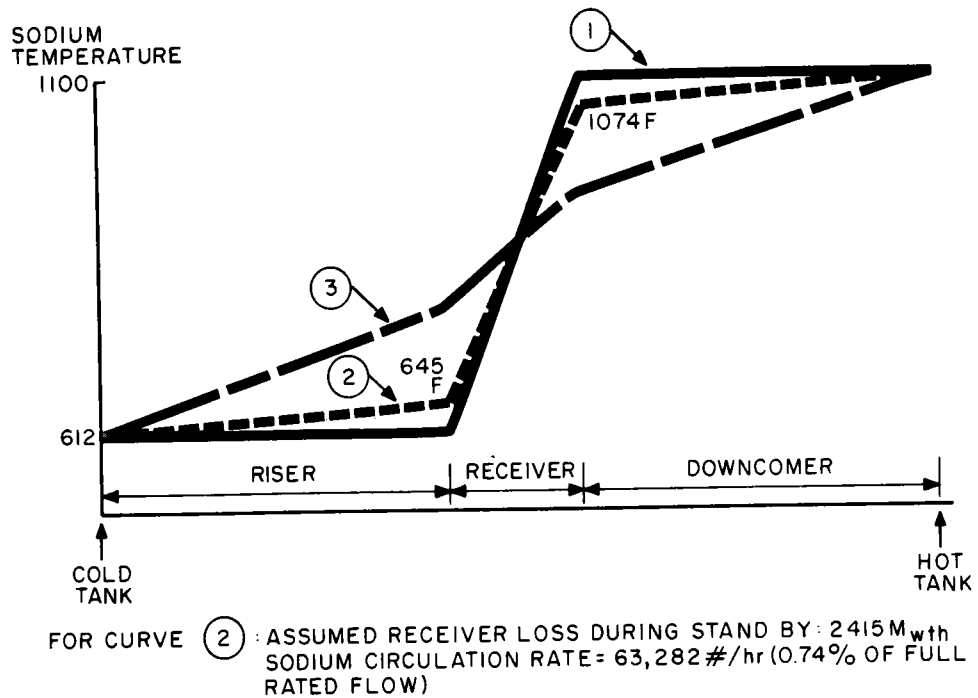


Figure 5-9. Temperature Levels In Tower Loop (Reverse Recirculation Scheme During Short Term Standby)

The temperature equalization and cooldown phenomenon in a steam generator involves the following three heat transfer processes:

- Heat transfer through the tube wall to the colder water/steam.
- Heat loss through the insulation to the ambient.
- Heat transfer by conduction from the hotter sodium to the colder sodium in the SG component.

Analysis has shown that the highest amount of heat flux, at least initially, is through the tube wall to the water/steam because of the relatively large temperature gradient and small heat transfer resistance in this path. This does not present a problem as this process decreases the temperature gradient across the tube wall and relaxes the stress which is present during normal operation.

Because the heat transfer area is large and the heat content of sodium is many times that of steam in the reheater and the superheater, the steam temperature would rise quickly to approach that of the sodium and little further heat transfer takes place. The remaining two processes would produce relatively low heat flux levels and therefore slow temperature transients. The summation of the effect of the latter two cooldown processes for the superheater and the reheater is illustrated in Figure 5-6. The initial transients are the highest. However, even in the first hour after shutdown, the metal temperatures are well within the 150°F/hr limit.

Cooldown of the evaporator was not modeled since the effort required for such an analysis would be beyond the resources available for this study. The evaporator temperature is expected to drop faster than the superheater and reheater because a large amount of heat in sodium is absorbed due to water evaporation. Judging from the rate of cooldown of the superheater and reheater, it does not seem likely for the evaporator to change temperature at a rate that would exceed the 150°F/hr limit. Therefore, it is concluded that the "bottled-up" configuration will be an acceptable standby mode. A detailed analysis of the evaporator cooldown process, however, is recommended.

The energy consumption for the bottling-up approach can be estimated as follows. From Figure 5-6, the steam generator is expected to drop about a maximum of 95°F in a 15 hour standby. Using the 150°F/hr transient limit, the time required to bring the steam generators back to normal operating temperatures is $\frac{95}{150} = 0.65$ hr. The corresponding energy drawn from hot sodium during warm up, assuming 10% of rated sodium flow, is $100 \text{ MW}_e \times 0.1 \times 0.65 \text{ hr.} = 6.5 \text{ MW}_e\text{-hr}$ (full rated flow sodium would produce 100 MW_e). Note that this energy is expended during the startup following,

rather than during, the standby period. The only energy expended during the standby is the passive loss of thermal energy to the ambient.

Alternative Approaches

The following system configurations were considered as candidates for the short term standby mode:

- Part Load Operation
- Trickle Flow
- SG Shutdown by Hot Sodium Temperature Control.

Part load operation has an advantage over the "bottled-up" configuration in that all normal operating temperature levels are maintained. There is no warm-up the following day, hence no delays or energy losses. The drawback is loss of energy due to the increased turbine heat rate at part load.

The operating load level is dependent upon the amount of energy in the hot storage tanks and the expected duration of the standby period. At full capacity the hot storage tanks hold sufficient sodium for three hours of full load operation, or sodium which can be used to generate 300 MW-hr of electric energy. For an expected overnight duration of 15 hours, for example, the turbine could be operated at $\frac{3}{15} = 20\%$ load. At this load level the increase in turbine heat rate could possibly be as much as 12-15%, resulting in output losses as high as 36 to 45 MW_e-hrs.

In the trickle flow approach a flow of 2% sodium (minimum flow requirement, per Ref. 5.2) and water/steam through the steam generators would be maintained. Again, this has the advantage of maintaining component temperatures and permitting a rapid startup the next morning. The energy loss is less than part load operation. For example, for a 15 hour hold duration, the energy expended would be 100 MW_e x 15 hr x 0.02 = 30 MW_e-hr.

Another advantage of the trickle flow approach over the part load approach is that it would allow the plant to operate in this mode for a longer period of time. For example, with full hot tanks (3 hrs full operation capacity), the plant can stay in standby for 15 hrs (at 20% load) using the part load approach, but it can last 150 hrs ($3 \div 2\% = 150$) using the trickle flow approach, allowing the standby to extend to a longer duration (e.g., an intermediate standby). Note that in either scheme the energy loss is proportional to the duration of the standby mode.

The trickle flow scheme however contains two drawbacks. Since the turbine and its feedwater heating system are not operating, the condensate must be heated to an

acceptable evaporator inlet temperature by other means. One possible way is to utilize the reheater discharge steam, but this would involve additional heat exchangers and associated controls. In addition, the flow levels are so low that the capability of the existing pump, valves and instrumentation would be deficient. A separate bypass system for the trickle flow would be required. A more detailed description of the trickle flow approach is contained in Appendix F.

The third alternative considered involves reducing the steam generator temperatures by controlling the inlet hot sodium temperature until a uniform temperature of 612°F (the cold tank temperature) is achieved. The steam generators would then be maintained at this temperature level. Sodium from the hot and the cold tanks are mixed to provide a controlled rate of reduction in steam generator inlet sodium temperature such that the maximum transient temperature change rate limit of 150°F/hr is not violated.

This approach was used for the shutdown of the steam generators of the Clinch River Breeder Reactor plant (Ref. 5.3). In such a baseload nuclear application, energy consumption and elapsed time during startup/shutdown were of little concern. However, for a solar plant it is desirable to maintain the steam generators near their respective normal operating temperatures to facilitate rapid restart following a shutdown. Therefore, this approach, which deliberately brings the temperature down, is deemed unsuitable for solar application.

5.3.1.2 Intermediate Term (Warm) Standby Receiver/Tower Side

For an intermediate standby (between 2 and 7 days) the Bottled-up approach described in the Short Term Standby Mode will also be used. However, as delineated in Figure 5-3, the temperature of sodium in the receiver panels would drop down below 400°F after about two days. This results from the large surface area, small sodium content, and relatively poor insulation of the receiver panels. The riser and the downcomer temperature after a two-day standby period are about 475°F and 750°F, respectively (Figure 5-2).

In order to avoid solidification of sodium in the receiver panel, it becomes necessary to provide a way of keeping the tower loop warm for standby periods longer than two days. Two options are available as discussed in the two alternatives considered below.

Referenced Approach

The selected scheme is to use sodium from the cold storage tanks to replenish the sodium in the tower loop and keep the loop near 600°F. This operation would be repeated periodically to maintain the loop temperature. Temperature monitoring would determine when recirculation of storage sodium is required. The frequency has been estimated to be once every 12 hours. The consideration is that the sodium temperature would drop by about 50°F in 12 hours and larger temperature drops may create thermal shocks in both the loop and the cold storage tanks during a startup.

The different rates of cooldown of the various parts in the tower loop require care in the operation. As described earlier, at the end of a 48 hr standby period the sodium temperature in the riser, receiver panel, and downcomer would be about 475, 400, and 750°F, respectively. If the replenishing operation begins at this time and the 600°F sodium from storage is circulated through the loop, the riser and the receiver panels would both be experiencing a temperature shock of 125°F (the 475°F sodium in the riser would first pass through the receiver and heat up the panels before the 600°F sodium enters the panels); but the downcomer would be subjected to a temperature shock of 350°F. In the event of a failure of the receiver insulation curtain drive mechanism which prevents the use of a curtain during standby, the receiver panels would be cooled at an even faster rate, resulting in more serious temperature shocks in the downcomer.

Appendix E, which addresses the question of downcomer temperature cycling, has shown that the temperature shock must be limited to below 125°F if the shock occurs once a week in order to avoid fatigue failure. Therefore, at the end of the 48 hour standby period the downcomer would still be too hot to accept the cold sodium. For this reason in the first replenishment operation cold sodium passage through the downcomer should be avoided. Instead, the overflow line valve would be opened and the circulating sodium would go from the receiver panel outlet header through the overflow line and back to the cold tanks. The circulation would be terminated once the sensors indicated that the temperature of the loop is near 600°F, and the tower loop will be left idle again.

The tower loop would cool down further if the standby period continues. The downcomer would eventually become suitable for accepting the circulating sodium. At this point the overflow line would be closed and the throttle valves opened, and sodium would return to the cold tank by way of the downcomer. The periodic replenishment operating would be repeated as necessary.

It should be mentioned that it has been assumed in the discussion above that the receiver panel exit main header, which connects the panels to the downcomer, would cool down at such a rate that it could accept the cold sodium from the panels without the temperature shock problem. Otherwise, a separate lower temperature header would have to be installed for the recirculation purpose. In order to avoid such a need, the insulation for the main header must be carefully designed.

Alternative Approach

The simplest approach to maintain the tower loop piping above 550°F would be the use of electric heaters. Trace heaters are available in the sodium piping, except the receiver panels, for the purpose of prewarming drained sodium piping before a fill (the receiver panels will be prewarmed by solar energy). Trace heaters would need to be installed at the backside of the receiver panels to keep them warm during a long standby period. In addition to this equipment cost, replacing the lost thermal energy by drawing electric energy from the utility grid would not be a favorable approach. Therefore, it does not appear to be economically attractive to use the heater scheme.

SG/EPGS Side

Referenced Approach

The bottled up mode of operation is continued for standby period of several days with only one modification, that being the capability to circulate cold sodium through the evaporator. The sodium in the evaporator loses its temperature faster than that in the superheater or reheater due to the presence of water in this component. Through evaporation the water absorbs larger amounts of heat from the sodium. The increase in pressure is controlled by the steam drum which vents off the generated steam. This causes a flow of steam through the upper half of the evaporator, carrying away even more heat. If this cooldown is permitted to continue the evaporator sodium could not be introduced into the storage system without some thermal shock and its associated stress. For this reason, when the evaporator sodium bulk temperature approaches 550° a circulating flow is set up which replaces the existing evaporator sodium with an amount from the cold storage tank at 612°F. This circulation is repeated each time the temperature decreases to 550°. A temperature history and recirculation loop is illustrated in Figure 5-10. Note that this system utilizes the same components (pump, mixing tee, etc.) as are required for evaporator startup, described in Section 5.3.2. The temperature decrease of the superheater and reheater lags behind that of the evaporator. Calculations show that circulation through these components will probably not be required for intermediate hold periods.

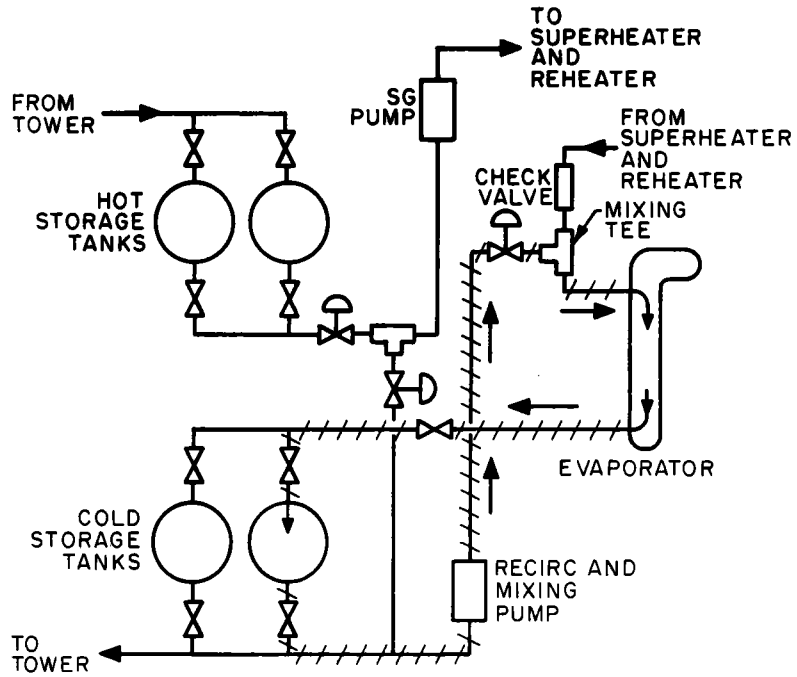
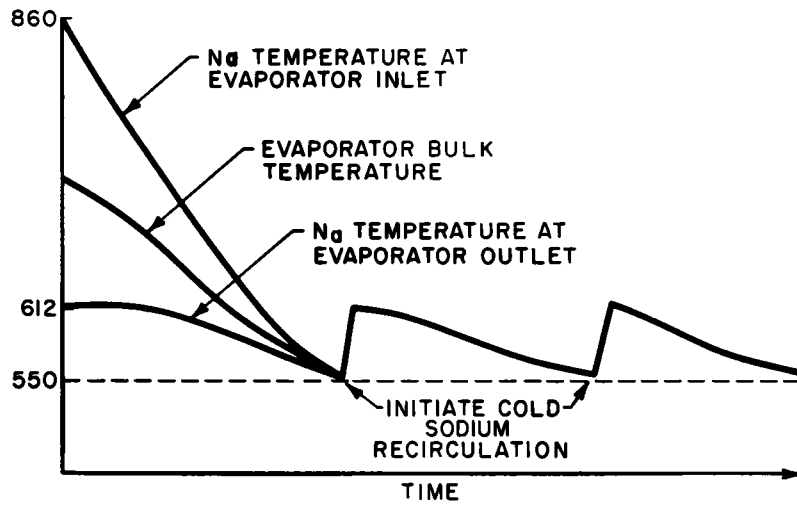


Figure 5-10. Evaporator Circulation Loop and Temperature History During Intermediate Term Standby

Alternative Approaches

Alternatives to the sodium circulation scheme include:

- using trace heaters
- using auxiliary boiler.

The additional costs of trace heater installation and operation for steam generators make the trace heater approach undesirable. The auxiliary boiler is an existing piece of equipment intended for steam generator prewarming from ambient temperature during a sodium fill/refill. However, the cost of the fuel used for the boiler made the scheme less economically attractive compared to the referenced approach.

5.3.1.3 Long Term (Cold) Standby

Receiver/Tower Side

Referenced Approach

For a long term hold (> 7 days) the "bottling-up with periodic replenishment" approach would continue to be used in the receiver/tower side. This mode of operation would continue until the sodium temperature in the storage tanks reaches 400°F. Beyond this point the system temperature will be maintained by electric trace heating. It should be pointed out that during a long term standby, if the cause of the standby does not occur on the receiver/tower side of the plant, sodium in the system can always be kept warm using solar energy collected such that the use of the trace heating system would not be required.

Alternate Approach

An alternative to the above scheme is to drain the sodium in the tower loop and fill the loop with argon cover gas for a long term standby of greater than 7 days. The sodium in the loop would be put into the storage tanks which are the best insulated components in the plant and will minimize heat losses. However, corrosion problems may develop in the drained tower piping due to possible contamination of the cover gas. Therefore, it is planned to drain the tower loop only when necessitated by maintenance or repair.

SG/EPGS Side

Preferred Approach

Standby period of this duration will see the superheater and reheater temperatures decay below the cold sodium storage temperature of 612°. When this happens, these components can be included in the evaporator sodium circulation loop as shown in Figure 5-11. The system is then maintained in this mode, recirculating as required, until the cold sodium temperature in the storage tanks reaches 400°F. At

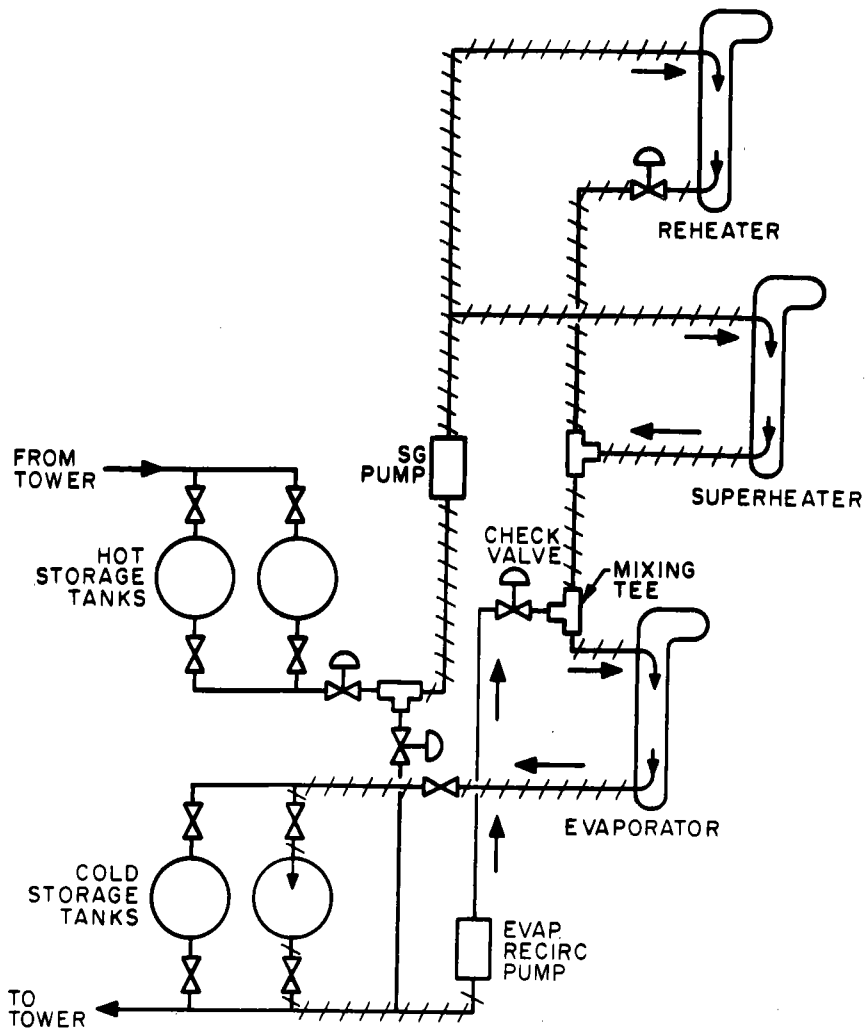
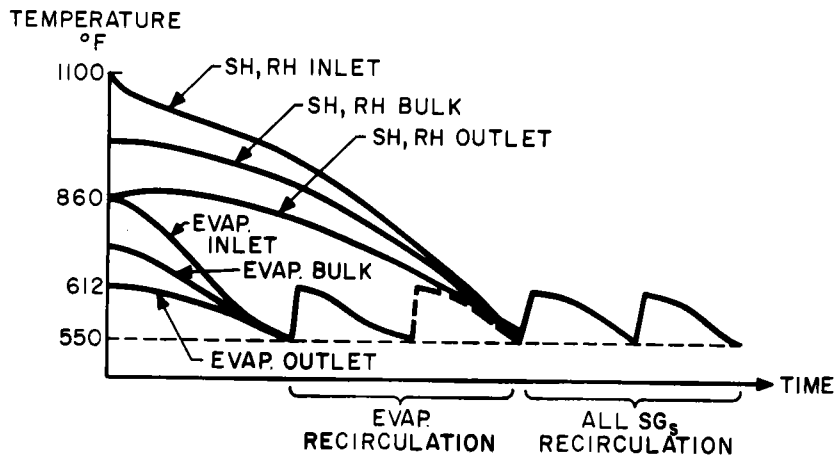


Figure 5-11. Steam Generator Circulation Loop and Temperature History During Long Term Standby

this point the temperature is maintained by trace heating and no further recirculation is required.

Preliminary calculation shows that by circulating sodium from cold storage tanks in the tower loop and the steam generator loop, the system temperature can be maintained above 400°F for a standby period on the order of four weeks.

Alternative Approaches

Considering the indefinite time period, the only possible alternative mode would involve draining of the sodium from the steam generator components. Because of the possibility of contamination in the argon cover gas, this alternative is recommended for emergency situations or for the maintenance/repair of the steam generator components.

A discussion of the sodium drainage approach is provided in Section 5.3.5.2.

5.3.2 STARTUP MODES

These modes cover the transition between the various standby modes and normal operation. The plant will be in either the hot, warm or cold start mode depending on the duration of the standby period prior to a start. Startup procedures for these modes are described in this section.

Standard startup constraints described in the GE operating manual for the reheat turbines, Ref. 5.1, must be complied with during the startup. The readers are also referred to the discussion on turbine warmup rates during a startup included in the Phase I report. The restrictions on the sodium component temperature change rates must also be observed.

5.3.2.1 Cold Start

A cold start condition exists when the plant has been shut down for more than a week. The temperature conditions of the plant prior to a cold start are:

- All sodium containing piping and components are at temperatures near the cold storage tank temperature as a result of the circulation scheme using cold tank sodium. The extent of temperature drop from the 612°F normal cold tank temperature depends on the length of the shutdown period. All are kept above 400 by trace heaters.
- The steam turbine first stage inner metal temperature is below 300°F.

Tower Side

The insulation curtain covering the receiver is dropped to expose the receiver panels. The tower pump is started to establish a flow through the receiver. Selected heliostats are focused on the receiver. The temperature set point for the

EM pump control is gradually ramped from the initial value to the rated temperature as the receiver sodium flow rate is slowly increased. The sodium flow rate would be ramped as necessary to accomplish an acceptable rate of change of temperature of the various sodium system components. As the warmup progressed, more heliostats would be focused on the receiver to increase the heat input. When the rated outlet temperature (1100°F) is achieved, the receiver is then operating under automatic control.

The return flow from the receiver can initially be valved to either the cold or the hot tanks depending on the sodium temperature in the downcomer. Later as the temperature increases, the return flow would be only to the hot tanks. The warmup of the cold and hot tanks to their respective normal operating temperatures (612°F and 1100°F) must be maintained and controlled such that the limits of the following parameters would not be exceeded:

- the rate of change of tank wall temperature
- the temperature differential between the inner and outer walls of the tank
- the temperature differential from the top to the bottom of the tank.

Determination of the limits for the above parameters is recommended in the preliminary design phase of the plant.

Steam Generators

The steam generator sodium pump would be started and controlled to supply sodium to the steam generation sections. The sodium to the superheater and reheater would be a mixture of the hot and cold tanks' supply to obtain the proper heating rate of 150°F/hr. The sodium flow will be maintained at 10% until the steam turbine is ready for loading. The steam drum recirculation pump is activated, establishing a flow of water through the evaporator. In this way the water in the evaporator and steam drum is heated along with the sodium. When the evaporator outlet sodium temperature reaches 612°F, it will be maintained at this level while the superheater/reheater inlet sodium temperature continue to rise at the 150°F/hr rate. The sodium temperature at the evaporator outlet is maintained by controlling the amount of feedwater flow to the evaporator. As the feedwater heating system is not operative at this time, the condensate must be heated to approximately 500°F by the auxiliary boiler. A typical flow and temperature history for the water and sodium is illustrated in Figure 5-12.

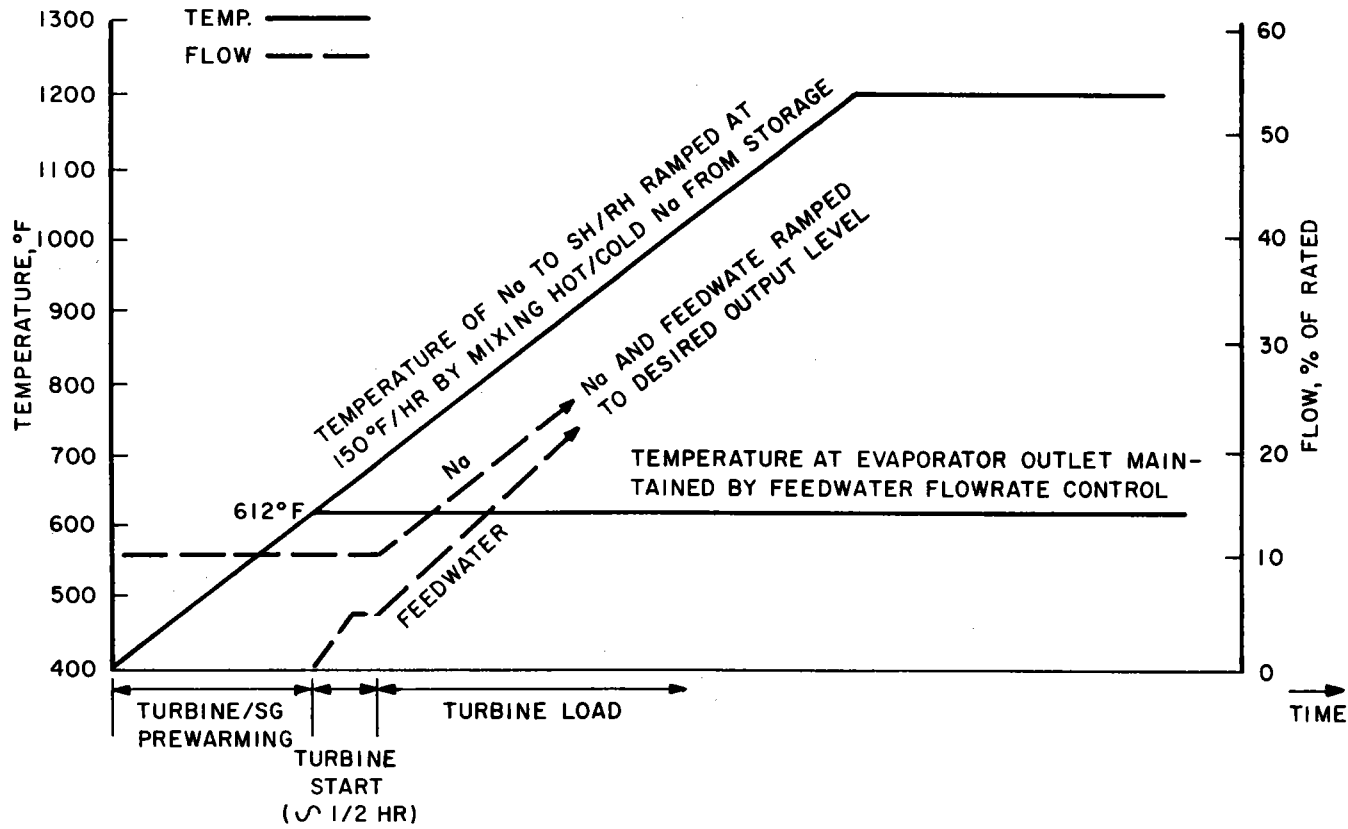


Figure 5-12. Flow and Temperature History of Steam Generator During Cold Start

EPGS

A cold start condition exists when the steam turbine first stage inner metal temperature is below 300°F and the turbine rotor must be preheated. It is assumed that the turbine lube oil system is fully operational and that the turbine generator unit has been on turning gear for a sufficient period of time to have the shaft eccentricity near a value that will be acceptable for turbine roll.

Shortly after the warmup of the steam generators is started, the warmup of the EPGs can be started. Steam for this operation is obtained from the steam drum, with the pressure being reduced to 55-70 psig prior to admission to the turbine. The main steam line drains would be open and the turbine bypass system would be placed in the startup control mode for the warmup period. Condensate pumps, boiler feed pumps and other necessary pumps would be started. The coordinated warmup of the entire sodium and steam systems would continue until the main steam pressure has reached approximately 25% of rated (600 psia). At this point the turbine steam seals would be applied and condenser vacuum established so that the turbine prewarming can be started. The prewarming of the steam turbine rotor would continue until the manufacturer's recommendations for prewarming (Ref. 5.1) are satisfied.

After turbine rotor prewarming is completed, the warmup of the sodium and steam system would continue until steam pressure and temperature conditions are established for turbine roll. This may involve adjustment of the turbine bypass system and steam temperature controls to establish a satisfactory steam-metal mismatch for the turbine cold start requirements.

When the proper conditions for turbine roll have been established, the turbine would be accelerated and loaded based on turbine rotor stress requirements and the heating limitations for the steam generators.

5.3.2.2 Warm Start

A warm start condition exists when the plant has been shutdown for a period of between 2 to 6 days. The conditions of the plant before a warm start are:

- The piping and components in the sodium loops (tower side and SG side) are near the cold storage tank temperature.
- The hot storage tank temperature is not much lower than 1100°F (for a 1/4 full hot tank, the temperature drop after a 7 day standby period is estimated to be 115°F).
- The steam turbine first stage inner metal temperature is greater than 300°F.

Procedures for a warm start would be similar to a cold start. However, assuming enough quantity of hot sodium near 1100°F is available in the hot storage tanks, the steam generators would be started a few hours before sunrise since they are the time limiting item.

A unique situation exists between the superheater/reheater outlets and the evaporator inlet which requires special attention. As shown in Figure 5-6, the sodium temperature at the bottom of the SH/RH is relatively constant at 860°. The evaporator inlet, however, cools relatively quickly for reasons explained in the discussion of SG standby modes, Section 5.3.1. At some time during an intermediate standby the temperature difference between these two points exceeds 150° and a re-establishment of sodium flow is not possible without a substantial thermal shock to the evaporator. For this reason the sodium coming from the SH/RH outlet is mixed with sodium from the cold storage tank to match the evaporator temperature. This temperature is then ramped up to 150°/hour until the normal operating point (860°) is reached. From this point on, all sodium flow to the evaporator comes from the SH/RH outlets and the warmup procedure is identical to that described for the cold start, Section 5.3.2.1.

5.3.2.3 Hot Start

The plant is in a hot start condition after a standby period of less than 1 day. This condition will, in general, exist after an overnight standby. All the startup procedures will follow the warm startup sequence.

For shorter standby such as a unit trip or some other rapid unloading of the steam turbine generator unit, the tower/receiver side of the plant could continue its operation, as only the SG/EPGS side is affected. The steam flow (rejected by the turbine) will be taken by the turbine bypass system for some interim period of time until the plant is shut down or the turbine generator unit can be restarted, synchronized and reloaded. To avoid severe cooling of the turbine metal during hot restart conditions, the turbine bypass system would be operated at a steam flow which will enable the superheater and reheater to operate in a region which will provide the required steam temperatures and thus avoid severe negative stresses in the turbine rotor.

5.3.3 NORMAL OPERATION MODES

Normal full load operation has been discussed extensively in the Phase I study and will not be repeated in this report.

System configurations during part load operation is identical to full load operation. Variable pressure operation is expected during part load. To better define the system conditions during part load operation, information on performance, flow rates, and state points at several part load levels are required.

5.3.4 SHUTDOWN MODES

5.3.4.1 Normal Shutdown

When there is a loss of insolation coincident with the end of the day, as determined by the master control clock, or when directed by the utility or the local operator, the plant is placed in the shutdown mode. The sequence of the shutdown is essentially the reverse of the startup sequence.

As insolation decreases, the hot sodium output from the receiver also decreases until there is essentially no more hot sodium being generated. The tower pump is secured and the throttle valves are shut off. The tower loop is then bottled up and placed in the standby mode. Coincident with the above actions, the heliostats are all returned to the stow position, and the receiver insulation curtain is raised to cover the receiver panels.

While the tower loop has been shut down, hot sodium in the storage tanks will continue to be discharged to the steam generators and electric power produced by the EPGs. The operation will continue until the hot sodium inventory in storage is reduced to a predetermined amount at which time the steam generators and the EPGs will be shut down. The amount of hot sodium left in the storage tanks must be enough to meet the SG/EPGs warmup sodium requirement.

When the shut down signal is received, flow rates in the SG and EPGs will be reduced to about 10% (expected minimum operating range of pumps, valves, instrumentations, etc.) at which time the steam generator pump is secured and the steam generators bottled up. The steam turbine is tripped and steam is bypassed to the condenser. The system is then in the standby mode.

5.3.4.2 Emergency Shutdown

The emergency shutdown sequence will be initiated for major malfunctions or alarm indications such as the following:

Sodium Side

- Receiver panel overtemperature
- EM pump malfunction
- Loss of sodium flow to tower

- Loss of sodium flow to steam generators
- Sodium/water reaction

Water/Steam Side

- Generator breaker trip
- Turbine overspeed trip
- Steam header overpressure/loss of pressure
- Steam header loss-of-flow
- Loss of feedwater flow
- Loss of steam drum recirculation flow
- Loss of condenser vacuum
- Condenser high/low level limits exceeded
- Loss of condensate flow.

The plant will be shut down in a manner similar to that used in the shutdown sequence. A local reset will be required prior to recommending plant startup to ensure that the cause of the emergency shutdown has been corrected and to ensure no plant damage has been incurred.

Since the storage tanks effectively decouples the tower loop operation from the power generating activity, it is possible to shut down only the receiver/tower side or the steam generator/EPGS side. That is, if the cause of emergency shutdown occurs on the tower loop side, only the collector and the receiver subsystems need be shutdown, while the steam generator/EPGS operation can continue as long as hot sodium from storage is available. If the problem occurs on the steam generator/EPGS side, the collector and the receiver subsystems can go on producing hot sodium until the hot storage tanks' capacity limit is reached.

The flexibility of shutting down only the side of the plant where emergency conditions have occurred would reduce the time required to recommence plant operation once the cause of the emergency shutdown is corrected, thereby minimizing the interruption of power generation.

A unique situation associated with the plant is the potential for a sodium/water reaction in the Steam Generator modules. A reaction can occur as a result of a leakage of water/steam through a faulty/defective tube into the sodium side. Steam Generator tube leaks, although uncommon, usually begin as very small tube defects due

to material or fabrication abnormalities. Hydrogen, oxygen and or acoustic detectors are placed at strategic location in the loop to detect micro size leaks before the leak becomes large enough to damage adjacent tubes. Upon detection operation is terminated, the leak located and suspect tubes plugged.

If leaks are allowed to grow, damage to adjacent tubes or structure can occur. With an increase in pressure generated from the reaction, rupture discs in the loop will burst, thereby relieving the loop pressure and discharging the generated reaction products into the relief system storage vessel.

5.3.5 OTHER TOPICS

Several topics related to plant operating modes are included in this section. The subjects include: cloud cover standby, drainage approach, and initial fill and refill of sodium.

5.3.5.1 Cloud Cover Standby

A situation similar to a hot standby is the cloud cover standby. During a short term cloud cover, the receiver/tower side will be bottled-up as is done in a hot hold. But normally the steam turbine power generation is continued by operating from storage during short term cloud cover. However, if the hot storage tanks are at a low level (i.e., expected cloud cover duration exceeds storage capacities required to generate desired load) then it may be necessary to revert temporarily to a standby condition. The system configuration in such a situation is essentially identical to the short term standby mode.

5.3.5.2 Drainage Approach

In the Phase I study, it was proposed to store all the drained sodium from the steam generator loop and the tower loop in a separate drain tank. The tank size required was 17,000 ft³ and SA515 carbon steel was specified as the material. To

avoid material problems, hot Na (1100°F) in the piping would have to be cooled before drainage, by losing heat to the ambient, until its temperature drops to the allowable temperature for storage in the drain tank. Since the sodium containment piping is well insulated, the cooling process would be slow and might adversely affect the capability of shutting down the plant in a reasonable amount of time.

The required drain tank size would be greatly reduced if the storage tanks are used to receive drained sodium. It is proposed to drain hot (~1100°F) sodium in the receiver, downcomer, superheater and reheater into the hot storage tanks, and drain the cold (~612°F) sodium in the riser, and evaporator into the cold storage tanks. The drainage paths are illustrated in Figures 5-13 and 5-14. Estimated reduction in the required drain tank size using this approach is 6,200 ft³.

To overcome the gravity heads, pressurized argon will be used at two locations: the top of the receiver and the point of split of sodium entering the superheater and reheater, as indicated in Figures 5-13 and 5-14. The only line added to facilitate this drainage approach is the line from a point after the superheater reheater exit sodium mixing tee to the bottom of the hot storage tank.

All sodium in the remaining piping and components will be drained by gravity force into the drain tank. It is proposed to use one drain tank made of 316SS to accommodate both hot and cold sodium. An alternative would be to employ two smaller drain tanks; one made of 316SS for hot sodium drainage, the other made of carbon steel for cold sodium drainage. The one-tank concept is preferable since the savings in material cost by using carbon steel for cold sodium will be outweighed by the costs of field assembling one more tank and the associated piping/valving. It should be mentioned that care must be exercised in putting the hot/cold sodium into the drain tank because of the big difference in their temperatures. A sequence which would drain the cold sodium first is recommended. This will warm the drain tank to ~600° prior to the draining of the hot sodium, thereby minimizing the thermal shock to the tank/piping.

5.3.5.3 Initial Fill and Refill of Sodium

Before a filling operation, all piping or components except the storage tanks which are filled with argon would first undergo several cycles of pressure reduction to full vacuum followed by back filling of argon at 14.7 psia. This would ensure their being free from contamination and leakage. The approach is not suitable for the storage tanks since they are not designed to take external pressure. Instead, multiple purging will be used for the storage tanks.

5-36

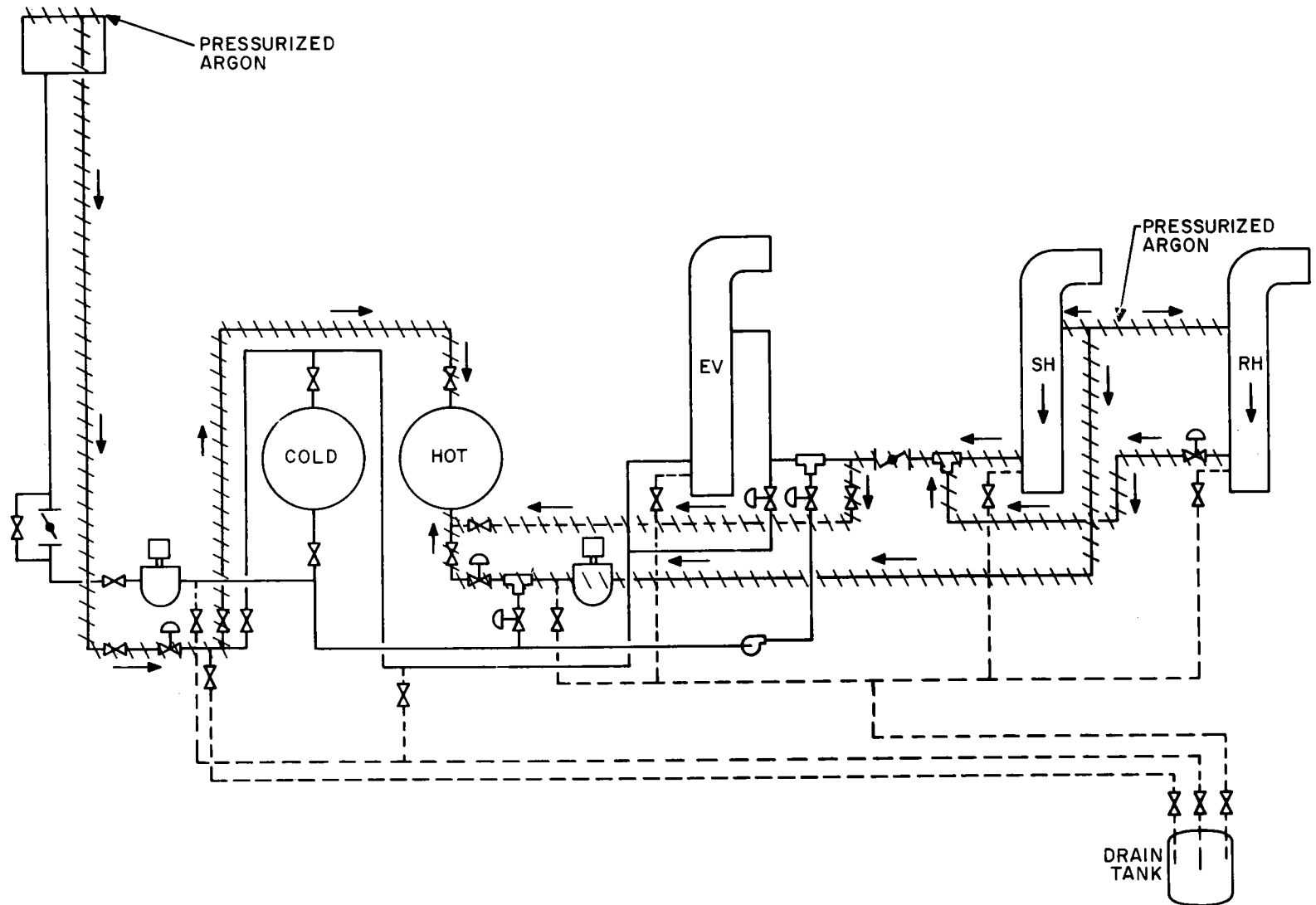


Figure 5-13. Sodium in Components/Piping Drained Into Hot Storage Tanks

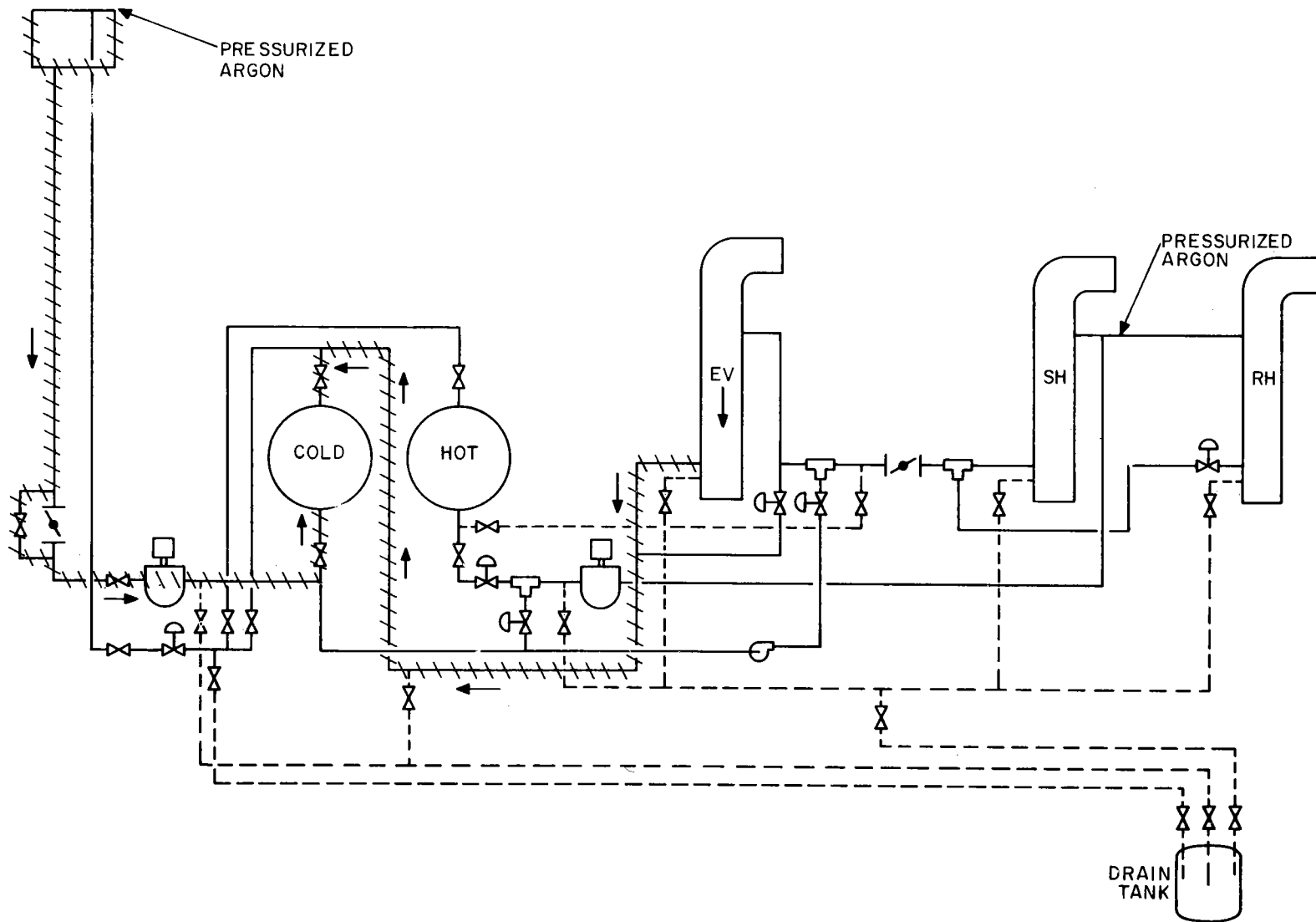


Figure 5-14. Sodium in Components/Piping Drained Into Cold Storage Tank

Initial Fill

Initial fill of sodium into the system is accomplished by filling sodium at a minimum of 400°F into the storage tanks. Sodium in the railroad tank cars is moved through the fill lines into the storage tanks using argon gas. The fill lines and the storage tanks will be preheated by trace heaters to 400°F before the filling operation.

Refill

As described in Section 5.3.1, sodium drainage is planned only when the removal of sodium is required for maintenance and repair purposes. The drainage approach selected in Section 5.3.5.2 calls for draining the majority of sodium in the system into the storage tanks, and the rest into the drain tank. Prior to filling sodium, all sodium containing piping and components are preheated to a temperature of 400°F. This is accomplished by the trace heaters except for the receiver panels and the steam generators; the receiver panels will be preheated using the solar energy from the collector field, and the steam generator preheated using hot water and steam from an auxiliary boiler.

Sodium in the drain tank is first forced back to the cold storage tanks by pressurizing the drain tank with argon gas. The insulation curtain covering the receiver is dropped to expose the receiver panels and selected heliostats are focused on the receiver to preheat the receiver panels. The panel temperatures are monitored until reaching 400°F. At this point, sodium in the cold tanks is pumped into the tower loop to displace the cover gas (the throttle valves at the bottom of downcomer are closed). A filled loop is detected by the overflow of sodium from the overflow line at the top of the receiver. The throttle valves are then opened and the flow from the receiver returns to the cold tanks, thus establishing a flow through the tower loop. The tower loop is then ready for a cold start.

In preheating the steam generators, care must be exercised to minimize temperature differentials between the steam generator module shell and the tubes. The following (Ref. 5.4) are to be followed.

- Before initiating the warmup, the steam generators is subjected to several cycles of pressure reduction to full vacuum followed by back filling of argon, while the tubes are filled with nitrogen.
- After the vacuum cycles are completed, and it is determined that there are no leaks, the tube side of the SG is filled with ambient temperature water. The water is circulated through the steam generators which are in series with an auxiliary boiler. The temperature of the circulating water is heated at 10°F per hour using the auxiliary boiler. The heat of the circulating water is

increased from ambient ($70^{\circ} + 15^{\circ}\text{F}$) temperature until the inlet water of the SG is 450°F . The time required for the inlet water temperature to get to 450°F is approximately 38 hours. The 450°F temperature of the inlet water is maintained for approximately 62 hours to soak the outer shell of the SG module to obtain a nominal shell temperature of 400°F . At the end of the soak period, the inlet water temperature is reduced at 10°F per hour until the approximately isothermal conditions of 400°F exist in the SG modules. The shell side of the modules is thus subjected to one pressure reduction to full vacuum cycle followed by back filling with argon to 14.7 psia. The SG modules are then filled with 400°F sodium, and are in a position for a cold start.

5.4 RECOMMENDED REVISIONS TO THE PHASE I PLANT DESIGN

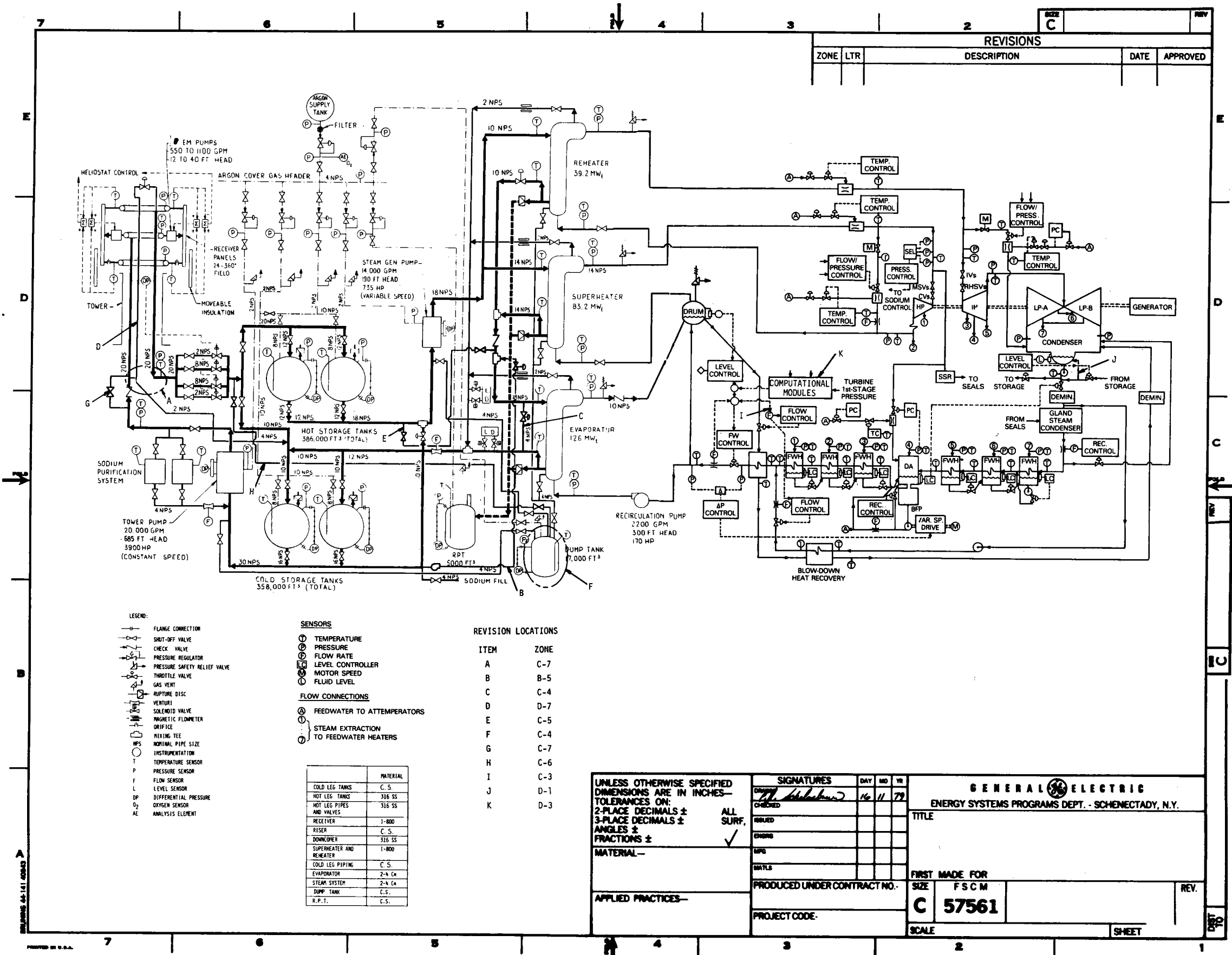
As a result of the operating mode analysis described in the previous sections, several revisions to the commercial plant design are made. These revisions are listed in Table 5-4 (Items a to h) and are indicated in the overall plant schematic shown in Figure 5-15. Also included in Table 5-4 and Figure 5-15 are the corrections of the errors contained in the Phase I schematic diagram (Items i to k) discovered in the present analysis.

5.5 AREAS FOR FUTURE STUDY AND RESOLUTION

Several areas of concern were revealed during the course of the present study which require future study and resolution. These areas are identified in Table 5-5 along with the recommended actions.

Table 5-4
 REVISIONS TO OVERALL PLANT SCHEMATIC

<u>Item</u>	<u>Revision</u>	<u>Reason</u>	<u>Referenced Section in this Report</u>
a	Elimination of shunt valve at bottom of tower.	Revised short term standby mode approach.	3.1.1
b	Addition of the line from cold storage tank to SH/RH exit Na line. Also associated pump, valve, and mixing tee.	To provide temperature control of Na entering evaporator during startup or standby recirculation.	3.2.1 and 3.1.2
c	Na bypass line between inlet and outlet of evaporator.	To bypass part of the mixture of Na (item b above) to obtain correct flow rate entering evaporator during startup.	3.2.1
d	Increase diameter of overflow line from 2" to 6".	Overflow line is also used for receiver Na recirculation during standby. Original size too small to achieve reasonable rate.	3.1
e	Addition of line from SH/RH exit mixing tee to bottom of hot storage tanks.	For SH/RH hot Na drainage.	3.5.2
f	Reduction in drain tank size by 6,200 ft ³ . Also material change from carbon steel to 316SS.	Use of storage tanks for Na drainage. Material changed to accept hot Na.	3.5.2
g	Addition of bypass around riser check valve.	To allow reversed flow direction during draining operation.	3.5.2
h	Addition of line from tower downcomer throttle valve exit to drain tank.	Hot sodium drainage.	3.5.2
i	Reverse direction of arrowhead.	To represent the correct signal direction	
j	Rerouted line from condensate storage tank, for condenser level control.	To represent the correct path.	
k	Changed from "compressor" to "computational modules."	A typo.	



REVISIONS				
ZONE	LTR	DESCRIPTION	DATE	APPROVED

- LEGEND:**
- FLANGE CONNECTION
 - SHUT-OFF VALVE
 - CHECK VALVE
 - PRESSURE REGULATOR
 - PRESSURE SAFETY RELIEF VALVE
 - THROTTLE VALVE
 - GAS VENT
 - RIPTURE DISC
 - VENTURI
 - SOLENOID VALVE
 - MAGNETIC FLOWMETER
 - ORIFICE
 - MIXING TEE
 - NOMINAL PIPE SIZE
 - INSTRUMENTATION
 - TEMPERATURE SENSOR
 - PRESSURE SENSOR
 - FLOW SENSOR
 - LEVEL SENSOR
 - DP
 - DIFFERENTIAL PRESSURE
 - O₂
 - OXYGEN SENSOR
 - AE
 - ANALYSIS ELEMENT

- SENSORS**
- ① TEMPERATURE
 - ② PRESSURE
 - ③ FLOW RATE
 - ④ LEVEL CONTROLLER
 - ⑤ MOTOR SPEED
 - ⑥ FLUID LEVEL
- FLOW CONNECTIONS**
- ⑦ FEEDWATER TO ATTEMPERATORS
 - ⑧ STEAM EXTRACTION TO FEEDWATER HEATERS

REVISION LOCATIONS

ITEM	ZONE
A	C-7
B	B-5
C	C-4
D	D-7
E	C-5
F	C-4
G	C-7
H	C-6
I	C-3
J	D-1
K	D-3

	MATERIAL
COLD LEG TANKS	C. S.
HOT LEG TANKS	316 SS
HOT LEG PIPES AND VALVES	316 SS
RECEIVER	1-800
RISER	C. S.
DOWNCOMER	316 SS
SUPERHEATER AND REHEATER	1-800
COLD LEG PIPING	C. S.
EVAPORATOR	2-1/2 Cn
STEAM SYSTEM	2-1/2 Cn
DUMP TANK	C. S.
R.P.T.	C. S.

UNLESS OTHERWISE SPECIFIED DIMENSIONS ARE IN INCHES— TOLERANCES ON: 2-PLACE DECIMALS ± 3-PLACE DECIMALS ± FRACTIONS ±

MATERIAL—

APPLIED PRACTICES—

PROJECT CODE—

SIGNATURES				DAY	MO	YR
DESIGNED	<i>[Signature]</i>			16	11	79
CHECKED						
DRAWN						
ENG'G						
INSTR.						
PRODUCED UNDER CONTRACT NO.	C 57561					
PROJECT CODE						

GENERAL ELECTRIC
ENERGY SYSTEMS PROGRAMS DEPT. - SCHENECTADY, N.Y.

TITLE

FIRST MADE FOR

SIZE F S C M

SCALE

SHEET

Figure 5-15. Revision To Plant Design

Table 5-5

AREAS OF CONCERN FOR FUTURE STUDY AND RESOLUTION

<u>Component</u>	<u>Operating Mode</u>	<u>Concern</u>	<u>Recommended Action</u>
Steam Generators	Standby, startup shutdown	Temperature change rate limits need substantiation	Detailed analysis to establish confident values
Evaporator	Standby	Cooldown rate dur- ing standby may exceed limits	Detailed modeling to confirm compliance with limits
Storage Tanks	Startup	Warmup rate limits not established	Analysis to determine limits
Receiver Insulation Curtain	Standby	Sketchy design specifications	Better definition
Hot/Cold Sodium Mixing Device	Cold startup/full	Sketchy design specifications	Better definition

SECTION 6

SYSTEM ANNUAL PERFORMANCE ANALYSIS

6.1 INTRODUCTION

A computer program has been developed to facilitate system annual performance calculations. It performs hour-by-hour simulations of system performance based on given system/subsystem design parameters along with insolation and weather data. The computer model is a valuable tool for performing future system level design/trade-off studies. This section summarizes the development of the computer program.

The model is structured with a main program containing input and output sections and with a number of interpolating polynomials which predict the performance of the components/subsystems. Three modes of system operation (normal operation, warmup, and standby) are considered. Following the plant operating logic, the efficiencies of the subsystems are combined to determine how much of the solar energy is converted to electricity. System performance can be printed out at hourly, daily, monthly, or annual intervals as desired. A description of the model is presented in Section 6.2.

The model was used to generate plant performance information using a magnetic tape containing insolation and weather data for Barstow, California for the year 1976. The results are given in Section 6.3.

A listing of the computer program is included in Appendix G.

6.2 COMPUTER MODEL DESCRIPTION

6.2.1 PROGRAM STRUCTURE

Figure 6-1 shows the top level flow chart for the model, identifying major sections in the program.

System inputs include the following two categories:

- Weather Tape - an hourly tape containing climatology data such as direct normal insolation, ambient temperature, etc.
- System Design Information - data such as total heliostat reflective area, thermal storage size, etc., which defines the system configuration.

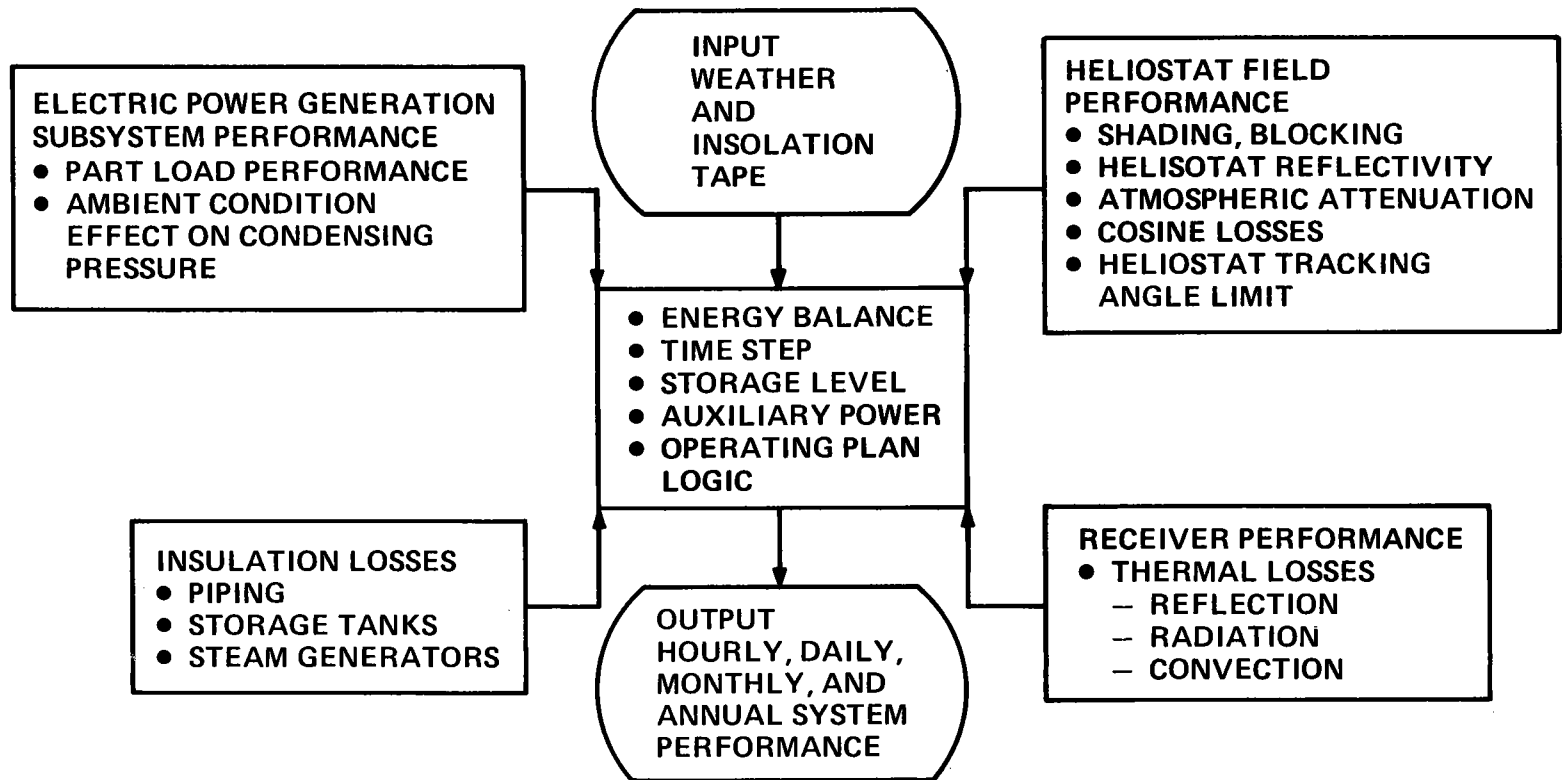


Figure 6-1. System Annual Performance Model Program Structure

The program output provides printout of complete energy balances and efficiencies of the system and various subsystems at hourly, daily, monthly, and annual intervals.

The main program controls the simulation to generate the desired performance output on the basis of the data inputs and component/subsystem performance models. As such, it maintains the simulation hourly time-step and in doing so updates and sums the variables which reflect the system energy balance. Within each time step, the main program selects the proper component performance polynomials based on the system operating plan control logic and the weather tape. Also, based on component operation, the program sums up operating auxiliaries.

6.2.2 OPERATING PLAN LOGIC

Figure 6-2 shows the operating plan logic flow chart. Since the storage tanks decouple the receiver/tower side of the plant from the steam generator (SG)/Electric Power Generation Subsystem (EPGS) side, operation of the two sides of the plant is independent of each other most of the time. An exception is when the storage is filled which requires that defocusing action be taken in the heliostat field.

Receiver/Tower Side

Operation of the receiver/tower side depends on the direct normal insolation level. The collection system would be put into operation if the insolation level is sufficiently high such that the net energy absorbed by the sodium in the receiver panels is at least enough to

- overcome the thermal losses from the receiver and tower loop piping, and
- feed into hot storage tanks the amount of thermal energy equivalent to the auxiliary electric energy consumed by the tower loop pumps and the heliostats.

This minimum energy absorbed by the receiver is very low, about 2 MW compared to the 408 MW design point value (Table 6-3). The corresponding "adequate" insolation level is time dependent, since the heliostat field efficiency varies throughout the year and the receiver efficiency decreases with decreasing incident flux on receiver (Figure 6-5). If the insolation level falls below the adequate value, the tower loop goes into the standby mode. The time required to bring the tower loop back to its normal operating temperature following a short or an intermediate term standby period is short (order of minutes), and its impact on operation is neglected.

SG/EPGS Side

According to the state of the hot sodium storage, the SG/EPGS side of the plant operates in one of the three modes: normal operation, warmup, and standby. In determining when to start the SG/EPGS in the morning, two possibilities exist:

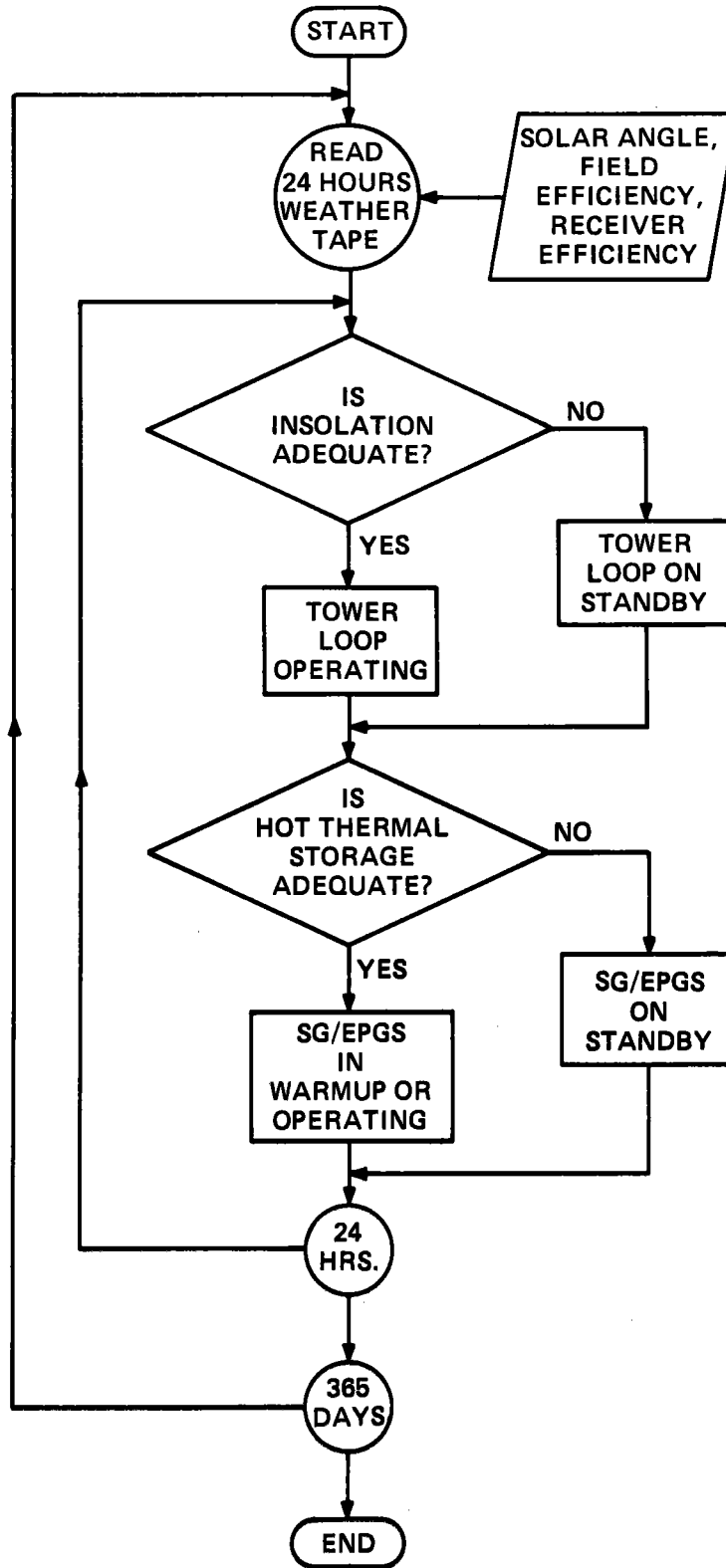


Figure 6-2. System Operation Logic Flow Chart

Approach 1: Start the SG/EPGS as soon as hot sodium is available.

Approach 2: Store hot sodium until some level of inventory has been established, then discharge to SG/EPGS.

Approach 1 has the advantage that space is made available in the hot tanks such that the chance of the tank's capacity being filled, thus requiring heliostat defocusing, is minimized. This advantage is particularly important for a day with high insolation levels. However, early in the morning when the insolation level is lower, the hot sodium produced may only be sufficient for EPGS to operate in part load, resulting in lower efficiency.

The situations are just the opposite for Approach 2. In this approach, hot sodium will be accumulated to allow EPGS to operate at higher load fractions for better performance. For a day with poor insolation, this approach would be preferred. However, on a high insolation day, the hot tanks would be quickly filled thus necessitating heliostat defocusing.

From the above discussions, it is apparent that Approach 1 should be taken for a sunny day, and Approach 2 for a cloudy day. The plant operator would make his decision based on weather forecast. In the present study the total daily insolation is known in advance from the weather data tape. In the computer model, for a day with daily insolation greater than $\frac{6 \text{KwHr}}{\text{m}^2}$ Approach 1 would be used. The selection of this number is based on the following considerations:

- Arbitrarily defining a sunny day as one which provides sufficient energy for 10 hours of EPGS operation at full power
- Assume an average of 10 sunny hours a day
- Total heliostat Reflective Surface Area = $1.108 \times 10^6 \text{ m}^2$
- Required solar energy incident on heliostats for one hour of EPGS full power operation = $(1.108 \times 10^6 \text{ m}^2 \times 950 \text{ w/m}^2) / 1.5 = 701 \text{ MW}$ (the heliostat field is sized to produce a 1.5 solar multiple at 950 w/m^2 insolation level)
- $\frac{701 \text{ MW} \times 10 \text{ hr}}{1.108 \times 10^6 \text{ m}^2} = 6.33 \frac{\text{KwHr}}{\text{m}^2}$ per day.

Therefore, a value of $6 \frac{\text{KwHr}}{\text{m}^2}$ has been chosen as a criterion for storage discharge method selection.

Other operating assumptions were made to simplify the computer model:

Approach 1 (for a sunny day)

- Hot sodium will be used to produce electricity as soon as it becomes available early in the morning, if the solar energy collected can at least provide enough hot sodium for EPGS to operate at half load

- All hot sodium in storage will be used up at the end of the day. Since for a sunny day the EPGS will be operating from storage after sunset, full load operation can be maintained during this period.

Approach 2 (for a cloudy day)

- The SG/EPGS will not be put into operation unless the accumulated hot sodium in storage is enough to sustain at least one hour of full load EPGS operation.
- If at the end of the day the amount of residual sodium in storage is small (not enough to supply one hour of full load operation), it is allowed to be stored overnight. Therefore, in those days when the insolation levels are very low, the receiver/tower side of the plant can still collect energy, but the EPGS side would not be started
- Full load operation of EPGS is assumed for simplicity. In reality, a plant operator could allow the EPGS to operate in part load to stretch the hot sodium storage inventory over a longer operating period should the need arise. For example, if it is forecasted that the insolation levels would be high in the morning and late afternoon, but low around noon, the plant operator could manipulate the sodium discharge rate so that the solar energy collected in the morning can carry the plant through the low insolation noon period to avoid the need to shutdown/restart and the resulting interruption of power output.

6.2.3 MODEL DESCRIPTION

Insolation and Weather Data

The insolation and weather data used in the performance analysis is the hour-by-hour data for Barstow, California for the year 1976. An Aerospace Corporation magnetic tape (Ref. 2.1) containing this information was used. The daily total insolation data for Barstow in 1976 is presented in Figure 6-3. It can be seen from this figure that the durations of the low or no insolation periods are less than 4 consecutive days. Therefore, there would be no long term standby (> 7 days) and therefore no cold start caused by weather conditions.

Heliostat Field Performance

The field efficiency is defined as

$$\text{field efficiency} = \frac{\text{power impinging on receiver}}{\text{total reflector surface area} \times \text{normal solar flux}}$$

The losses incurred include: heliostat shading and blocking, reflectivity, atmosphere attenuation, and geometric (cosine) losses.

The variation of field efficiency with time for the twenty first day of each month is shown in Figure 6-4. These trends are based on data presented in the Phase I study report (Ref. 1.1). In this figure, the heliostat tracking limit is

6-7

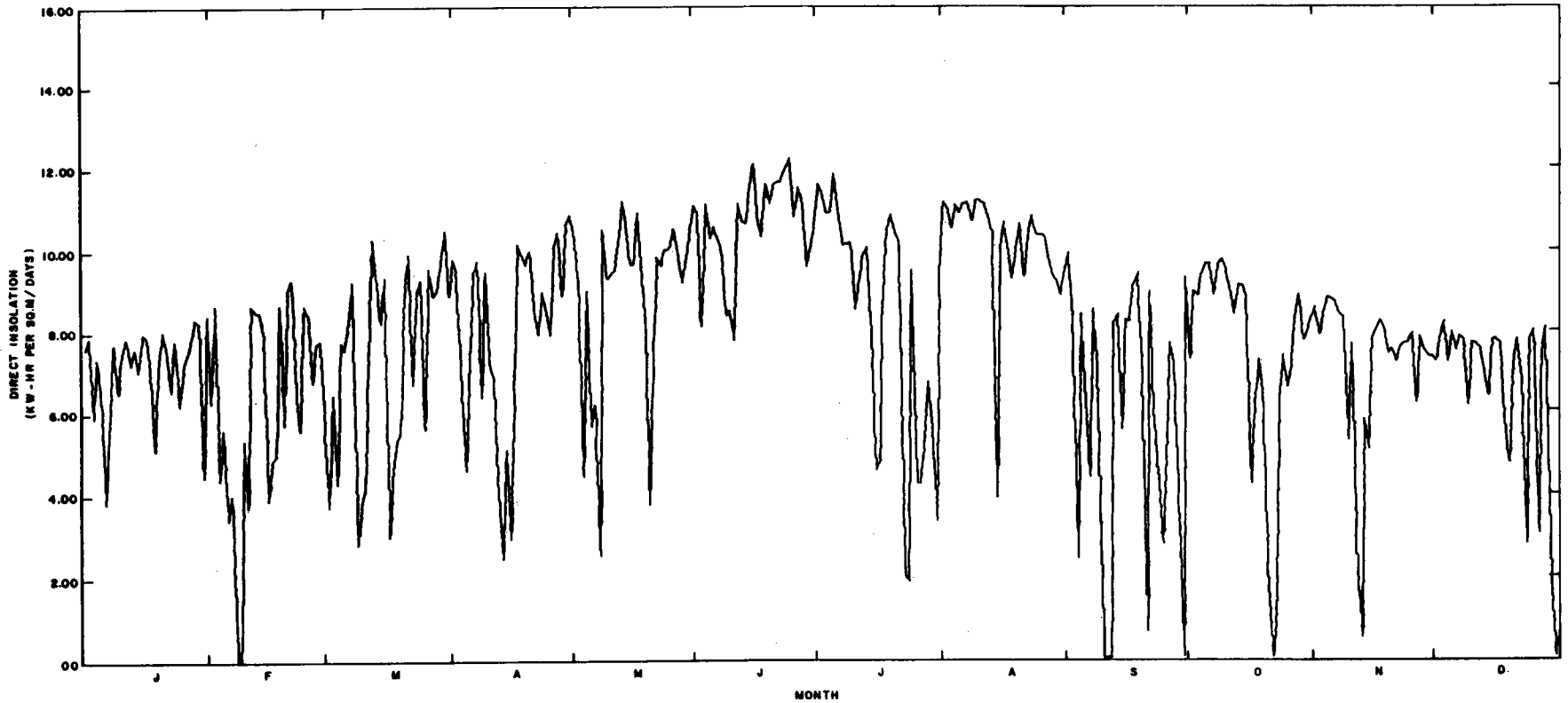


Figure 6-3. Daily Total Insolation Data for Barstow, California in 1976

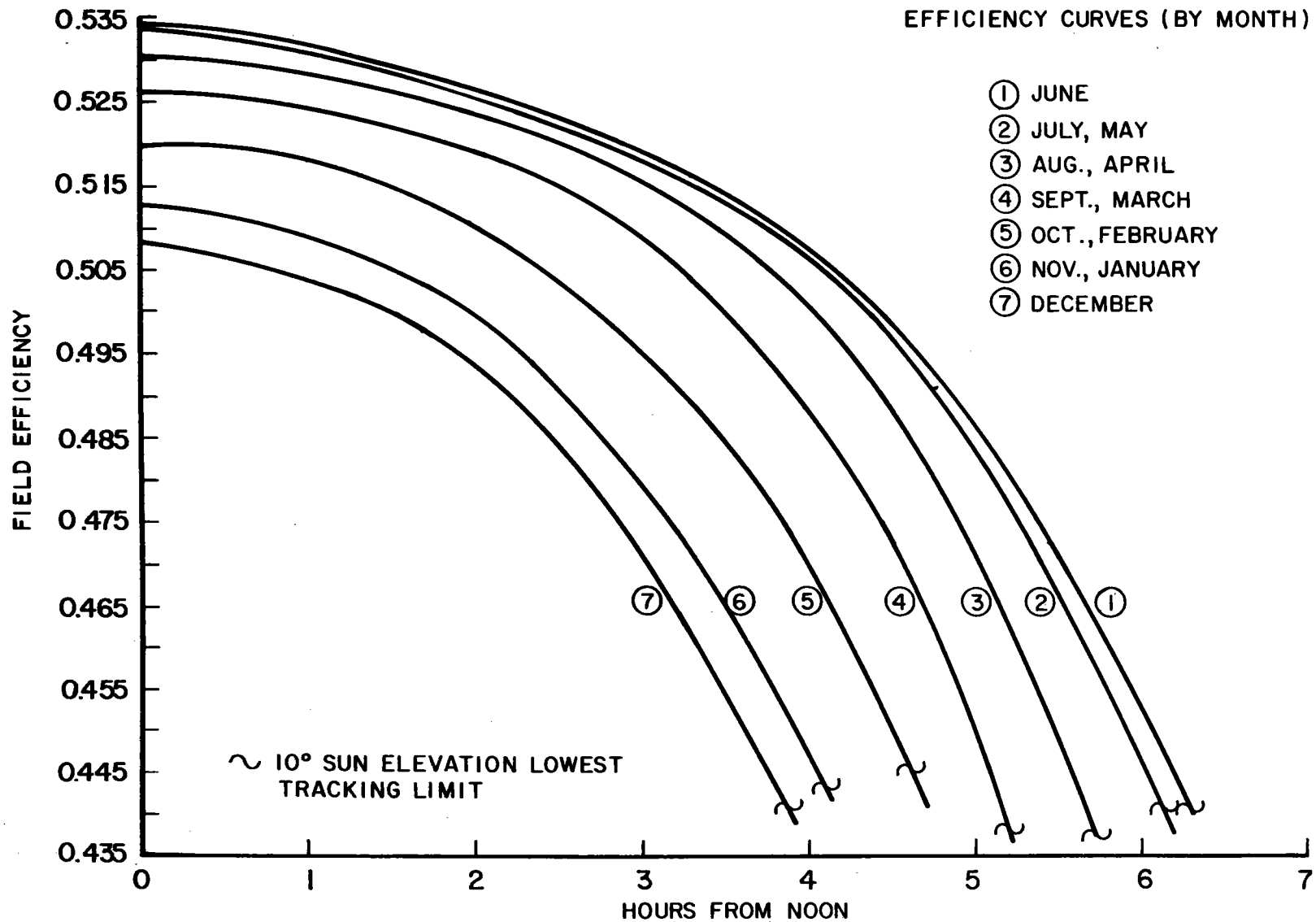


Figure 6-4. HelioStat Field Efficiency Variation
(Enclosed HelioStats)

also shown. This limit corresponds to a 10° sun elevation angle, below which the heliostats cannot track and hence do not collect any solar energy. In the present model each individual curve has been used for its respective month. Also, the value of efficiency at mid-hour has been used for the entire hour.

Receiver Performance

Thermal losses from the receiver include the reflected, radiative, and corrective losses. The receiver efficiency is defined as

$$\text{receiver efficiency} = \frac{\text{power absorbed by sodium in receiver}}{\text{power impinging on receiver}}$$

Receiver efficiency deteriorates when the incident flux is reduced. The receiver efficiency variation with incident power level is illustrated in Figure 6-5 (Ref. 6.1). The figure was derived by assuming that the incident flux varies in magnitude while maintaining the same shape. Note that if the incident flux drops below about 5% of the design point value, the thermal losses would exceed the incident power and the receiver efficiency would become negative.

Figure 6-5 is the efficiency for the revised two-header-panel receiver configuration with the heliostats aiming at the belt of receiver. Because of its higher efficiency compared to the original three-header-panel design (0.9033 vs. 0.8910 at design point), the number of heliostats in the field is reduced from 20,415 in the Phase I design to 20,137 in the present study.

Insulation Losses

Thermal losses from the system components via the insulation materials are summarized in Table 6-1. The values for standby periods were calculated by assuming that the hot components (except the hot storage tanks) are at the average temperature of hot and cold tanks ($\frac{1100 + 610}{2} = 855^\circ\text{F}$), cold components remain at 610°F, and hot storage tanks are assumed to be maintained at the 1100°F temperature level. Constant values are used throughout the standby periods.

Auxiliary Loads

A breakdown of the auxiliary loads is given in Table 6-2 (Ref. 1.1). The auxiliary loads for the receiver subsystem are assumed to vary linearly with the heat absorbed by sodium at the receiver. During a standby, the collector subsystem requires auxiliary power to keep the heliostat enclosures inflated. In addition, the steam turbine requires lubricating oil, sealing steam, and power to spin the rotor (turning gear). Lighting and other plant facility power requirements also continue during a standby. All other auxiliary equipment can be shut down as shown in Table 6-2.

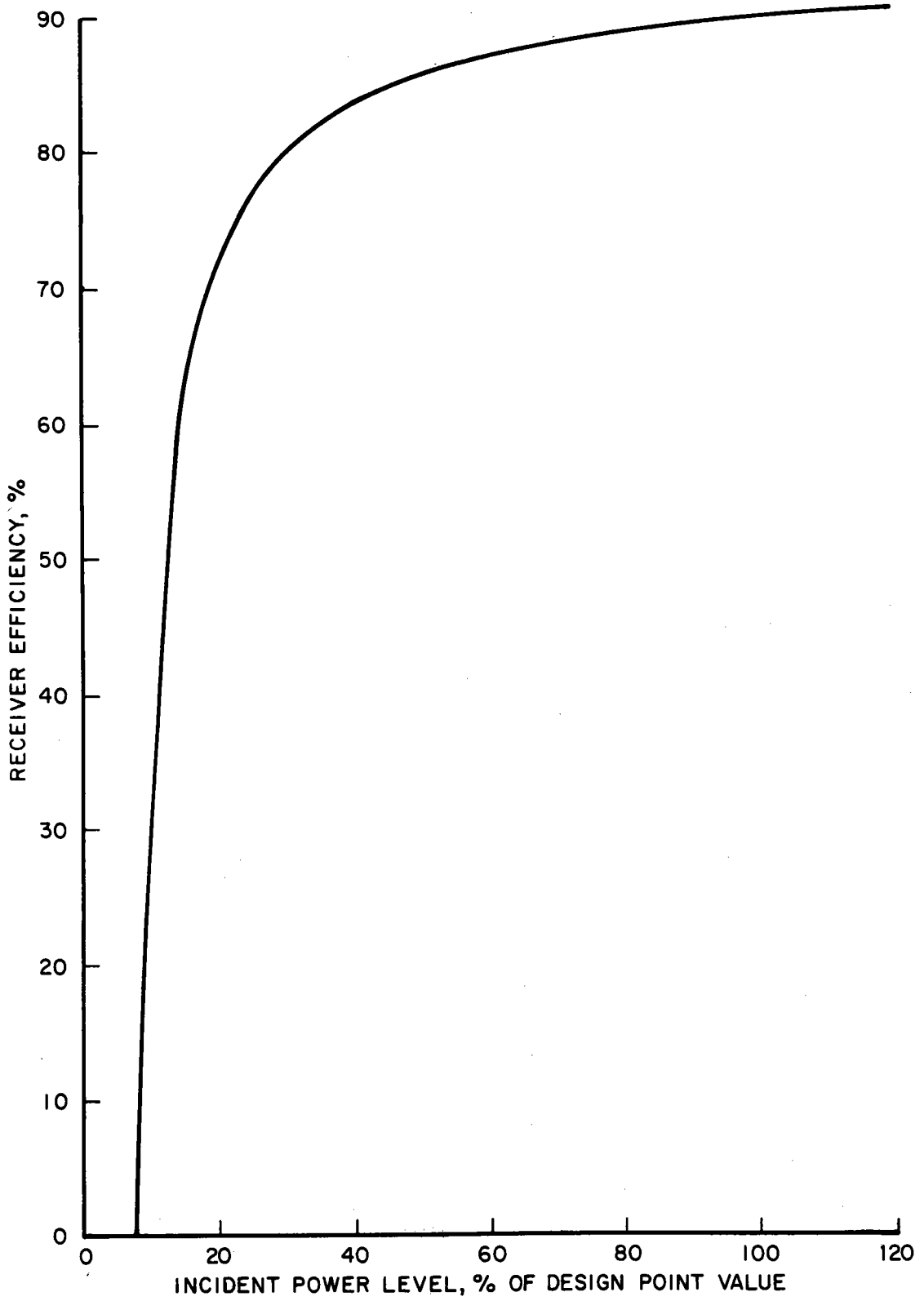


Figure 6-5. Receiver Efficiency Variation

Table 6-1

INSULATION LOSS SUMMARY

<u>Receiver/Tower Side</u>	<u>During Normal Operation</u> (Mwth)	<u>During Standby</u> (Mwth)
Hot Piping (receiver outlet header to hot tank inlet nozzle)	0.146	0.110
Cold Piping (cold tank outlet nozzle to receiver inlet header)	0.069	0.069
Receiver	Taken into account in receiver efficiency	0.128
<u>SG/EPGS Side</u>		
Piping	0.086	0.072
SG	0.036	0.026
<u>Storage Tanks</u>		
Cold	0.116	0.116
Hot	0.328	0.328

Table 6-2

SUMMARY OF AUXILIARY LOADS

<u>Description</u>	<u>Design Point</u> (MW _e)	<u>Standby</u> (MW _e)
<u>Collector Subsystem</u>		
Electronics and Drives	0.40	0
Blowers on Enclosures	0.31	0.31
<u>Receiver Subsystem</u>		
Electromagnetic Pumps	0.32	0
EM Pump Cooling Blower	0.03	0
Main Tower Pump	2.91	0
Steam Generator Pump	0.55	0
<u>Electronic Power Generation Subsystem</u>		
Boiler Feed Pumps - Main	2.86	0
- Blowdown	0.29	0
Condensate Pump	0.08	0
Feed Heater Drain Pump	0.01	0
Evaporator Recirculation Pump	0.12	0
Cooling Tower - Fans (5 units)	0.52	0
- Circulating Water Pumps (5 units)	2.06	0
<u>Hotel Load*</u>	0.76	0.76
<u>Transformer</u>	<u>0.55</u>	<u>0</u>
TOTAL	11.77	1.07

*Includes lighting, air conditioning, machine shop, and steam turbine auxiliaries using small motors such as lubricating oil pumps and generator cooling blowers.

Plant auxiliary power is supplied by the EPGs when the EPGs is in operation, and by the utility grid when the EPGs is shut down.

EPGS Performance

The design point EPGs efficiency is 0.445 (2" Hga condensing pressure at 73°F web bulb temperature). The efficiency varies with condensing pressure as well as load fraction. Variations in EPGs efficiency are given in Figures 6-6 and 6-7, estimated based on data provided by GE Medium Steam Turbine Department. The change in condensing temperature with ambient wet bulb temperature is delineated in Figure 6-8. Part load condenser performance is illustrated in Figure 6-9. There is a limit to part load condenser performance due to air ejector performance limitations near an absolute vacuum. In the present model, it is assumed that the condensing pressure is not allowed to go below 1" Hga.

SG/EPGS Warmup Energy Consumption

During a standby period, heat loss to the ambient would result in component temperature drops. In the warmup period following a standby, the components would be brought back to their respective normal operating temperatures by absorbing heat from the circulating sodium. The rate of the warmup process is limited by the temperature change rate limitations of the components. Therefore, for a component with a stringent limitation, the major portion of the energy in the circulating sodium would not be utilized, since only a small fraction of the heat content of the circulating sodium is used to warmup the components while the rest is released to steam, part of which is used for turbine startup.

Since the tower loop temperatures can be brought back to normal levels in a very short period (Ref. 6.2), the impact of its warmup time requirement is neglected in the present study. The time limiting components are the steam generators which impose a 150°F/hr temperature change rate limit. The method used to estimate the energy consumption associated with the warmup process of the steam generators is illustrated in the following example.

Assuming the steam generators have lost 60°F during a standby period, the warmup time required would be $\frac{60}{150} = 0.4$ hr. The circulating sodium flow is assumed to be 10% of the design point value during this warmup period. The steam generator inlet sodium is a mixture of sodium from the cold (610°F) and the hot (1100°F) storage tanks. At the beginning of this 0.4 hr. warmup period, the mixture (at $1100 - 60 = 1040$ °F) would be 12.2% from cold storage and 87.8% from hot storage (since $610 \times 0.122 + 1100 \times 0.878 = 1040$). When the warmup is completed at the end of the

6I-9

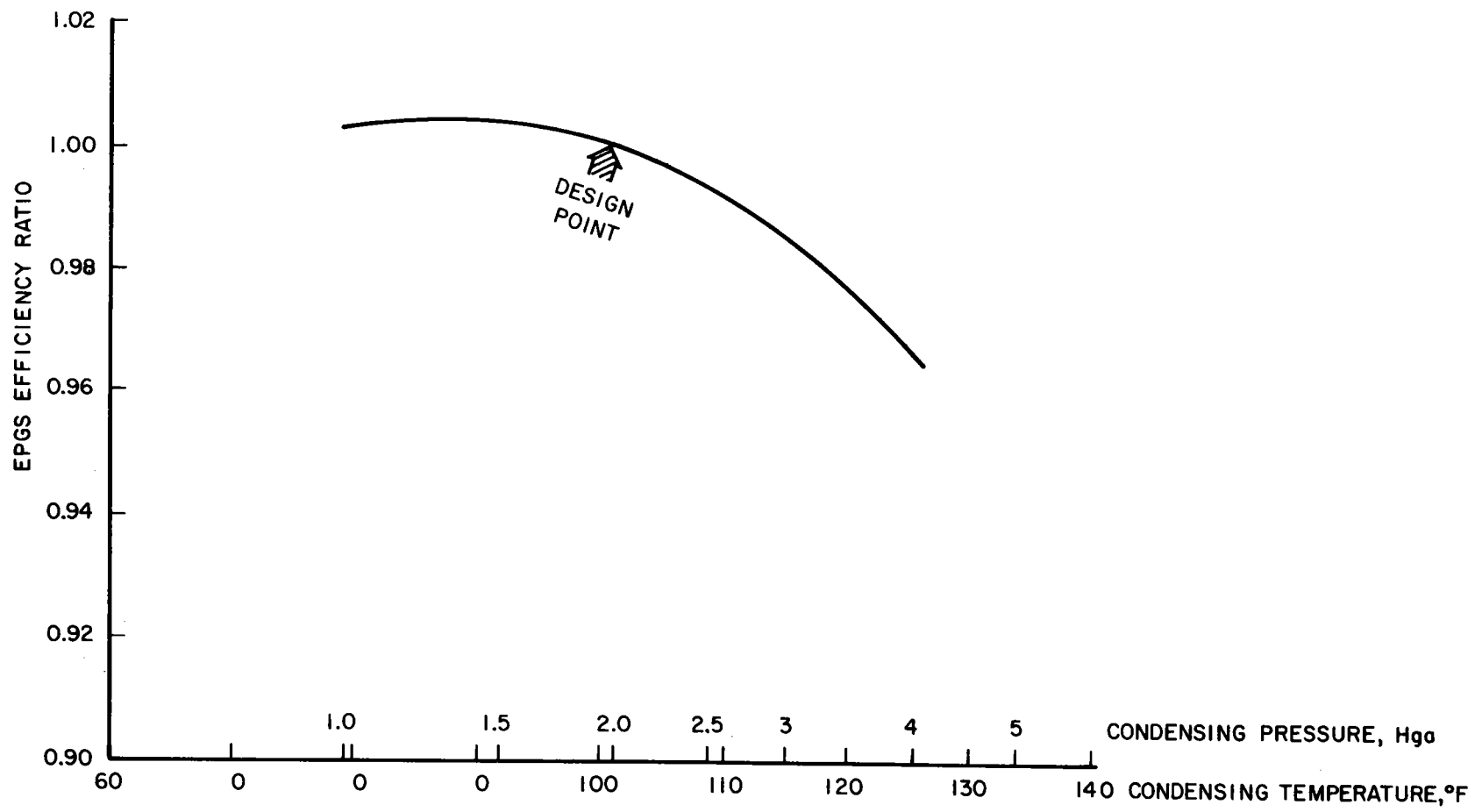


Figure 6-6. EPGs Efficiency Variation With Condensing Condition

6-14

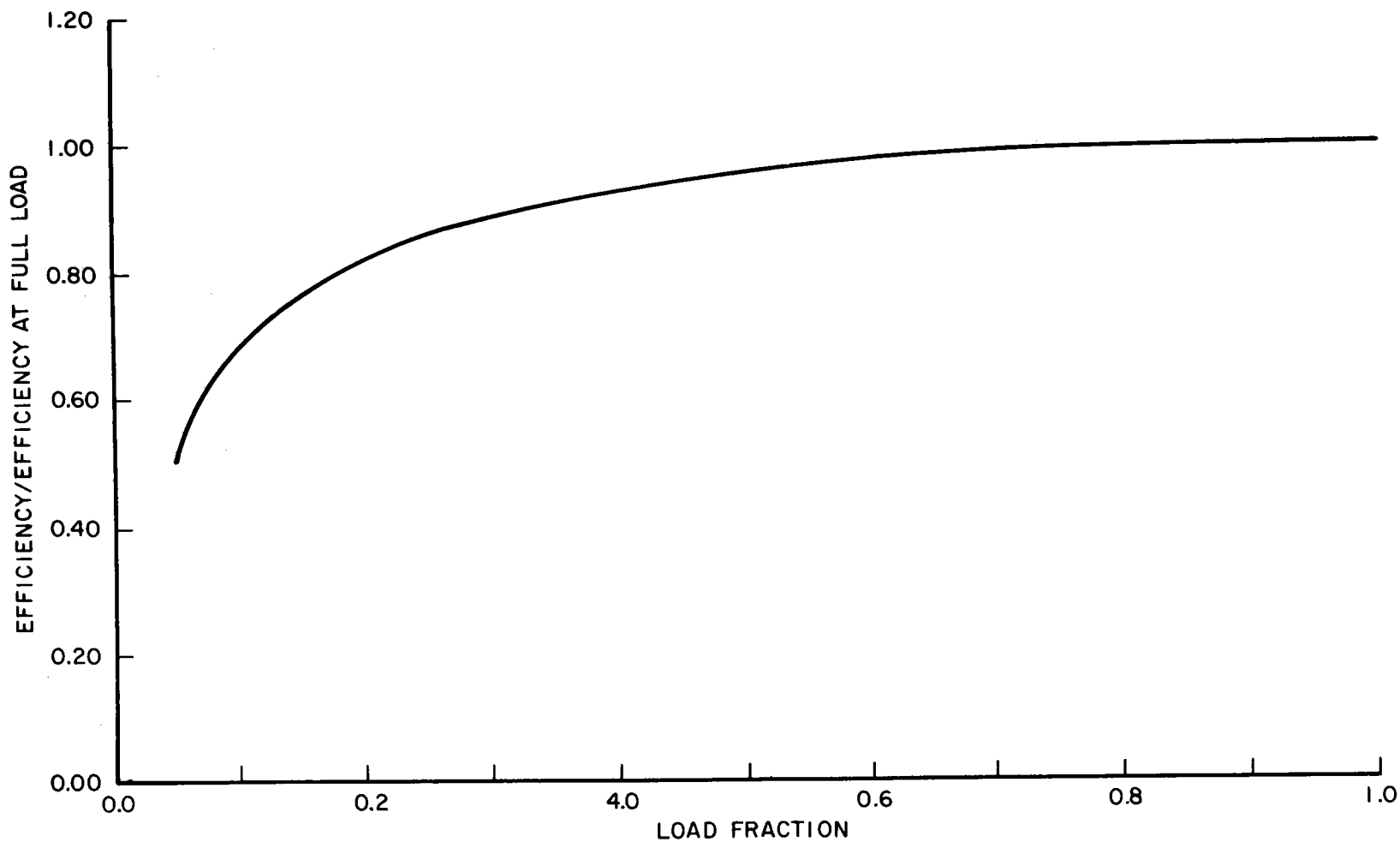


Figure 6-7. Steam Turbine/Generator Performance Variation With Load

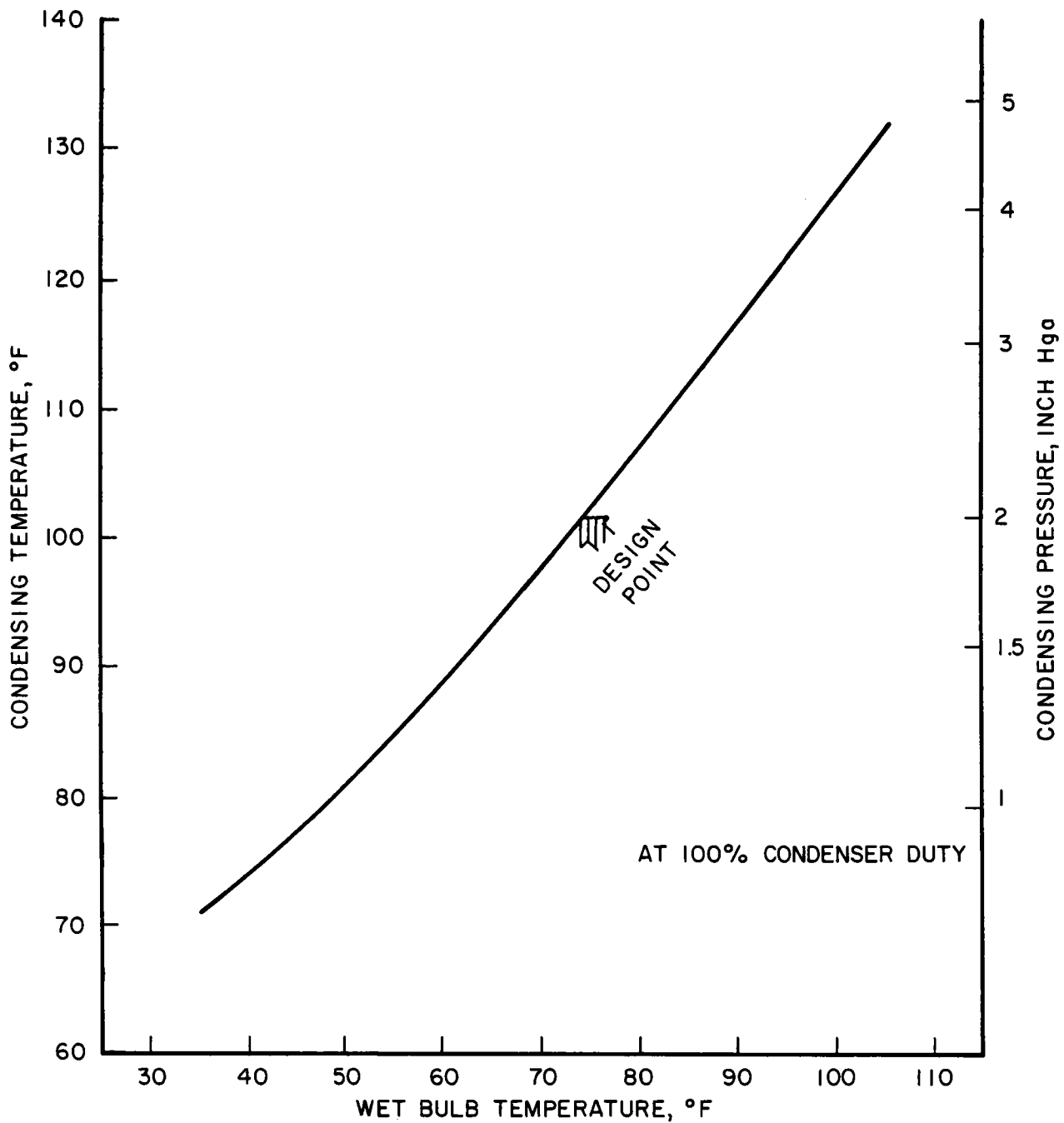


Figure 6-8. Variation of Condensing Condition With Ambient Wet Bulb Temperature

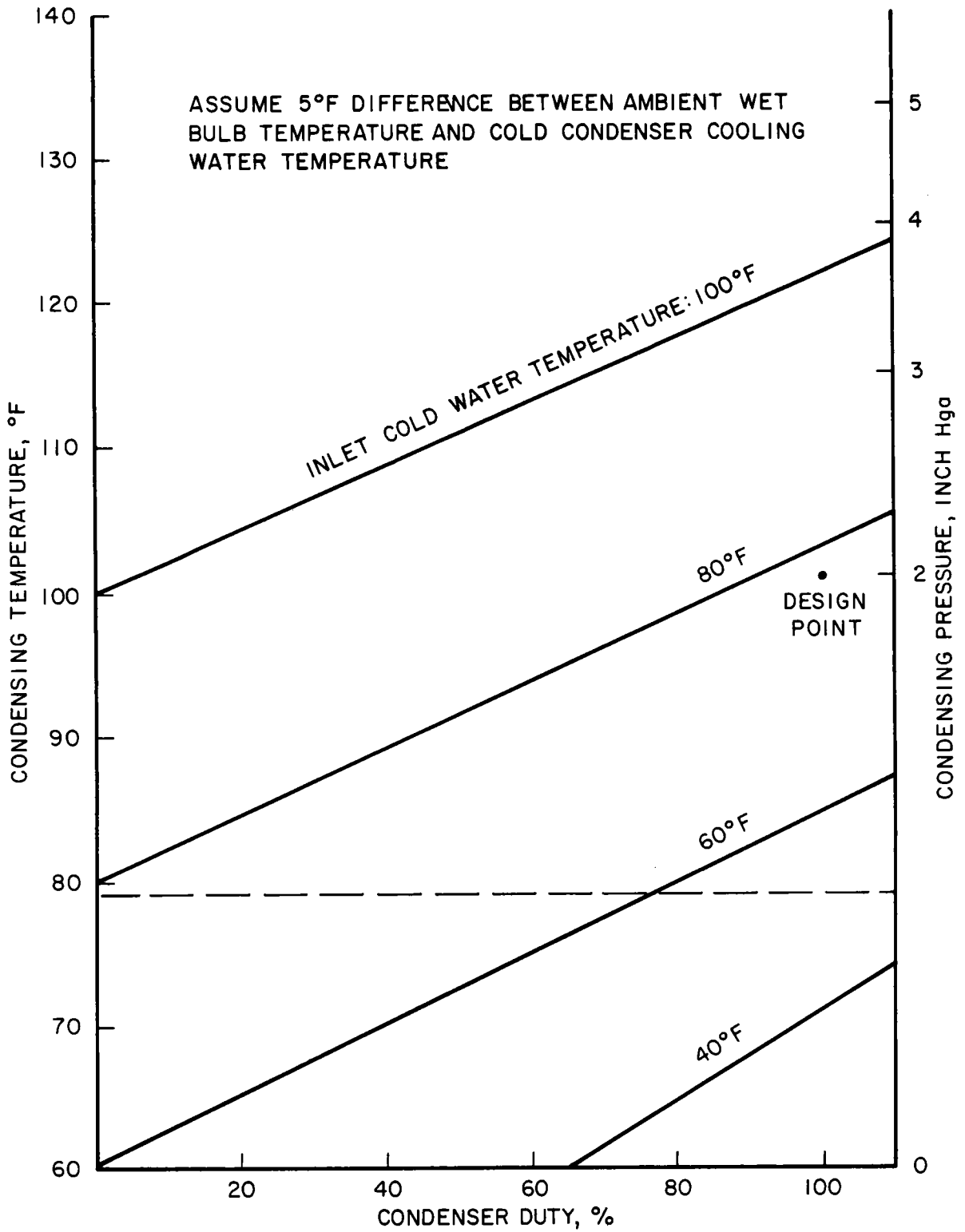


Figure 6-9. Condenser Part Load Performance

0.4 hr. period, the steam generator inlet sodium would be 100% from the hot storage tanks. With the hot sodium proportion in the mixture increasing linearly, the energy lost during the warmup periods is then

$$\underbrace{\left(\frac{0.878+1}{2}\right)}_{\text{averaged proportion of 1100°F sodium used during warmup}} \times \underbrace{(0.1)}_{\text{10\% of rated flow}} \times \underbrace{\left(247.89 \frac{\text{Mwth}}{\text{hr}}\right)}_{\text{heat released from 1100°F sodium at rated flow to steam in SG}} \times \underbrace{0.4 \text{ hr.}}_{\text{warmup period duration}} = 9.31 \text{ Mwth}$$

For ease of modeling, in the present computer model it is assumed that the warmup energy required will be obtained from solar energy collected during the first hour of solar energy collection in the morning. Furthermore, since a plant operator can use the hot sodium stored from the previous day to start warming up the steam generators prior to sunrise, the effect of the warmup time requirement on operation is not considered in the present model.

6.3 PLANT PERFORMANCE

6.3.1 DESIGN POINT

The design point specifications are as follows:

- Insolation = 950 w/m^2
- Ambient Temperature = 73°F wet bulb
= 82°F dry bulb
- Reference Site: Barstow, California (35° latitude)

The performance of the ACR plant under these conditions are summarized in Table 6-3. The differences between the values in this table and the data reported in the Phase I study result from a change in receiver panel design and a re-evaluation of insulation losses in the receiver/tower side of the plant.

6.3.2 HOURLY VARIATION DURING TYPICAL DAYS

To illustrate the variation of plant net output during a day, the power output profiles for June 21 and December 23 are presented in Figures 6-10 and 6-11, respectively. The hourly variations in incident insolation level and net hot storage tank energy level are also shown. The simulation is done on an hour-by-hour basis, hence the insolation level and net power output have flat tops. The net energy level in hot storage tanks varies constantly, and a linear profile is assumed between the beginning and the end of each hour.

Table 6-3
DESIGN POINT ENERGY BALANCE

Description	MW
Ideal Incident Power on Heliostats	1052.2
Incident Power on Receiver	408.2
Net Power to Sodium in Receiver	368.8
Net Power into Tanks ¹	371.2
Power Discharged from Hot Tanks	247.5
(Power Stored in Hot Tanks)	(123.7)
Net Power to Steam in Steam Generators ²	247.9
Net Heat to Steam ³	251.1
Gross Generator Output	111.8
Net Plant Output	100.0
<u>Gross Electricity</u> = $\frac{111.8}{251.1} = 0.445$	
<u>Net Heat to Steam</u>	
$\frac{\text{Net Electricity}}{\text{Solar Incident on Heliostats}} = \frac{100}{1052.2/1.5} = 0.143$	
$\frac{\text{Net Electricity}}{\text{Solar Incident on Receiver}} = \frac{100}{408.2/1.5} = 0.367$	
Solar Multiple = $\frac{371.2}{247.5} = 1.5$	

¹ Include Tower Piping Loss 0.215 Mwth, Tank Heat Loss 0.444 Mwth, Heat Input from Tower/Receiver Pumps 3.04 Mwth

² Include SG piping Heat Loss (Including SG Surface Heat Loss) 0.22 Mwth, Heat Input from SG Pump 0.44 Mwth

³ Include Heat Input from EPGS Pumps 3.19 Mwth

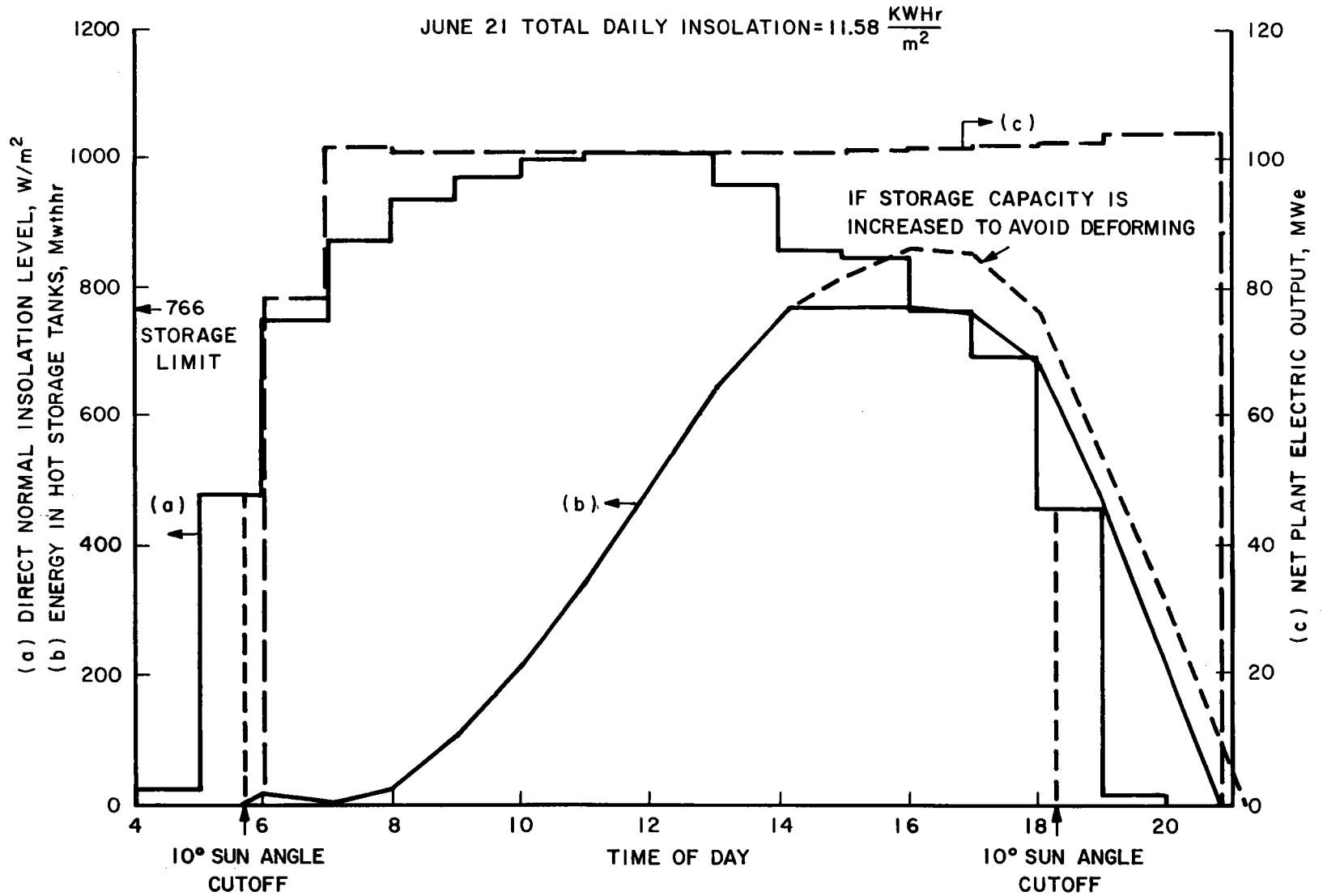


Figure 6-10. Daily Output Variation, June 21

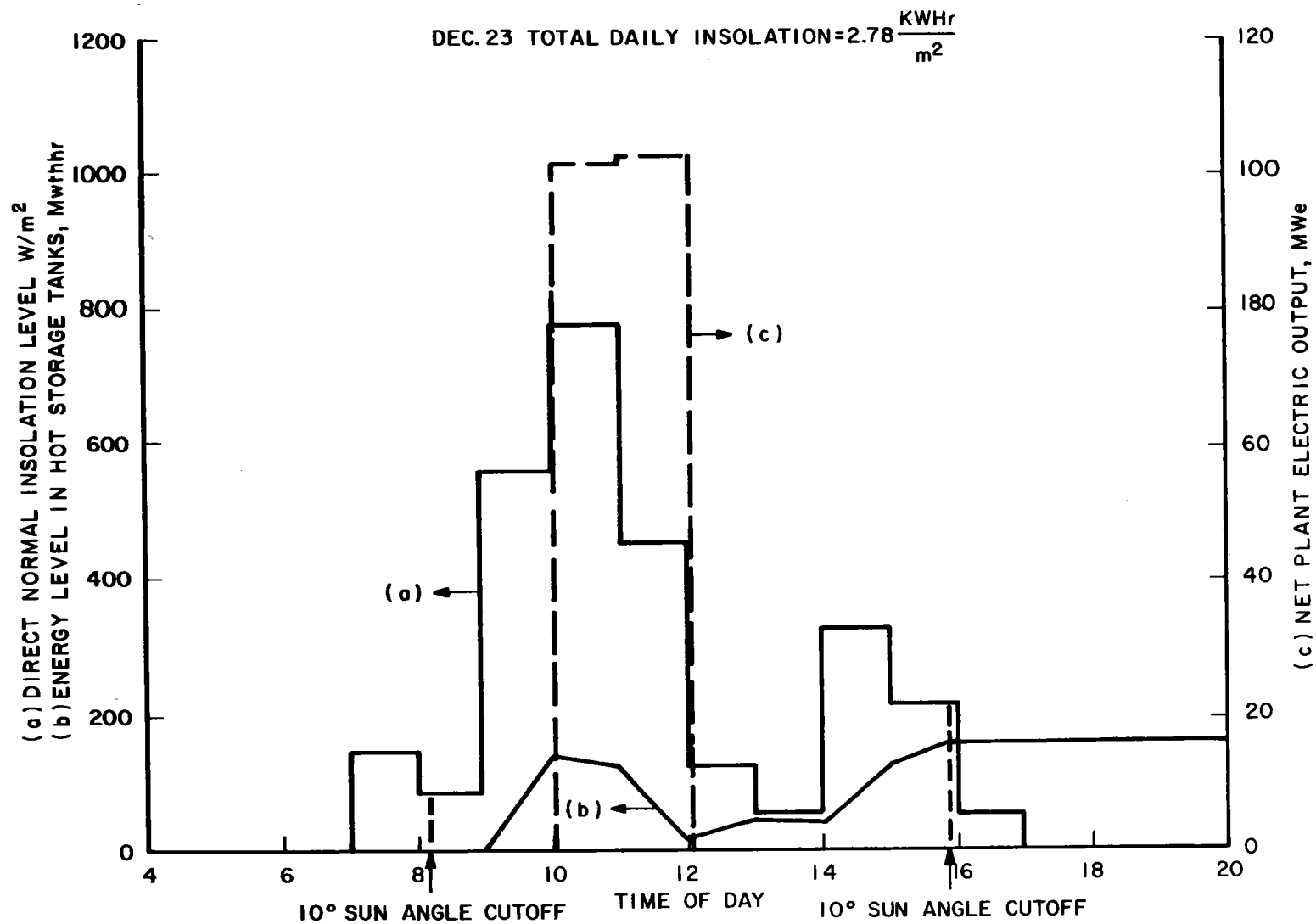


Figure 6-11. Daily Output Variation, December 23

Sunny Day

June 21 (Figure 6-10) is a day with high insolation levels. According to the plant operating plan discussed in Section 6.2.2., hot sodium would be used to generate power once it is produced, if the hot sodium is at least enough for half-load EPGS operation. Therefore, in the period between 5:43 a.m., when sun elevation angle = 10° and heliostat field starts collecting solar energy, and 6:00 a.m. hot sodium generated at the receiver is stored in the tanks, without discharging to the steam generators. Between 6:00 a.m. and 7:00 a.m., the insolation level is sufficient to start the EPGS system and operate at 50% load. In this period, hot sodium from the receiver is supplemented by hot sodium from storage, and is discharged to the steam generators for power generation. The hot storage energy level is drawn down to zero at 7:00 a.m. Between 7:00 a.m. and 4:00 p.m., excess solar power becomes available and storage fills up. At about 2:10 p.m., the storage tanks would reach their maximum fill levels with a 3-hour design (766 Mwth-Hr) and thermal power would have to be dumped in the collector field by heliostat defocusing. Therefore, storage level is maintained at 766 Mwth-Hr between 2:10 p.m. and 4:00 p.m. After 4:00 p.m. energy drawn from storage exceeds the input to storage from tower, and storage level begins to fall. At 6:17 p.m., the sun elevation angle reaches 10° and the heliostat field stops collecting solar energy. Operation of SG/EPGS would continue until 8:51 p.m. when the storage is depleted.

If the dumped energy (necessitated due to hot storage tank capacity limit) could be stored, the storage energy level would be as shown by the dotted line in Figure 6-10.

The EPGS operates at full load from 7:00 a.m. until shutdown. Since the auxiliary loads on the tower side increases with increasing insolation level, the lowest net plant output is between 12:00 noon and 1:00 p.m. when the insolation level is the highest, and the highest net output is when the EPGS operates out of storage (tower shutdown).

Cloudy Day

December 23 (Figure 6-11) is a day with low and intermittent solar insolation. Recall that the operating plan used in the present model for a cloudy day (Section 6.2.2) is that no hot sodium would be used to generate power unless the accumulated hot sodium in storage can sustain at least one-hour of full load operation. Between 8:09 a.m. (sun elevation angle = 10°) and 9:00 a.m. the insolation level is too low to be worthy of collecting. Between 9:00 a.m. and 10:00 a.m. hot sodium is generated

but its amount is low and SG/EPGS would stay idle, and the stored energy level increases during this period. From 10:00 a.m. to 12:00 noon electric power is produced using hot sodium from receiver supplemented by hot sodium from storage. Note that full load EPGS operation has been assumed. At 12:00 noon, the EPGS is shut-down since the insolation levels are low in the afternoon. The tower side of the plant continue to operate except between 1:00 p.m. and 2:00 p.m. when the insolation level is too low, and hot sodium is put into storage with the storage level ending at 157 Mwth-Hr at the end of the day. This energy is allowed to be stored overnight.

6.3.3 MONTHLY AND ANNUAL VARIATION

Information on monthly variation of performance is summarized in Table 6.4. In this table, the ideal available energy incident on heliostats column (A) is the amount of sunlight available at the heliostat location based on the surface area of the heliostats. As explained in Section 6.2.2, the heliostat field would collect energy only when the insolation levels are above certain values below which auxiliary losses exceed collected energy. Also, the heliostat field can collect energy only when the sun's elevation angle is above 10° . Furthermore, there are times when the hot storage tanks are filled to their capacity and part of the heliostat field would have to be defocused. Excluding the above three circumstances during which solar energy is not collected, the energy incident on heliostats during collection can be calculated and is shown in column (B). All other items are self-explanatory. The net plant output variation is plotted in Figure 6-12. Plant annual performance is summarized in Figure 6-13.

Heliostat defocusing necessitated by hot storage tank capacity limit results in loss of energy. With the 766 MWhr hot storage capacity, this energy loss is calculated and shown in Table 6-5. Note that the months for which heliostat defocusing is exercised (March to August) correspond to the months with high insolation (Figure 6-3).

Table 6-4

MONTHLY PERFORMANCE VARIATION (UNIT: MWhr PER MONTH)

	(A) Ideal Available Energy Incident On Heliostats	(B) Energy Incident On Heliostats During Collection	(C) Energy Impinging On Receiver	(D) Energy Absorbed By Na In Receiver	(E) Net Heat To Steam	(F) Gross Electric Output	(G) Net Plant Output
J	243,832	224,593	69,396	61,278	62,034	27,604	24,835
F	197,881	184,567	59,988	52,754	53,121	23,697	21,445
M	252,277	239,490	80,995	71,371	72,599	32,364	29,238
A	265,871	255,313	87,802	77,350	78,619	35,059	31,665
M	307,833	295,907	102,512	90,619	92,237	41,130	37,127
J	351,295	328,415	113,400	100,876	102,735	45,801	41,298
J	283,474	268,432	92,888	81,986	83,361	27,127	33,492
A	348,158	320,796	109,291	97,416	99,037	44,216	40,032
S	192,293	181,225	61,482	54,096	54,708	24,364	21,971
O	256,573	235,097	76,399	67,667	68,526	30,586	27,660
N	238,929	214,730	66,207	58,529	59,190	26,384	23,789
D	220,226	195,957	58,670	51,336	52,017	23,150	20,973

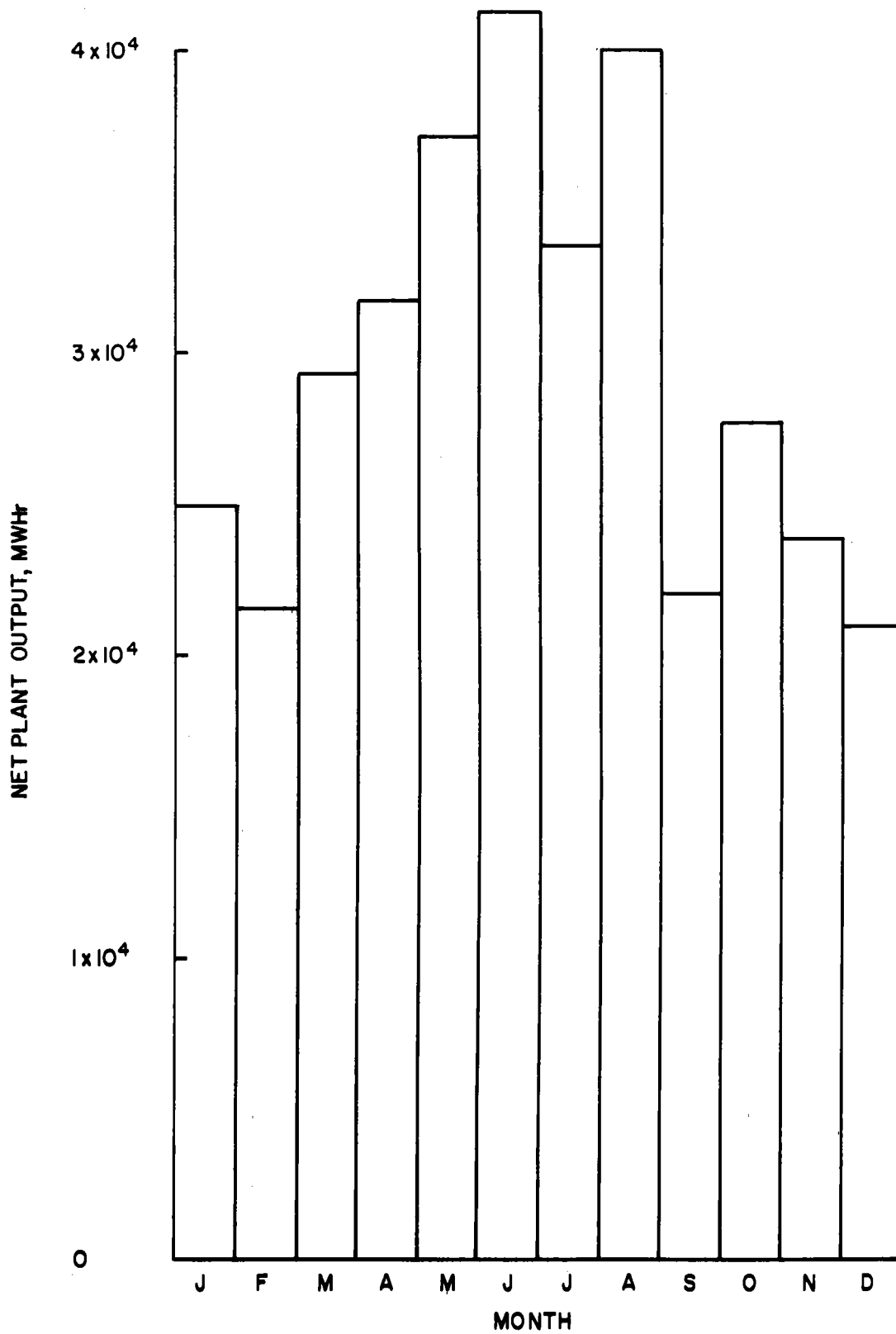
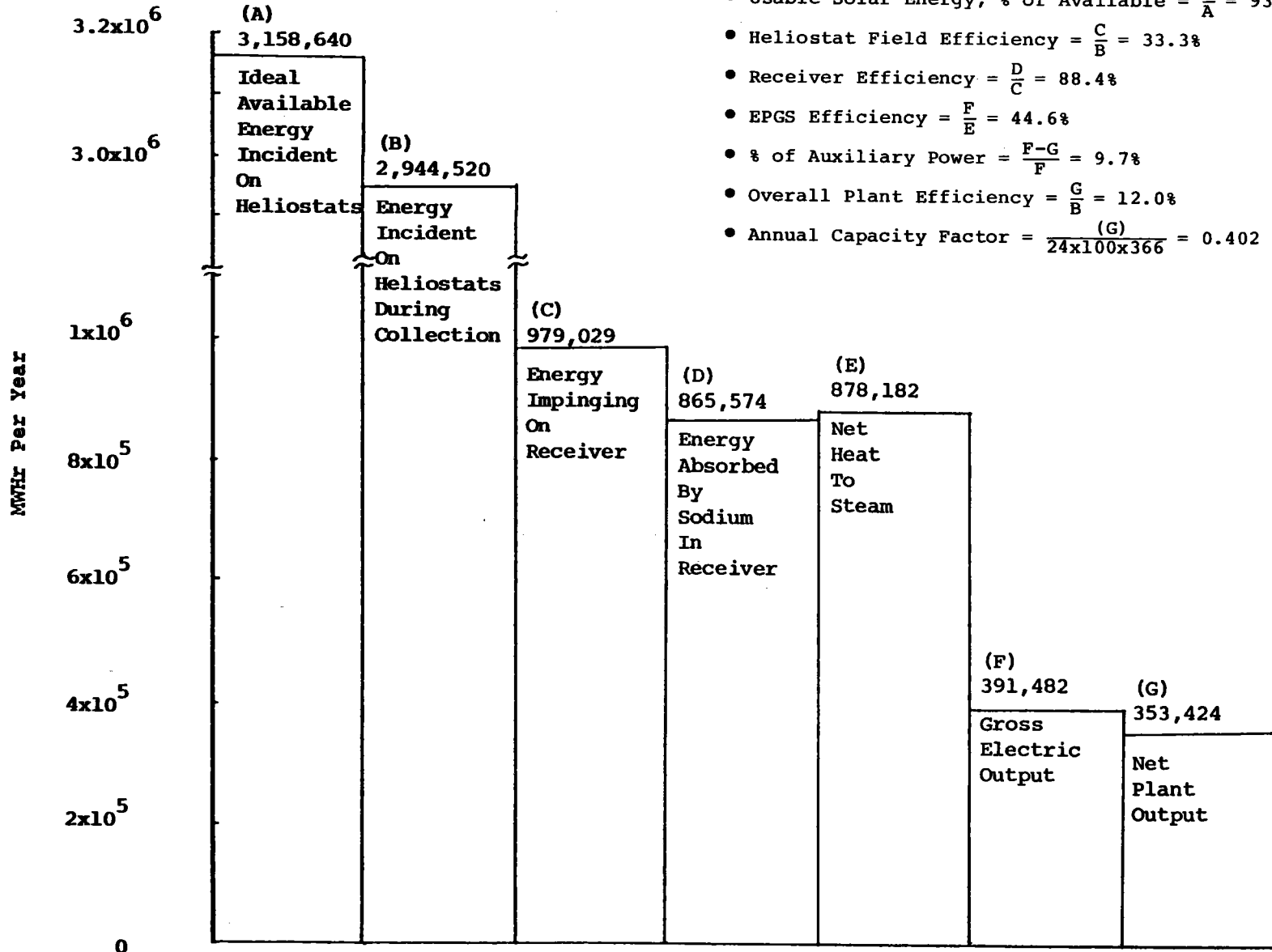


Figure 6-12. Monthly Net Plant Output Variation



Annual Performance Summary

- Usable Solar Energy, % of Available = $\frac{B}{A} = 93.2\%$
- Heliostat Field Efficiency = $\frac{C}{B} = 33.3\%$
- Receiver Efficiency = $\frac{D}{C} = 88.4\%$
- EPGS Efficiency = $\frac{F}{E} = 44.6\%$
- % of Auxiliary Power = $\frac{F-G}{F} = 9.7\%$
- Overall Plant Efficiency = $\frac{G}{B} = 12.0\%$
- Annual Capacity Factor = $\frac{(G)}{24 \times 100 \times 366} = 0.402$

Figure 6-13. Annual Plant Energy Flow

Table 6-5
ENERGY LOSS DUE TO HELIOSTAT DEFOCUSING

	J	F	M	A	M	J	J	A	S	O	N	D	ANNUAL
Energy	0	0	0.18%	0.29%	0.29%	1.67%	0.38%	2.00%	0	0	0	0	0.53%
Loss*													

*Defined as $\frac{\text{(energy dumped evaluated at hot storage tanks)}}{\text{(actual energy put into hot storage tanks)}}$

SECTION 7

REFINED CONCEPTUAL DESIGN

7.1 INTRODUCTION

The commercial plant configuration selected at the end of the Advanced Central Receiver Program - Phase I has been refined as part of Task 2.1 of this Phase II program. Figure 7-1 indicates those subsystems that have been modified to incorporate improved performance and/or lower cost. Table 7-1 shows the impact of these changes, along with the specified heliostat usage based on availability, all of which directly affect the overall system optimal design.

Detailed analyses of the modified subsystems have been presented in previous sections of this report. The results of these analyses formed the basis for a refined collector field optimization study which is presented in this section. Overall plant performance is also presented. A refined cost estimate for the modified commercial plant configuration is presented in Section 8 of this report.

7.2 FIELD OPTIMIZATION ANALYSIS

Refinement of the commercial plant configuration was accomplished with the DELSOL computer code (Ref. 7.1). DELSOL has two principle capabilities, as shown in Table 7-2: (1) to evaluate the optical performance of a prescribed solar central receiver power plant system, and (2) to determine the optimal system design incorporating a specified technology.

As a system design tool, DELSOL determines the best combination of field layout, tower height and receiver size based on the performance, total plant capital cost, and energy cost. The optimal design is evaluated by searching over a range of tower heights and two components of the receiver dimension (e.g., diameter and height of an external cylindrical receiver) at the design point power level to find the system with the minimum cost of energy.

The input information required for the DELSOL code consists of heliostat specifications, receiver performance and a capital cost model that is representative of a reference plant design. The necessary heliostat data were basically the same as were used in Phase I (Ref. 1.1, Table 3.2-2) except as noted in Table 7.3.

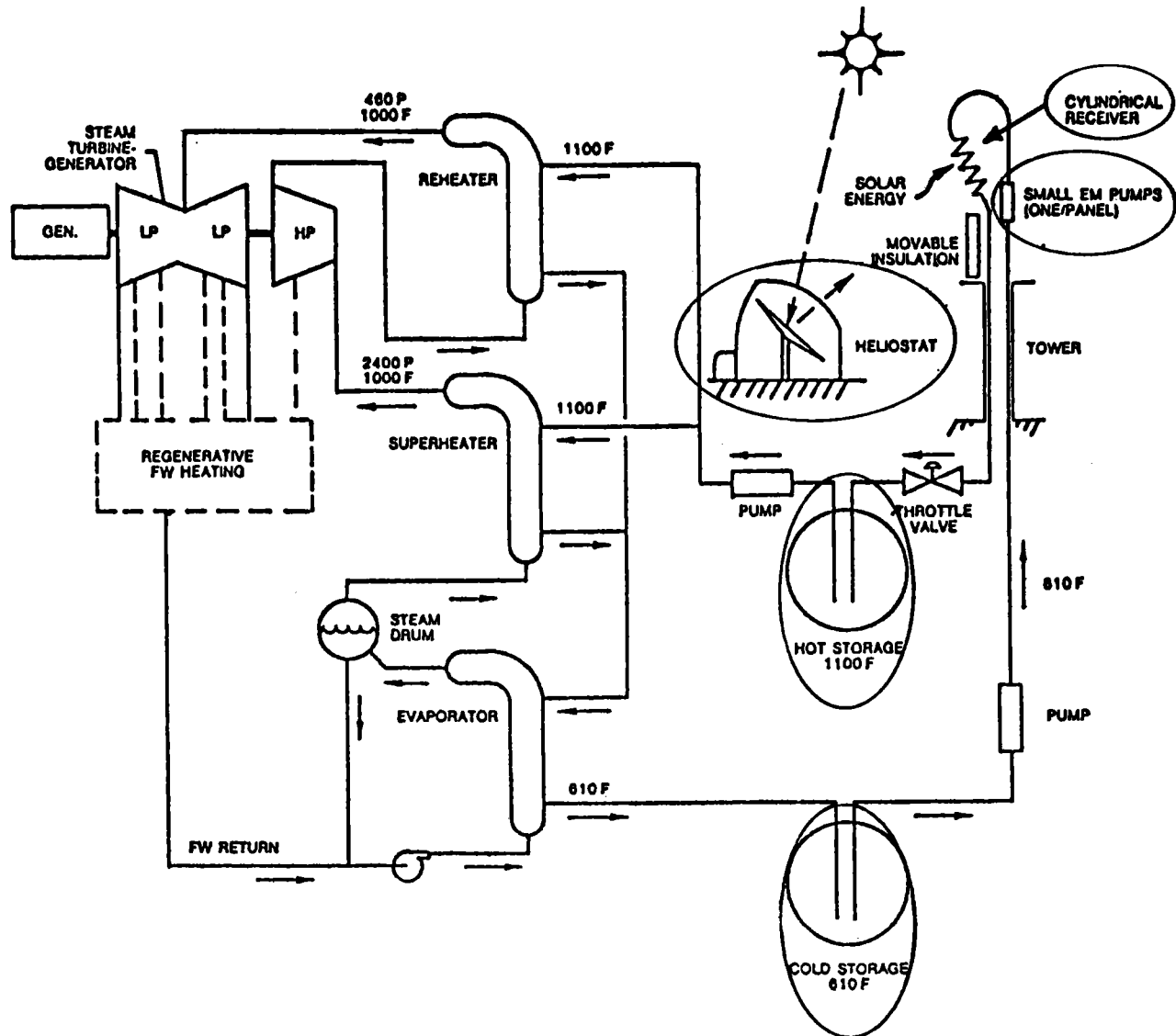


Figure 7-1. Modified Subsystems in Phase I Commercial Plant Configuration

Table 7-1

IMPACT OF CHANGES TO PHASE I CONCEPTUAL DESIGN

ITEM	ØI	ØII	IMPACT
Receiver Panel	3 Header	2 Header	<ul style="list-style-type: none"> ● Increased Efficiency ● Decreased Cost
Receiver Flow Control	1 EM Pump Per Panel (24)	Grouped Panels (8)	Reduced Cost
Storage System	6 Spherical Tanks	4 Modified Hemispherical Tanks	Reduced Cost
1st Plant Heliostats	GE/Enclosed	Glass/Unenclosed	Near Term Application
Nth Plant Heliostats	GE/Enclosed	GE/Enclosed	Mature Technology With Development

Table 7-2

DELSOL - CAPABILITIES

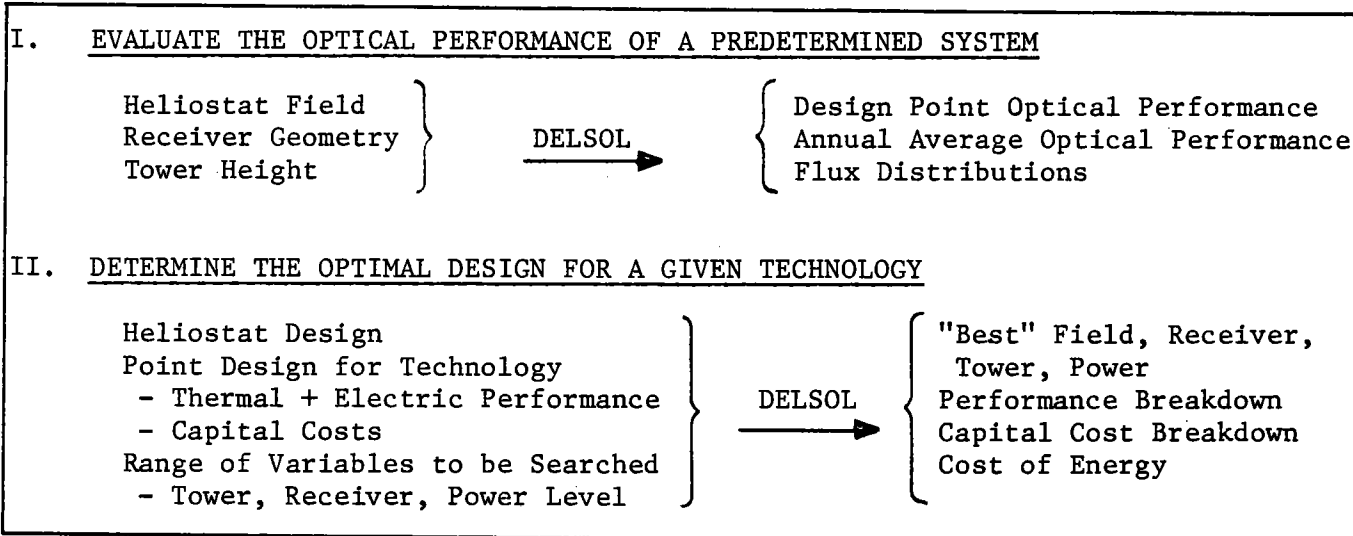


Table 7-3

REVISED HELIOSTAT SPECIFICATIONS

<u>COSTS</u>	<u>ENCLOSED (PLASTIC)</u>	<u>EXPOSED (GLASS)</u>
Unit Cost*	\$18.60/m ²	\$59.24/m ²
Land Cost	\$ 0.62/m ²	\$ 0.62/m ²
<u>PERFORMANCE</u>		
Effective Reflectivity	0.724**	0.92
* Does not include distributables or wiring cost.		
** Combined performance of:		
● transmittance of Kynar enclosure, in and out, each 0.93		
● reflectance of silvered LLumar 0.91		
● surface degradation 0.92		

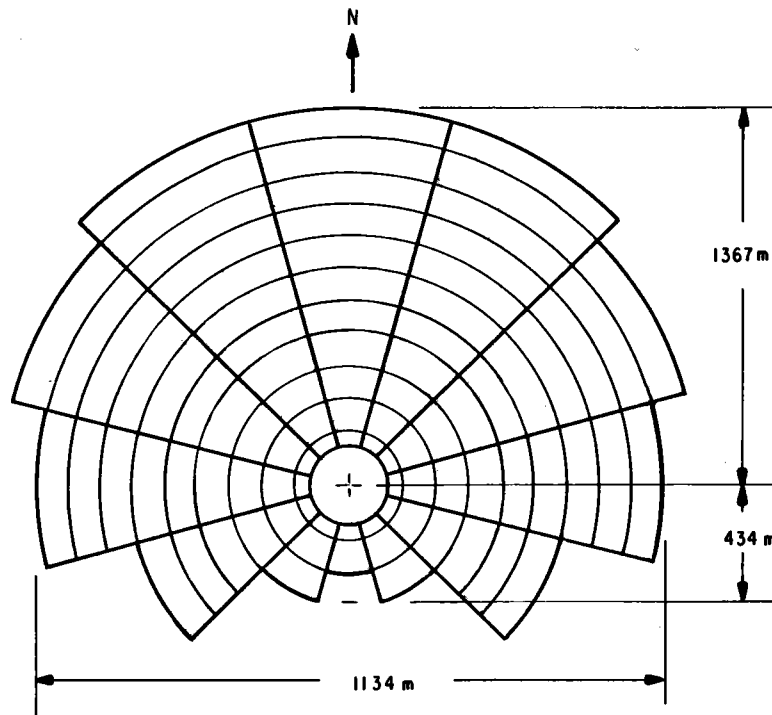
The unenclosed glass heliostat data were extracted from Ref. 7.2 and represent the current technology corresponding to a production level of 25,000 units per year. For the enclosed heliostat, the performance data reflects the latest available plastic material properties obtained from a current on-going development program (Ref. 7.3) while the cost data was extracted from Ref. 7-4 and appropriately modified to account for the change in materials. Enclosed heliostat costs represent a mature technology corresponding to a production level of 1,000,000 units per year.

Cost and performance models used in this optimization analysis were those contained in the DELSOL code with the default cost parameters modified to be representative of the ACR conceptual design. The Phase I cost breakdown shown in Volume III of Ref. 1.1 forms the basis of this cost modification. These modified costs then become the reference plant capital costs which are optimally scaled within DELSOL.

7.2.1 OPTIMUM FIELD LAYOUT

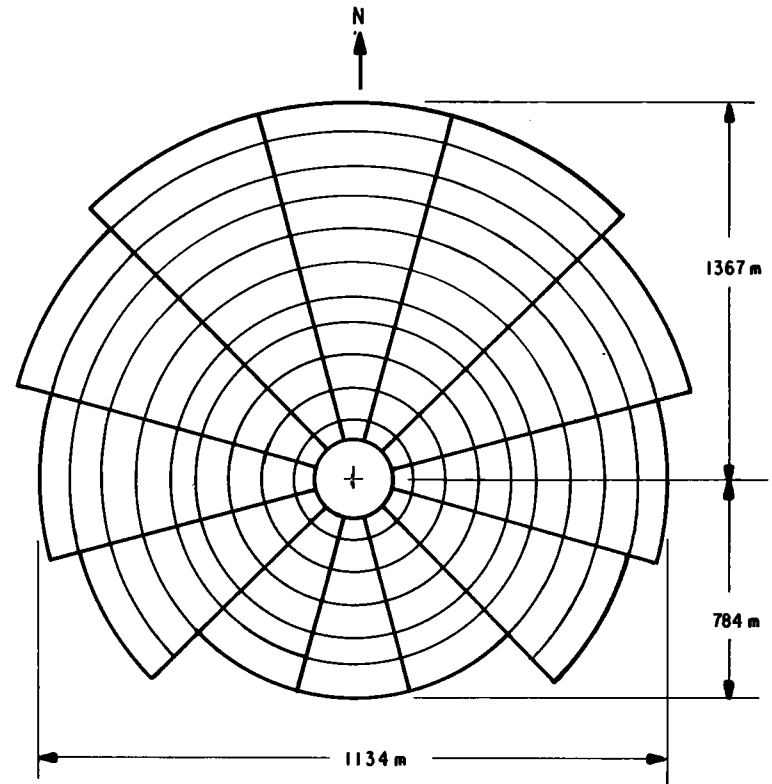
An optimized field/receiver which delivers 375 MWt net power at the design point (noon summer solstice, 950 W/m²) has been redesigned using DELSOL. Figure 7-2 shows the optimized field layout for both the 1st plant using glass heliostats and the Nth plant using enclosed heliostats.

7-5



TOWER HEIGHT = 190m
 RECEIVER SIZE = 18.5m (H) X 18.5m (D)
 NUMBER OF HELIOSTATS = 12957
 HELIOSTAT SIZE = 49m²
 LAND AREA = 2.930 Km²
 ANNUAL POWER IMPINGING ON RECEIVER = 1.269×10^6 MW_TH
 SUMMER SOLSTICE NOON NET POWER = 375.12 MW_T

(a) 1st PLANT



TOWER HEIGHT = 190m
 RECEIVER SIZE = 16.5m (H) X 16.5m (D)
 NUMBER OF HELIOSTATS = 15304
 HELIOSTAT SIZE = 55m² (FOCUSED)
 LAND AREA = 3.801 Km²
 ANNUAL POWER IMPINGING ON RECEIVER = 1.226×10^6 MW_TH
 SUMMER SOLSTICE NOON NET POWER = 374.79 MW_T

(b) Nth PLANT

Figure 7-2. Optimized Field Layout

In computing the flux impinging on the receiver, the DELSOL calculated "smart" heliostat aiming procedure was utilized. This procedure takes advantage of the fact that the size of the image from near heliostats is smaller than from far heliostats and produces a more uniform flux profile along with reduced peak fluxes. The resulting circumferential flux variation is illustrated in Figure 7-3 and the axial flux variations are shown in Figure 7-4. Tabulated values of the calculated receiver flux are given in Figures 7-5 and 7-6.

The field efficiency is defined as

$$\text{field efficiency} = \frac{\text{power impinging receiver}}{\text{total reflector surface area} \times \text{normal solar flux}}$$

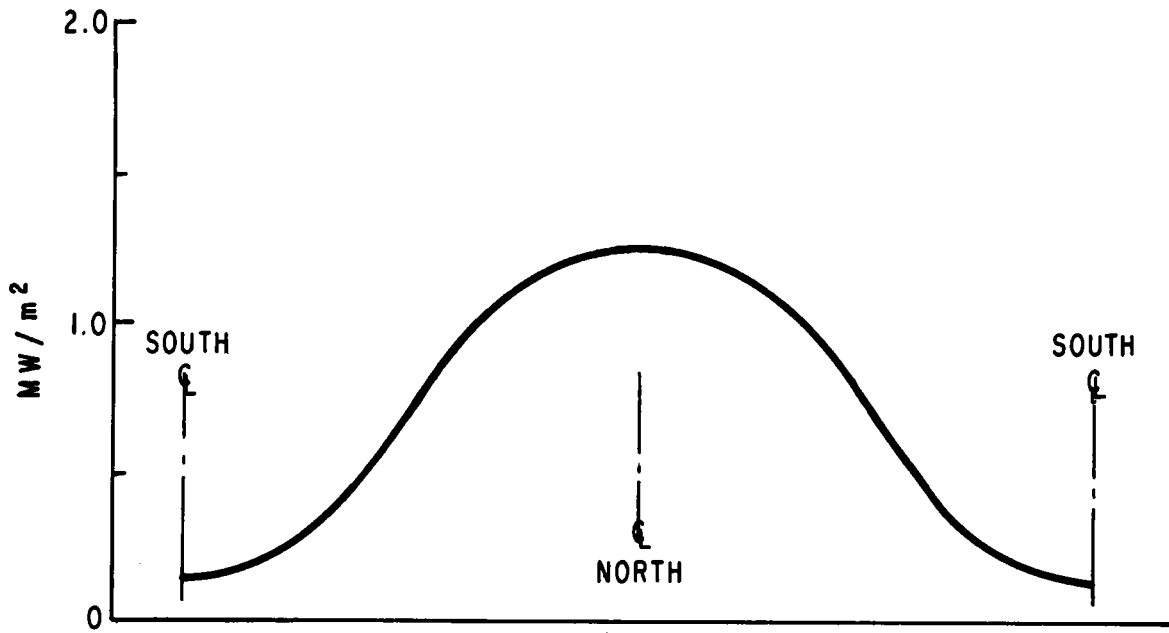
The variation of field efficiency with time for the summer and winter solstices and the equinox are shown in Figure 7-7.

Table 7-4 summarizes the annual performance of the collector subsystem and also describes the DELSOL sun model used in estimating the annual energy incident on the receiver. Note that this sun model does not exactly match the design point insolation of 950 W/m² at summer solstice noon, and therefore the incident power does not coincide with the design value.

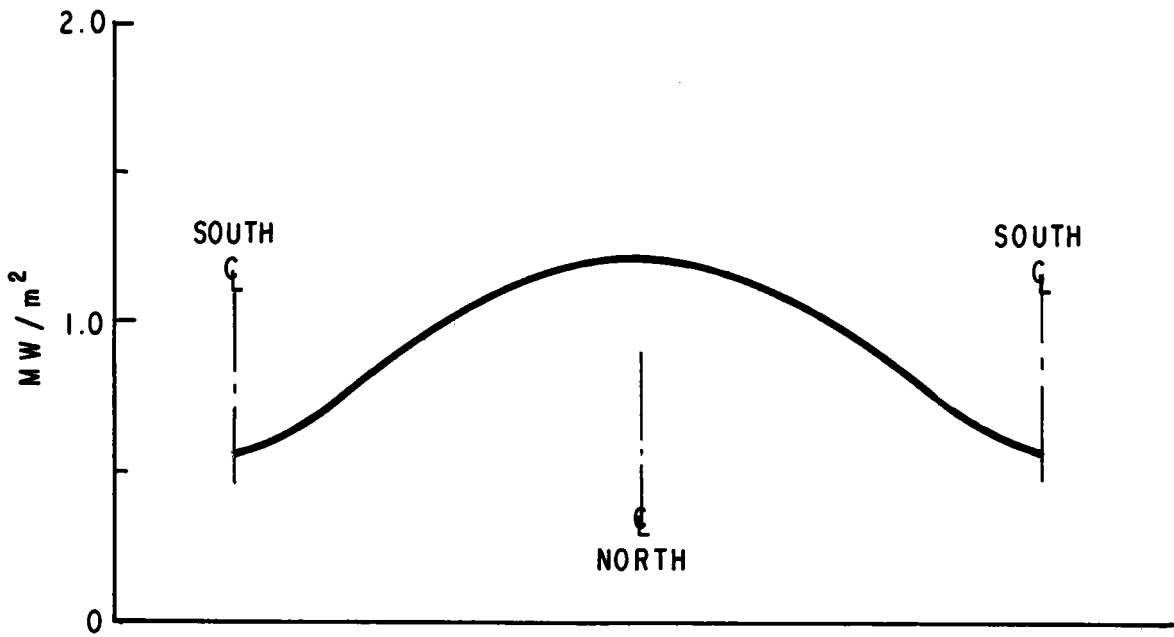
7.2.2 RECEIVER DESIGN

Figure 7-8 is the modified ACR-Phase II receiver concept which includes previously described improvements that affect both performance and cost. As in the original design, the sodium cooled absorber surface consists of 24 separate panels. However, the receiver size will depend upon heliostat application. For the first plant with flat glass heliostats the receiver will be 18.5 meters (60.7 feet) high by 18.5 meters (60.7 feet) in diameter while the Nth plant with focused GE enclosed heliostats will have a receiver that is 16.5 meters (54.1 feet) high by 16.5 meters (54.1 feet) in diameter.

Unlike the original design the panels are of a two header configuration. Cold sodium enters at the bottom of each panel into a header and is heated as it flows upward to an exit header at the top of the panel. Recent studies have resulted in system optimization at lower peak flux levels and design analysis provided in Section 2 shows acceptable fatigue life at projected strain levels for a two header panel with a slightly higher panel efficiency. The two header panel is projected to be of lower cost as a result of fewer welds.

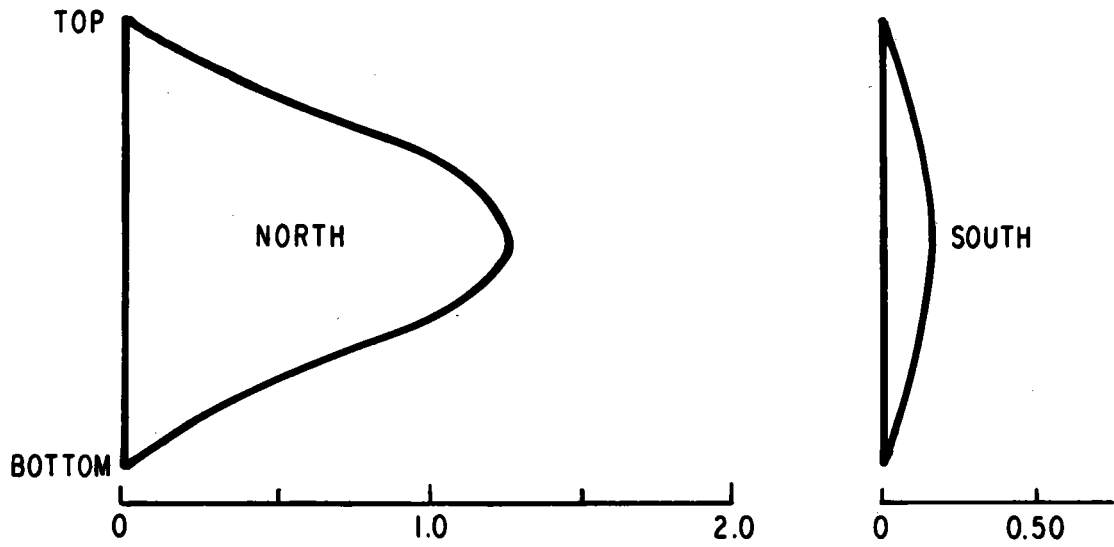


(a) 1ST PLANT

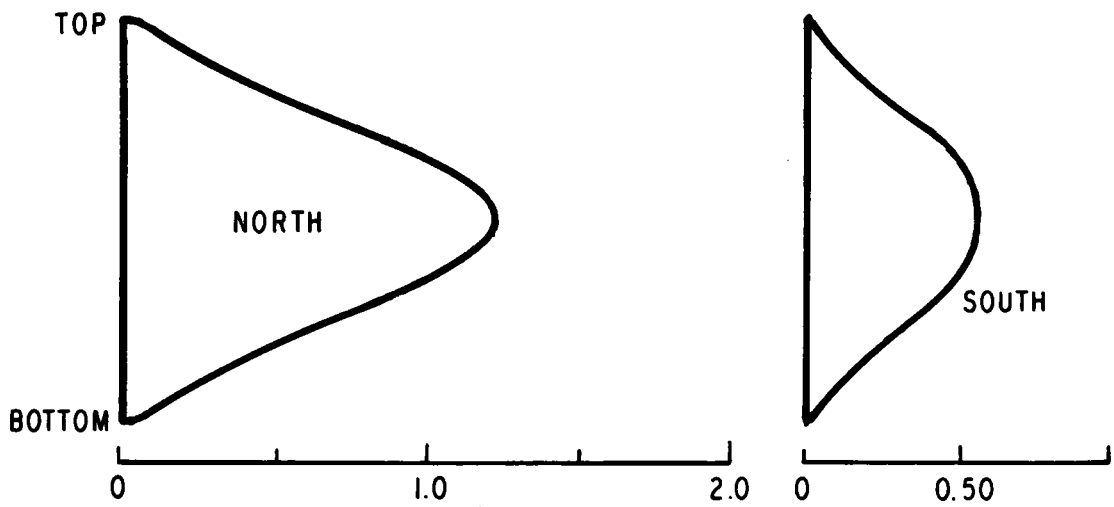


(b) NTH PLANT

Figure 7-3. Design Point Circumferential Flux Variation of Receiver Midline



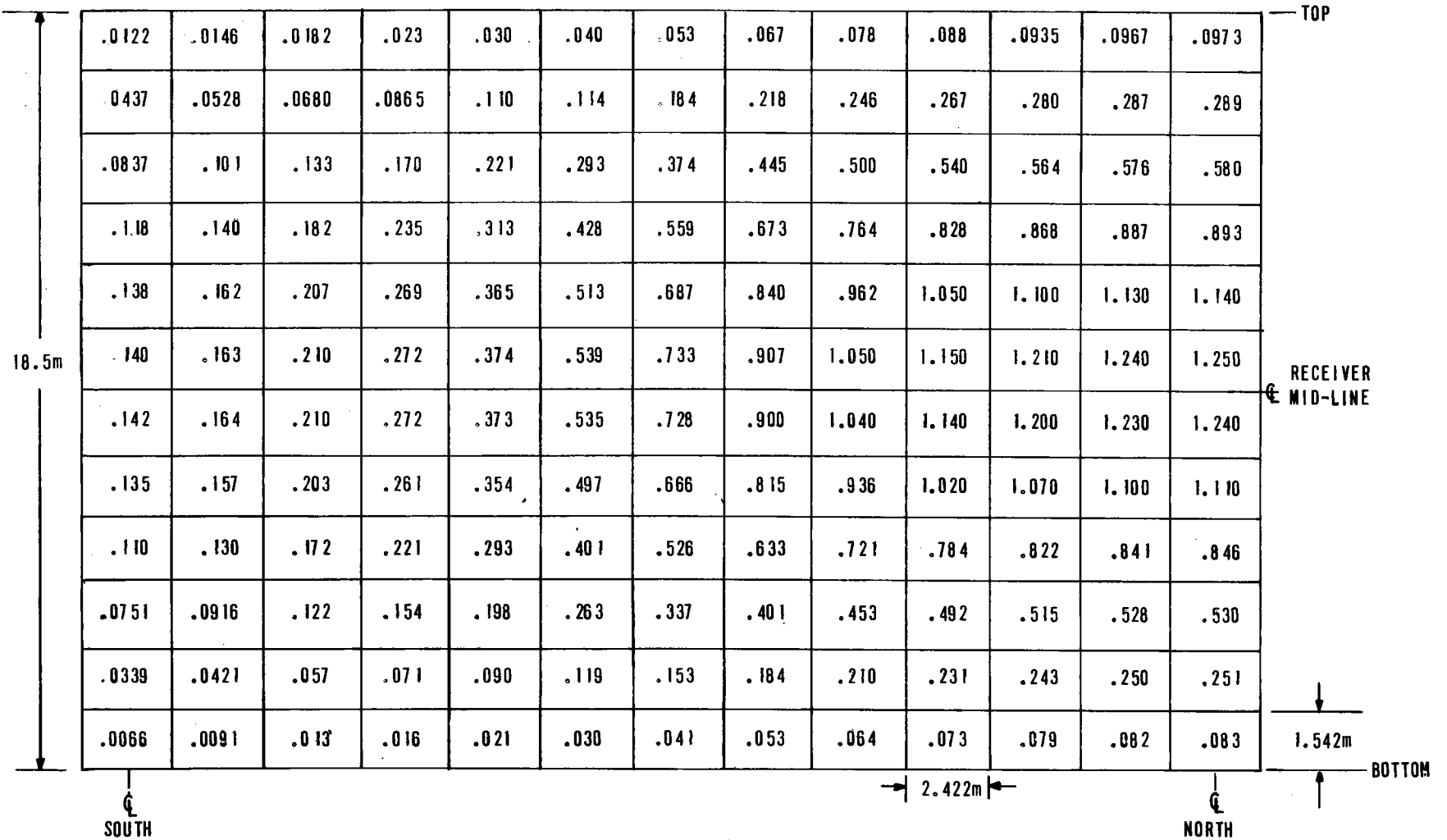
(a) 1ST PLANT



(b) NTH PLANT

Figure 7-4. Design Point Axial Flux Variations

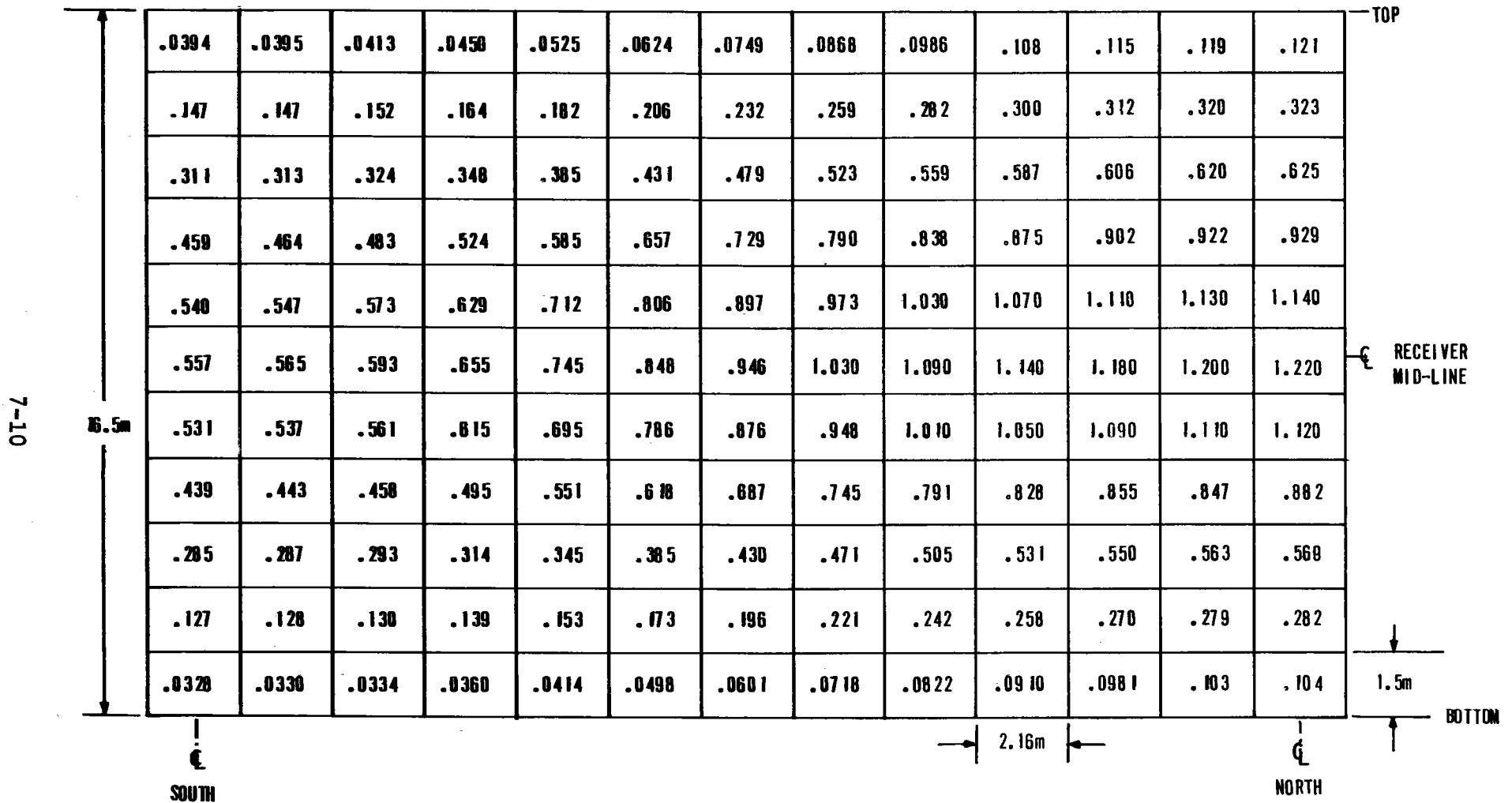
7-9



Receiver Size: 18.5 m (H) x 18.5 m (D)

Units: MW/m²

Figure 7-5. Design Point Incident Flux (1st Plant)



Receiver Size: 16.5 m (H) x 16.5 m (D)

Units: MW/m²

Figure 7-6. Design Point Incident Flux (Nth Plant)

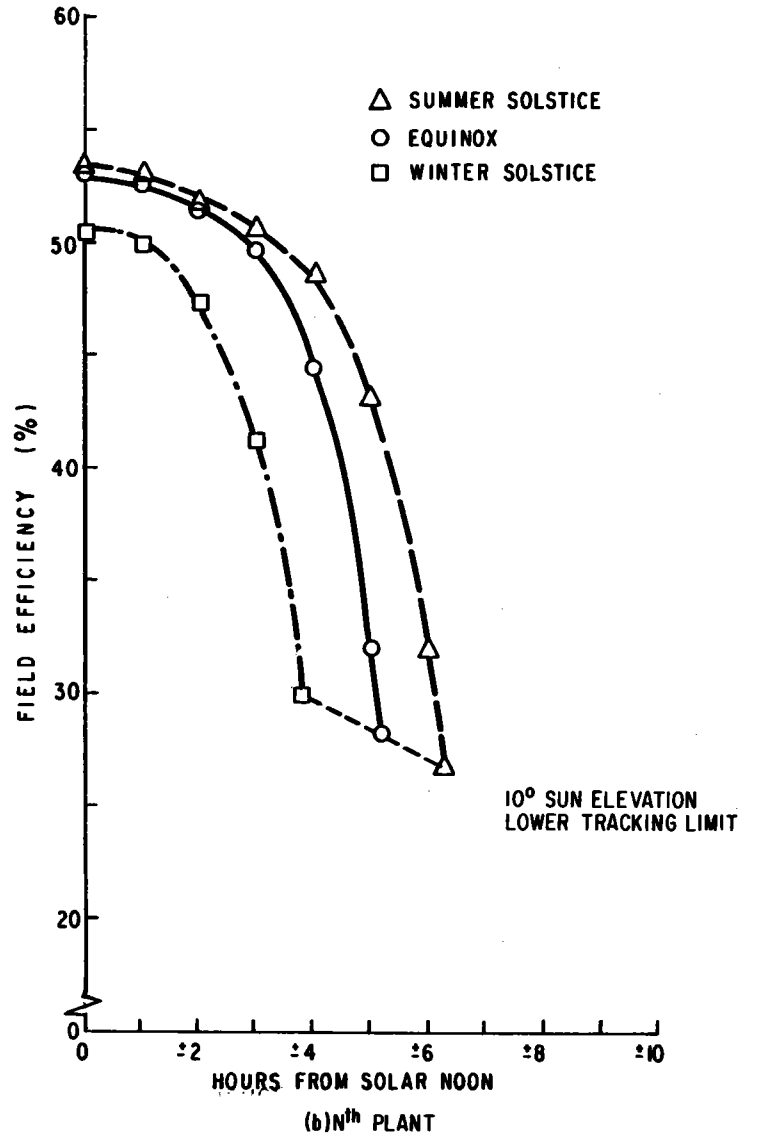
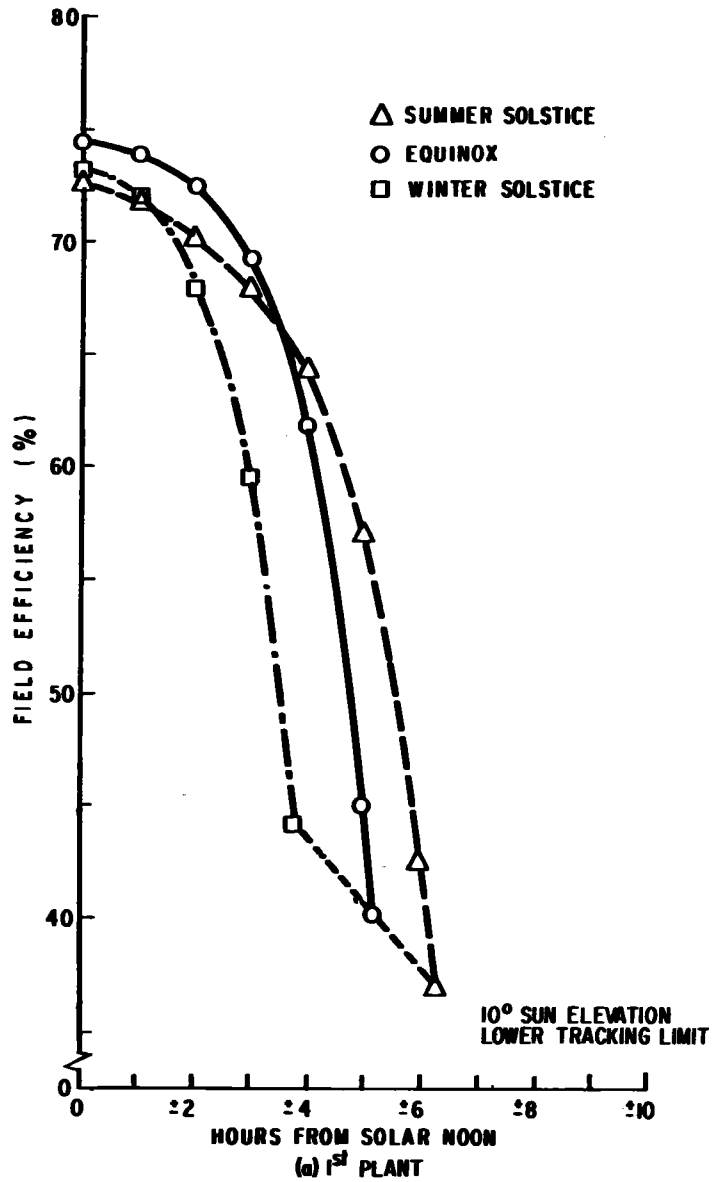
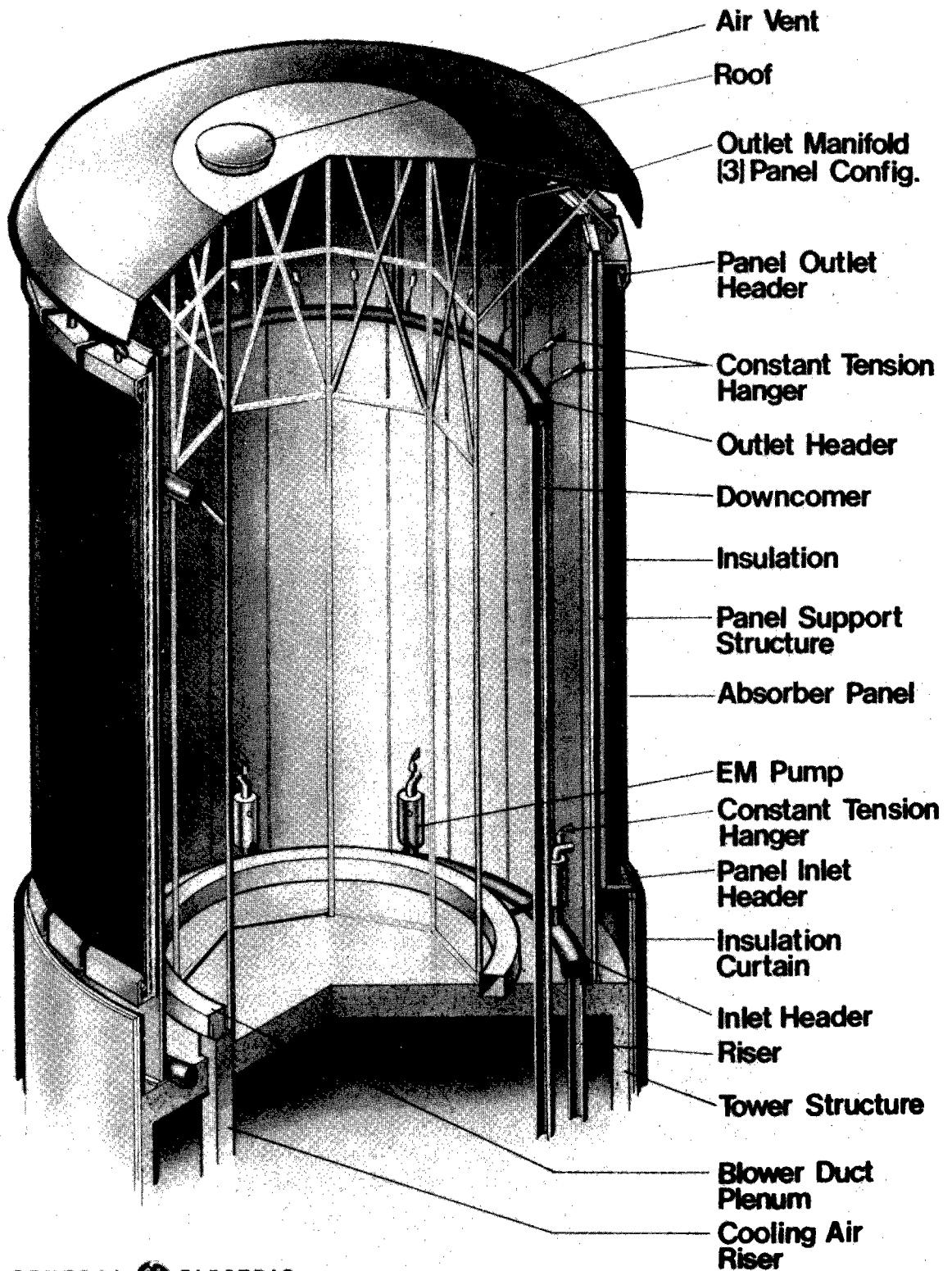


Figure 7-7. Variations in Field Efficiency

Table 7-4

ANNUAL PERFORMANCE SUMMARY

DAY OF YEAR	HOURS FROM NOON	ELEVATION (DEGREES)	AZIMUTH (DEGREES)	NORMAL INSOLATION (W/M ²)	1st PLANT		Nth PLANT	
					INCIDENT POWER ON RECEIVER (MWT)	FIELD EFFICIENCY	INCIDENT POWER ON RECEIVER (MWT)	FIELD EFFICIENCY
WINTER SOLSTICE	0.0	31.55	0.00	858.	397.589	.730	363.864	.504
	1.0	29.84	15.89	844.	385.666	.720	354.163	.499
	2.0	25.00	30.40	797.	343.849	.680	316.321	.472
	3.0	17.65	42.90	697.	283.239	.595	241.856	.412
	3.8	10.0	51.92	522.	146.619	.442	131.322	.299
DAY 35	0.0	38.42	0.00	895.	423.557	.754	390.876	.519
	1.0	36.49	17.97	884.	413.363	.737	381.299	.512
	2.0	31.08	34.02	846.	382.239	.712	353.562	.497
	3.0	23.04	47.43	768.	314.127	.644	291.287	.451
	4.0	13.23	58.50	603.	188.919	.493	175.194	.345
4.3	10.00	61.50	517.	136.780	.417	124.897	.287	
SPRING EQUINOX	0.0	55.00	0.00	941.	444.223	.744	419.382	.529
	1.0	52.30	25.04	933.	437.871	.739	412.966	.526
	2.0	45.19	45.19	907	416.834	.724	392.846	.514
	3.0	35.40	60.16	857.	376.391	.692	358.471	.497
	4.0	24.18	71.68	763.	299.495	.618	286.532	.446
	5.0	12.24	81.26	566.	181.785	.450	151.884	.319
5.2	10.00	82.91	505.	128.522	.401	120.115	.283	
DAY 127	0.0	71.58	0.00	950.	441.361	.732	426.874	.534
	1.0	67.22	39.85	944.	434.415	.725	419.437	.528
	2.0	57.52	63.18	925.	415.853	.708	405.415	.521
	3.0	45.96	77.12	889.	386.499	.685	376.244	.503
	4.0	33.80	87.17	826.	336.273	.641	332.951	.479
	5.0	21.52	95.64	714.	245.594	.542	246.520	.410
6.0	10.00	103.31	493.	121.156	.387	117.232	.283	
SUMMER SOLSTICE	0.0	78.45	0.00	947.	436.586	.726	424.652	.533
	1.0	72.58	52.49	941.	428.979	.718	418.478	.528
	2.0	61.53	74.21	924.	411.068	.701	402.316	.517
	3.0	49.43	85.93	892.	383.804	.678	379.084	.505
	4.0	37.16	94.53	838.	341.568	.642	341.197	.484
	5.0	25.01	102.09	746.	289.480	.589	270.799	.431
	6.0	13.19	109.56	569.	153.876	.425	152.321	.318
	6.3	10.00	111.71	488.	114.324	.389	110.000	.268



GENERAL  ELECTRIC

COMMERCIAL SOLAR PLANT RECEIVER

Figure 7-8. ACR-Phase II Receiver Concept

In the original design a single electromagnetic (EM) pump was provided for each absorber panel. A recently conducted optimization effort has studied reducing the number and hence cost of the EM pumps and the results which gang three panels with one pump is illustrated in the receiver plan view (Figure 7-9). Details of this optimization study are provided in Section 3.

In the original three header configuration the panel was fixed to the support structure at the cold header at the panel midpoint and was permitted to expand due to thermal growth both upward and downward. In the arrangement illustrated (Figure 7-9) the full panel axial expansion, about 3.2 inches, is downward and is accommodated by length change in the cold riser pipe. The inlet header pipe and EM pump unit is allowed to move downward as the panel expands. The radial expansion of the inlet header pipe is provided by permitting the bottom of the solar panels to move radially outward by pivoting the panels at the top. The panel support structure is at near ambient temperature and rigidly attached to the tower structure. The radial growth between the hot outlet header and this structure is accommodated by bends in the panel outlet pipes. The length of this pipe can be designed to provide sufficient fatigue life per the method of ANSI B31.1 American National Standard Power Piping. The axial growth of the panel outlet pipes will be accommodated by flexibility in the downcomer.

Bolted flange joints are shown at the inlet and exit from the solar panel to permit ease of panel replacement. This feature may be modified to a welded joint based on fatigue analysis and test of the bolted joint.

Based on recent design work for the Advanced Central Receiver, the method of mounting the panel to the strong back to allow for axial thermal differential growth will be changed from a guided roller as used in the initial study to a linkage system as shown in Figure 7-9. Lateral differential expansion, as in the initial study, will be accommodated with clips brazed to the back of the panel.

7.3 OVERALL PLANT PERFORMANCE

The performance of the refined commercial plant configuration has been estimated at the design point (noon summer solstice). The results are presented in this section for both the 1st plant and the Nth plant.

The design point energy cascades at various points in the plant are shown in Figure 7-10. A detailed listing of the collector/receiver power inputs, outputs, and losses is given in Table 7-5. The field losses are based on the field performance estimates described in Section 7.2.1. The absorber losses and the remainder of the energy balance shown in Table 7-5 are based on the results of Phase I.

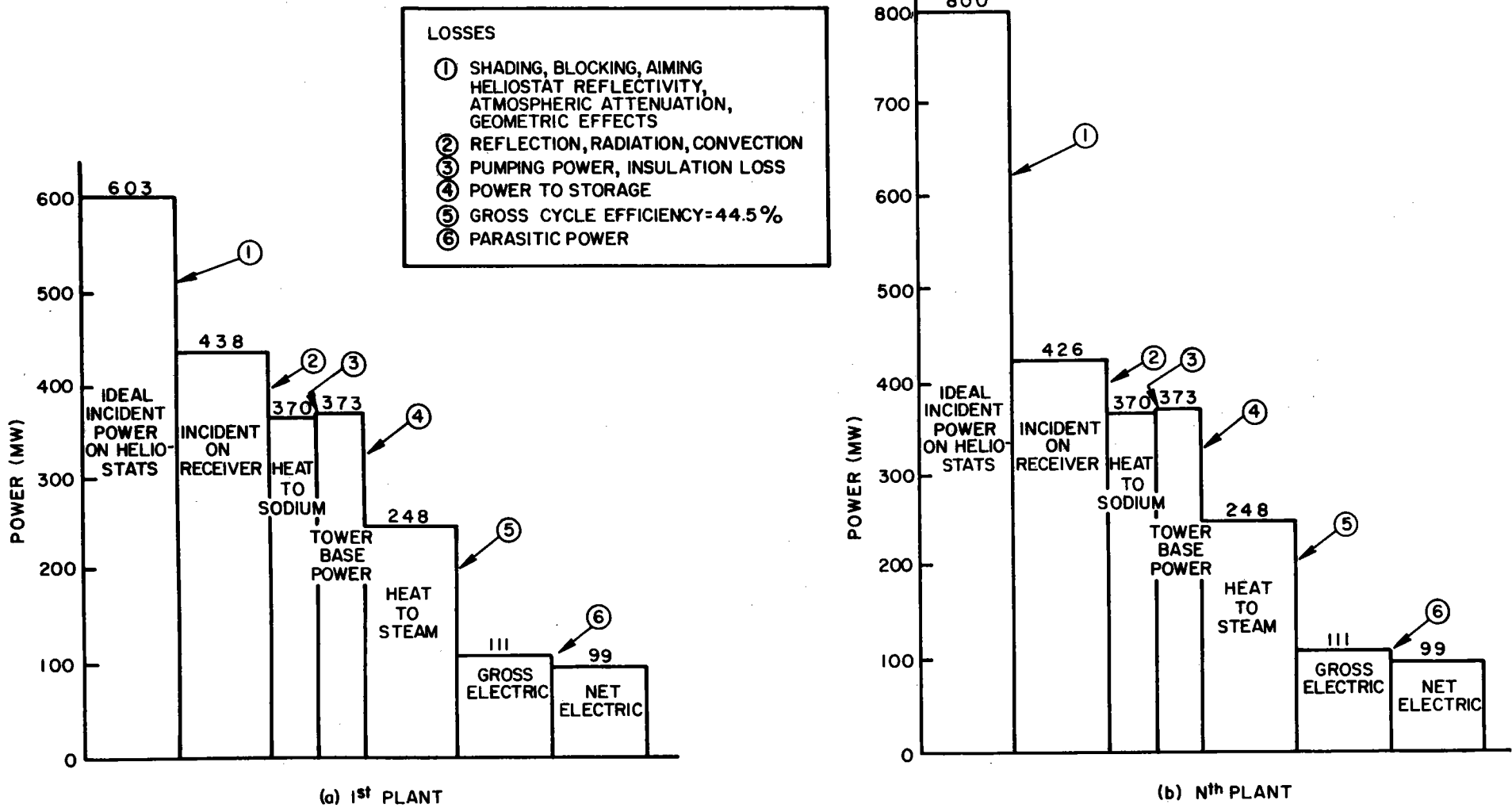


Figure 7-10. Refined Energy Cascade at Design Point (Noon, Summer Solstice)

Table 7-5

PLANT ENERGY BALANCE

	1ST PLANT (MW)	NTH PLANT (MW)
Available Insolation (950 W/m ² x mirror area)	603.15	799.63
Losses:		
Shading, Blocking, Aiming, Heliostat Reflectivity, Atmospheric Attenuation, Geometric Effects	-165.26	-373.83
Receiver Reflectivity	- 21.89	- 21.29
Radiation & Convection	- 46.09	- 34.70
Net Power to Sodium	369.91	369.81
Power Input from Pumps	+ 3.23	+ 3.23
Insulation Losses	- .52	- .52
Net Power at Tower Base	372.62	372.52
Power to Storage	-124.21	-124.17
Gross Heat to Steam Generators	248.41	248.35
Gross Electric Output	110.54	110.52
Parasitic Power Losses (10%)	- 11.05	- 11.05
Net Electric Output	99.49	99.47

Section 8

REFINED PLANT COST ESTIMATE

A number of potential improvements in performance and cost were identified in the Phase I Study (Reference 1.1, Section 6.3 Potential Improvements in Performance and Cost). This list was reviewed and optimized using the DELSOL computer code as part of Task 2.1 and is described in Section 7. Four improvements were selected which had the potential of the greatest cost and performance impact (note all costs are in 1978 dollars). The four improvements (Figure 8-1) resulted in a \$20 million cost reduction in the First Solar Power Plant and \$17.8 cost reduction for the Mature Solar Power Plant. The cost improvements were for the Absorber Unit, Receiver Circulation Equipment (EM Pumps), Thermal Storage Equipment, Collector Equipment (Heliostats) and are described in the following sections. These four sections are the only areas that have been changed, and this refined estimate does not reflect a total update of the Phase I (Ref. 1.1) cost estimate. For easy cross-referencing to Phase I report, account title, volume number and page number are listed for each improvement.

8.1 RECEIVER EQUIPMENT

The Phase I design* consisted of a three-header absorber panel with a separate electromagnetic (EM) pump for each of the 24 panels. This design had the advantage of reducing tube wall temperature in the high flux region which reduced the thermal stress. The selection of a lower peak flux reduced the requirements of the sodium cooled absorber panel. These new ground rules were the basis for the revised design described in section 7.2.2 which called for a two-header absorber panel with 8 electromagnetic pumps serving the 24 panels.

8.1.1 ABSORBER UNIT

The Phase I conceptual design study** selected a three-headed panel to accommodate high peak solar fluxes on the order of 4 MW/M^2 , which were anticipated prior to the final selection of the 360° heliostat field configuration. Since the peak

*Ref. 1.1 - Volume III, page 6-38.

**Ref. 1.1 - Volume III, page 6-41.

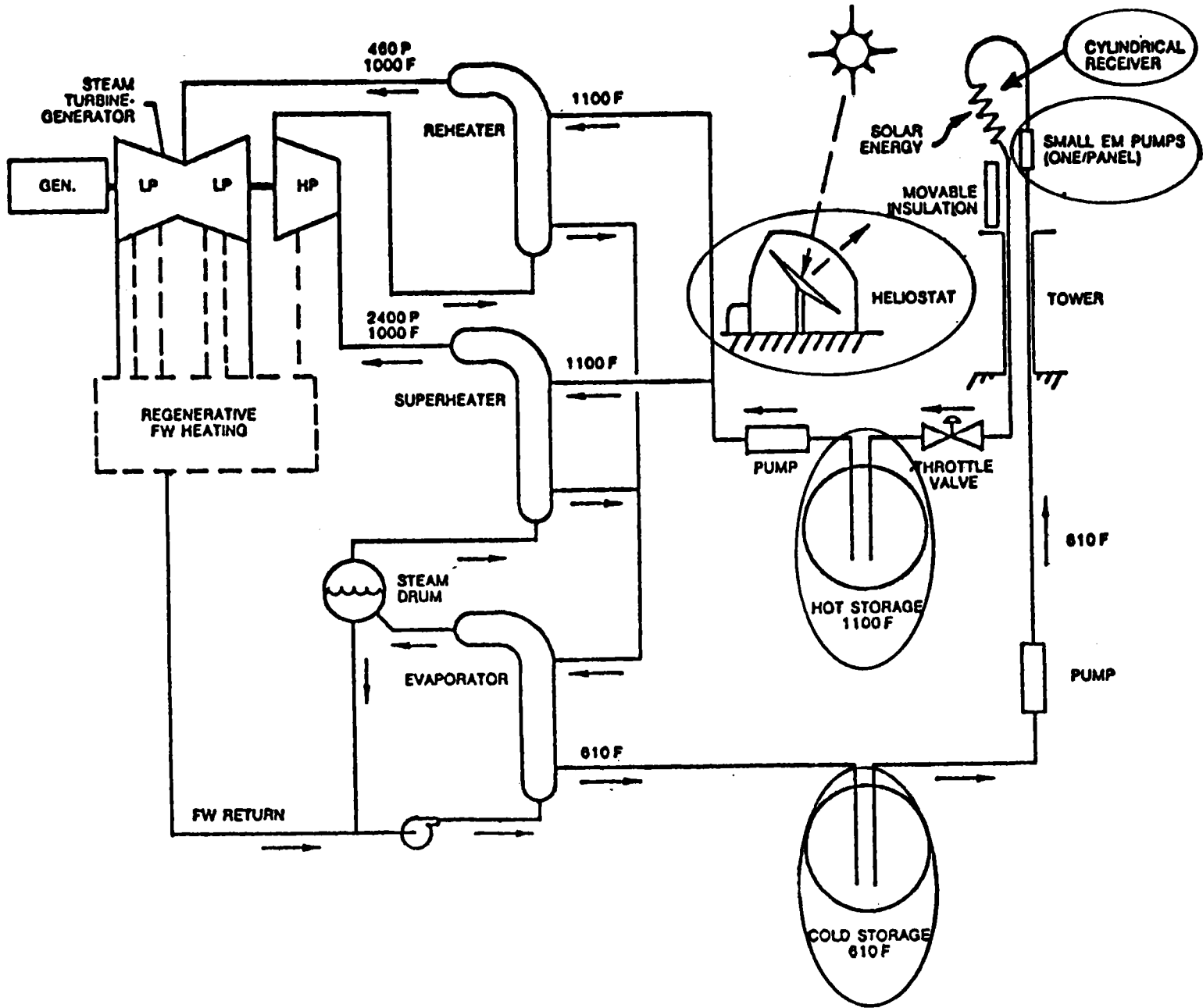


Figure 8-1. Phase I - Commercial Plant Configuration with Changes Highlighted

flux in the present design is significantly lower (1.2 MW/M^2) a less expensive two-header panel was designed. By eliminating the extra header, it is possible to reduce the welding operation by a factor of two and eliminate a reverse tube bending operation (Figure 8-2). The efficiency of the panel also increased from 89.1% to 90.4 which results in a 1.4% reduction in the number of heliostats required.

In addition to two-header design change, the list of manufacturing operations (Table 8-1) was modified to incorporate the "hourglass" insert and the nickel plating operation. The "hourglass" insert (Figure 8-3) was incorporated into the design to improve braze wetting and joint strength. The nickel plating operation provides superior wetting action and eliminates sporadic flow observed when no plating samples were brazed in the brazing evaluation program.

The shop labor hours saved by eliminating half of the welds on the headers was partially offset by increased cost due to the "hourglass" inserts and the additional operation for plating the panel tubes and inserts. The net effect of these changes (Table 8-1) in the manufacturing cost of the panel was a saving of \$134,005 over the Phase I cost for 24 panels (Tables 8-2 and 8-3).

8.1.2 RECEIVER CIRCULATION EQUIPMENT*

The receiver electromagnetic (EM) trim pumps used to control the sodium flow to each absorber panel represent a significant cost factor. An optimization study was conducted and it concluded that 16 EM trim pumps could be eliminated by grouping panels as illustrated in Figure 8-4. Selective grouping of three absorber panels together reduced the required EM pumps from 24 to 8. This resulted in a 3.1 million dollar cost reduction. The Phase I cost for E.M. Pumps (account 4513.1)* was \$4,606,000 and the revised cost is \$1,535,000**.

8.2 THERMAL STORAGE EQUIPMENT***

The Phase I thermal storage equipment cost were based on 3 hot and 3 cold spherical tanks. During the current contract Kaiser Engineers identified the tank

**Notes: Above costs are based on utilization of the same pump design for all pumps although duct geometry will be different for different flow rating: different duct geometry does not significantly affect the cost. Cost are based on a 600 gpm pump recently manufactured by General Electric.

*Ref. 1.1, Volume III, page 6-41.

***Ref. 1.1, Volume III, page 6-45.

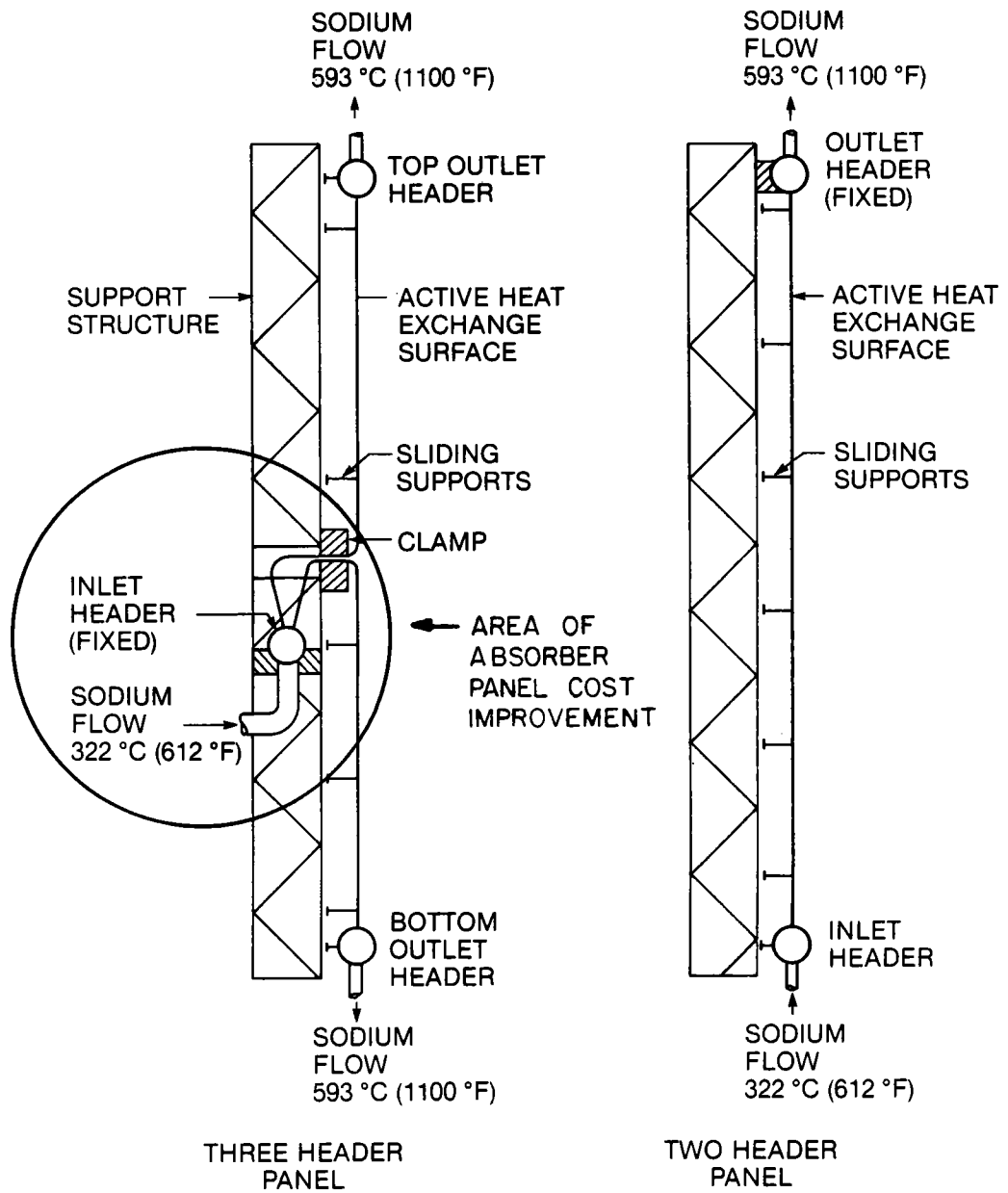


Figure 8-2. Comparison of Two and Three Header Panels

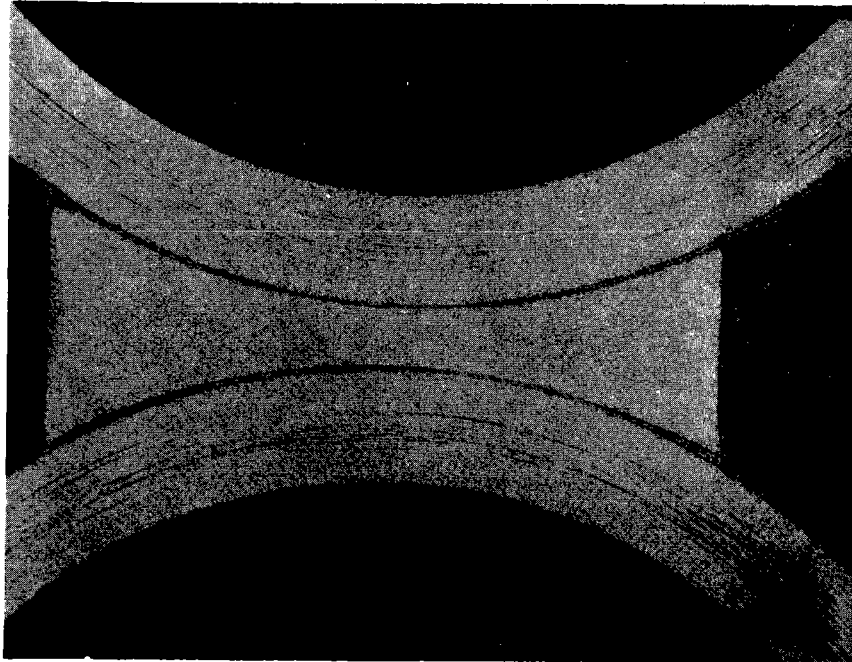


Figure 8-3. Hour Glass Insert

Table 8-1

COMMERCIAL REUSED RECEIVER PANEL MANUFACTURING OPERATIONS

CHANGES

- ➔ 1. Inspect, Cut to Size, and Machine End Tubes
- (NEW) ➔ 2. Manufacture Hour Glass Inserts
- ➔ 3. Bend Tubes
- (NEW) ➔ 4. Nickel Plate Tubes and Inserts
- 5. Set Up Tube Bundle in Fixture
- 6. Apply Braze Alloy
- 7. Furnace Braze Tube Bundles
- ➔ 8. Fabricate Inlet Header
- ➔ 9. Fabricate Outlet Header
- ➔ 10. Weld Tubes to Headers
- 11. Pressure and Helium Leak Test
- 12. Fabricate Support Structure
- 13. Fabricate Expansion Devices
- 14. Attach Tube Bundle to Support Structure
- 15. Install Insulation
- 16. Paint
- 17. Prepare for Shipment
- 18. Load on Railroad Car

Table 8-2
 ABSORBER PANEL COST DETAIL
 (24 Panels)

Shop Material	\$ 654,000	
Shop Labor and Overhead	896,744	
Incoming Freight	<u>2,880</u>	
Total Shop Cost	\$1,553,624	\$1,553,624
Design Drafting	58,000	
Blueprints	5,000	
Contract Control	100,000	
Engineering Department	12,300	
Estimating Department	7,000	
Contract Reserve (4%)	74,000	
Purchase Department and Q.C. Manufacturing	<u>6,000</u>	
Total Main Office Cost	\$ 263,600	<u>\$ 263,600</u>
Subtotal		\$1,817,224
SGA and Overhead		127,205
Fee (8%)		<u>145,793</u>
4511 Total		\$2,089,807

Table 8-3

ABSORBER PANEL MATERIALS AND FACTORY LABOR (ONE PANEL)

	Weight* (lb)	Material Cost (\$)	Factory Man-Hours
Panel Fabrication			
Tubing, 0.75-in. dia x 0.049-in wall 6230 ft @ \$1.85/ft, Incoloy 800H	2,490	11,530	438
100% XOray of Tube-to-Stub Welds	--	--	162
Hour Glass Inserts Incoloy 800	46	115	10
Nickel Plating Tubine & Inserts		2,160	
Header Fabrication			
(a) Inlet Header Plate, 0.25-in. Thick, 320 lb @ \$2.52/lb Incoloy 800H	544	1,386	308
Stubs	85	425	--
End Caps, Vents, Drains, Nipples, Straight Stops, and Saddles	175	690	--
Dye Penetrant Weld Inspection	--	--	10
10% X-ray Stubs and Headwelds	--	--	11
(b) Outlet Header Plate, 0.25-in Thick 485 lb @ \$2.52/lb. Incoloy 800H	412	1,040	200
Stubs	85	425	--
End Caps, Vents, Drain, Nipples and Straight Stops	240	1,010	--
Dye Penetrant Weld Inspection	--	--	13
100% X-ray Stubs and Head Welds	--	--	114
Support Structure			
Carbon Steel @ \$0.22/lb	10,360	2,300	414
Insulation			
Stainless Steel Pins Fibrefrac, Alumium Cover	2,900	840	70
Expansion Roller Assemblies			
Cor-ten, T-22, Incoloy Parts @ \$1.75/lb	800	1,000	45
Paint			
Black and White Pyromark	50	130	--
Brazing Operations and Materials			
Microbraz Metal, 24 lb @ \$25/lb	--	600	--
Furnace Charges	--	2,500	--
Purge Gases			
N ₂ 32,000 ft ³ @ \$6.60/1000 ft ³	--	240	--
H ₂ 32,000 ft ³ @ \$11.00/1000 ft ³	--	360	--
Gas Preheat Charge	--	360	--
Totals (per panel)	18,187	27,111	1,840
For 24 panels			

*Includes an allowance for scrap

support structure as an area of potential cost reduction and develop in improved tank design approach (Figure 805). A 38% cost reduction was accomplished utilizing a cylindrical tank top for increased volume per tank which eliminates two tanks, and improved tank support structure based on proven commercial design. The cost reduction is summarized in Table 8-4.

8.3 COLLECTOR EQUIPMENT*

Through the use of the DELSOL computer code new optimized field/receiver configurations were developed (see Section 7.2 for analysis) for both the 1st Commercial Plant and the Nth Commercial Plant. The near term application used glass heliostats with data extracted from Reference 7.2 for a production level of 25,000 units per year. The Nth Plant enclosed heliostat cost represents a mature mass-production projection of 1,000,000 heliostats per year (Reference 7.4). The enclosed heliostat cost and performance data was obtained from the current on-going material development program (Reference 7.3). The heliostat cost data was put into the DELSOL program and the optimized results are shown in Table 8-5 for the 1st Commercial Plant. The optimization study showed a 6.8 million dollar cost reduction using the enclosed heliostats in the mature plant configuration (Table 8-6).

8.4 REVISED FIRST SOLAR POWER PLANT CAPITAL COST SUMMARY

Table 8-7 summarizes all the revised cost estimates in Sections 8.1 - 8.3. The grand total of all costs for the 1st Commercial version of the General Electric solar plant concept was found to be \$190.4 million. Dividing this cost by the design point net electrical output translates the cost into \$1930/kw. Note that all costs are quoted in mid-1978 dollars, and that the bottom line does not include escalation and interest during construction.

8.5 REVISED MATURE SOLAR POWER PLANT CAPITAL COST SUMMARY

The mature plant cost estimate represents the expected capital cost of the solar power plant after 30 plants have been built to the commercial plant configuration. The results (Table 8-8) show a projected cost of \$146 million dollars; this is a cost reduction of \$17.8 million over the Phase I (Reference 1.1) cost estimate. At the design point this cost is translated into \$1480/kw (1978 dollars).

*Ref. 1.1, Volume III, pages 6-36.

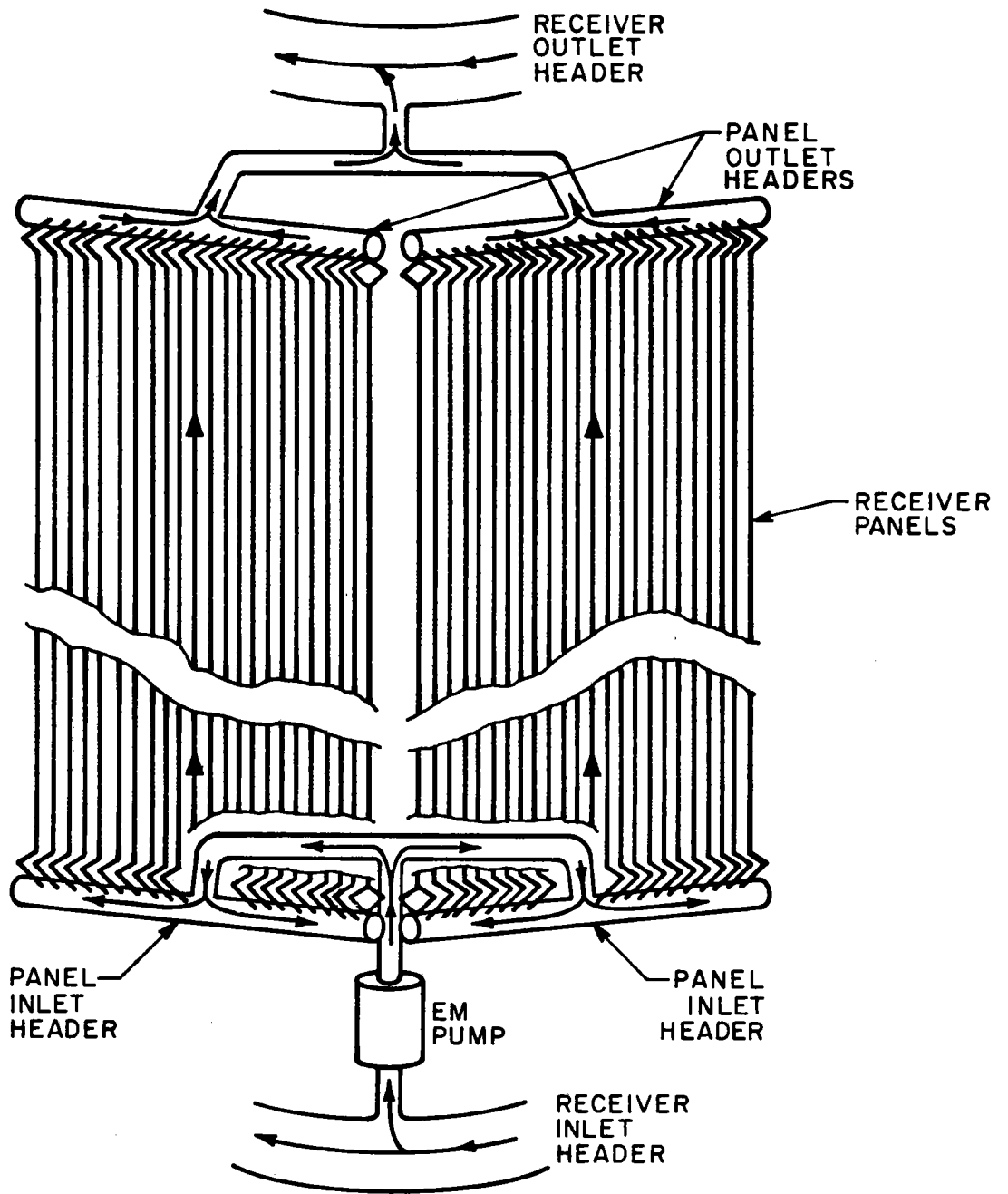


Figure8-4. Panel Grouping Concept

Table 8-4

COMMERCIAL PLANT STORAGE COST
(1978 Dollars)

<u>ACCOUNT</u>	<u>ØI</u>	<u>REVISED</u>
4611 HOT STORAGE TANKS	10,065,000	4,600,000
4612 COLD STORAGE TANKS	2,802,000	1,420,000
ADDITIONAL OUTER TANKS W/LEGS		2,050,000
4660 STORAGE FOUNDATION	190,000	127,000
	<hr/>	<hr/>
	12,057,000	8,197,000

\$4.86 MILLION
LABOR AND MATERIAL
COST REDUCTION

Table 8-5

1st COMMERCIAL HELIOSTAT COST
(1978 Dollars)

	<u>ØI</u>			<u>REVISED</u>		
	<u>UNIT</u>	<u>TOTAL</u>	(ENCLOSED)	<u>UNIT</u>	<u>TOTAL</u>	(UNENCLOSED)
4400 COLLECTOR EQUIPMENT (HELIOSTATS)	2334	45,607,110		3241	43,870,176	
4800 DISTRIBUTABLES (HELIOSTATS ONLY)	433	8,839,695		344	4,656,384	
TOTAL	2667	54,448,366		3585	48,526,580	

\$5.9 MILLION MATERIAL,
LABOR AND DISTRIBUTABLE
COST REDUCTION

Table 8-6

MATURE HELIOSTAT COST
(1978 DOLLARS)

	<u>ØI</u>			<u>REVISED</u>		
	<u>UNIT</u>	<u>TOTAL</u>	(ENCLOSED)	<u>UNIT</u>	<u>TOTAL</u>	(ENCLOSED)
4400 COLLECTOR EQUIPMENT (HELIOSTATS)	1093	22,312,983		1114	17,050,332	
4800 DISTRIBUTABLES (HELIOSTATS ONLY)	297	6,063,255		297	4,545,288	
TOTAL	1390	28,376,238		1411	21,595,620	

\$6.8 MILLION MATERIAL
LABOR AND DISTRIBUTABLE
COST REDUCTION

Table 8-7

FIRST SOLAR POWER PLANT
(1978 DOLLARS)

	<u>ØI</u>	<u>REVISED</u>
4100 SITE STRUCTURES AND MISCELLANEOUS EQUIPMENT	10,714,750	10,714,750
4200 TURBINE PLANT EQUIPMENT	20,070,400	20,070,400
4300 ELECTRIC PLANT EQUIPMENT	6,759,000	6,759,000
4400 COLLECTOR EQUIPMENT	45,828,746	43,870,176
4500 RECEIVER EQUIPMENT	36,174,418	32,993,713
4600 THERMAL STORAGE EQUIPMENT	19,178,700	14,318,500
4800 DISTRIBUTABLES	71,790,190	61,662,275
	<hr/>	<hr/>
TOTAL	210,516,204	190,388,814
(\$/KW)*	2,135	1,930

\$20 MILLION
COST REDUCTION
IN 1ST PLANT COST

*98.63 MWe @ DESIGN POINT

Table 8-8
MATURE SOLAR POWER PLANT
(1978 DOLLARS)

4100 SITE STRUCTURES AND MISCELLANEOUS EQUIPMENT	10,714,750	10,714,750
4200 TURBINE PLANT EQUIPMENT	20,070,400	20,070,400
4300 ELECTRIC PLANT EQUIPMENT	6,759,000	6,759,000
4400 COLLECTOR EQUIPMENT	22,312,983	17,050,332
4500 RECEIVER EQUIPMENT	31,714,312	31,580,307
4600 THERMAL STORAGE EQUIPMENT	19,178,700	14,318,500
4800 DISTRIBUTABLES	53,013,001	45,488,832
	<hr/>	<hr/>
TOTAL	163,763,146	145,982,121
(\$/KW*)	1,660	1,480

\$17.8 MILLION
COST REDUCTION
IN MATURE PLANT

*98.63 MWe @ DESIGN POINT

8-16

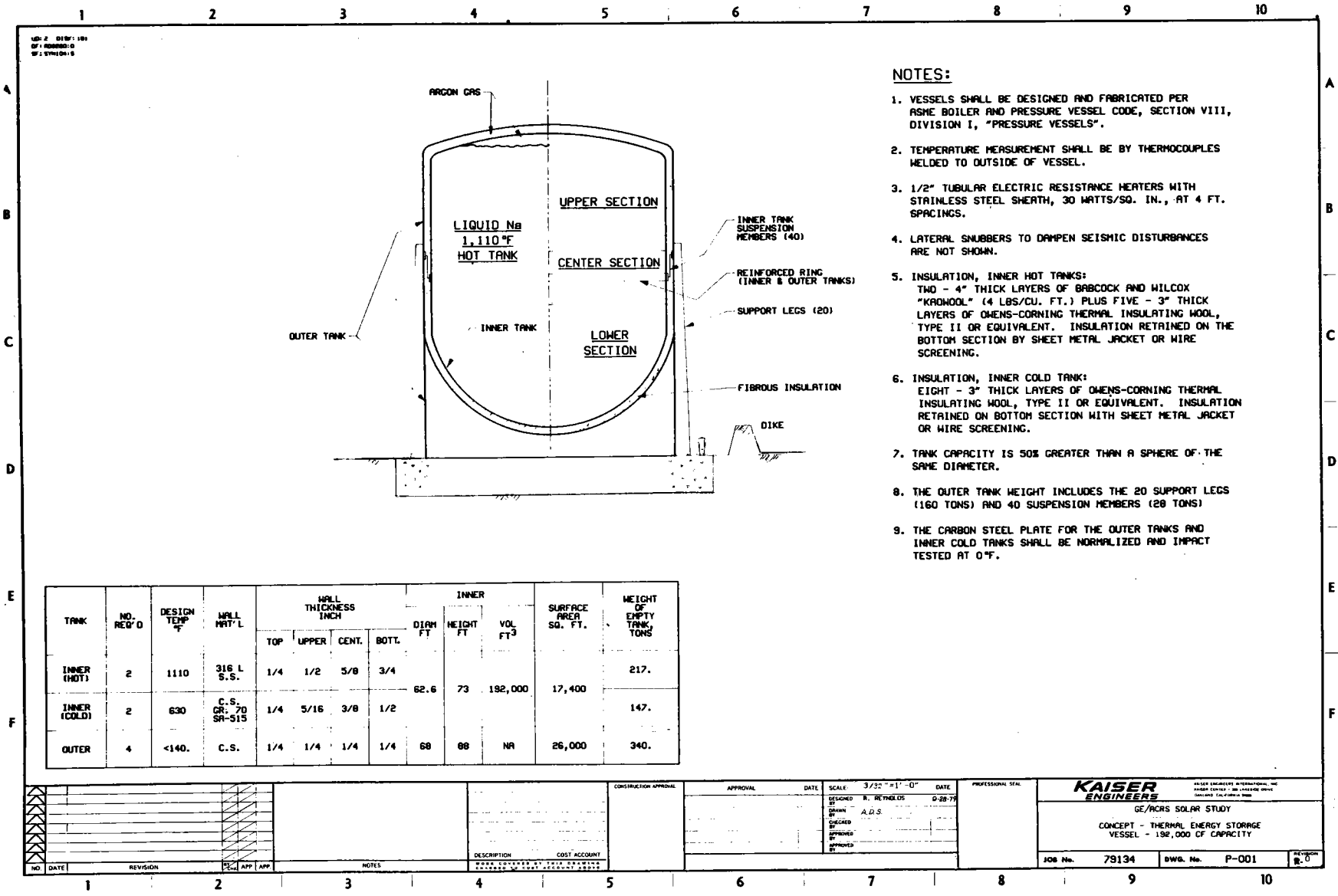


Figure 8-5. Thermal Energy Storage Vessel

The estimate is intended to be the expected value of the plant cost with roughly equal probabilities for being too high or too low. The estimate is based on the Phase I, Volume III Report (Reference 1.1) and only modified to reflect the changes previously described in Sections 8.1 - 8.3.

The Phase I estimate (Reference 1.1) covers all construction, engineering, and major component costs incurred between the time a utility orders the plant and the time the plant is fully operational. It has been assumed that an architect/engineer would design the plant, procure the major components, and manage a construction contractor who would procure the field materials and provide the construction labor force. There are other contracting options possible. Some result in higher total plant costs; others result in lower costs.

It has been assumed that this plant will be constructed at Barstow, California; the materials costs and sales tax used in the estimate are appropriate for Central California. In some cases, the labor cost was estimated as a fraction of the material cost based on historical data rather than being calculated from a man-hour estimate.

A number of items have been excluded from the estimate. These items are:

- Land right-of-way
- Owner's administrative costs
- Interest and escalation during construction
- Training
- Permits and licenses
- Soil testing
- Office furniture
- Construction models
- Capital investment for additional rail cars to deliver sodium.

Section 9

REFERENCES

Section 1

1. Conceptual Design of Advanced Central Receiver Power Systems, Phase I Final Report, General Electric Company, U.S. Department of Energy Report No. SAN/20500-1, June 29, 1979.

Section 2

1. Barstow Insolation and Meteorological Data Base, The Aerospace Corporation, March 1978.
2. L.F. Coffin, "Time Dependent Fatigue - Phenomenology and Life Prediction," Proceedings of U.S. Dept. of Energy Workshop on Time Dependent Fracture of Materials at Elevated Temperatures, Washington, D.C., February 1979.
3. S. Majumdar, Compilation of Fatigue Data for Incoloy 800 Alloys, Argonne National Laboratories, Report No. ANL/MSD-78-3, March 1979.
4. I. Berman et al., An Interim Structural Design Standard for Solar Energy Application, Sandia Laboratories Report No. SAND 790S183, April 1979.

Section 4

1. N.I. Hamilton, Heat and Mass Flow Analysis of Packed-Bed Thermal Regenerators, Massachusetts Institute of Technology Lincoln Laboratory, U.S. Department of Energy Contract No. EX-76-A-01-2295, August 1978.
2. Touloukian, Y.S. and E.H. Buyco, Thermophysical Properties of Matter, Thermophysical Properties Research Center, Purdue University, Plenum Press, NY, 1970.
3. Kreith, F., Principles of Heat Transfer, 2nd Edition, International Textbook Co., Scranton, Pa., 1965.
4. R.B. Bird, W.E. Stewart and E.N. Lightfoot, Transport Phenomena, John Wiley and Sons, NY, 1960.
5. R.K. Reynolds, "Storage Tank Support Analysis," Kaiser Engineers Final Report, Subcontract No. ESPD-79-0014, October 5, 1979.

Section 5

1. Basic Information for Starting and Loading Reheat Fossil-Fired Units, GE MSTD publication GEK-50804.
2. Personal communication with E.E. Gerrels, GE-ARSD, 7/27/79
3. Clinch River Breeder Reaction Plant Equipment Specification, Steam Generator, GE ARSD, Revision Number 30, 3/79.
4. Clinch River Plant Steam Generator Operation, Transmitted from J.C. Amos (ARSD) to J.A. Bond (ESPD), 8/10/79.

REFERENCES (Cont'd)

Section 6

1. ACR Phase II Technical Progress Report No. 1, GE ESPD, May 1979.
2. A.C. Ku and D.J. Muller, Operating Mode Analysis, ACR Phase II Mid-term Report, Volume 1, Section 5.0 of this report.

Section 7

1. T.A. Dellin and M.J. Fish, A User's Manual for DELSOL: A Computer Code for Calculating the Optical Performance, Field Layout, and Optimal System Design for Solar Central Receiver Plants, Sandia Laboratories, Report No. SAND79-8215, June 1979.
2. Solar Central Receiver Prototype Heliostat, Final Technical Report No. MDC-G7399, McDonnell Douglas Astronautics Company, August 1978.
3. Heliostat Materials Development and Evaluation, Sandia Laboratories Contract No. 83-0024B.
4. Solar Central Receiver Prototype Heliostat, Phase I Final Technical Report No. SAN-1468-1, General Electric Company, October 1978.

APPENDIX A

PANELGR2 - RECEIVER LOSS ANALYSIS CODE

```

100 REAL KN,KT,N,NU
110 DIMENSION W(12),QS(12,16),ET(12,16),TNA(12,16),TN(15),HN(12,16),
120 & KT(12,16),U(12,16),QCP(12),WP(12),TTP(12,16),
130 & TT(12,16),QR(12,15),QC(12,16),EFP(12),QIP(12),QRP(12)
140 DIMENSION P(6),WZ(6),IP(12)
150 FILENAME FLUX
160 DATA DX,DY,CN,TH,TC,PI/1.0,2.0944,.30353,1097.22,612.95,3.14159/
170 DATA ET/192*0.90/
180 DATA TT/192*1100./
190 DATA DL,D,N,SIG,EPS,ALPHA/.75,.65,108...1714E-8,.90,.95/
200 PRINT,"PANEL GROUPING (TWELVE VALUES)"
210 READ,(IP(I), I=1,12)
220 PRINT,"AIR TEMP., CONV. COEFF.,CI"
230 READ, TA,HT,CI
240 PRINT,"FLUX PLOT FILENAME"
250 READ, FLUX
260 READ(FLUX,500) ((QS(I,J),I=1,12),J=1,16)
270 500 FORMAT(4X,12F6.3)
280 20 PRINT,"FULL PRINT(YES=1,NO=0)"
290 READ,L
300 DO 160 M=1,5
310 WR=0.
320 QIR=0.
330 QRR=0.
340 QCR=0.
350 DO 125 I=1,12
360 SUM=0.
370 DO 120 J=1,16
380 SUM = SUM + QS(I,J)*ET(I,J)
390 120 CONTINUE
400 W(I) = SUM*DX*DY*3.413E6/CN/(TH-TC)
410 CONTINUE
420 125 CONTINUE
430 DO 2 K=1,6
440 P(K)=0.0
450 WZ(K)=0.0
460 DO 1 I=1,12
470 IF (IP(I) .NE. K) GO TO 1
480 WZ(K) =WZ(K) +W(I)
490 P(K) =P(K) +1.
500 WAV =WZ(K) / P(K)
510 1 CONTINUE
520 DO 3 I= 1,12
530 IF (IP(I) .EQ. K) W(I)= WAV
540 3 CONTINUE
550 2 CONTINUE
560 DO 150 I=1,12
570 WP(I)=W(I)
580 TN(I) = TC + QS(I,1)*ET(I,1)*DX*DY*3.413E6/W(I)/CN
590 TNA(I,1) = (TC + TN(I))/2.

```

```

600      DO 130 J=2,16
610      TN(J)= TN(J-1) + QS(I,J)*ET(I,J)*DX*DY*3.413E6/W(I)/CN
620      TNA(I,J)= (TN(J-1)+TN(J))/2.
630  130 CONTINUE
640      QIP (I)=0.
650      QRP(I)=0.
660      QCP(I)=0.
670      DO 140 J=1,16
680      KN= 125.3-12.74*ALOG(TNA(I,J))
690      PE= 48.*W(I)*CN/(PI*D*KN*N)
700      NU= 7.0 + .025*(PE**(.8))
710      HN(I,J)= KN*NU*12./D
720      KT(I,J)= 6.7 + .004705 *(TNA(I,J)+TT(I,J))/2.
730      U(I,J)= DL/HN(I,J)/D + DL/24./KT(I,J)*ALOG(DL/D)
740      U(I,J)= 1./U(I,J)
750      QT= C1*QS(I,J)*ET(I,J)*3.413E6/10.7636
760      TT(I,J)= TNA(I,J) + QT/U(I,J)
770      TTP(I,J)= TNA(I,J) + QT/U(I,J)/C1
780      QR(I,J) = SIG*EPS*DX*DY*10.7636*((TT(I,J)+460.)**4 -
790 &          (TA+460.)**4)/3.413E6
800      QC(I,J)= HT*DX*DY*10.7636*(TT(I,J) - TA)/3.413E6
810      ET(I,J)= ALPHA - (QR(I,J)+QC(I,J))/QS(I,J)/DX/DY
820      QIP(I)= QIP(I) + QS(I,J)*DX*DY
830      QRP(I)= QRP(I) + QR(I,J)
840      QCP(I)= QCP(I) + QC(I,J)
850  140 CONTINUE
860      QIP(I)= QIP(I)
870      QRP(I)= QRP(I)
880      QCP(I)= QCP(I)
890      EFP(I)= ALPHA - (QRP(I)+QCP(I))/QIP(I)
900      WR=WR + WP(I)*2.
910      QIR=QIR+QIP(I)*2.
920      QRR=QRR+QRP(I)*2.
930      QCR=QCR+QCP(I)*2.
940  150 CONTINUE
950      QREF = QIR*.05
960      EFR= ALPHA-(QRR +QCR)/QIR
970  160 CONTINUE
980      PRINT 510,WR,QIR,QRR,QCR,QREF,EFR
990  510 FORMAT(1X,"RECEIVER SUMMARY"/1X,"FLOW=",F13.6,"LB/HR"/
1000 &          1X,"INCIDENT=",F8.2,"MW"/
1010 &          1X,"RAD. LOSS=",F8.2,"MW"/
1020 &          1X,"CONV. LOSS=",F8.2,"MW"/
1030 &          1X,"REFL. LOSS=",F8.2,"MW"/
1040 &          1X,"EFFICIENCY=",F6.4/"0")
1050      PRINT 520
1060  520 FORMAT (1X,"PANEL",2X,"FLOW",9X,"INCIDENT",2X,"RADIATION",2X,
1070 &          "CONVECTION",2X,"EFFICIENCY"/
1080 &          8X,"LB/HR",8X,"MW",8X,"MW",9X,"MW")
1090      PRINT 530,(I,WP(I),QIP(I),QRP(I),QCP(I),EFP(I),I=1,12)

```

```

1100 530 FORMAT(1X,12,5X,F8.0,5X,F8.3,2X,F8.3,3X,F8.3,4X,F7.4)
1110 PRINT 540
1120 540 FORMAT("OOUTSIDE TUBE TEMPERATURES(DEG. F)")
1130 PRINT 550,((TT(I,J),I=1,12),J=1,16)
1140 550 FORMAT(1X,12F8.1)
1150 PRINT 560
1160 560 FORMAT("ONODE EFFICIENCIES(P.U.)")
1170 PRINT 570,((ET(I,J),I=1,12),J=1,16)
1180 570 FORMAT(1X,12F8.4)
1190 IF (L.EQ.0) GO TO 200
1200 PAUSE
1210 PRINT 580
1220 580 FORMAT("OINCIDENT FLUX(MW/SQ.M)")
1230 PRINT 590,((QS(I,J),I=1,12),J=1,16)
1240 590 FORMAT(1X,12F7.3)
1250 PRINT 600
1260 600 FORMAT ("ORADIATION LOSS(MW)")
1270 PRINT 570,((QR(I,J),I=1,12),J=1,16)
1280 PRINT 620
1290 620 FORMAT("OCONVECTION LOSS(MW)")
1300 PRINT 570,((QC(I,J),I=1,12),J=1,16)
1310 PRINT 640
1320 640 FORMAT("ONODE SODIUM TEMPERATURES(DEG. F)")
1330 PRINT 550 , ((TNA(I,J),I=1,12),J=1,16)
1340 PAUSE
1350 PRINT 660
1360 660 FORMAT("OSODIUM HEAT TRANSFER COEFFICIENTS(BTU/HR*F*FT**2)")
1370 PRINT 550,((HN(I,J),I=1,12),J=1,16)
1380 PRINT 680
1390 680 FORMAT("OTUBE CONDUCTANCE(BTU/HR*F*FT**2)")
1400 PRINT 550,((U(I,J),I=1,12), J=1,16)
1410 PRINT 700
1420 700 FORMAT("OTUBE WALL CONDUCTIVITY(BTU/HR*F*FT)")
1430 PRINT 710,((KT(I,J),I=1,12), J=1,16)
1440 710 FORMAT(1X,12F7.1)
1450 PRINT 720
1460 720 FORMAT("OPEAK TUBE TEMPERATURE (DEG. F)")
1470 PRINT 550,((TTP(I,J),I=1,12),J=1,16)
1480 200 CONTINUE
1490 PRINT,"CONTINUE ITERATION?(YES=1,NO=0)"
1500 READ,L1
1510 IF(L1.EQ.1) GO TO 20
1520 STOP
1530 END

```

Table A-1
VARIABLE LIST FOR PANEL GR

ALPHA	= absorptivity
CI	= heat flux factor to account for two dimensional tube wall conduction
CN	= average specific heat of sodium
D	= tube i.d.
DX	= panel width
DY	= node height
EFP(I)	= efficiency of panel i
EFR	= efficiency of receiver
EPS	= emissivity
ET(I,J)	= efficiency of node i in panel j
HN(I,J)	= sodium side heat transfer coefficient
HT	= air side convective heat transfer coefficient
IP(I)	= group number of panel i
KN	= sodium thermal conductivity
KT(I,J)	= tube wall thermal conductivity
N	= number of tubes per panel
NU	= Nusselt number of sodium
P(K)	= number of panels in group K
PE	= Peclet number of sodium
QC(I,J)	= convection loss from node i in panel j
QR(I,J)	= radiative loss from node i in panel j
QS(I,J)	= incident solar flux on node i in panel j
QCP(I)	= convective loss from panel i
QCR(I)	= radiative loss from panel i
QIP(I)	= incident power on panel i
QIR	= solar incident power on receiver
QRP(I)	= radiative loss on panel i
QRR	= radiative loss from receiver
SIG	= Stefan Boltzmann Constant
TA	= ambient air temperature
TC	= sodium inlet temperature
TH	= sodium outlet temperature
TN(I)	= sodium temperature at outlet of node i, TH(0) = TC
TNA(I,J)	= average sodium temperature in node i of panel j
TT(I,J)	= average sodium temperature in node i of panel j
U(I,J)	= tube conductance
W(I)	= sodium flowrate in one half of panel i
WP(I)	= sodium flowrate in panel i
WR	= receiver sodium flowrate
WZ(K)	= total flow of panels in group K
WAV	= average flow in panel group

APPENDIX B

PANELGR2 OUTPUT FOR SELECTED GROUPING SCHEME

PANEL GROUPING (TWELVE VALUES)?1,1,1,2,2,2,3,3,3,4,4,4

AIR TEMP., CONV. COEFF., C1?83., 2...6366

FLUX PLOT FILENAME?FLUX2.H

FULL PRINT(YES=1, NO=0)?1

RECEIVER SUMMARY

FLOW= 0.858614E+07LB/HR
 INCIDENT= 414.14MW
 RAD. LOSS= 15.14MW
 CONV. LOSS= 4.19MW
 REFL. LOSS= 20.71MW
 EFFICIENCY=0.9033

PANEL	FLOW LB/HR	INCIDENT MW	RADIATION MW	CONVECTION MW	EFFICIENCY
1	457969.	22.628	0.685	0.180	0.9118
2	457969.	21.623	0.652	0.177	0.9117
3	457969.	20.655	0.621	0.174	0.9115
4	393825.	19.692	0.673	0.179	0.9067
5	393825.	18.707	0.637	0.176	0.9066
6	393825.	17.731	0.603	0.172	0.9063
7	330006.	16.768	0.664	0.178	0.8998
8	330006.	15.796	0.623	0.174	0.8996
9	330006.	14.837	0.584	0.170	0.8992
10	265890.	13.852	0.659	0.177	0.8897
11	265890.	12.876	0.609	0.172	0.8893
12	265890.	11.905	0.553	0.168	0.8886

OUTSIDE TUBE TEMPERATURES(DEG. F)

620.6	620.1	619.8	619.5	619.2	618.6	618.8	618.2	617.9	617.7	617.1	616.8
629.7	628.9	628.2	628.0	627.3	626.4	626.7	625.6	624.8	624.8	624.0	622.9
647.5	645.5	644.2	644.4	642.6	641.1	641.6	639.9	638.1	638.7	636.7	634.5
674.9	671.8	669.1	670.3	667.2	664.3	665.8	662.4	659.5	661.1	657.6	653.8
718.4	713.2	708.9	711.3	706.3	701.1	704.2	698.8	693.5	697.1	691.1	684.9
789.8	781.9	774.3	778.7	770.4	762.2	767.8	758.8	749.8	757.3	746.6	736.3
895.4	883.2	871.3	879.2	866.0	852.9	863.2	848.5	834.2	847.5	830.7	814.2
1011.1	994.1	977.4	991.4	972.9	954.5	971.8	951.3	931.0	953.3	929.6	905.7
1094.0	1073.4	1053.3	1075.7	1053.1	1030.6	1057.6	1032.4	1007.2	1041.7	1012.0	981.9
1127.0	1105.1	1083.3	1114.5	1089.8	1055.3	1102.7	1074.5	1046.6	1093.4	1059.7	1026.1
1130.9	1108.5	1086.3	1124.5	1099.1	1074.1	1119.2	1090.0	1061.0	1117.1	1081.3	1045.9
1129.4	1106.7	1084.7	1127.2	1101.7	1076.1	1126.0	1096.4	1066.9	1128.4	1091.9	1055.6
1128.7	1105.9	1083.8	1128.9	1103.0	1077.4	1130.0	1100.0	1070.4	1134.7	1097.7	1060.9
1127.0	1104.1	1082.1	1128.4	1102.4	1077.0	1130.8	1101.0	1071.1	1136.9	1099.7	1062.7
1123.7	1101.0	1079.2	1126.0	1100.3	1074.8	1129.4	1099.4	1069.7	1135.9	1099.1	1061.9
1121.5	1098.8	1077.1	1124.0	1098.4	1072.9	1127.7	1097.7	1068.1	1134.2	1097.2	1060.4

NODE EFFICIENCIES(P.U.)

0.8045	0.7954	0.7904	0.7792	0.7730	0.7592	0.7552	0.7383	0.7287	0.7122	0.6863	0.6711
0.8625	0.8587	0.8554	0.8497	0.8456	0.8401	0.8348	0.8265	0.8202	0.8090	0.8029	0.7888
0.8995	0.8970	0.8950	0.8922	0.8891	0.8867	0.8825	0.8796	0.8749	0.8693	0.8636	0.8570
0.9166	0.9153	0.9139	0.9122	0.9104	0.9087	0.9061	0.9038	0.9015	0.8976	0.8944	0.8904
0.9264	0.9256	0.9248	0.9234	0.9225	0.9213	0.9194	0.9181	0.9164	0.9137	0.9117	0.9094
0.9323	0.9320	0.9315	0.9303	0.9298	0.9292	0.9276	0.9269	0.9260	0.9238	0.9225	0.9212
0.9350	0.9348	0.9345	0.9334	0.9332	0.9328	0.9314	0.9310	0.9305	0.9284	0.9277	0.9270
0.9345	0.9345	0.9344	0.9330	0.9329	0.9328	0.9310	0.9309	0.9306	0.9280	0.9278	0.9274
0.9312	0.9312	0.9312	0.9293	0.9293	0.9293	0.9266	0.9266	0.9266	0.9228	0.9228	0.9226
0.9236	0.9238	0.9239	0.9206	0.9207	0.9208	0.9164	0.9165	0.9166	0.9101	0.9103	0.9104
0.9085	0.9088	0.9090	0.9031	0.9034	0.9036	0.8956	0.8960	0.8962	0.8847	0.8849	0.8853
0.8822	0.8824	0.8829	0.8725	0.8732	0.8733	0.8590	0.8599	0.8605	0.8391	0.8405	0.8414
0.8410	0.8414	0.8419	0.8248	0.8253	0.8263	0.8021	0.8032	0.8050	0.7689	0.7715	0.7725
0.7712	0.7708	0.7724	0.7425	0.7429	0.7463	0.7043	0.7094	0.7090	0.6495	0.6527	0.6545
0.6249	0.6270	0.6311	0.5731	0.5795	0.5811	0.5120	0.5100	0.5175	0.4026	0.4238	0.4191
0.3960	0.3901	0.3999	0.2935	0.3078	0.2964	0.1933	0.1807	0.1984	0.0093	-0.0105	0.0166

PAUSE

INCIDENT FLUX(MW/SQ.M)

0.066	0.062	0.060	0.056	0.054	0.050	0.049	0.045	0.043	0.040	0.036	0.034
0.113	0.108	0.104	0.098	0.094	0.089	0.085	0.079	0.075	0.069	0.065	0.060
0.207	0.196	0.188	0.179	0.169	0.162	0.152	0.145	0.135	0.126	0.117	0.108
0.341	0.325	0.310	0.297	0.281	0.267	0.252	0.237	0.224	0.208	0.194	0.179
0.549	0.523	0.501	0.478	0.455	0.429	0.406	0.383	0.360	0.335	0.312	0.289
0.901	0.862	0.822	0.784	0.745	0.707	0.668	0.630	0.591	0.554	0.512	0.474
1.404	1.344	1.283	1.223	1.161	1.101	1.042	0.980	0.920	0.860	0.799	0.739
1.821	1.742	1.663	1.586	1.507	1.428	1.349	1.272	1.194	1.115	1.038	0.959
1.821	1.742	1.663	1.586	1.507	1.428	1.349	1.272	1.194	1.115	1.038	0.959
1.404	1.344	1.283	1.223	1.161	1.101	1.042	0.980	0.920	0.860	0.799	0.739
0.901	0.862	0.822	0.784	0.745	0.707	0.668	0.630	0.591	0.554	0.512	0.474
0.549	0.523	0.501	0.478	0.455	0.429	0.406	0.383	0.360	0.335	0.312	0.289
0.341	0.325	0.310	0.297	0.281	0.267	0.252	0.237	0.224	0.208	0.194	0.179
0.207	0.196	0.188	0.179	0.169	0.162	0.152	0.145	0.135	0.126	0.117	0.108
0.113	0.108	0.104	0.098	0.094	0.089	0.085	0.079	0.075	0.069	0.065	0.060
0.066	0.062	0.060	0.056	0.054	0.050	0.049	0.045	0.043	0.040	0.036	0.034

RADIATION LOSS(MW)

0.0130	0.0130	0.0130	0.0130	0.0129	0.0129	0.0129	0.0129	0.0129	0.0129	0.0128	0.0128
0.0135	0.0134	0.0134	0.0134	0.0134	0.0133	0.0133	0.0133	0.0132	0.0132	0.0132	0.0131
0.0144	0.0143	0.0143	0.0143	0.0142	0.0141	0.0141	0.0140	0.0139	0.0140	0.0139	0.0137
0.0160	0.0158	0.0157	0.0157	0.0156	0.0154	0.0155	0.0153	0.0151	0.0152	0.0150	0.0148
0.0188	0.0184	0.0181	0.0183	0.0180	0.0176	0.0178	0.0175	0.0172	0.0174	0.0170	0.0166
0.0240	0.0234	0.0228	0.0231	0.0225	0.0218	0.0223	0.0216	0.0209	0.0215	0.0207	0.0200
0.0335	0.0323	0.0311	0.0319	0.0306	0.0294	0.0303	0.0290	0.0277	0.0289	0.0274	0.0260
0.0468	0.0447	0.0426	0.0443	0.0421	0.0399	0.0419	0.0395	0.0373	0.0398	0.0371	0.0346
0.0585	0.0555	0.0525	0.0558	0.0525	0.0494	0.0532	0.0497	0.0463	0.0509	0.0469	0.0432
0.0637	0.0602	0.0569	0.0617	0.0579	0.0543	0.0599	0.0556	0.0516	0.0584	0.0535	0.0488
0.0644	0.0608	0.0574	0.0633	0.0593	0.0555	0.0625	0.0579	0.0536	0.0622	0.0566	0.0515
0.0641	0.0605	0.0571	0.0638	0.0597	0.0558	0.0636	0.0589	0.0545	0.0640	0.0582	0.0529
0.0640	0.0604	0.0570	0.0640	0.0599	0.0560	0.0642	0.0595	0.0550	0.0650	0.0591	0.0536
0.0637	0.0601	0.0567	0.0640	0.0598	0.0560	0.0644	0.0596	0.0551	0.0654	0.0594	0.0539
0.0632	0.0596	0.0563	0.0636	0.0595	0.0557	0.0641	0.0594	0.0549	0.0652	0.0593	0.0538
0.0629	0.0593	0.0560	0.0633	0.0592	0.0554	0.0639	0.0591	0.0547	0.0649	0.0590	0.0535

CONVECTION LOSS(MW)

0.0071	0.0071	0.0071	0.0071	0.0071	0.0071	0.0071	0.0071	0.0071	0.0071	0.0071	0.0071
0.0072	0.0072	0.0072	0.0072	0.0072	0.0072	0.0072	0.0072	0.0072	0.0072	0.0071	0.0071
0.0075	0.0074	0.0074	0.0074	0.0074	0.0074	0.0074	0.0074	0.0073	0.0073	0.0073	0.0073
0.0078	0.0078	0.0077	0.0078	0.0077	0.0077	0.0077	0.0077	0.0076	0.0076	0.0076	0.0075
0.0084	0.0083	0.0083	0.0083	0.0082	0.0082	0.0082	0.0081	0.0081	0.0081	0.0080	0.0080
0.0093	0.0092	0.0091	0.0092	0.0091	0.0090	0.0090	0.0089	0.0088	0.0089	0.0088	0.0086
0.0107	0.0106	0.0104	0.0105	0.0103	0.0102	0.0103	0.0101	0.0099	0.0101	0.0099	0.0097
0.0123	0.0120	0.0118	0.0120	0.0118	0.0115	0.0117	0.0115	0.0112	0.0115	0.0112	0.0109
0.0134	0.0131	0.0128	0.0131	0.0128	0.0125	0.0129	0.0125	0.0122	0.0127	0.0123	0.0119
0.0138	0.0135	0.0132	0.0136	0.0133	0.0130	0.0135	0.0131	0.0127	0.0133	0.0129	0.0125
0.0138	0.0135	0.0133	0.0138	0.0134	0.0131	0.0137	0.0133	0.0129	0.0137	0.0132	0.0127
0.0138	0.0135	0.0132	0.0138	0.0135	0.0131	0.0138	0.0134	0.0130	0.0138	0.0133	0.0128
0.0138	0.0135	0.0132	0.0138	0.0135	0.0131	0.0138	0.0134	0.0130	0.0139	0.0134	0.0129
0.0138	0.0135	0.0132	0.0138	0.0135	0.0131	0.0138	0.0134	0.0131	0.0139	0.0134	0.0129
0.0137	0.0134	0.0132	0.0138	0.0134	0.0131	0.0138	0.0134	0.0130	0.0139	0.0134	0.0129
0.0137	0.0134	0.0131	0.0138	0.0134	0.0131	0.0138	0.0134	0.0130	0.0139	0.0134	0.0129

NODE SODIUM TEMPERATURES(DEG. F)

614.3	614.2	614.2	614.3	614.2	614.1	614.3	614.1	614.1	614.2	614.0	614.0
618.2	617.9	617.7	618.0	617.8	617.5	618.1	617.7	617.4	617.9	617.5	617.1
625.5	624.8	624.3	625.3	624.7	624.0	625.4	624.5	623.8	625.3	624.3	623.3
638.3	636.9	635.9	638.2	636.8	635.5	638.4	636.7	635.2	638.4	636.5	634.4
659.4	657.0	655.1	659.5	657.0	654.6	659.8	656.9	654.2	660.2	656.7	653.1
694.1	690.1	686.7	694.5	690.3	686.1	695.3	690.3	685.5	696.4	690.3	684.1
749.4	743.1	737.2	750.4	743.4	736.4	752.0	743.7	735.6	754.4	744.0	733.8
826.9	817.3	808.0	828.8	817.8	807.0	831.4	813.5	805.8	835.6	819.5	803.5
914.3	900.8	887.8	917.1	901.7	886.5	920.9	902.8	884.9	927.0	904.5	882.1
991.2	974.4	958.1	994.9	975.6	956.4	999.5	976.9	954.4	1007.3	979.2	951.0
1045.6	1026.5	1007.7	1049.7	1027.7	1005.9	1055.0	1029.1	1003.4	1063.6	1031.5	999.4
1079.1	1058.5	1038.3	1083.3	1059.7	1036.2	1088.7	1061.0	1033.4	1097.8	1063.1	1028.8
1099.0	1077.4	1056.4	1103.1	1078.5	1054.0	1108.4	1079.5	1050.9	1117.3	1081.4	1045.7
1110.4	1088.3	1066.9	1114.4	1089.2	1064.2	1119.4	1090.0	1060.7	1128.0	1091.4	1054.9
1115.4	1094.0	1072.3	1120.1	1094.5	1069.3	1124.8	1095.1	1065.5	1132.9	1096.0	1059.2
1118.8	1096.3	1074.6	1122.2	1096.7	1071.3	1126.7	1096.8	1067.2	1134.1	1097.2	1060.3

PAUSE

SOIUM HEAT TRANSFER COEFFICIENTS (BTU/HR*F*FT**2)

9393.7	9394.0	9394.1	8964.9	8965.1	8955.4	8524.0	8524.4	8524.6	8063.6	8064.1	8064.3
9381.9	9382.9	9383.5	8953.6	8954.3	8955.4	8512.6	8514.0	8514.8	8052.7	8054.1	8055.3
9360.0	9362.1	9363.6	8932.1	8933.9	8936.0	8491.3	8493.9	8496.1	8031.7	8034.4	8037.4
9322.1	9326.1	9329.1	8894.5	8898.4	8902.2	8454.1	8458.8	8463.1	7994.5	7999.9	8005.6
9261.2	9268.0	9273.5	8833.9	8840.8	8847.6	8393.9	8402.0	8409.6	7934.3	7943.7	7953.6
9165.3	9176.0	9185.3	8738.4	8749.6	8761.0	8298.7	8311.8	8324.5	7838.5	7854.5	7870.6
9021.3	9037.3	9052.2	8595.1	8612.5	8630.0	8155.7	8176.0	8196.0	7694.9	7719.9	7744.8
8836.2	8858.4	8879.9	8410.9	8435.6	8460.5	7972.2	8000.9	8029.6	7511.0	7546.2	7581.6
8646.7	8674.8	8702.4	8222.6	8254.1	8285.9	7785.1	7821.4	7858.2	7323.9	7368.2	7413.6
8493.8	8526.1	8558.3	8070.8	8107.4	8144.3	7634.5	7676.6	7719.3	7174.0	7225.1	7277.8
8392.4	8427.4	8462.5	7970.5	8010.2	8050.3	7535.2	7580.9	7627.4	7075.4	7131.0	7188.1
8332.5	8369.1	8405.7	7911.5	7952.8	7994.8	7477.1	7524.7	7573.3	7018.2	7076.3	7135.8
8297.8	8335.5	8372.9	7877.6	7919.9	7962.9	7444.2	7492.8	7542.4	6986.2	7045.5	7106.3
8278.1	8316.3	8354.2	7858.5	7901.4	7944.9	7425.9	7475.0	7525.2	6968.9	7028.8	7090.3
8268.0	8306.5	8344.6	7849.0	7892.2	7935.8	7417.1	7466.4	7516.9	6961.1	7021.1	7083.1
8263.7	8302.4	8340.5	7845.4	7888.6	7932.3	7414.0	7463.5	7514.0	6959.1	7019.1	7081.1

TUBE CONDUCTANCE (BTU/HR*F*FT**2)

1699.5	1699.3	1699.2	1682.3	1682.2	1682.0	1663.5	1663.3	1663.2	1642.0	1641.8	1641.7
1703.3	1703.0	1702.7	1685.8	1685.6	1685.2	1666.7	1666.2	1666.0	1644.8	1644.5	1644.1
1710.7	1709.9	1709.4	1692.6	1691.9	1691.2	1672.7	1672.0	1671.3	1650.3	1649.5	1648.7
1722.4	1721.1	1720.0	1703.4	1702.1	1701.0	1682.7	1681.3	1680.1	1659.3	1657.9	1656.5
1740.9	1738.7	1736.9	1720.6	1718.5	1716.4	1698.5	1696.3	1694.2	1673.8	1671.4	1669.0
1770.8	1767.5	1764.4	1748.4	1745.0	1741.7	1724.2	1720.6	1717.0	1697.5	1693.4	1689.3
1814.9	1809.9	1805.0	1789.6	1784.3	1779.1	1762.5	1756.7	1751.1	1732.7	1726.3	1720.0
1864.9	1857.9	1851.2	1836.9	1832.6	1822.3	1805.9	1799.0	1791.1	1774.4	1765.5	1756.5
1905.2	1896.8	1888.5	1876.1	1867.2	1858.1	1844.8	1835.1	1825.3	1811.0	1800.0	1788.7
1928.2	1919.0	1909.8	1899.6	1889.6	1879.6	1868.7	1857.7	1846.8	1835.0	1822.6	1809.9
1938.7	1929.0	1919.4	1911.1	1900.6	1890.1	1881.0	1869.5	1857.9	1848.1	1834.9	1821.5
1944.0	1934.1	1924.3	1917.1	1906.4	1895.5	1887.6	1875.8	1863.9	1855.2	1841.6	1827.8
1947.2	1937.1	1927.2	1920.6	1909.7	1898.8	1891.3	1879.4	1867.4	1859.1	1845.4	1831.4
1948.6	1938.4	1928.5	1922.2	1911.2	1900.3	1893.1	1881.1	1869.0	1861.0	1847.1	1833.0
1948.7	1938.6	1928.6	1922.5	1911.5	1900.5	1893.5	1881.4	1869.3	1861.3	1847.5	1833.4
1948.5	1938.3	1928.5	1922.2	1911.3	1900.3	1893.3	1881.2	1869.1	1861.0	1847.2	1833.1

TUBE WALL CONDUCTIVITY (BTU/HR*F*FT)

9.6	9.6	9.6	9.6	9.6	9.6	9.6	9.6	9.6	9.6	9.6	9.6
9.6	9.6	9.6	9.6	9.6	9.6	9.6	9.6	9.6	9.6	9.6	9.6
9.7	9.7	9.7	9.7	9.7	9.7	9.7	9.7	9.7	9.7	9.7	9.7
9.8	9.8	9.8	9.8	9.8	9.8	9.8	9.8	9.8	9.8	9.8	9.8
9.9	9.9	9.9	9.9	9.9	9.9	9.9	9.9	9.9	9.9	9.9	9.8
10.2	10.2	10.1	10.2	10.1	10.1	10.1	10.1	10.1	10.1	10.1	10.0
10.6	10.5	10.5	10.5	10.5	10.4	10.5	10.4	10.4	10.5	10.4	10.3
11.0	11.0	10.9	11.0	10.9	10.8	10.9	10.9	10.8	10.9	10.8	10.7
11.4	11.3	11.3	11.4	11.3	11.2	11.4	11.3	11.2	11.3	11.2	11.1
11.7	11.6	11.5	11.7	11.6	11.5	11.5	11.4	11.4	11.5	11.5	11.4
11.8	11.7	11.6	11.8	11.7	11.6	11.8	11.7	11.6	11.8	11.7	11.5
11.9	11.8	11.7	11.9	11.8	11.7	11.9	11.8	11.6	11.9	11.8	11.6
11.9	11.8	11.7	12.0	11.8	11.7	12.0	11.8	11.7	12.0	11.8	11.7
12.0	11.9	11.8	12.0	11.9	11.7	12.0	11.9	11.7	12.0	11.9	11.7
12.0	11.9	11.8	12.0	11.9	11.7	12.0	11.9	11.7	12.0	11.9	11.7
12.0	11.9	11.8	12.0	11.9	11.7	12.0	11.9	11.7	12.0	11.9	11.7

PEAK TUBE TEMPERATURE (DEG. F)

524.2	623.4	623.0	622.5	622.1	621.2	621.3	620.5	620.0	619.7	618.8	618.4
636.3	635.1	634.2	633.7	632.8	631.5	631.6	630.1	629.1	628.7	627.7	626.2
660.0	657.4	655.5	655.2	652.9	650.9	650.9	648.7	645.2	645.3	643.7	641.1
695.8	691.7	688.1	688.6	684.5	680.8	681.4	677.1	673.3	674.1	669.6	664.9
752.1	745.3	739.7	740.8	734.5	727.6	729.5	722.6	715.9	718.2	710.7	703.0
844.5	834.3	824.3	825.8	816.2	805.7	809.2	797.9	786.5	792.0	778.7	766.0
978.8	963.2	947.8	952.7	935.9	919.5	926.6	908.4	890.6	900.6	880.2	860.1
1116.3	1095.1	1074.2	1084.3	1061.5	1038.7	1051.8	1027.2	1002.5	1020.5	992.4	964.0
1196.5	1172.0	1147.8	1166.2	1139.6	1112.9	1135.7	1106.5	1077.1	1107.2	1073.3	1038.9
1204.5	1179.6	1154.9	1182.8	1154.9	1127.5	1161.6	1130.2	1099.2	1142.5	1105.7	1068.9
1179.5	1155.3	1131.2	1167.2	1139.9	1113.0	1155.8	1124.8	1093.8	1147.7	1109.7	1072.5
1158.1	1134.2	1111.2	1152.3	1125.7	1098.8	1147.3	1115.7	1086.1	1145.8	1108.3	1071.0
1145.7	1122.2	1099.4	1143.6	1117.0	1090.8	1142.3	1111.6	1081.5	1144.6	1107.1	1069.6
1136.4	1113.0	1090.7	1136.3	1110.0	1084.3	1137.4	1107.3	1077.0	1142.0	1104.5	1067.1
1127.8	1105.0	1083.1	1129.3	1103.6	1078.0	1132.1	1101.9	1072.1	1137.6	1100.8	1063.5
1123.1	1100.3	1078.5	1124.9	1099.4	1073.8	1128.3	1098.2	1068.7	1134.2	1097.2	1060.4

CONTINUE ITERATION? (YES=1, NO=0) ?0

APPENDIX C

COMPONENT COOL DOWN ANALYSIS
(INITIAL UNIFORM TEMPERATURE)

C.1 INTRODUCTION

This appendix presents the analysis performed to determine the rate of cool down of an isolated component which is initially at a uniform temperature. The analysis is applicable to components such as the riser, downcomer, and the storage tanks during a standby period.

Since the component considered is wrapped in thermal insulation materials, the effect of heat content of the insulation materials on the cool down rate is also included in the analysis.

C.2 ANALYSIS

The major assumptions are:

1. The temperature of the fluid inside the component, T_F , is uniform at all times.
2. The metal (pipe or tank wall) has the same temperature as the fluid ($T_P = T_F$).
3. The "average" temperature of insulation material, T_I , is equal to $\frac{T_P + T_A}{2}$, where T_A is the ambient temperature.

The energy balance for the component (fluid + metal + insulation) can be written as

$$\frac{dT_B}{dt} = \frac{-UA (T_P - T_A)}{\sum_i MC_i} \quad (C-1)$$

where T_P = metal temperature, $^{\circ}F$

T_A = ambient temperature, $^{\circ}F$

UA = product of heat transfer conductance and area, $\frac{Btu}{^{\circ}F \cdot hr}$

$\sum_i MC_i$ = $MC_F + MC_P + MC_I$, the summation of thermal capacities

of fluid, metal, and insulation, $\frac{Btu}{^{\circ}F}$

T_B = "bulk" temperature of component, $^{\circ}F$

t = time, hr

T_B , by definition, is expressed as

$$T_B = \frac{[T_P \times (MC_F + MC_P) + \left(\frac{T_P + T_A}{2}\right) \times MC_I]}{MC_F + MC_P + MC_I} \quad (C-2)$$

$$= \frac{Q_B}{\sum_i MC_i}$$

where Q_B is the total heat content (Btu) of the system.

To solve Eq. (C-1), an expression relating T_P to the T_B must be found. This expression can be obtained from Eq. (C-2) as follows:

$$\text{Let } RF = \frac{MC_F + MC_P}{\sum_i MC_i} \quad (C-3)$$

$$RRF = \frac{MC_I}{\sum_i MC_i} \quad (C-4)$$

$$\text{Then } RRF = 1. - RF \quad (C-5)$$

From Eqs. (C-3), (C-4) and (C-5), Eq. (C-2) becomes

$$T_B = T_P \times RF + \frac{T_P + T_A}{2} \times RRF \quad (C-6)$$

Expanding and collecting terms, we have

$$T_P = \frac{T_B - T_A \times RRF/2}{RF + \frac{RRF}{2}} \quad (C-7)$$

$$\text{Define } C1 = \frac{T_A \times RRF}{2} \quad (C-8)$$

$$C2 = RF + \frac{RRF}{2} \quad (C-9)$$

Then Eq. (C-7) is reduced to

$$T_P = \frac{T_B - C1}{C2} \quad (C-10)$$

This is the desired relationship between T_P and T_B .

Now solving Eq. (C-1) by substituting Eq. (C-10) into Eq. (C-1),

$$\begin{aligned} \frac{dT_B}{dt} &= \frac{-UA}{\sum_i MC_i} \left(\frac{T_B - C1}{C2} - T_A \right) \\ &= \frac{-UA}{C2 \cdot \sum_i MC_i} \left[T_B - \left(T_A + \frac{C1}{C2} \right) \times C2 \right] \end{aligned} \quad (C-11)$$

$$\text{Let } T = (T_A + \frac{C1}{C2}) C2 \quad (C-12)$$

$$\text{EXPON} = \frac{-UA}{C2 \sum_i MC_i} \quad (C-13)$$

$$\text{then } \frac{dT_B}{dt} = - \text{EXPON} (T_B - T') \quad (C-14)$$

The solution is

$$T_B = T' + (T_{Bo} - T') e^{- \text{EXPON} \times t} \quad (C-15)$$

where T_{Bo} is the initial value of T_B .

Having found T_B , the value of $T_p (=T_F)$ can then be obtained from Eq. (C-10).

APPENDIX D

COMPONENT COOL DOWN ANALYSIS
(INITIAL NONUNIFORM TEMPERATURE)

D.1 INTRODUCTION

The method used to estimate the rate of cool down of an isolated component which is initially nonuniform in temperature is described in this Appendix. At the initial moment, the component is hot at the top, cold at the bottom, with a linear temperature profile in between.

The method presented here was applied to the receiver panels to determine their cool down rate (note that the temperature profile in the panel actually has a S shape rather than a straight line). It was also applied to the superheater and the re-heater. The steam inside the latter two components has small thermal content and its effect can be neglected.

D.2 ANALYSIS

There are two mechanisms that cause the temperature in the component to vary. The first is the conduction along the longitudinal direction (from the hot top to the cold bottom) that tends to equalize the temperature in the component. The second mechanism is the heat loss through the surface of the component to the ambient.

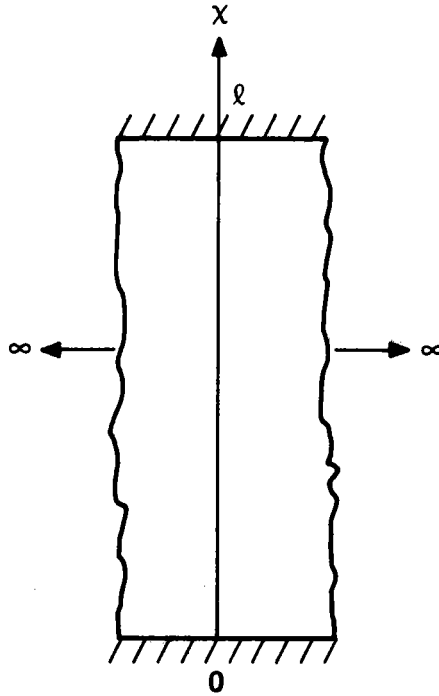
In the present method, it was assumed that the local temperature change in the component due to the two mechanisms described above are independent of each other, and therefore can be separately calculated and then superimposed to arrive at the total change.

Granted, this method is approximate. However, it serves the purpose of obtaining qualitative trends to aid in the operating mode analysis. A more rigorous approach would involve the use of numerical techniques to analyze the transient behavior of the component together with the insulation material wrapped around it. The level of effort required in such an approach would not be justified for the purpose of this study.

Methods used to estimate the temperature change due to the two mechanisms are described below.

Longitudinal Conduction

Considering only the longitudinal conduction in the component, the problem becomes that of a solid bounded by two parallel planes, both ends insulated, with an initial temperature distribution. The situation is illustrated in Figure D-1. The analytical solution* of this problem is also included in Figure D-1. For the present problem where the initial temperature distribution is linear, the integrations can be carried out and the general solution is reduced to:



GOVERNING EQUATION $\frac{\partial^2 T}{\partial x^2} = \frac{1}{K} \frac{\partial T}{\partial t}$

BOUNDARY CONDITIONS $\frac{\partial T}{\partial x} = 0$ AT $x = 0$ AND $x = l$

INITIAL CONDITION $T = T_0 + bx$ $0 \leq x \leq l$

WHERE $K =$ THERMAL DIFFUSIVITY OF SODIUM, FT²/HR

$t =$ TIME, HR

$b =$ INITIAL TEMPERATURE GRADIENT, F/FT

SOLUTION $T = \frac{1}{l} \int_0^l f(x') dx' + \frac{2}{l} \sum_{n=1}^{\infty} e^{-Kn^2 \pi^2 t / l^2} \omega S \frac{n\pi x}{l} \int_0^l f(x) \omega S \frac{n\pi x'}{l} dx'$

WHERE $f(x') =$ INITIAL TEMPERATURE DISTRIBUTION

Figure D-1. Heat Transfer Problem Statement and Solution

$$T = T_o + \frac{b\ell}{2} + \frac{2b\ell}{\pi^2} \sum_{n=1}^{\infty} \left[\rho \frac{-Kn^2 \pi^2 t}{\ell^2} \cos \frac{n\pi x}{\ell} \left(\frac{(-1)^n - 1}{n^2} \right) \right]$$

Note that at the midpoint of the component, $x = \frac{\ell}{2}$, the temperature remains constant and is equal to the equilibrium temperature. Also, the temperature profile is always symmetric with respect to the midpoint.

Heat Loss to Ambient

The method described in Appendix C was used to estimate this part of heat loss. The procedure was to first obtain the rate of temperature decrease for the midpoint (initially its temperature is equal to the average between the hot and cold ends) using the method described in Appendix C, then arrive at the local temperature decrease rate by multiplying the midpoint value by the ratio

$$\frac{T_{\text{local}} - T_{\text{ambient}}}{T_{\text{midpoint}} - T_{\text{ambient}}}$$

The temperature drop estimates derived for the two temperature change mechanisms were added to obtain the total temperature drop. Note that the hot end of the component loses heat to the ambient as well as to the cold end of the component, and its temperature is monotonically decreasing with time. The cold end, on the other hand, receives heat from the hot end while losing heat to the ambient. Near the beginning of the transient, the heat received exceeds the heat lost, resulting in a rise in temperature in the cold end. But as the temperature gradient in the component decreases with time, the heat lost to the ambient would then outweigh the heat received and the temperature would decrease.

* H.S. Carslaw and J.C. Jaeger, Conduction of Heat in Solids, Oxford University Press, N.Y. 1959.

APPENDIX E

TEMPERATURE CYCLING CHARACTERISTICS
IN THE DOWNCOMER PIPE

E.1 INTRODUCTION

In the proposed approach for receiver tower loop standby modes, the riser and the downcomer pipes are bottled up. Heat transfer analysis indicated that the downcomer temperature would drop at a rate of about 100°F in a 12 hour (nominal overnight standby) period. During the tower loop startup process following a standby period (may be longer than 12 hours), hot sodium generated in the receiver would be introduced into the downcomer. The temperature difference between the hot sodium and the cold pipe raises the concern about possible cyclic fatigue problem of the downcomer. The purpose of this Appendix is to address this concern.

The analysis begins with the derivation of the maximum allowable temperature difference across the downcomer pipe wall during pipe warmup in order to avoid cyclic fatigue failure. Calculations are then made to estimate the pipe inner/outer surface temperature difference for various sodium warmup rates. The results show that no problem with downcomer piping temperature cyclic fatigue is expected during a startup.

E.2 ANALYSIS

Allowable ΔT Across Downcomer Pipe Wall

The fatigue life curve for the downcomer material (316SS) given by Chopra, et.al.* is reproduced in Figure E-1. It shows that the number of cycles to failure, N_f , is insensitive to the total strain range, $\Delta\epsilon$, for $N_f > 10^4$ ($\Delta\epsilon \approx 5 \times 10^{-3}$) which is the N_f range of interest in the problem under consideration (daily warmup for 365 cycles/year x 30 years = 10950 cycles over the life of the plant). The ASME pressure vessel code requires that a safety factor of $\frac{N_f}{20}$ or $\frac{\Delta\epsilon}{2}$, whichever is more conservative, be applied. Therefore, an allowable total strain range value of $\Delta\epsilon_{\text{allowable}} = 2.5 \times 10^{-3}$ was selected.

The equations used to calculate the total strain range are presented below. The downcomer pipe was assumed to be a flat plate because of its small thickness to radius ratio. From Roark**, the stress developed in the surface layer of the downcomer when suddenly subjected to a temperature change ΔT is

$$\sigma = \frac{\Delta T \alpha E}{1 - \nu} \quad (E-1)$$

* O.K. Chopra, J.Y.N. Wang and K. Natesan, Review of Sodium Effects on Candidate Materials for Central Receiver Solar - Thermal Power Systems, Argonne National Laboratory, Report No. ANL-79-36, May 1979 (Draft).

**R.J. Roark, Formulas for Stress and Strain, McGraw-Hill, 1954, pg. 374.

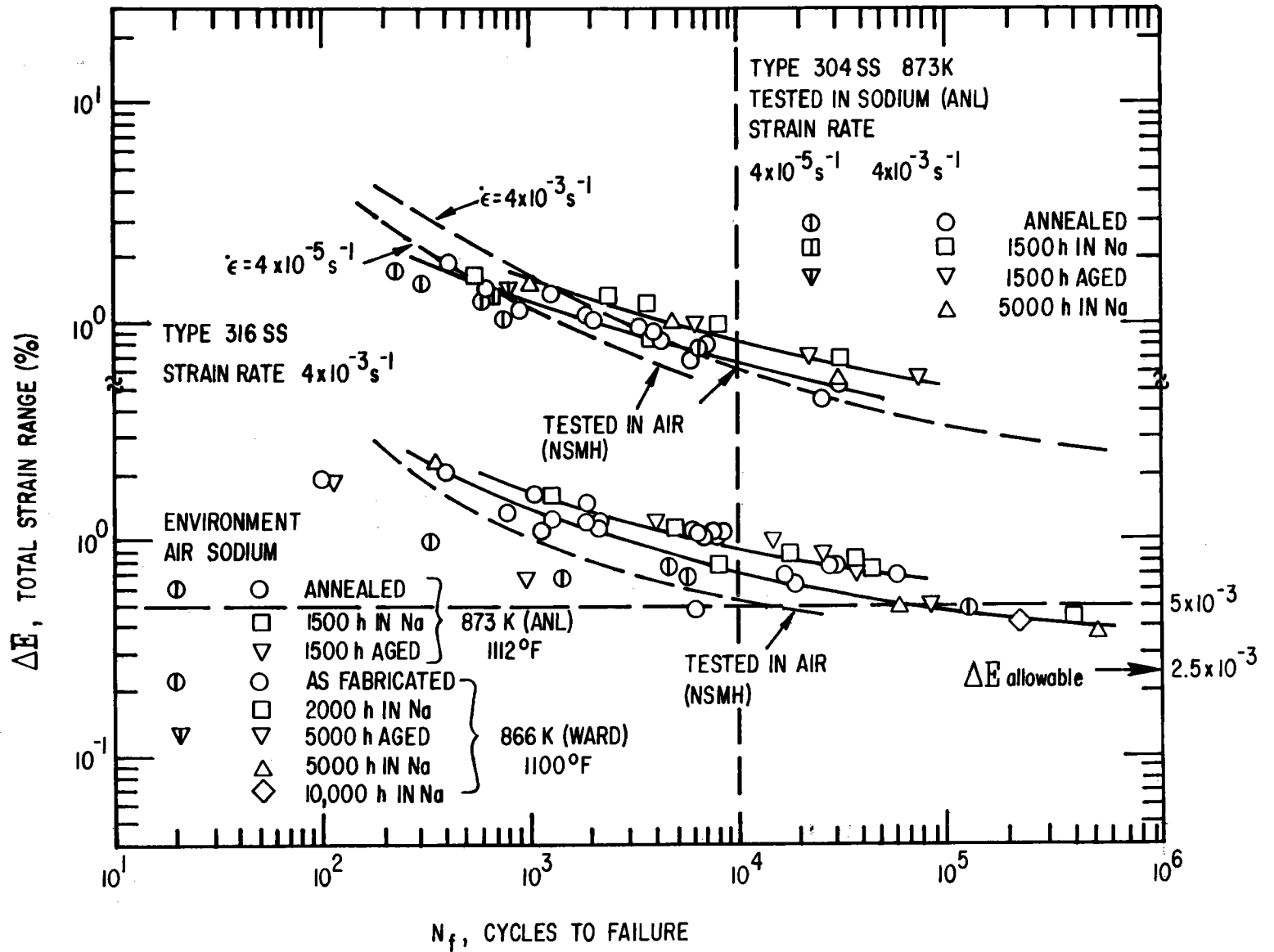


Figure E-1. Fatigue Life Curve for 316SS at High Temperature

where

α = coefficient of thermal expansion

E = modulus of elasticity, psi

ν = poissons ratio.

The total strain range (from Mendelson*) is

$$\Delta\epsilon = \frac{2\sigma}{E} \quad (E-2)$$

Combining Equations E-1 and E-2:

$$\Delta\epsilon = \frac{2\Delta T\alpha}{1-\nu} \quad (E-3)$$

Using $\alpha = 9.7 \times 10^{-6} \text{F}^{-1}$ and $\nu = 0.3$ for 316SS, Eq. E-3 becomes

$$\Delta\epsilon = (2.77 \times 10^{-5}) \Delta T \quad (E-4)$$

To keep $\Delta\epsilon$ below the allowable value of 2.5×10^{-3} , Eq. E-4 gives the value of maximum allowable ΔT :

$$(\Delta T)_{\text{allowable}} = 90^{\circ}\text{F} \quad (E-5)$$

Therefore, to avoid fatigue problems due to daily temperature cycling, the ΔT across the pipe wall should be maintained below 90°F . Consequently, it is unacceptable to suddenly put hot sodium at rated condition temperature of 1100°F into a cooler downcomer pipe (cooled down to 1000°F overnight as previously stated). Instead, the hot sodium temperature should be gradually ramped up during a startup to allow the high temperature to propogate across the pipe wall, thus reducing the ΔT .

For standby durations longer than overnight the downcomer temperture would become even lower. Analysis showed that for a 36-hour standby (corresponding to one day and two nights) the downcomer temperature would drop by 260°F . The hot sodium temperature ramping approach would be even more important in these cases. Note that, however, longer than overnight standby occurs much less frequently than overnight shutdown. Assuming the 36-hour standby occurs once per week, Figure E-1 gives an allowable $\Delta\epsilon$ of 3.5×10^{-3} (including the safety factor) for $N_f = 52 \text{ cycles/year} \times 30 \text{ years} = 1560 \text{ cycles}$. Applying Eq. E-4, the value of maximum allowable ΔT is about 125°F . Therefore, the less frequent 36-hour standby actually requires a less stringent ΔT limit, thus allowing a faster sodium temperature ramp up rate during warmup. The total time required to reach normal operating temperature is

* Design and Fabrication of Brayton Cycle Solar Heat Receiver, Final Report, Contract NAS 3-10944, GE Nuclear Systems Programs, Edited by I. Mendelson, July 1971.

of course longer since the starting temperature is lower.

Receiver Exit Sodium Temperature Ramp Rate Evaluation

The problem now is to evaluate the acceptable ramp rate of receiver exit hot sodium temperature during a startup. Due to heat transfer resistance, the pipe outer surface temperature would lag behind the inner surface temperature which increases with the increasing sodium temperature. Therefore, the ΔT across the pipe wall begins to increase from zero when the hot sodium is first introduced. After a while it reaches a constant value. This constant value is maintained until the sodium temperature reaches the normal operating value. At this point the ΔT across the wall starts to diminish as the outer wall surface temperature catches up with the inner wall, and finally the wall temperature reaches an equilibrium. The sodium temperature ramp rate should be chosen such that the ΔT across the pipe at any instant is lower than the maximum allowable value of 90°F.

To determine the transient variation in ΔT across the pipe wall, the following assumptions are made in the analysis:

- The pipe wall is approximated by an infinite slab.
- One dimensional heat transfer is assumed (no variation along pipes length).
- The pipe wall is initially at a uniform temperature T_i , reached after a standby period.
- The pipe outer surface is insulated perfectly.
- The pipe inner surface is assumed to be at the same temperature as the hot sodium (convective film resistance neglected).
- The pipe inner surface temperature is ramped up linearly from T_i , beginning at time zero.

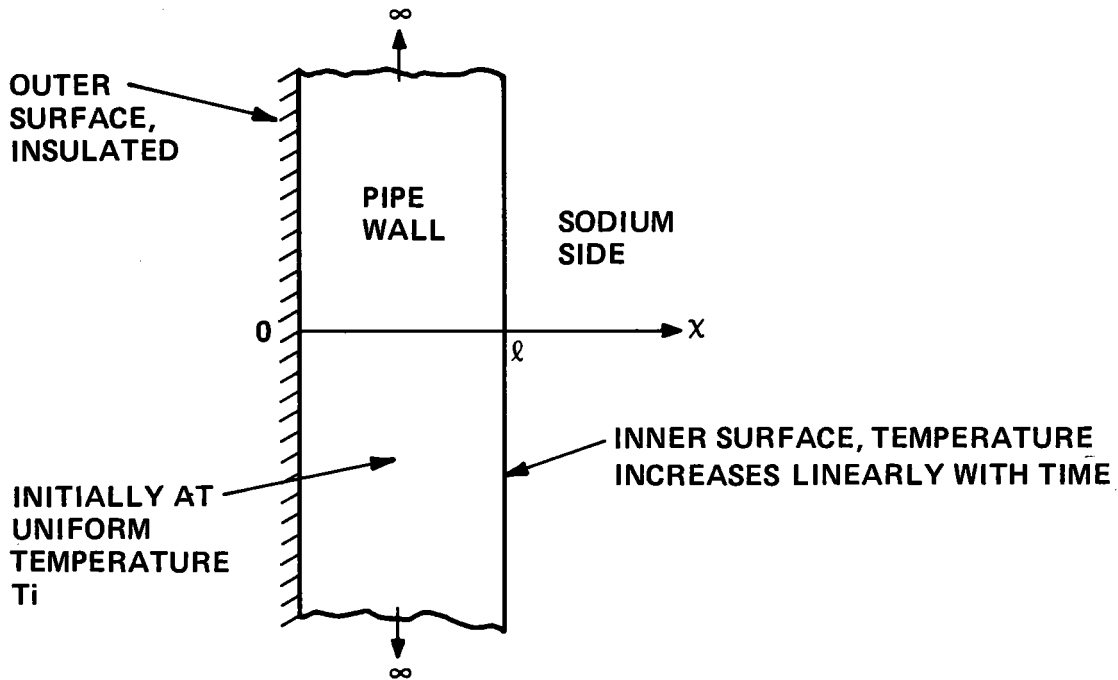
The situation is illustrated in Figure E-2. The general solution to this problem, taken from Carslaw and Jaeger* is also included in Figure E-2.

For the present problem the integrations in Figure E-2 can be performed and the solution is reduced to:

$$T = \frac{2}{\ell} \sum_{n=0}^{\infty} \left\{ (-1)^n \cos cx \left[\frac{T_i}{c} (1 - e^{-KC^2 t}) + b \left(\frac{t}{c} - \frac{1}{KC^3} \right) + \frac{be^{-KC^2 t}}{KC^3} \right] + \frac{T_i}{c} \left[\rho^{-KC^3 t} \operatorname{sinc} \ell \right] \right\} \quad (E-6)$$

where $C = \frac{(2n+1)\pi}{2\ell}$

* H.S. Carslaw and J.C. Jaeger, Conduction of Heat in Solids, Oxford University Press, New York, 1959.



GOVERNING EQ.

$$\frac{\partial^2 T}{\partial x^2} = \frac{1}{K} \frac{\partial T}{\partial t}$$

BOUNDARY CONDITIONS

$$\frac{\partial T}{\partial x} = 0 \text{ AT } x = 0$$

$$T = T_i + bt \text{ AT } x = l$$

INITIAL CONDITION

$$T = t_i \quad 0 < x < l$$

WHERE

K = THERMAL DIFFUSIVITY OF PIPE MATERIAL, FT^2/HR

t = TIME, HR

b = TEMPERATURE RAMP RATE, F/HR

SOLUTION:

$$T = \frac{2}{l} \sum_{n=0}^{\infty} e^{-\frac{K(2n+1)^2\pi^2 t}{4l^2}} \cos \frac{(2n+1)\pi x}{2l} \left\{ \frac{(2n+1)\pi K(-1)^N}{2l} \int_0^t e^{-\frac{K(2n+1)^2\pi^2 \lambda}{4l^2}} \Phi_2(\lambda) d\lambda + \int_0^l f(x') \cos \frac{(2n+1)\pi x'}{2l} dx' \right\}$$

WHERE $\Phi_2(\lambda)$ = TIME DEPENDENT BOUNDARY CONDITION

$f(x')$ = SPARE DEPENDENT INITIAL CONDITION

Figure E-2. Heat Transfer Problem Statement and Solution

A computer program was written to facilitate the computation of the series solution. Note that the quantity of interest is the maximum value of the ΔT across the pipe wall, $\Delta T = T(x=l) - T(x=0)$. The following parameters are used in the calculation:

$$l = 0.03125' \text{ (pipe wall thickness)}$$

$$K = 0.209 \text{ ft}^2/\text{hr} \text{ (thermal diffusivity of 316SS)}$$

The results of the calculations are present in Figure E-3 for three values of sodium temperature ramp rate. The time required for the sodium temperature to increase from the initial temperature of 1000°F to the normal operating temperature of 1100°F at the ramp rates of $166.7^\circ\text{F}/\text{min}$, $83.3^\circ\text{F}/\text{min}$ and $16.7^\circ\text{F}/\text{min}$ are 0.6 min., 1.2 min., and 6 min., respectively. The corresponding max. ΔT s across the pipe wall are 23.2°F , 11.5°F , and 2.2°F , well within the ΔT limit imposed by the cycle fatigue failure criteria. Therefore, it is concluded that the downcomer temperature cycling during startup would not present a fatigue failure problem.

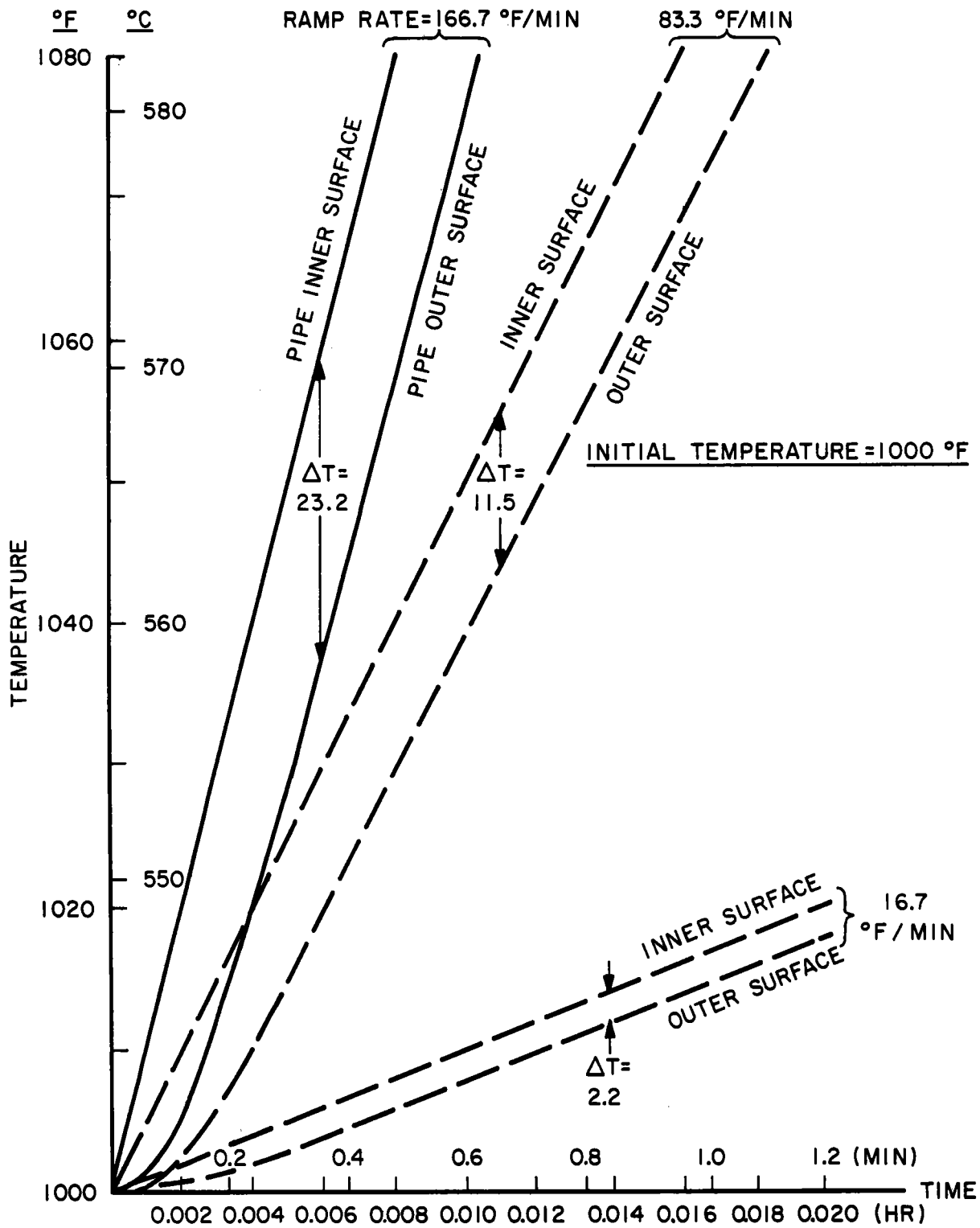


Figure E-3. Downcomer Pipe Inner/Outer Surface Temperature Variation with Different Sodium Temperature Ramp Up Rates During Startup

APPENDIX F
TRICKLE FLOW SCHEME FOR
SHORT TERM STANDBY

A more detailed discussion on the trickle flow scheme for plant short time standby is presented in this appendix.

In this scheme, the steam generator temperatures are maintained near their normal operating values by a trickle flow of sodium, about 2% of design point flow, through the steam generators. Sodium flow paths are identical to those for normal operation. On the water/steam side a proportionate flow picks up the heat from the sodium. Bypass lines around the steam turbine and the desuperheating systems are utilized as illustrated in Figure F-1. A mass and energy balance for this system is illustrated in Figure F-2 which was generated based on the assumption that total heat transferred varies linearly with flow rates.

The mass flows in Figure F-2 are based on a sodium flow of 2%. Sufficient water/steam is circulated to maintain sodium temperature at or near their design point level. The pony motor on the sodium steam generator pump will permit low flow operation without any hardware modification.

A smaller feedwater recirculation pump and a smaller sodium flow control valve at reheater exit are required (not shown in Figure F-1) to handle the low flow during the hold mode of operation. These additional equipments will be installed in bypass lines parallel to their larger counterparts.

The system pressure on the water/steam side are based on the assumption of variable pressure operation. During a shutdown, the system pressure is reduced as the load decreases. At 1250 psia, the temperature in the steam drum is 572°F and is approaching the 300°F sodium-steam ΔT limit. Load reduction beyond this point are accomplished by throttling the flow through the steam turbine control valves. After shutdown, the steam drum pressure level is maintained at 1250 psia by the overnight standby mode. As shown in Figure F-1, condenser water is pumped to 1400 psia and utilized for SG cooling and desuperheating. The feedwater flow is mixed with a portion of the hot reheat (HRH) steam to produce a temperature of 521°F. This is shown as a single step on the schematic, but will actually involve a series of FW heaters which will first condense the HRH steam then mix the condensed fluid with the feedwater. The flow is then mixed with steam drum condensate (1.13 recirculation ratio) and pumped through the evaporator to the steam drum. Saturated steam flows from the steam drum through the superheater where the temperature is raised to 1000°F. The superheated steam is routed through a HP turbine bypass leg where a pressure control system reduces the pressure from 1200 psia to 420 psia and a temperature control

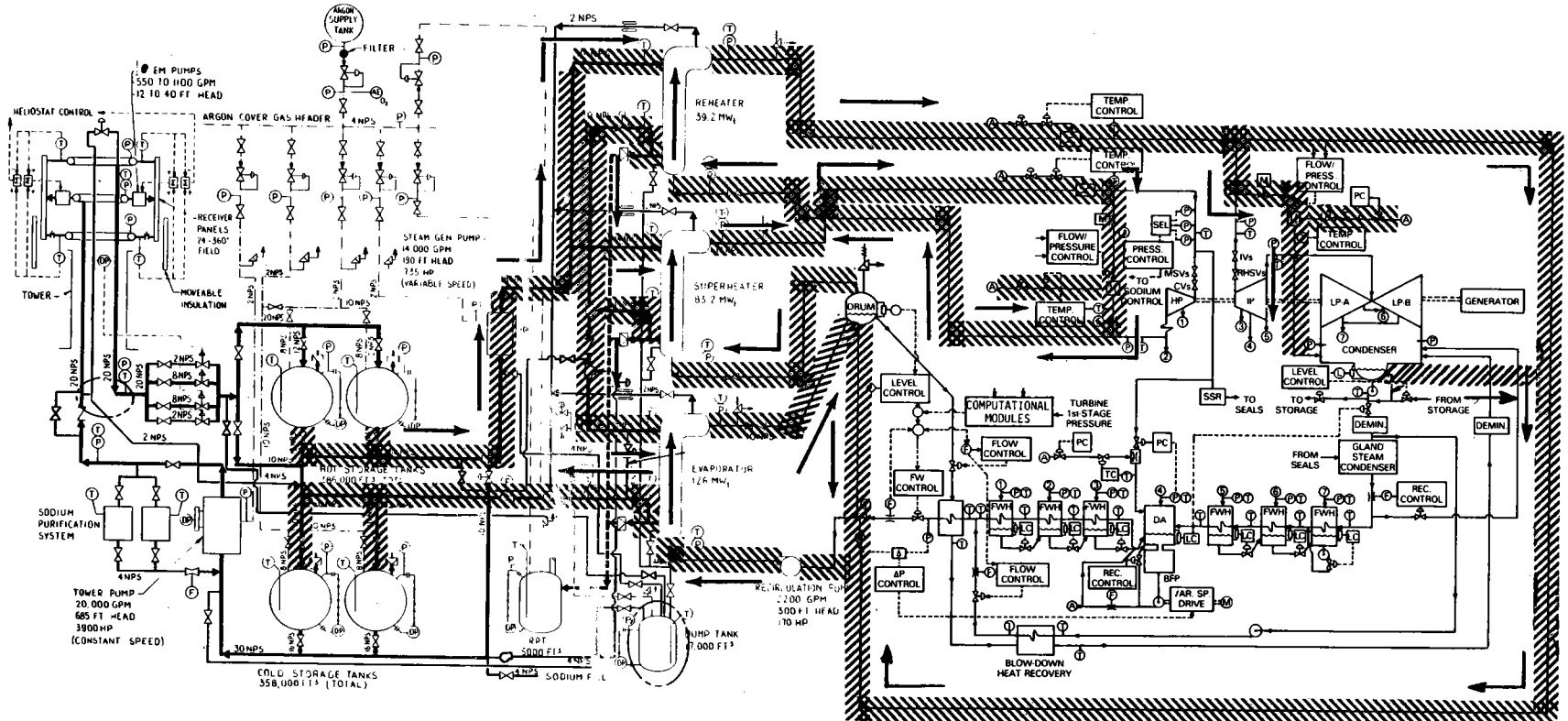


Figure F-1. Flow Path During Hold Mode Using Trickle Flow Approach

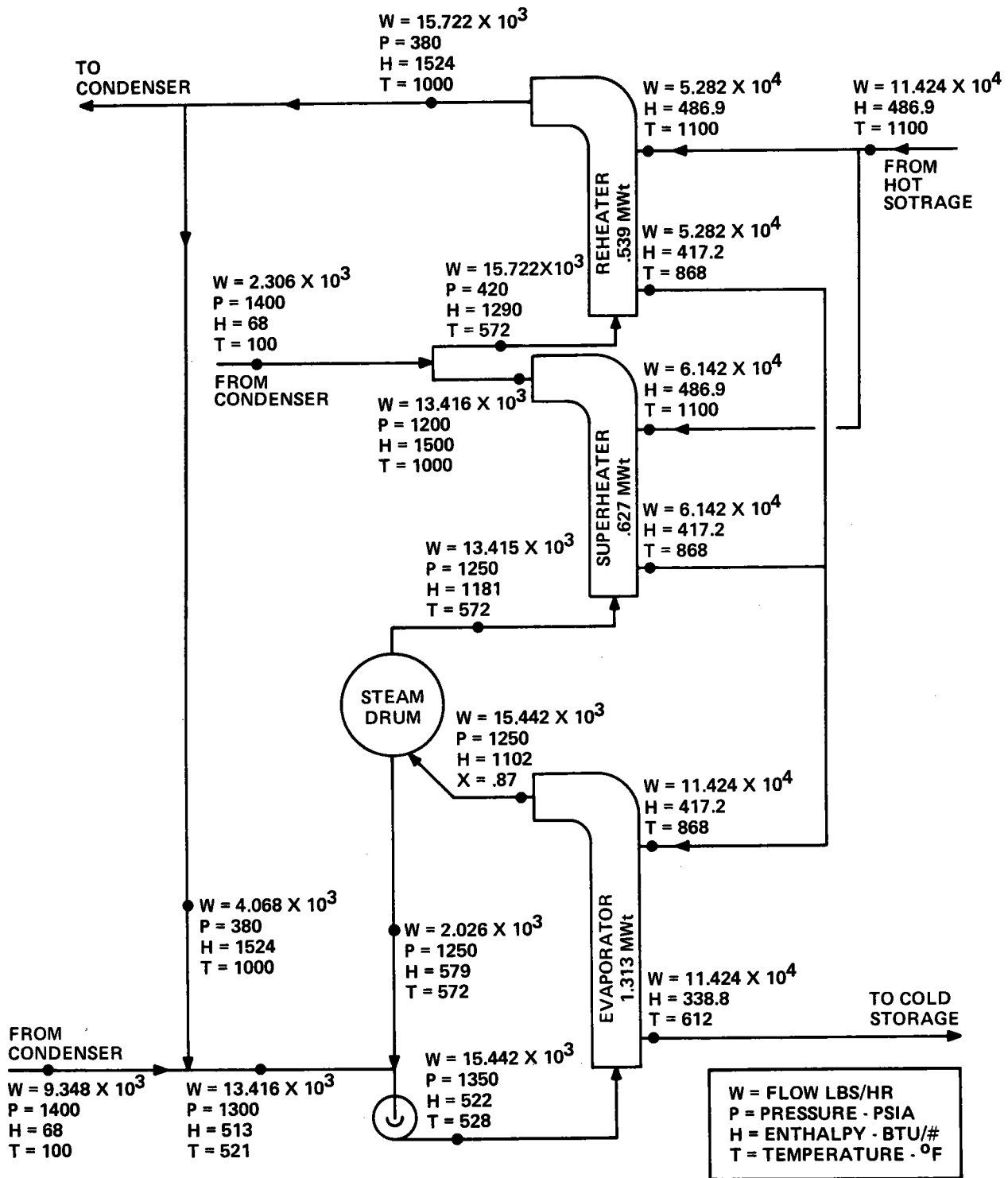


Figure F-2. Steam Generator Heat Balance in Hold Mode, Trickle Flow Approach (2% of Design Point Sodium Flow), English Units

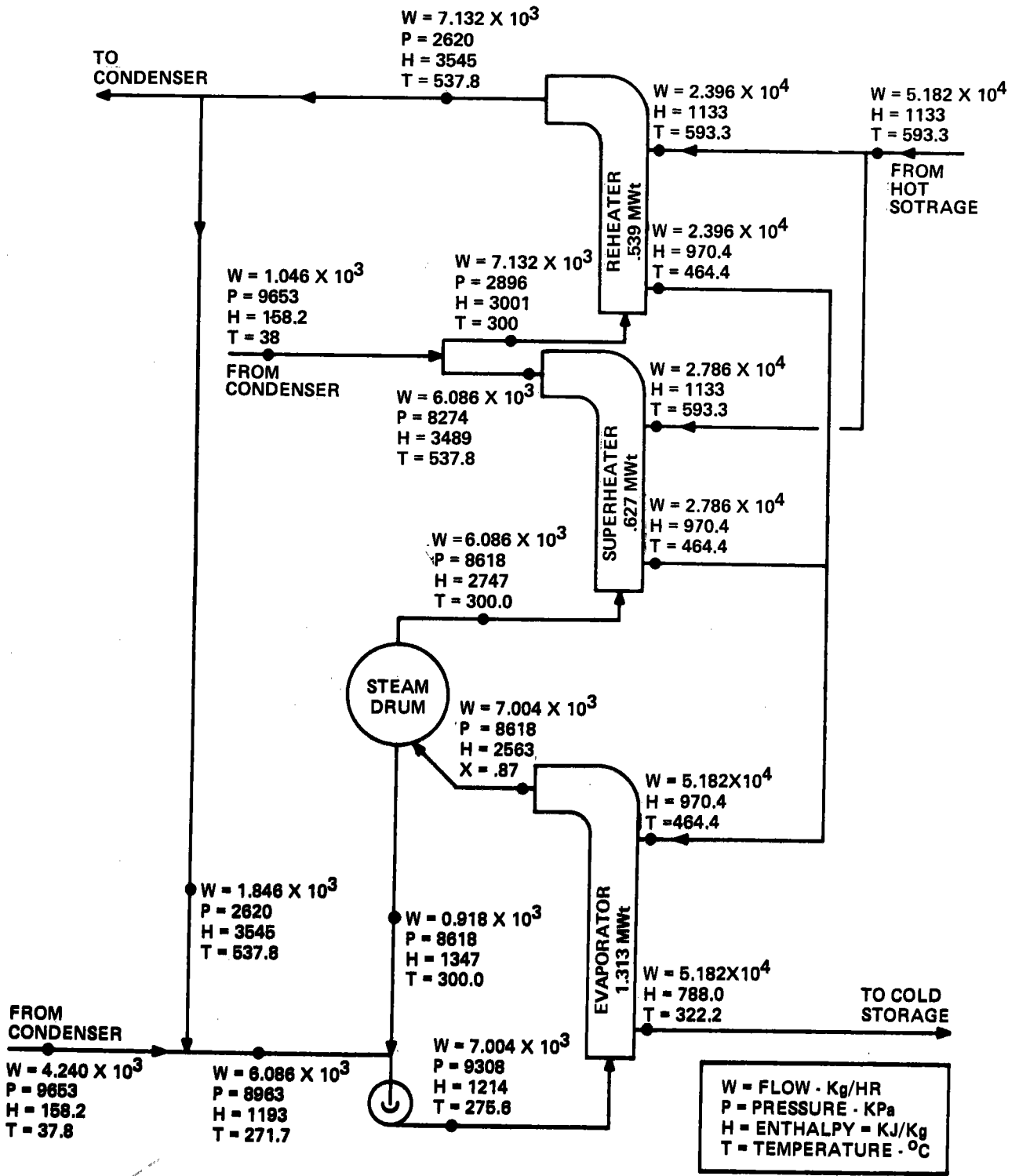


Figure F-2A. Steam Generator Heat Balance in Hold Mode, Trickle Flow Approach (2% of Design Point Sodium Flow), Metric Units

system adds sufficient condensate to reduce the temperature to 572^o, the normal design point values of the cold reheat (CRH) steam. The CRH steam passes through the reheater where the temperature is increased to 1000^oF. A portion of this hot reheat steam is utilized for feedwater heating. The remaining HRH steam is routed through a LP turbine bypass system where both the pressure and temperatures are reduced to levels suitable for the condenser.

It should be pointed out that there is an element of uncertainty associated with this scheme. At very low flow dynamic instability in the evaporator may be induced due to two-phase flow heat transfer characteristics. This concern must be resolved. However, it is beyond the scope of the present analysis. Should it be determined in future studies that there actually would be a problem with instability, it is proposed to pressurize the feedwater (say, 2600 psia) to maintain the fluid in the evaporator subcooled thus eliminating the problem, then employ a flash tank (at 1250 psia) at evaporator outlet to obtain dry steam for the superheater.

The steam generator low flow characteristics study would also help in determining the minimum required sodium flow rate which has been tentatively chosen to be 2% of the rated value in the present analysis. Naturally, the lower value is more desirable since the circulation of hot sodium in the steam generators during standby represents an energy loss.

APPENDIX G

**COMPUTER PROGRAM LISTING FOR
SYSTEM ANNUAL PERFORMANCE ANALYSIS**

04/15/80 9.698

```

09C*****"ANNUAL*****
10C*****THIS PROGRAM CALCULATES ANNUAL PERFORMANCE FOR THE*****
11C*****ALTERNATE CENTRAL RECEIVER SOLAR PLANT (100 MW)*****
20C*****
30 DIMENSION IHR(24),DNI(24),TEMPDP(24),TEMPDB(24),TEMPWB(24)
40 DIMENSION EFFLD(12,24),SUNANG(12,24)
50 DIMENSION PMONTH(12),PDAY(12,31),PWST(12,31),PWSTMO(12),THRSTO(366)
60 DIMENSION PAVABL(12),PUSABL(12),PUSED(12),PFOCUS(12),PRCV(12),PRCVD(12)
70 DIMENSION PCHA(12),PDIS(12),PEPGS(12),PGRSS(12),PPARA(12)
80 DIMENSION PORID(12),PLOFF(12),PLON(12),PLWARM(12),MODAY(12)
90C
91 DATA MODAY/31,29,31,30,31,30,31,31,30,31,30,31/
100 DATA PAVABL,PUSABL,PUSED,PFOCUS,PRCV,PRCVD/72*0./
110 DATA PCHA,PDIS,PEPGS,PGRSS,PPARA/60*0./
120 DATA PORID,PLOFF,PLON,PLWARM/48*0./
130 DATA EAVABL,EUSABL,EUSED,EFOCUS,ERCV,ERCVED/6*0./
140 DATA ECHA,EDIS,EPEGS,EGRSS,E PARA/5*0./
150 DATA EGRID,ELOFF,ELON,ELWARM/4*0./
160 DATA PDAY,PMONTH,PWST,PWSTMO/768*0./
170 DATA ((EFFLD(I,J),I=1,12),J=1,5)/60*0./
180 DATA (EFFLD(1,J),J=6,12)/0.,0.,0.210,0.250,0.302,0.330,0.343/
190 DATA (EFFLD(2,J),J=6,12)/0.,0.,0.221,0.289,0.328,0.351,0.360/
200 DATA (EFFLD(3,J),J=6,12)/0.,0.207,0.266,0.320,0.351,0.364,0.372/
210 DATA (EFFLD(4,J),J=6,12)/0.,0.218,0.297,0.339,0.361,0.373,0.380/
220 DATA (EFFLD(5,J),J=6,12)/0.205,0.253,0.314,0.347,0.365,0.377,0.385/
230 DATA (EFFLD(6,J),J=6,12)/0.184,0.262,0.318,0.349,0.366,0.378,0.387/
240 DATA (EFFLD(12,J),J=6,12)/0.,0.,0.,0.229,0.289,0.320,0.333/
250 DATA ((SUNANG(I,J),I=1,12),J=1,5)/60*0./
260 DATA (SUNANG(1,J),J=6,12)/0.,0.,0.09,1.,1.,1.,1./
270 DATA (SUNANG(2,J),J=6,12)/0.,0.,0.61,1.,1.,1.,1./
280 DATA (SUNANG(3,J),J=6,12)/0.,0.20,1.,1.,1.,1.,1./
290 DATA (SUNANG(4,J),J=6,12)/0.,0.73,1.,1.,1.,1.,1./
300 DATA (SUNANG(5,J),J=6,12)/0.12,1.,1.,1.,1.,1.,1./
310 DATA (SUNANG(6,J),J=6,12)/0.28,1.,1.,1.,1.,1.,1./
320 DATA (SUNANG(12,J),J=6,12)/0.,0.,0.,0.85,1.,1.,1./
330 DATA PARCOL,PARENC/0.40,0.31/
340 DATA PAREMP,PARTOW,PARSOP/0.35,2.91,0.55/
350 DATA PARBFP,PARCND,PARCIR,PARCT/3.15,0.09,0.12,2.58/
360 DATA PARTHL,PARTNF/0.76,0.55/
370 DATA QLTWON,QLSGON,QLTWOF,QLSGOF/0.215,0.122,0.179,0.098/
380 DATA GLTANK,QLRCV/0.444,0.128/
390 DATA DNIREF,QLNCDE,QUSEDE,QUSSMIN/950.,408.2,368.7,2./
400 DATA STOCAP,QDISDE,QEPGSD/766.,247.54,251.08/
410 DATA GRATED,FRARAT/111.7,0.445/
420 DATA MODULE,ACOLL/20137,55./
430 DATA IPDAY,IPMON/0,1/
440C
450 DO 40 I=1,5
460 N=12-I
470 DO 40 J=1,12
480 SUNANG(N,J)=SUNANG(I,J)
490 DO 40 EFFLD(N,J)=EFFLD(I,J)
500 DO 30 I=1,12
510 DO 30 J=1,12
520 M=25-J
530 SUNANG(I,M)=SUNANG(I,J)
540 DO 30 EFFLD(I,M)=EFFLD(I,J)
550C
560 AREATL=ACOLL*MODULE
570 STOMAX=STOCAP+QDISDE
580C
590C*****
600C*****DAILY CYCLE*****
610C*****
620C
630 QSTBYT=0.
640 QSTBYS=0.
650 HRSTBY=0.
660 THRSTO(1)=0.
670 CALL ATTACH(15,"BARSTOW3;",1,0,ISTAT, )
680 CALL ATTACH(16,"WETBULB;",1,0,ISTAT, )
690 DO 9999 NDAY=1,366
700 READ(15) IYR,MO,IDAY,(IHR(K),DNI(K),TEMPDB(K),TEMPDP(K),K=1,24)
710 READ(16) (TEMPWB(K),K=1,24)
720 DAYDNI=0.

```

04/15/80 9.698

```

730 D0 305 JJ=1,24
740 305 DAYDNI=DAYDNI+DNI(JJ)/1000.
750 IWARM=0
760 IF(NDAY.NE.1) THRST0(NDAY)=THRST0(NDAY-1)
770C
780 D0 500 K=1,24
790 IF(IPDAY.EQ.0) G0 T0 502
800 IF(NDAY.NE.300.AND.NDAY.NE.301.AND.NDAY.NE.302) G0 T0 502
810 I HOUR=IHR(K)/100
820 PRINT 90,M0, IDAY, I HOUR, DNI(K), TEMPWB(K), EFFLD(M0,K), SUNANG(M0,K)
830 90 FORMAT("****M0=",I2,1X,"DAY=",I2,1X,"HR=",I2,1X,"DNI=",F6.1,1X,
840& "TEMPWB=",F5.1,1X,"EFFLD=",F5.3,1X,"SUNANG=",F5.3)
850 502 CONTINUE
860 PAVABL(M0)=PAVABL(M0)+DNI(K)*AREATL/1.E6
870C
880C*****
890C*****TOWER SIDE*****
900C*****
910C
920 QINCID=AREATL*DNI(K)*EFFLD(M0,K)/1.E6
930 RINCID=QINCID/QINCDE
940 IF(RINCID.LT.0.0531) G0 T0 111
950 IF(RINCID.GE.0.3) EFRCV=7.2119874E-1+4.3483832E-1*RINCID
960& -3.6340616E-1*RINCID**2+1.106691E-1*RINCID**3
970 IF(RINCID.LT.0.3) EFRCV=0.9843858-0.0522086/RINCID
980 111 IF(RINCID.LT.0.0531) EFRCV=0.
990 QUSE=QINCID*EFRCV
1000C
1010C***** STANDBY MODE*****
1020C
1030 IF(QUSE.GT.QUSMIN.AND.SUNANG(M0,K).GT.0.05) G0 T0 666
1040 QSTBYT=QSTBYT+QLTW0F+QLRCV+QLTANK
1050 PLOFF(M0)=PLOFF(M0)+QLTW0F+QLRCV+QLTANK
1070 QCHA=0.
1080 PARTW=PARENC
1090 IF(JPDAY.EQ.0) G0 T0 1913
1100 IF(NDAY.NE.300.AND.NDAY.NE.301.AND.NDAY.NE.302) G0 T0 1913
1110 PRINT,"TOWER SIDE ON STANDBY"
1120 1913 CONTINUE
1130 G0 T0 667
1140C
1150C***** OPERATING MODE*****
1160C
1170 666 CONTINUE
1180C COUNT LOSSES DURING THE FRACTION OF THE HOUR WHEN SUN ANGLE IS LOW
1190 QSTBYT=QSTBYT+(QLTW0F+QLRCV+QLTANK)*(1.-SUNANG(M0,K))
1200 PLOFF(M0)=PLOFF(M0)+(QLTW0F+QLRCV+QLTANK)*(1.-SUNANG(M0,K))
1220C
1230 PUSABL(M0)=PUSABL(M0)+DNI(K)*AREATL/1.E6
1260 QCHA=(QUSE-QLTW0N-QLTANK+PAREMP*0.86+PART0W*0.95)*SUNANG(M0,K)-QSTBYT
1270 QSTBYT=0.
1280 PL0N(M0)=PL0N(M0)+(QLTW0N+QLTANK)*SUNANG(M0,K)
1290 THROD=THRST0(NDAY)
1291 QCHA0D=QCHA
1300 THRST0(NDAY)=THRST0(NDAY)+QCHA
1310C
1320C DUMP HOT SODIUM IF HOT TANKS ARE FULL
1321 FRACTI=1.
1330 IF(THRST0(NDAY).LT.ST0MAX) G0 T0 669
1340 PWST(M0, IDAY)=PWST(M0, IDAY)+THRST0(NDAY)-ST0MAX
1350 THRST0(NDAY)=ST0MAX
1360 QCHA=ST0MAX-THROD
1361 FRACTI=QCHA/QCHA0D
1370 669 CONTINUE
1380C
1390 PCHA(M0)=PCHA(M0)+QCHA
1400 PUSED(M0)=PUSED(M0)+DNI(K)*AREATL*SUNANG(M0,K)/1.E6
1401 PFOCUS(M0)=PFOCUS(M0)+DNI(K)*AREATL*SUNANG(M0,K)
1402& *FRACTI/1.E6
1403 PRCV(M0)=PRCV(M0)+QINCID*SUNANG(M0,K)*FRACTI
1404 PRCVED(M0)=PRCVED(M0)+QINCID*EFRCV*SUNANG(M0,K)*FRACTI
1410 PARTW=PARENC+(PARCOL+(PAREMP+PART0W)*(QUSE*FRACTI/QUSEDE))*SUNANG(M0,K)
1420 IF(IPDAY.EQ.0) G0 T0 667
1430 IF(NDAY.NE.300.AND.NDAY.NE.301.AND.NDAY.NE.302) G0 T0 667
1440 PRINT 131,EFRCV,QINCID,QUSE,QCHA,THRST0(NDAY)

```

04/15/80 9.698

```

1450 131 FORMAT("EFRCV=",F5.3,1X,"QINCID=",F6.1,1X,"QUSE=",F6.1,1X,
1460& "QCHA=",F5.1,1X,"THRST0=",F6.1)
1470 667 CONTINUE
1480C
1490C*****
1500C*****SG/EPGS SIDE*****
1510C*****
1520C
1530 IF(DAYDNI.LT.6.AND.THRST0(NDAY).LT.QDISDE) GO TO 600
1540 IF(IWARM.EQ.0.AND.THRST0(NDAY).LT.QDISDE/2.) GO TO 600
1550 IF(IWARM.EQ.1.AND.THRST0(NDAY).LT.0.5) GO TO 600
1560 IF(IWARM.EQ.1) GO TO 800
1570 GO TO 700
1580C
1590C*****STANDBY MODE*****
1600C
1610 600 CONTINUE
1620 IWARM=0
1630 HRSTBY=HRSTBY+1.
1640 QSTBYS=QSTBYS+QLSG0F
1650 PLOFF(M0)=PLOFF(M0)+QLSG0F
1660 PARSG=PARHTL
1670 PGRID(M0)=PGRID(M0)+PARSG+PARTW
1680 IF(IPDAY.EQ.0) GO TO 913
1690 IF(NDAY.NE.300.AND.NDAY.NE.301.AND.NDAY.NE.302) GO TO 913
1700 PRINT,"SG/EPGS SIDE ON STANDBY"
1710 913 CONTINUE
1720 QDIS=0.
1730 TDR0P=6.*HRSTBY
1740 IF(TDR0P.GT.490.) TDR0P=490.
1750 GO TO 500
1760C
1770C*****WARM UP MODE*****
1780C
1790 700 CONTINUE
1800 TIMEWM=TDR0P/150.
1810 TENDWM=1100.-TDR0P
1820 QLWARM=(1.+(TENDWM-610.)/490.)/2.*0.1*QDISDE*TIMEWM-QSTBYS
1830 PLWARM(M0)=PLWARM(M0)+QLWARM
1840 THRST0(NDAY)=THRST0(NDAY)-QLWARM-QSTBYS
1850 IF(IPDAY.EQ.0) GO TO 1500
1860 IF(NDAY.NE.300.AND.NDAY.NE.301.AND.NDAY.NE.302) GO TO 1500
1870 PRINT,"WARMUP OF SG/EPGS"
1880 PRINT 132, HRSTBY,QSTBYS,TIMEWM,QLWARM
1890 132 FORMAT("HRSTBY=",F4.0,1X,"QSTBYS=",F4.1,1X,"TIMEWM=",F4.2,1X,
1900& "QLWARM=",F6.1)
1910 1500 CONTINUE
1920 IWARM=1
1930 HRSTBY=0.
1940 QSTBYS=0.
1950C
1960C*****NORMAL MODE*****
1970C
1980 800 CONTINUE
1990 QDIS=QDISDE
2000 IF(THRST0(NDAY).LT.QDISDE) QDIS=THRST0(NDAY)
2010 THRST0(NDAY)=THRST0(NDAY)-QDIS
2020 PDIS(M0)=PDIS(M0)+QDIS
2030C
2040C CONDENSING PRESSURE EFFECT ON EPGS EFFICIENCY
2050 IF(THRST0(NDAY).LT.QDISDE.AND.SUMANG(M0,K).LT.0.05) GO TO 5555
2060 QEPGS=QDIS+(PARSGP*0.8015)-QLSG0N+(PARBFP+PARCND+PARCIR)*0.95
2070 SRATIO=QEPGS/QEPGS0
2080 GO TO 5556
2090C
2100C END OF DAY DEPLETION OF NA AT FULL LOAD FOR A FRACTION OF AN HOUR
2110 5555 CONTINUE
2120 FRACT=QDIS/QDISDE
2130 QEPGS=QDIS+((PARSGP*0.8015)-QLSG0N+(PARBFP+PARCND+PARCIR)*0.95)*FRACT
2140 SRATIO=1.
2150 5556 CONTINUE
2160 T100=51.90024*EXP(0.0089967*TEMPWB(K))
2170 TSLOPE=T100-(TEMPWB(K)+5.)
2180 TCOND=TEMPWB(K)+5.+TSLOPE*SRATIO
2190 IF(TCOND.LT.79.) TCOND=79.

```

04/15/80 9.698

```

2200 FACCON=0.94044787+4.021048E-4*TCOND+1.5824425E-5*TCOND**2
2210&      -1.3853331E-7*TCOND**3
2220 FRACON=FRARAT*FACCON
2230C
2240C PART LOAD EFFECT ON EPGs EFFICIENCY
2250 IF(THRSTO(NDAY)+QDIS.LT.QDISDE.AND.SUNANG(MO,K).LT.0.05) GO TO 1801
2260C ITERATE FOR LOAD FRACTION
2270 KLOAD=0
2280 FRALDE=SRATIO
2290 802 CONTINUE
2300 IF(FRALDE.GE.0.4) FACLD=7.3499496E-1+6.7252457E-1*FRALDE
2310&      -5.5128706E-1*FRALDE**2+1.4376755E-1*FRALDE**3
2320 IF(FRALDE.LT.0.4) FACLD=FRALDE/(0.0519473+0.9531657*FRALDE)
2330 FRAGEN=FRACON*FACLD
2340 KLOAD=KLOAD+1
2350 QGROSS=QEPGS*FRAGEN
2360 FRALOD=QGROSS/QRATED
2370 DIFF=ABS(FRALDE-FRALOD)
2380 IF(KLOAD.GE.10) GO TO 801
2390 IF(DIFF.LT.0.005) GO TO 801
2400 FRALDE=(FRALDE+FRALOD)/2.
2410 GO TO 802
2420 801 CONTINUE
2430 GO TO 1802
2440C
2450 1801 CONTINUE
2460 FACLD=1.
2470 FRALDE=1.
2480 FRALOD=1.
2490 FRAGEN=FRACON*FACLD
2500 QGROSS=QEPGS*FRAGEN
2510 1802 CONTINUE
2520C
2530 PARSG=PARSGP+PARBFP+PARCND+PARCIR+PARCT+PARHTL+PARTNF
2540 IF(THRSTO(NDAY)+QDIS.LT.QDISDE.AND.SUNANG(MO,K).LT.0.05) PARTW=PARTW*FRACT
2550 IF(THRSTO(NDAY)+QDIS.LT.QDISDE.AND.SUNANG(MO,K).LT.0.05) PARSG=PARSG*FRACT
2560 QPARTL=PARTW*PARSG
2570 QNET=QGROSS-QPARTL
2580 FRAPAR=QNET/QGROSS
2590 PLON(MO)=PLON(MO)+QLSGON
2600 PEPGS(MO)=PEPGS(MO)+QEPGS
2610 PGRROSS(MO)=PGRROSS(MO)+QGROSS
2620 PPARA(MO)=PPARA(MO)+PARTW*PARSG
2630 PDAY(MO, IDAY)=PDAY(MO, IDAY)+QNET
2640C
2650C*****
2660C*****PRINT DAILY PERFORMANCE*****
2670C*****
2680C
2690 312 CONTINUE
2700 IF(IPDAY.EQ.0) GO TO 500
2710 IF(NDAY.NE.300.AND.NDAY.NE.301.AND.NDAY.NE.302) GO TO 500
2720 PRINT 91, SRATIO, TCOND
2730 91 FORMAT("SRATIO=", F5.3, 2X, "TCOND=", F5.1)
2740 PRINT 105, FRALDE, FRALOD
2750 105 FORMAT("FRALDE=", F6.4, 3X, "FRALOD=", F6.4)
2760 PRINT 106, FACCON, FACLD
2770 106 FORMAT("FACCON=", F6.4, 3X, "FACLD=", F6.4)
2780 PRINT 99, FRAGEN, FRAPAR
2790 99 FORMAT("FRAGEN=", F6.4, 3X,
2800&      "FRAPAR=", F6.4)
2810 PRINT 81, PARTW, PARSG, QPARTL
2820 81 FORMAT("PARTW=", F4.2, 2X, "PARSG=", F4.2, 2X, "QPARTL=", F5.1)
2830 PRINT 98, QDIS, QEPGS, QGROSS
2840 98 FORMAT("QDIS=", F6.2, 2X, "QEPGS=", F6.2, 2X, "QGROSS=", F6.1)
2850 PRINT 96, QNET, THRSTO(NDAY)
2860 96 FORMAT("QNET=", F5.1, 2X, 3X, "THRSTO=", F5.1)
2870C
2880 500 CONTINUE
2890 IF(IPDAY.EQ.0) GO TO 907
2900 IF(NDAY.NE.300.AND.NDAY.NE.301.AND.NDAY.NE.302) GO TO 907
2910 PRINT 890, MO, IDAY, PDAY(MO, IDAY), PWST(MO, IDAY), DAYDNI, THRSTO(NDAY)
2920 890 FORMAT("MO=", I2, 1X, "DAY=", I2, 1X, "PDAY=", E10.4, 1X,
2930&      "PWST=", E10.4, 1X, "DAYDNI=", F5.2, 1X, "THRSTO=", F5.1)
2940 907 CONTINUE

```

04/15/80 9.698

2950 9999 CONTINUE

2960C

2970C*****

2980C*****CALCULATE MONTHLY AND YEARLY PERFORMANCE*****

2990C*****

3000C

3010 IF(IPMON.EQ.0) GO TO 9994

3020 PYEAR=0.

3030 DO 9997 NMONTH=1,MO

3070 DO 9996 ID=1,MODAY(NMONTH)

3080 PMONTH(NMONTH)=PMONTH(NMONTH)+PDAY(NMONTH, ID)

3090 PWSTMO(NMONTH)=PWSTMO(NMONTH)+PWST(NMONTH, ID)

3100 9996 CONTINUE

3110 PCTUSA = PUSABL(NMONTH)/PAVABL(NMONTH)

3120 PCTUSD = PUSED(NMONTH)/PUSABL(NMONTH)

3121 PCTFOC=PFOCUS(NMONTH)/PUSED(NMONTH)

3130 PCTFLD = PRCV(NMONTH)/PFOCUS(NMONTH)

3140 PCTRCV=PRCVD(NMONTH)/PRCV(NMONTH)

3150 PCTWST=PWSTMO(NMONTH)/PCHA(NMONTH)

3151 PCTLWM=PLWARM(NMONTH)/PCHA(NMONTH)

3160 PCTEPG = PGRSS(NMONTH)/PEPGS(NMONTH)

3170 PCTOVL = PMONTH(NMONTH)/PFOCUS(NMONTH)

3180 PCTPAR=(PGRSS(NMONTH)-PPARA(NMONTH))/PGRSS(NMONTH)

3190 PCTL0F=PL0FF(NMONTH)/PRCVD(NMONTH)

3200 PCTL0N=PL0N(NMONTH)/PRCVD(NMONTH)

3210C

3220 IF(IPMON.EQ.2) GO TO 3333

3230 PRINT 9995, NMONTH, PMONTH(NMONTH)

3240 9995 FORMAT("*****PMONTH(", I2, ")=", F7.1, "(MW-HR)")

3250 PRINT 9981, PAVABL(NMONTH), PUSABL(NMONTH), PUSED(NMONTH)

3260 9981 FORMAT("PAVABL=", E13.7, 1X, "PUSABL=", E13.7, 1X, "PUSED=", E13.7)

3270 PRINT 9982, PFOCUS(NMONTH), PRCV(NMONTH), PRCVD(NMONTH)

3280 9982 FORMAT("PFOCUS=", E13.7, 1X, "PRCV=", E13.7, 1X, "PRCVD=", E13.7)

3290 PRINT 9983, PEPGS(NMONTH), PGRSS(NMONTH), PPARA(NMONTH)

3300 9983 FORMAT("PEPGS=", E13.7, 1X, "PGRSS=", E13.7, 1X, "PPARA=", E13.7)

3310 PRINT 9984, PLOFF(NMONTH), PL0N(NMONTH)

3320 9984 FORMAT("PLOFF=", E13.7, 1X, "PL0N=", E13.7)

3330 PRINT 9985, PGRID(NMONTH), PWSTMO(NMONTH)

3340 9985 FORMAT("PGRID=", E13.7, 1X, "PWSTMO=", E13.7)

3350 PRINT 9775, PCHA(NMONTH), PDIS(NMONTH), PLWARM(NMONTH)

3360 9775 FORMAT("PCHA=", E13.7, 1X, "PDIS=", E13.7, 1X, "PLWARM=", E13.7)

3370 PRINT 9770, PCTUSA, PCTUSD, PCTFOC, PCTFLD, PCTRCV

3380 9770 FORMAT("PCTUSA=", F6.4, 1X, "PCTUSD=", F6.4, 1X,

3390 9770 "PCTFOC=", F6.4, 1X, "PCTFLD =", F6.4, 1X, "PCTRCV =", F6.4)

3400 PRINT 9771, PCTWST, PCTEPG, PCTOVL

3410 9771 FORMAT("PCTWST=", F6.4, 1X, "PCTEPG=", F6.4, 1X, "PCTOVL=", F6.4)

3420 PRINT 9971, PCTPAR, PCTL0F, PCTL0N, PCTLWM

3430 9971 FORMAT("PCTPAR=", F6.4, 1X, "PCTL0F=", F6.4, 1X, "PCTL0N=", F6.4,

3431 9971 "PCTLWM=", F6.4)

3440 9997 CONTINUE

3450C

3460 PYEAR=PYEAR+PMONTH(NMONTH)

3470 EAVABL=EAVABL+PAVABL(NMONTH)

3480 EUSABL=EUSABL+PUSABL(NMONTH)

3490 EUSED=EUSED+PUSED(NMONTH)

3491 EFOCUS=EFOCUS+PFOCUS(NMONTH)

3500 ERCV=ERCV+PRCV(NMONTH)

3510 ERCVD=ERCVD+PRCVD(NMONTH)

3520 ELOFF=ELOFF+PLOFF(NMONTH)

3530 EL0N=EL0N+PL0N(NMONTH)

3540 EEPGS=EEPGS+PEPGS(NMONTH)

3550 EGRSS=EGRSS+PGRSS(NMONTH)

3560 EPARA=EPARA+PPARA(NMONTH)

3570 EGRID=EGRID+PGRID(NMONTH)

3580 EWST=EWST+PWSTMO(NMONTH)

3590 ELWARM=ELWARM+PLWARM(NMONTH)

3600 ECHA=ECHA+PCHA(NMONTH)

3610 EDIS=EDIS+PDIS(NMONTH)

3620 9997 CONTINUE

3630C

3640 EFFUSA=EUSABL/EAVABL

3650 EFFUSD=EUSED/EUSABL

3651 EFFFOC=EFOCUS/EUSED

3660 EFFFLD=ERCV/EFOCUS

3670 EFFRCV=ERCVD/ERCV

04/15/80 9.698

```
3680 EFFWST=EWST/ECHA
3690 EFFEPG=EGROSS/EEPGS
3700 EFFPAR = (EGROSS - EPARA)/EGROSS
3710 EFFLOF=ELOFF/ERCVED
3720 EFFLON=ELON/ERCVED
3730 EFFLWM=ELWARM/ECHA
3740 EFFOVL=PYEAR/EFOCUS
3750 CAPFAC=PYEAR/(8784.*100.)
3760 PRINT, "*****YEARLY PERFORMANCE SUMMARY*****"
3770 PRINT 9992, PYEAR, CAPFAC
3780 9992 FORMAT("PYEAR=", E13.7, 2X, 2X, "CAPFAC=", F6.4)
3790 PRINT 4001, EAVABL, EUSABL, EUSED
3800 4001 FORMAT("EAVABL=", E13.7, 1X, "EUSABL=", E13.7, 1X, "EUSED=", E13.7)
3810 PRINT 4002, EFOCUS, ERCV, ERCVED
3820 4002 FORMAT("EFOCUS=", E13.7, 1X, "ERCV=", E13.7, 1X, "ERCVED=", E13.7)
3830 PRINT 4003, ELOFF, ELON
3840 PRINT 4006, ECHA, EDIS, ELWARM
3850 PRINT 4004, EEPGS, EGROSS, EPARA
3860 PRINT 4005, EGRID, EWST
3870 4003 FORMAT("ELOFF=", E13.7, 1X, "ELON=", E13.7)
3880 4006 FORMAT("ECHA=", E13.7, 1X, "EDIS=", E13.7, 1X, "ELWARM=", E13.7)
3890 4004 FORMAT("EEPGS=", E13.7, 1X, "EGROSS=", E13.7, 1X, "EPARA=", E13.7)
3900 4005 FORMAT("EGRID=", E13.7, 1X, "EWST=", E13.7)
3910 PRINT 9875, EFFUSA, EFFUSD, EFFFOC, EFFFLD, EFFRCV
3920 9875 FORMAT("EFFUSA=", F6.4, 1X, "EFFUSD=", F6.4, 1X,
3930& "EFFFOC=", F6.4, 1X, "EFFFLD=", F6.4, 1X, "EFFRCV=", F6.4)
3940 PRINT 4010, EFFWST, EFFEPG, EFFOVL
3950 4010 FORMAT("EFFWST=", F6.4, 1X, "EFFEPG=", F6.4, 1X, "EFFOVL=", F6.4)
3960 PRINT 4011, EFFPAR, EFFLOF, EFFLON, EFFLWM
3970 4011 FORMAT("EFFPAR=", F6.4, 1X, "EFFLOF=", F6.4, 1X, "EFFLON=", F6.4,
3971& 1X, "EFFLWM=", F6.4)
3980 9994 CONTINUE
3990C
4000 CALL DETACH(15, ISTAT, )
4010 CALL DETACH(16, ISTAT, )
4020 STOP
4030 END
```